DESIGN, MODELLING AND IMPLEMENTATION OF SEVERAL MULTI-STANDARD HIGH PERFORMANCE SINGLE-WIDEBAND AND MULTI-WIDEBAND MICROWAVE PLANAR FILTERS

Y. X. TU

PhD

UNIVERSITY OF BRADFORD

2016

DESIGN, MODELLING AND IMPLEMENTATION OF SEVERAL MULTI-STANDARD HIGH PERFORMANCE SINGLE-WIDEBAND AND MULTI-WIDEBAND MICROWAVE PLANAR FILTERS

Y. X. TU

Ph. D.

2016

DESIGN, MODELLING AND IMPLEMENTATION OF SEVERAL MULTI-STANDARD HIGH PERFORMANCE SINGLE-WIDEBAND AND MULTI-WIDEBAND MICROWAVE PLANAR FILTERS

Analysis, Simulation and Measurements of Multi-Standard Uniplanar High Performance Asymmetric Stepped Impedance Resonator Single / Dual-Wideband Filters With Wide Stopband And Triple-Wideband / Quadruple-Wideband / Quint-Wideband Filters

YUXIANG TU

BSc, MSc

Submitted for the degree of

Doctor of Philosophy

School of Engineering and Informatics

University of Bradford

2016

DESIGN, MODELLING AND IMPLEMENTATION OF SEVERAL MULTI-STANDARD HIGH PERFORMANCE SINGLE-WIDEBAND AND MULTI-WIDEBAND MICROWAVE PLANAR FILTERS

Analysis, Simulation and Measurements of Multi-Standard Uniplanar High Performance Asymmetric Stepped Impedance Resonator Single / Dual-Wideband Filters With Wide Stopband And Triple-Wideband / Quadruple-Wideband / Quint-Wideband Filters

Keywords:

Microwave Planar Filters, Asymmetric Stepped Impedance Resonator (ASIR), Multi-standard, Single-wideband, Dual-wideband, Triple-wideband, Quadruple-wideband, quint-wideband filters, Wide Stopband, Wireless Communication.

Abstract

The objectives of this work are to review, investigate and model the microwave planar filters of the modern wireless communication system. The recent main stream of microwave filters are classified and discussed separately. Various microwave filters with detailed applications are investigated in terms of their geometrical structures and operational performances. Theoretical

A comprehensive theoretical study of microwave filters is presented. The main types of microwave filters including the basic low-pass filters such as Butterworth and Chebyshev filters are fully analysed and described in detail. The transformation from low-pass prototype filters to high-pass filters, band-pass filters and band-stop filters are illustrated and introduced. Research work on stepped impedance resonator (SIR) and asymmetric stepped impedance resonator (ASIR) structure is presented. The characteristics of $\lambda g/4$, $\lambda g/2$ and λg (λg is the guided wavelength of the fundamental frequency in the free space) type SIR resonators, and the characteristic of asymmetric SIR resonator are categorized and investigated.

Based on the content mentioned above, novel multi-standard high performance asymmetric stepped impedance resonator single-wideband and dual-wideband filters with wide stopbands are proposed. The methodologies to realize wide passband and wide stop-band filters are detailed. In addition, multi-standard high performance triple-wideband, quadruple-wideband and quint-wideband filters are suggested and studied. The measurement results for all prototype filters agree well with the theoretical predictions and simulated results from Ansoft HFSS software. The featured broad bandwidths over single/multiple applicable frequency bands and the high performances of the proposed filters make them very promising for applications in future multi-standard wireless communication.

Table of Contents

Acknowledgment

The completion of this report would not have been possible without the help and support of the following people. First and foremost I would like to express my appreciation and gratitude to my supervisor Prof. R. A. Abd-Alhameed and Dr. James. M. Noras. They have been very generous in their time and always a source of invaluable guidance, encouragement and inspiration to me. Also, I would like to express my appreciation for Dr. Prashant Pillai's support and help throughout completion of my PhD study.

Moreover, I extend my thanks to Dr. C. H. See for his continuous help and kindness.

Last but by no means least, I convey my warmest thanks to my parents for their endless support and encouragement throughout my life, letting me reach this far in my studies.

Acronyms

ASIR	Asymmetric Stepped Impedance Resonator
BPF	band-pass Filter
BSF	band-stop Filter
CF	Central Frequency
CPW	Coplanar Wave Guide
DGS	Defected Ground Structure
FBW	Fractional Bandwidth
GPA	Ground Plane Aperture
GPS	Global Positioning System
GSM	Global System for Mobile Communication
HPF	High-pass filter
IL	Insertion Loss
LCP	Liquid Crystal Polymer
LPF	Low-pass filter
LTCC	Low-Temperature Co-fire Ceramic
LTCF	Low-Temperature Co-fire Ferrite
LTE	Long Term Evolution
MEMC	Mixed Electronic and Magnetic Coupling

MEMC	Micro Electro-Mechanical Systems
MEMS	Micro Electro-Mechanical Systems
MMR	Multi-Mode Resonators
PBG	Photonic Band Gap
RF	Radio Frequency
RL	Return Loss
SIR	Stepped Impedance Resonator
SIW	Substrate Integrated Waveguide
TZ	Transmission Zeros
UMTS	Universal Mobile Telecommunications System
UWB	Ultra-Wide-band
WiMAX	Worldwide Interoperability for Microwave Access
WLAN	Wireless Local Area Network

List of Figures

List of Tables

Chapter 1

Introduction

1.1 Background and Motivation

In recent years, wireless communication facilities such as wireless transceivers have been exerting an increasingly vital impact in the field of microwave and radio frequency communication. One of the most important modules in wireless communication systems is the microwave filter [1-7]. Microwave filters play a critical role in passing desired frequency bands and stopping unwanted ones including noise interference signals in communication systems. Figure 1.1 shows the positions of the microwave filters in a generic wireless transceiver system. Therefore, developing high performance multi-standard filters with compact size, low in-band insertion loss (IL), and high out-of-band rejection skirts is our goal in the following steps. Compared to the traditional stepped impedance resonator (SIR) with two step discontinuities, the asymmetric SIR (ASIR) has only one discontinuity but still keeps the characteristic of controllable spurious modes. Thus, it has the advantage of compact size, less loss, and strong design feasibility, particularly in designing of high-order BPFs such as dual band [8][10], triple band and quad band[16] BPFs because of its inherently higher order resonant modes. Therefore, the motive of this thesis is to analyse, design and measure the high performance single- and multi-band ASIR filters for advanced communication systems.

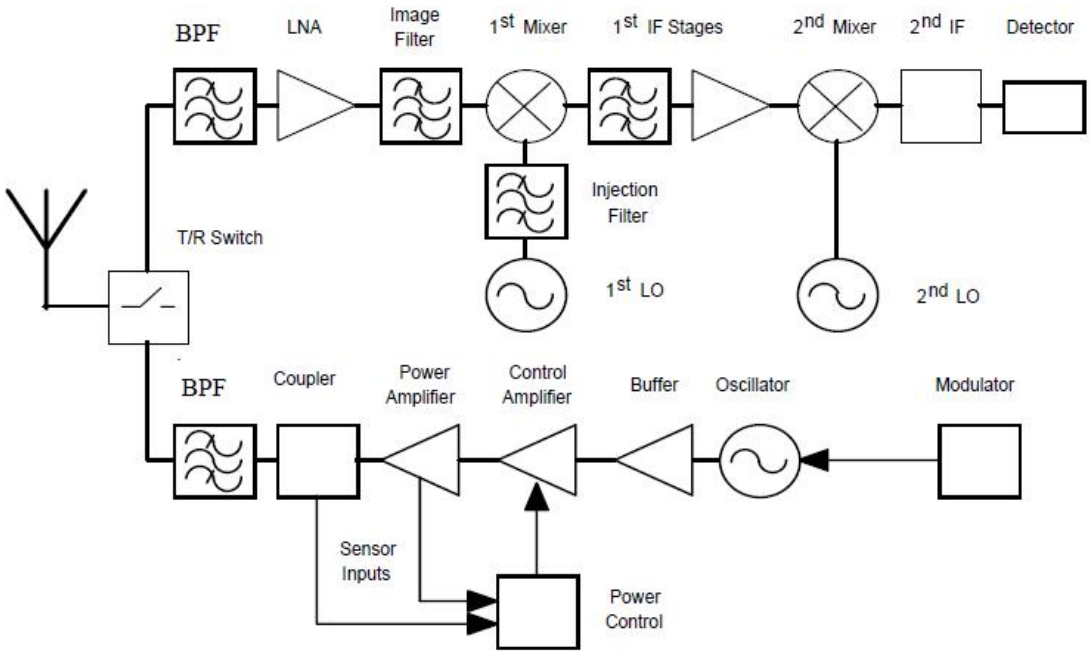

Figure 1.1. A generic wireless transceiver

1.2 Thesis Objectives

The currently proposed ASIR filters are mainly ~~about~~ the traditional Anti-Parallel-Coupled ASIR (APC-ASIR) which consists of two ASIR units with their high and/or low impedance lines anti-coupled with each other and is usually folded at its open end. In [13], the high impedance lines of two ASIRs are bent and coupled with each other to form a signal transmission route, and the first spurious frequency is utilized to form the second operating band [14]. Because the frequency response characteristic of the anti-parallel-coupled line is determined by the frequency response characteristic of the ASIR, the APC-ASIR frequency response is easy to calculate. However, the bandwidth characteristic of the APC-ASIR structure [12, 13], as with the multi-stage coupled ASIR structure [15, 16], has two disadvantages: one is its narrow band characteristic within the pass-band range; and another one is

limited number of pass-bands. Therefore, this approach cannot fully meet the multi-service broad band requirement of current wireless communications.

The objective of this thesis is to develop, design and characterize methodologies for the proposed wide-band ASIR filters with single- and multi-band characteristics. Hence, it involves the analysis, design, simulation and fabrication of wide-band ASIR filters with critical parameters including the desired central frequency, wide-bandwidth, low loss and small size.

Based on the current single-band ASIR with narrow band disadvantages, single-wide-band ASIR structures with wide stop-bands are analysed and designed, as shown in chapter 6 and chapter 7, respectively.

Based on the current dual-band ASIR with narrow band disadvantages, dual-wide-band ASIR structures with wide stop-bands are analysed and designed, and shown in chapter 5.

Based on the current ASIR with the disadvantage of limited band numbers, triple/quad/quint-wide-band ASIR structures are analysed and designed, as shown in chapter 5, chapter 6 and chapter 7, respectively.

Relevant communication standards includes the Global System for Mobile Communication(GSM): GSM850 (824-894 MHz), GSM900 (890-960 MHz), GSM1800 (1710-1880 MHz), GSM1900 (1850-1990 MHz), Universal Mobile Telecommunications System (UMTS) :1920-2170 MHz, Global Positioning System

(GPS) :L1 band: 1.57542 GHz, L2 band: 1.22760 GHz, L3 band: 1.38105 GHz, L4 band: 1.84140 GHz, IEEE 802.11a (frequency band centred at 5.2 GHz/5.8 GHz), IEEE 802. 11b/g/n (2.4-2.6 GHz), Worldwide Interoperability for Microwave Access (WiMAX): 3.3-3.7 GHz, Long Term Evolution (LTE): LTE2300: 2305-2400 MHz, LTE2500: 2500-2690 MHz and so on. These wireless communication standards are followed when analysing and designing the related single-and multi-wide-band filters.

1.3 Organization of the Thesis

Chapter 1: This chapter gives a brief introduction to microwave filters including their application fields and main function in wireless communications. Communication standards and relative operating frequency bands are proposed to guide the design of microwave filters.

Chapter 2: This chapter covers an introduction to microwave filters and sets out a comprehensive review of microwave filters, mainly planar microwave filters. The recent years' main stream of microwave filters are classified and discussed separately, which includes: (1) lumped-element LC filters, (2) planar structure filters, and (3) non-planar structure filters. Planar structure filters including microstrip filters, coplanar waveguide filters and so on are described especially in detail . In addition, this chapter introduces new materials, new structures and new technologies in the microwave filter field, including new materials such as low-temperature co-fire ceramic technology (LTCC), low-temperature co-fire ferrite (LTCF), liquid

crystal polymer (LCP), new structures such as photonic band gap (PBG), ground plane aperture (GPA), defected ground structure (DGS), substrate integrate waveguide (SIW), new technologies such as micro electro mechanical systems (MEMS) or micromachining, high temperature superconducting and so on . All these new materials, new structures and new technologies have been proposed in papers to enhance the performance of microwave filters as well as the performance of microwave systems.

Chapter 3: This chapter presents a comprehensive theoretical study of microwave filters. It covers the introduction to a diversity of filters including low-pass filters, high-pass filters, band-pass filters and band-stop filters as well as filter design parameters including (1) the central frequency, (2) insertion loss, (3) ripple coefficient, (4) bandwidth, (5) rectangular coefficient, (6) the stop-band rejection. Three basic classic types of filters including (1) Maximally flat filter (Butterworth filter), (2) Chebyshev Filter, and (3) Elliptic Filter are explained. Furthermore, filter frequency transforms are reviewed including: (1) frequency transform between low-pass filter and low-pass prototype, (2) frequency transform between high-pass filter and low-pass prototype, (3) frequency transform between band-pass filter and low-pass prototype, and (4) frequency transform between band-stop filter and low-pass prototype. All these can give a deeper understanding of the design of microwave filters.

Chapter 4: This chapter provides a comprehensive study of stepped impedance resonator (SIR) structures and asymmetric stepped impedance resonator (ASIR) structures. All three types of $\lambda_g/4$, $\lambda_g/2$ and λ_g SIR resonator (λ_g is the guide wave

length of the resonator's fundamental frequency in free space) are analysed and fully explained. The chapter reviews: (1) The basic SIP structure, (2) The characteristics of SIR including resonating requirements and electrical lengths, (3) Spurious frequencies, and (4) Equivalent circuits. Moreover, the asymmetric stepped-impedance resonator, which is a novel SIR structure and has appeared in publications in recent years, is studied because of its advantages over other structures including the SIR structure. Traditional anti-parallel coupled ASIR structures are described, simulated and studied. All these are helpful to the detailed design of ASIR filters in the next chapter.

Chapter 5: Based on the content mentioned above, a novel parallel-coupled ASIR structure is proposed and its characteristics are fully analysed and discussed, showing differences from the characteristics of current anti-parallel coupled ASIR structures. Based on this novel structure, two novel multi-standard dual-wideband asymmetric stepped impedance resonator type filters are proposed, in which the mathematical analyses and descriptions of the characteristic of filter circuit structure are derived, and the configuration, performance and transmission zero point are analysed. Novel parallel-coupled asymmetric SIRs with interdigital cross-coupled line structure are integrated together to realize optimized in-band performance and realize wide stop-bands by introducing extra transmission zeros. Besides, the novel parallel-coupled asymmetric SIRs with parallel uncoupled microstrip lines structure are integrated together to realize optimized in-band performance and realize wide stopbands by introducing extra transmission zeros. Both types of the proposed dual-wideband filter have large stop-band bandwidth with sufficient suppression level. To the author's knowledge, the proposed structures realize for the first time dual

wideband and wide stop-band resulting from the restriction of high order harmonic frequencies.

Chapter 6: This chapter proposes an ASIR coupled structure with a meander coupled section. The novel structure's mathematical analysis and filter characteristics are derived, and the transmission zero point generation condition is analysed. The even and odd phase velocity compensation technique is also considered in this novel structure. By using this knowledge, a single-wideband filter with wide-stopband resulting from the generation of multiple transmission zeros is proposed. The single-wideband filter has advantages including low insertion loss, low return loss, simple structure and wide stop-band to suppress undesired signal interception. Moreover, by tuning the locations of transmission zeros, the quint-wideband filter can be realized by this novel structure. The quint-wideband filter has advantages including low insertion loss, low return loss, simple structure and large fractional bandwidth, indeed the largest fractional bandwidth in currently proposed quint-band filters.

Chapter 7: This chapter proposes an ASIR spiral and open loop coupled structure to realize a single-wideband filter and a quint-wideband filter. A spiral and open-loop structure is used to realize a mixed electric coupling and magnetic coupling effect and at the same time facilitate the quint-band performance. Based on the structure, the single-wideband filter is also realized. The Ansoft HFSS software simulated results and measurement results agree well with the theoretical predictions. The broad bandwidths over dual applicable frequency bands and the miniaturized

size of the proposed filter make it very promising for applications in multi-standard wireless communication.

Chapter 8: This chapter summarizes the thesis findings and looks ahead to future work.

1.4 References

[1] J. Shi, L. L Lin, Jian-Xin Chen, et al. Dual-Band band-pass Filter With Wide Stop-band Using One Stepped-Impedance Ring Resonator With Shorted Stubs. IEEE Microwave and Wireless Components Letters. Vol. 24, no. 7, pp: 442 - 444, 2014.

[2] L. Gao, X. Y. Zhang. High-Selectivity Dual-Band band-pass Filter Using a Quad-Mode Resonator with Source-Load Coupling. IEEE Microwave and Wireless Components Letters, Vol. 23, no. 9, pp: 474 - 476, 2013.

[3] Shou-Jia Sun, T. Su, K. Deng, et al. Compact Microstrip Dual-Band band-pass Filter Using a Novel Stub-Loaded Quad-Mode Resonator. IEEE Microwave and Wireless Components Letters, Vol. 23, no. 9, pp: 465 - 467, 2013.

[4]S. Fu, B. Wu, J. Chen, et al. Novel Second-Order Dual-Mode Dual-Band Filters Using Capacitance Loaded Square Loop Resonator. IEEE Transactions on Microwave Theory and Techniques, Vol. 60, no. 3, Part. 1, pp 477 - 483, 2012.

[5] C. W. Tang, P. H. Wu. Design of a Planar Dual-Band band-pass Filter. IEEE Microwave and Wireless Components Letters, Vol. 21, no. 7, pp: 362 - 364, 2011.

[6] S. M. Wang, Chun-Hsiang Chi, Ming-Yu Hsieh, et al. Miniaturized spurious pass-band suppression microstrip filter using meandered parallel coupled lines. IEEE Transactions on Microwave Theory and Techniques, Vol. 53, no. 2, pp: 747-753, 2005.

[7] S. L. March. Phase velocity compensation in parallel-coupled microstrip. IEEE MTT-S International Microwave Symposium Digest, pp: 410-413, 1982.

[8] Ching-Wen Tang, Po-Hsien Wu. Design of a Planar Dual-Band band-pass Filter. IEEE Microwave and Wireless Components Letters, Vol. 21, no. 7, pp: 362 -364. 2011.

[9] X. Y. Zhang, J. X. Chen, Q. Xue, et al. Dual-band band-pass filters using stub-loaded resonators. IEEE Microwave Wireless Component Letters. Vol. 17, no. 8, pp: 583-585, Aug. 2007.

[10] P. Mondal and M. K. Mandal. Design of dual-band band-pass filters using stub-loaded open-loop resonators. IEEE Transactions on Microwave Theory and Techniques. Vol. 56, no. 1, pp: 150-155, Jan. 2008.

[11] J. Sun, T. Su, K. Deng, et al. Shorted-Ended Stepped-Impedance Dual-Resonance Resonator and Its Application to Bandpass Filters. IEEE Transactions on Microwave Theory and Techniques, Vol. 61, no. 9, pp. 3209-3215, Sept. 2013.

[12] C. H. Kim and K. Chang. Wide-Stopband Bandpass Filters Using Asymmetric Stepped-Impedance Resonators. IEEE Microwave Wireless Component Letter. Vol. 23, no. 2, pp. 69-71, Feb. 2013.

[13] C. H. Kim and K. Chang. Independently Controllable Dual-Band Bandpass Filters Using Asymmetric Stepped-Impedance Resonators. IEEE Transactions on Microwave Theory and Techniques, Vol. 59, no. 12, pp. 3037-3047, Dec. 2011.

[14] Y. C. Chang, C. H. Kao, M. H. Weng, et al. Design of the Compact Wideband Bandpass Filter With Low Loss, High Selectivity and Wide Stopband. IEEE Microwave Wireless Component Letter. Vol. 18, no. 12, pp. 770-772, Dec. 2008.

[16] H. W. Liu, B. P. Ren et al. High-Temperature Superconducting Bandpass Filter Using Asymmetric Stepped-Impedance Resonators with Wide-Stopband Performance. IEEE Transaction on Applied Superconductivity, Vol. 25, no. 5, pp. 1-6, Oct. 2015.

[16] H. W. Wu and R. Y. Yang. A New Quad-Band Bandpass Filter Using Asymmetric Stepped Impedance Resonators. IEEE Microwave Wireless Component Letter. Vol. 21, no. 4, pp. 203-205, April 2011.

Chapter 2

Microwave Filters Overview

2.1 Introduction

Most RF and microwave filters are made up of one or more coupled resonators, and the resonator is the basic unit to realize the filter. According to the different technologies used in filter realization, filters can be divided into lumped-element LC filters [1]-[5], planar structure filters such as microstrip transmission line filters [6]-[23],coplanar waveguide filters [24]-[28] and so on, non-planar structure filters such as waveguide filters [29]-[32], resonant cavity filters [33] and so on. The books by Cohn [34], Matthaei, Young and Jones [35], R. J. Cameron, C. M. Kudsia, and R. R. Mansour [36] provide good references to the concept, design and realization of RF and microwave filters.

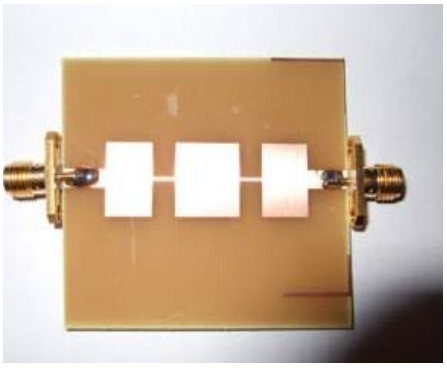

Figure 2.1. Planar structures. (microstrip, CPW, etc.)

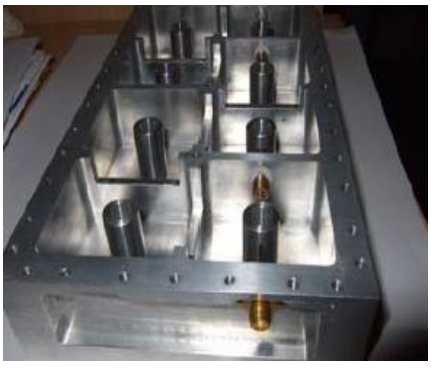

Figure2.2. Non-planar structures. (Cavity, non-planar, waveguide etc.)

2.2 Lumped-Element LC Filters

The simplest resonator structure that can be used in RF and microwave filters is an LC tank circuit consisting of parallel or series inductors and capacitors. These have the advantage of being very compact, but the low quality factor of the resonators leads to relatively poor performance.

Lumped-element LC filters [1]-[5] have both an upper and lower frequency range. As the frequency gets very low, into the low kHz to Hz range the size of the inductors used in the tank circuit becomes prohibitively large. Very low frequency filters are often designed with crystals to overcome this problem. As the frequency gets higher, into the 600 MHz and higher range, the inductors in the tank circuit become too small to be practical. An inductor of 1 nanoHenry (nH) at 600 MHz isn't even one full turn of wire. In recent years, miniature lumped element filters have come into use. The structures in [2], [4] and [5] have the advantages of compact size, light weight, easy for fabrication and fixing. Miniature lumped element filters are suitable for the use of narrow and wide-band filters ranges from 10-2000 MHz.

2.3 Planar Structure Filters

2.3.1 Microstrip Filters

The general structure of a microstrip is illustrated in Figure 2.3. A conducting strip (microstrip line) with a width W and a thickness t is on the top of a dielectric substrate that has a relative dielectric constant ε_r and a thickness h. The bottom of the substrate is

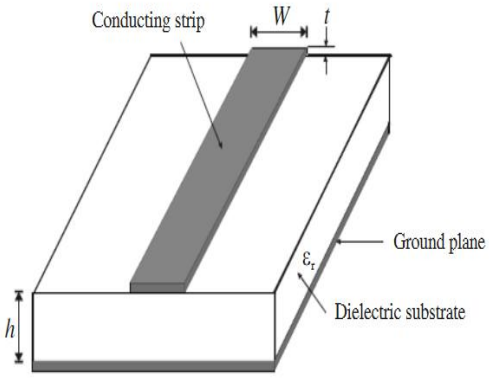

Figure 2.3. General microstrip structure

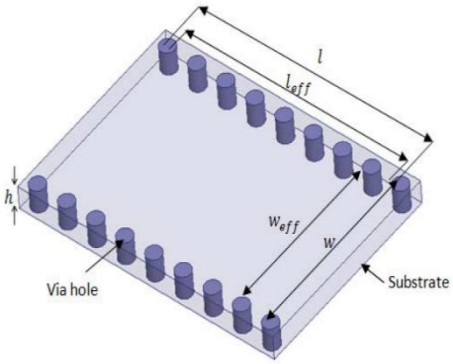

Figure 2.4. The basic structure of SIW

a ground (conducting) plane. Microstrip transmission lines can be used to make good resonators and filters to offer a better compromise in terms of size and performance than lumped element filters. Microstrip filters can be classified into stepped impedance resonators (SIRs) [6]-[12], hairpin filters [13]-[17], interdigital filters [18]-[23], parallel coupled filters and so on. In 1980, Makimoto et al. for the first time derived approximate design formulas for band-pass filters (BPFs) using parallel-coupled striped stepped-impedance resonators (SIRs) in ref. [6]. The formulas take into account the arbitrary coupling length and quarter wavelength coupling. The author showed that this type of filter had advantages of controlling spurious response and insertion loss by changing the structure of the resonator. Then two experimental filters are designed by using the formulas and measured.

In 1997, Sagawa et al. proposed in paper [7] to standardize $\lambda_g/4$ type, $\lambda_g/2$ type, λ_g type transmission-line stepped impedance resonators (SIRs) and systematically summarize their fundamental characteristics, such as resonance conditions, resonator length, spurious (higher order) responses, and equivalent circuits. Practical applications which employ features of three types of SIRs are investigated with demonstrations of specific

structures. Original design formulas with respect to λ_g type dual-mode resonators are analytically derived.

In [8], the ultra-wide-band (UWB) BPF comprised a cascade of low and high-pass structures. The concept of multimode resonators (MMR) used for UWB BPF was initially proposed in [9], where the first three resonant modes of the MMR were utilized to design the filter. In [10], pseudo interdigital stepped impedance resonators (PI-SIRs) were proposed to develop a UWB BPF.

In 2010, Qing-Xin Chu et al. presented an ultra-wide-band (UWB) band-pass filter (BPF) using a stepped-impedance stub-loaded resonator (SISLR) [11]. Characterized by theoretical analysis, the proposed SISLR is found to have the advantage of providing more degrees of freedom to adjust the resonant frequencies. Besides, two transmission zeros can be created at both lower and upper sides of the pass-band. Benefiting from these features, a UWB BPF is then investigated by incorporating this SISLR and two aperture-backed interdigital coupled-lines. Figure 2.5 shows the SISLR structure in [11].

In 2013, Liang Chen proposed a compact UWB filter with dual notched bands using cascaded shorted stub loaded stepped impedance resonators (SIRs) [12]. The basic UWB filter consists of multi-mode resonator (MMR) loaded with T-shaped stub and interdigital feed lines, having flat ultra-wideband response and sharp rejection skirt.

Two cascaded shorted-stub loaded SIRs are symmetrically coupled to MMR, introducing dual notched bands with deep and sharp shirt and providing freedom to

adjust the notch frequency. A UWB filter with 5.8Ghz/8.0Ghz notched bands is designed and fabricated.

Hairpin filters have been previously shown in many works. They have special properties, advantageous for the design of compact, narrow-band, and band-pass microstrip filters.

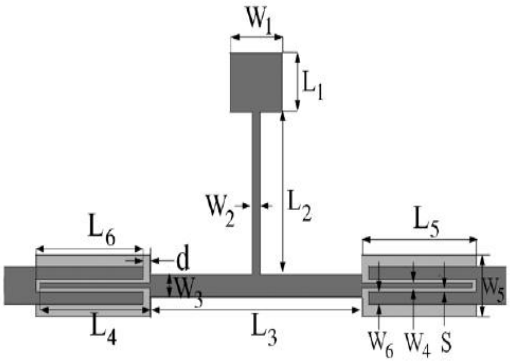

Figure 2.5. The SISLR structure in [11]

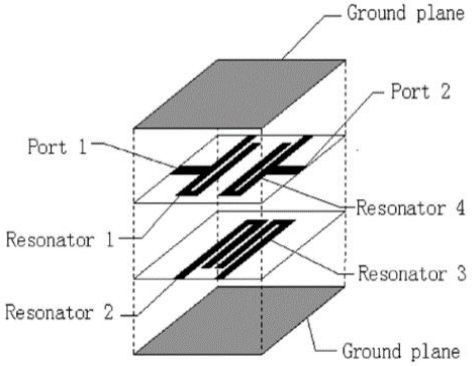

Figure 2.6. Multi-layer folded inter-digital resonators in [19]

In 2003, George L. Matthaei introduced a new "zig-zag" form of hairpin-comb filter [13], which is shown to have additional important advantages for designing compact narrow-band filters. Examples with computed responses and the measured results from high-temperature superconductor trial designs are presented. The considerable flexibility available in the design of band-pass filters of this sort is shown to be helpful in the design of tuneable band-pass filters having nearly constant bandwidth and pass-band shape as they are tuned. Measured results for tuning over nearly an octave range are presented.

In 2007, Vargas, J. M et al. proposed a superconductor circuit based on series Micro-Electro-Mechanical (MEM) switches to switch between two band-pass hairpin filters with 200 MHz bandwidth and nominal center frequencies of 2.1 GHz and 2.6 GHz [14].

This is accomplished using 4 switches actuated in pairs, one pair at a time. When one pair is actuated the first band-pass filter is coupled to the input and output ports. When the other pair is actuated the second band-pass filter is coupled to the input and output ports, thus corresponding output responses are obtained. The device is made of $YBa_2Cu_3O_7$ thin film deposited on a 20 mm by 20 mm $LaAlO_3$ substrate by pulsed laser deposition. $BaTiO_3$ deposited by RF magnetron sputtering is utilized as the insulation layer at the switching points of contact.

In 1995, J. S.Hong et al. proposed a new type of miniaturized microstrip band-pass filters with pseudo-interdigital structure without via hole grounded resonators [18] . A very compact filter of this type, having a size smaller than a quarter-wavelength by quarter-wavelength at a mid-band frequency of 1.1 GHz was designed and fabricated. This filter gains its compactness from the fact that it has a size similar to that of the conventional inter-digital band-pass filter. It gains its simplicity from the fact that no short-circuit connections are required so the structure is fully compatible with planar fabrication techniques.

In 2005, Yani Mu et al. proposed a novel compact cross-coupled inter-digital band-pass filter (BPF) [19]. (See in Figure. 2.6.) By using multilayer folded quarter-wavelength resonators, the size of the filter is reduced greatly, meanwhile a cross-coupling is introduced to produce transmission zeros and thereby improve the stop-band characteristics of the filter. As an example, a four-pole BPF centred at 2. 25 GHz with a fractional bandwidth of 31% is designed, fabricated, and measured. In the same year, G. Q. Wang et al. proposed a compact interdigital stripline band-pass filter embedded in low temperature co-fired ceramic for 5GHz wireless LAN applications, including

design, simulation, fabrication, and measurements [20]. The filter measures 8mm, by 7mm, by 1.1 mm and exhibits an insertion loss of 3.6 dB, a return loss of 20 dB, and a 212MHz pass-band with the midband frequency at 5.28 GHz. The filter is highly reproducible with good tolerance. A low noise amplifier (LNA) built on the top of the LTCC substrate with an embedded filter has the same bandwidth and midband frequency as those of the filter.

In 2012, S. W. Wong et al. proposed an interdigital microstrip coupled-line band-pass filter for millimetre-wave application [21]. A quadruple-mode microstrip-line resonator is designed to constitute the pass-band. The interdigital coupled-line sections are designed as the input/output network of the resonator. The measured results show that the filter achieves a pass-band insertion loss of 1.07dB at 40GHz, the lower- and upper-stop-band rejections are larger than 18 dB and 3 dB fractional bandwidth is 20%.

2.3.2 Coplanar Waveguide Filters

A coplanar waveguide (CPW) structure is used for the filter design since it can be well integrated into existing RFICs on Si substrates without the need to incorporate via-holes. For the design of microwave components, the CPW structure is less sensitive to the substrate thickness and substrate dielectric constant than microstrip structures.

In the case of coplanar waveguide based stub designs, crosstalk and parasitic radiation can be minimized by using series stubs which are patterned in the centre conductor, as opposed to a shunt stub configuration. At low frequencies or on low permittivity substrates, however, they tend to occupy considerable amounts of space since they are often designed to be a quarter-wavelength long. As a solution to this problem, the concept of folded series stubs is introduced in [24]. At the resonant frequency, these

inner slots are a quarter wavelength long and thus the short- circuit at point A is transferred to an open-circuit at point B, resulting in a band-stop response (see in Figure 2.7(a)). Using the new approach, the inner slots are simply folded back upon themselves two times (see in Figure 2.7(b)). This effectively reduces the stub length from $\lambda_g/4$ to $\lambda_g/12$, while achieving the same open-circuit effect at the input port. What's more, the bandwidth has reduced the use of lumped elementcapacitors integrated with distributed element, series stubs.

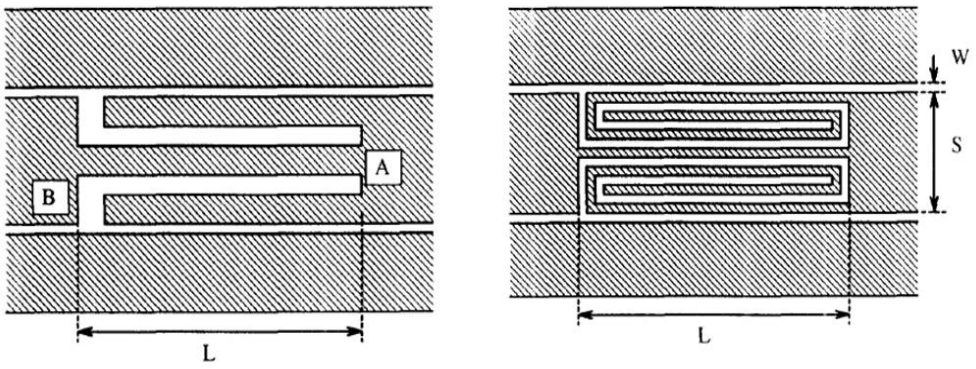

(a) (b)

Figure 2.7. (a) Folded series stubs, (b) Folded short-end stubs.

In 2002, K.T.Chan proposed a filter which has only 3.4 dB loss at peak transmission of 40GHz with a broad 9GHz bandwidth [26]. This was achieved using an optimized proton implantation process that converts the standard low-resistivity Si to a semi-insulating state to improve the filter performance. The filter shows a great potential for compact, low loss, and low-cost passive circuits in the future applications at high frequencies. This is the first demonstration of high performance filter at millimetre-wave regime on Si with process compatible to current VLSI technology. In 2003, K. T. Chan proposed a set of filters over the range from 22-91 GHz [27]. The bandpass filter consists of coupled lines to form a series resonator, of which a photographic image is shown in Figure 2.8 (a), while the band-stop filter was designed in a double-folded short-end stub structure, whose photographic image is shown in Figure 2.8(b), where

the dark area in the photograph is the metal pattern. At resonant frequencies, the inner slots transfer the equivalent open circuit to a short circuit, thus, a band-stop response was obtained [24], [25]. The band-stop filter has a double-folded short-end stub form, which reduces the filter size by folding stubs and slots in the filter structure.

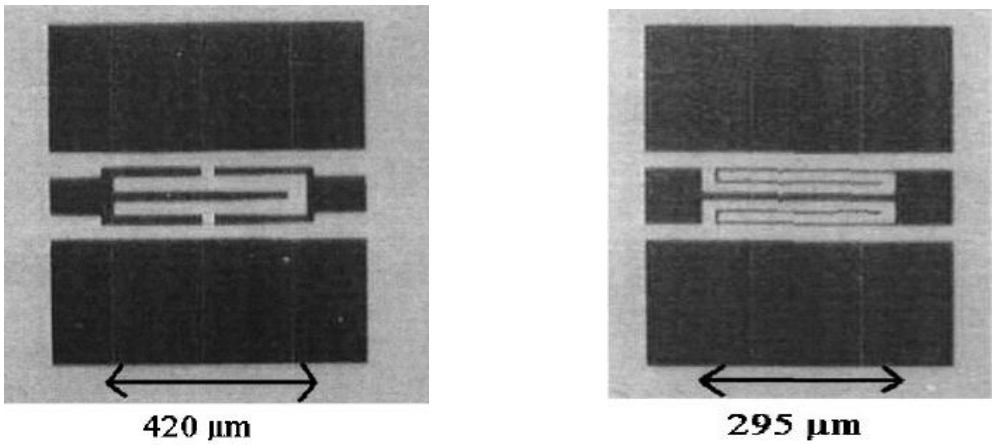

(a) (b)

Figure 2.8 (a). Image of the fabricated band-pass filters designed for the W-band of 94GHz. (b) Image of the fabricated band-stop filters for 52 GHz.

In ~~the~~ Figure 2.8, the values of the equivalent capacitance and inductance depend on the gap spacing between the coplanar couple lines and the width of the central line. The two parallel coupled-lines microstrip coplanar waveguide filter is one of the most common microwave filters in many practical wireless systems [28]. This kind of filters have a high order to produce a sharp transition band (TB). Therefore, one predicts the filter would be larger and have more insertion loss (IL) . In paper [29], the author used the bended stub with novel folded technology to improve the three parallel coupled-lines structure of BPF for N =1. This creates a sharp transition band (TB) and reduces the dimension of the circuit by 66.67% at 2.45 GHz. Its centre frequency can be shifted easily by adjusting the interfaces simultaneously.

2.4 Non-Planar Structure Filters

Non-planar structure filters include waveguide filters and dielectric resonator filters. The rectangular waveguide filter, which is shown in Figure 2.2, is widely used in microwave and millimetre-wave such as in communications, electronic warfare (EW), automatic test equipment (ATE), microwave subsystems and radar systems [30]. They are required for high-power applications and preferred for precision performance. At low signal levels, they are primarily used at frequencies from 8 to more than 100 GHz. This waveguide filter also provides a high Q factor, high selectivity and low insertion loss [31]. Meanwhile, the waveguide filter has a relatively bulky size, higher cost and is not easy to integrate between planar and non-planar circuits. In 2012, X. H. Zhao proposed a silicon micro-machined band-pass rectangular waveguide filter which is firstly fabricated by the deep reactivation etching (DRIE) processes for sub-millimetre wave applications. The filter circuit structure is formed using an ICP reactive ion etcher to etch through the full thickness of the silicon wafer, and is then bonded together with two metallized glass covers to form the waveguide cavity. The measured results show bandwidth of 21.2 GHz and 14.5 GHz centred at 140 GHz with 3-pole and 5-pole filters while the loaded quality factors are Q=139 and 163, respectively. In 2010, Q. F. Zhang proposed a four-pole waveguide band-pass filter with about 6% fractional bandwidth [32]. The filter is based on non-resonating 'T' junctions and the measured results agree well with the calculated results and show good in-band equal ripple performance and sharp rejection performance.

In 2009, paper [33] introduced a dual-band filter using dielectric resonator (DR) technology, based on the half-cut cylinder resonator shown in Figure 2.9. Two

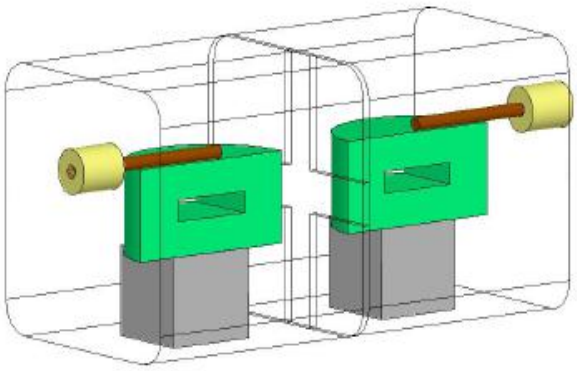

Figure 2.9. Structure of the dual-band 2-cavity (2x2-poles) filter in [33]

orthogonal modes of the resonator are used to carry the two operating pass-bands of the filter. It is shown that full control over the two pass-bands is achieved, through the independent control of the centre frequencies, inter-cavity couplings, and input/output couplings of each band. Filter design is simple and is carried out separately for each band, owing to the orthogonal modes. Various improvement techniques are also discussed.

2.5 New Materials, New Structures and New Technologies in Modern Microwave Filters

In recent years, there have been several new concepts applied to distributed microwave circuits in order to meet the requirement of high performance, compact size, low cost ,and so on. For example, some new materials such as low-temperature co-fire ceramic technology (LTCC) [37]-[42], low-temperature co-fire ferrite (LTCF) [43]-[44], liquid crystal polymer (LCP) [45]-[48], new technologies such as micro electro-mechanical systems (MEMS) or micromachining [49]-[55], high temperature superconducting and some new structures such as photonic band gap (PBG) [56]-[59],

ground plane aperture (GPA) [60]-[62], defected ground structure (DGS) [63]-[76], substrate integrated waveguide (SIW) [77]-[79], and others are proposed in papers to enhance the performance of microwave filters as well as whole microwave systems.

Liquid crystal polymer (LCP) is a new and promising thermoplastic material which can be used as both substrate and package material. Two types of liquid crystal polymer films, bonding film and core film, are available with different melting temperatures. Besides, the cost of LCP is comparable to that of conventional printed circuit board material and is much cheaper than that of low temperature co-fired ceramic (LTCC). In general, LCP is a good choice for developing devices with low cost, low loss, light weight, multilayer integration and packaging compatibility.

Photonic band gap (PBG) structure is a periodic structure which has been known as providing rejection of a certain frequency band. However, it is difficult to use a PBG structure for the design of the microwave or millimetre-wave components due to the difficulties of modelling.

A novel ground plane aperture structure (GPA) technique simply incorporates the microstrip line with a centred slot at the ground plane.The use of GPA has attractive applications in 3 dB edge coupler for tight coupling and band-pass filters for spurious band suppression and enhanced coupling. DGS based on GPA focuses not only on its application but also on its own characteristics and its ground plane metal of a microstrip (or stripline, or coplanar waveguide) circuit is intentionally modified to enhance performance [69]. For example, there are slot structures, slot variations, meander lines,

drum bell structures and so on [70]. Besides, additional applications of DGS can also be seen in delay lines, antennas [71] [72], and dividers [73]. The basic element of DGS is a resonant gap or slot in the ground metal, placed directly under a transmission line and aligned for efficient coupling to the line. DGS can change characteristics of the transmission line such as the line capacitance and line inductance. Besides, it can increase the characteristic impedance of the microstrip, achieve reduction in size and improve the performance of the microstrip components. Figure 2.10 shows various DGS structures. In 2003, a single resonator with the "notch" size DGS is proposed[64], which is shown in Figure 2.11 (a). This one-pole "notch" in frequency response can be used to provide additional rejection at the edges of a filter pass-band, or at an out-of-band frequency such as a harmonic, mixer image, or any frequency where the filter structure has poor rejection due to re-entry or moding effects. Moreover, DGS allows the designer to place a notch (zero in the transfer function) almost anywhere. When placed just outside a band-pass filter's pass-band, the steepness of the roll-off and the close-in stop-band are both improved.

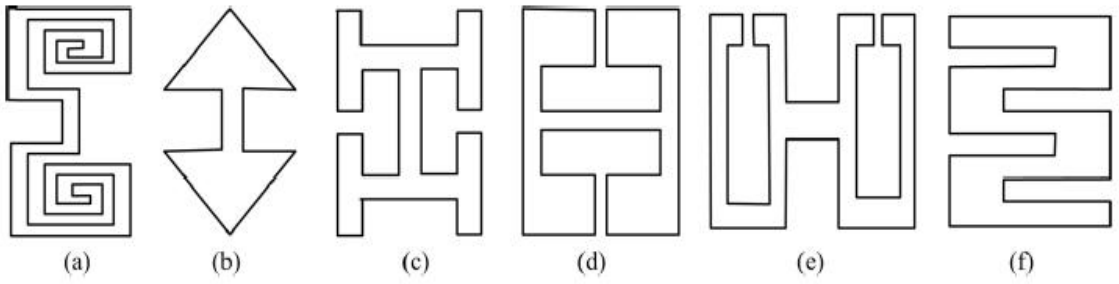

Figure 2. 10. Various DGSs: (a) Spiral head, (b) Arrowhead-slot, (c) "H" shape slots,(d) A square open-loop with a slot in middle section, (e) Open-loop dumbbell and (f) Inter-digital DGS.

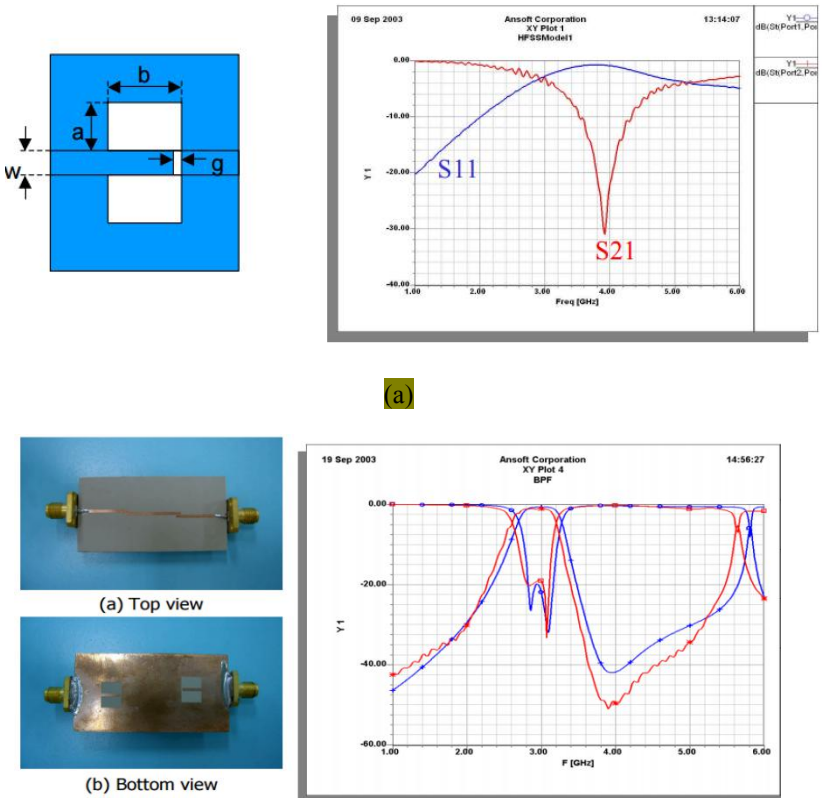

Figure 2.11 (a) Structure of a specific DGS type and its frequency response, obtained by electromagnetic simulation in paper [64]. (b) Layout, simulation and measurements of a coupled-line band-pass filter at 3.0 GHz. The filter includes two 3.92 GHz DGS elements, located adjacent to the input and output in paper [64].

The filter's centre frequency is 3.0 GHz, while the DGS resonators are designed for a notch at 3.92 GHz. The plot of Figure 2.11 (b) shows a fast roll-off on the high frequency side of the pass-band, which is much greater than that of the basic coupled line filter [64].

In 2010, Y.C.Guo published a paper containing an improved equivalent circuit parameters extraction method for the dumbbell-shaped defected ground structure [74]. The new extraction parameters equations are obtained in closed-form expressions, which contain S11 and S21. Compared with conventional methods, the proposed

method can give more accurate frequency response curves, and can be widely used in the design and analysis of DGS.

In 2013, Abdalla Abdulhadi published a paper named Combined Shaped Microstrip Line and DGS Techniques for Compact Low-pass Filter Design [75]. Inset feed and stub matching techniques are used to enhance the filter characteristics. The proposed filter is composed of double U-shaped DGS units at the ground plane and a shaped microstrip line on the top.

In the same year, Abdalla Abdulhadi published another paper "Combined Shaped Microstrip Line and DGS" [76] and its structure shown in Figure 2.12. The DGS is composed of two equilateral U-shaped DGS and one inverted U-shaped DGS unit, which provide higher attenuation for the high frequency harmonics. The shaped microstrip line consists of two sections of microstrip line of different widths and three parallel double stub sections of different widths, which provide impedance matching control for the input and output ports in order to obtain higher attenuation in the stop-band.

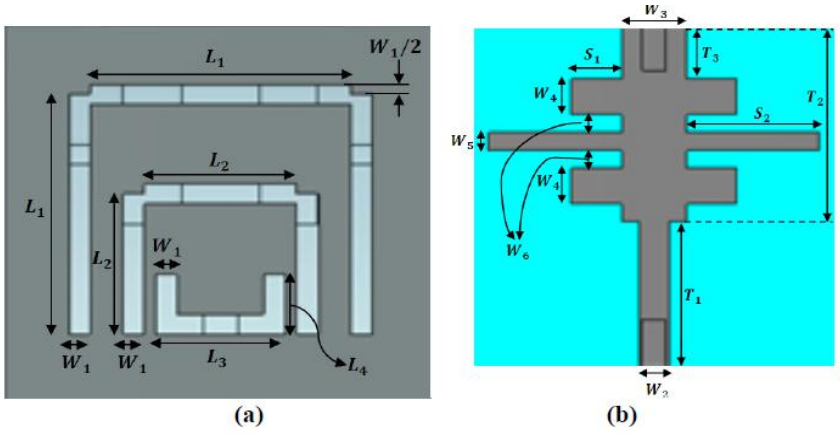

Fig 2.12. Description of the (a) DGS unit and (b) the transmission line dimensions in [76].

Because of the similarity between substrate integrated waveguide (SIW) structures and classical rectangular waveguides, most planar (H-plane) waveguide components are implemented in SIW technology. This solution usually permits a substantial reduction in size and in weight of components compared to classical waveguides. Moreover, losses of SIW components are lower than the corresponding microstrip devices and there are no radiation and packaging problems. SIW components are a good compromise between air-filled rectangular waveguides and microstrip lines.

In recent years, SIW technology was vastly explored to overcome the problems. Ke Wu introduced the substrate integrated circuit in 2003, which is the new concept for high-frequency electronics and optoelectronics [80]. In addition to SIW, Substrate Integrated Slab Waveguide (SISW) and Substrate Integrated Non Radiating Dielectric (SINRD) guide circuits are also included in this concept. The SIW structure is based on planar dielectric substrates with top and bottom layers perforated with arrays of metalized via holes. SIW provides low-cost waveguide filters by using standard printed circuit board (PCB) processes [80]-[82]. In terms of size, SIW is more compact and easy to integrate with other microwave and millimetre-wave circuits in the same substrate compared to conventional waveguides. Figure 2.2 shows the structure of an SIW, which consists of the top and bottom metal planes of a substrate and two parallel arrays of via holes, also known as via fence, in the substrate.

There are several designs of SIW band-pass filter for X-band applications is being introduced by researchers in the past years based on a different method. In 2005, Y. L. Zhang developed the compact band-pass filter with SIW triangular cavities [83]. The design filter was based on the coupling matrix synthesis method with a centre frequency

of 2.4 GHz. In 2010, Shahvirdi used the contour integral method to design a four pole Chebyshev X-band dual inductive post SIW filter based upon the discretization of the boundary of some structure [84]. It needs less memory than the full wave method. To decrease the computation time, circular vias were replaced by square ones. The centres of these square vias are the same as for the circulars.

In 2011, X.Zou suggests ~~the~~ transforming a band-pass filter to the equivalent conventional rectangular wave guide band-pass filter [85]. The designed waveguide filter has a sharp skirt characteristic. The symmetrical window SIW filter is designed with a 3 dB bandwidth of 5% from 9.77-10.27 GHz. The insertion loss is about 1.4 dB and return loss is more than 20dB.

2.6 References

[1] Hontsu Shigeki, Iguchi K, Agemura K, et al. Mechanical tuning of Superconducting lumped element filter. IEEE Transactions on Applied Superconductivity. Vol. 15, no. 2 (1). pp: 972-975. 2005.

[2] Brzezina G, Roy L, MacEachern L. Design Enhancement of Miniature Lumped-Element LTCC Bandpass Filters. IEEE Transactions on Microwave Theory and Techniques. Vol. 57, no. 4 (1). pp: 815- 823. 2009.

[3] Brzezina G, Roy L. Miniaturized. Lumped-Element Filters for Customized System-on-Package L-Band Receivers. IEEE Transactions on Components Packaging and Manufacturing Technology. Vol. 4. no.1. pp: 26-36.

[4] Shilong Qian, Jiasheng Hong. Miniature Quasi-Lumped-Element Wideband band-

pass Filter at 0.5-2 GHz Band Using Multilayer Liquid Crystal Polymer Technology, IEEE Transactions on Microwave Theory Technology.Vol. 60, no. 9, pp: 2799-2807.

[5] Yo-Shen Lin and Chien-Chun Cheng. Miniature CPW Parallel-Coupled band-pass Filter Based on Inductive Loaded Coupled-Lines and Lumped-Element J-Inverters. IEEE Microwave and Wireless Components Letters. Vol. 17, no. 5. pp: 343-345. 2007.

[6] Makimoto Mitsuo and Sadahiko Yamashita. Band-pass Filters Using Parallel Coupled Stripline Stepped Impedance Resonators. IEEE Transactions on Microwave Theory and Techniques. Vol. 28, no. 12. pp: 1413-1417. 1980.

[7]Sagawa M, Makimoto Mitsuo, Sadahiko Yamashita. Geometrical structures and fundamental characteristics of microwave stepped-impedance resonators. IEEE Transactions on Microwave Theory and Techniques. Vol. 45. pp: 1078-1085. 1997.

[8] C. L. Hsu, F. C. Hsu, and J. T. Kuo. Microstrip band-pass filters for ultra-wideband (UWB) wireless communications. IEEE MTT-S International Microwave Symposium Digest . pp: 679-682. Jun. 2005.

[9] L. Zhu, S. Sun, and W. Menzel. Ultra-wideband (UWB) band-pass filter using multiple-mode resonator. IEEE Microwave Wireless Component Letter. Vol. 15, no. 11, pp: 796-798, Nov. 2005.

[10] M. Z. Ji and Q. X. Chu. Compact UWB bandpass filter using pseudo-interdigital stepped impedance resonators," in Proceeding China Micro. Millimetre-Wave Conference, Ningbo, China. pp: 1096-1098. 2007.

[11] Qing-Xin Chu, Xu-Kun Tian. Design of UWB Bandpass Filter Using Stepped-

Impedance Stub-Loaded Resonator. IEEE Microwave and Wireless Components Letters, Vol. 20, no. 9, pp: 501-503. 2010.

[12] Xiaoyan Zhang, Wu. B. Compact UWB band-pass filter with dual notched bands using cascaded shorted-stub loaded SIRS. 2013 IEEE 5th International Symposium on Microwave, Antenna, Propagation and EMC Technologies for Wireless Communications (MAPE), pp: 198-201. 2013.

[13] Matthaei G. L. Narrow-band, fixed-tuned, and tuneable band-pass filters with zig-zag hairpin-comb resonators. IEEE Transactions on Microwave Theory and Techniques, Vol. 51, no. 4 (1). pp: 1214-1219. 2003.

[14] Vargas J. M. , Noel J, Brzhezinskaya M, et al. Design and Fabrication of Two Switch Superconducting Microstrip Hairpin Filters Using Series MEMS Switches. IEEE Transactions on Applied Superconductivity. Vol. 17, no. 2 (1), pp: 898-901. 2007.

[15] Jiwen Zhu, Zhenghe Feng. Microstrip Interdigital Hairpin Resonator with an Optimal Physical Length. IEEE Microwave and Wireless Components Letters. Vol. 16, no. 12. pp: 672-674. 2006.

[16] Yingjie Di, Gardner. P, Hall. P. S, et al. Multiple-coupled microstrip hairpin-resonator filter. IEEE Microwave and Wireless Components Letters, Vol. 13, no. 12. pp: 532-534. 2003.

[17] Alimenti F, Mariotti. C, Mezzanotte. P, et al. A 1.2 V, 0.9 mW UHF VCO Based on Hairpin Resonator in Paper Substrate and Cu. IEEE Microwave and Wireless Components Letters, Vol. 23, no. 4. pp: 214-216. 2013.

[18] Hong J. S., Lancaster M. J. Development of new microstrip pseudo-interdigital bandpass filters. IEEE Microwave and Guided Wave Letters, Vol. 5, no. 8. pp: 261-263. 1995.

[19] Yani Mu, Zhewang Ma, Deming Xu. A novel compact interdigital band-pass filter using multilayer cross-coupled folded quarter-wavelength resonators. IEEE Microwave and Wireless Components Letters, Vol. 15, no. 12. pp: 847-849. 2005.

[20] Gangqiang Wang, Van. M, Barlow. F, et al. An interdigital band-pass filter embedded in LTCC for 5- GHz wireless LAN applications. IEEE Microwave and Wireless Components Letters, Vol. 15, no. 5. pp: 357-359. 2005.

[21] Wong, S. W, Chen, Z. N, Chu, Q. -X. Microstrip-line millimetre-wave band-pass filter using interdigital coupled-line. Electronics Letters. Vol. 48, no. 4, 2012 pp: 224-225.

[22] Young-Ho Cho, Xu-Guang Wang, Sang-Won Yun. Design of Dual-Band Interdigital Bandpass Filters Using Both Series and Shunt Resonators. IEEE Microwave and Wireless Components Letters, Vol. 22, no. 3, 2012, pp: 111-113.

[23] Wenzel, R. J. Synthesis of Combline and Capacitively Loaded Interdigital band-pass Filters of Arbitrary Bandwidth. IEEE Transactions on Microwave Theory and Techniques. Vol. 19, no. 8. pp: 678-686. 1971.

[24] Weller T. M , Katehi L. P. Miniature stub and filter designs using the microshield transmission line. IEEE MTT-S International Microwave Symposium Digest. Vol. 2. pp: 675- 678. 1995.

[25] M. Duran-Sindreu, J. Bonache and F. Martin. Compact Elliptic-Function Coplanar

Waveguide Low-Pass Filters Using Backside Metallic Patterns. IEEE Microwave and Wireless Components Letters. Vol. 20, no. 11, pp: 601-603. 2010.

[26] Chan K. T, Chen, C. Y, Chin Albert. et al. 40- GHz Coplanar Waveguide band-pass Filters on Silicon Substrate. IEEE Microwave and Wireless Components Letters. Vol. 1, no. 11. pp: 429-431. 2002.

[27] K. T. Chan, Albert Chin, Ming-Fu Li, Dim-Lee Kwong, Sean P. McAlister, D. S. Duh, W. J. Lin, and C. Y. Chang, High-Performance Microwave Coplanar band-pass and band-stop Filters on Si Substrates, IEEE Transaction on Microwave Theory and Techniques. Vol. 51, no. 9, pp: 2036-2040, Sept. 2003.

[28] J. -T. Kuo and E. Shih, Wideband band-pass filter design with three-line microstrip structures, 2001 IEEE MTT-S International Microwave Symposium Digest. Vol. 3, pp: 1593-1596. 2011.

[29] Shry-Sann Liao, Pou-Tou Sun, Hsien-Ku Chen, et al. Compact-Size Coplanar Waveguide band-pass Filter. IEEE Microwave and Wireless Components Letters. Vol. 13, no. 6, 2003.

[30] Ian Hunter. Theory and Design of Microwave Filters. The Institution of Electrical Engineers, 2001.

[31] M. J. Hill, R. W. Ziolkowski, J. Papapolymerou. A High-Q Reconfigurable Planar EBG Cavity Resonator. IEEE Microwave and Wireless Components Letters. Vol. 11, no. 6, 2001.

[32] Zhang Q. F, Lu Y. L. Design of waveguide band-pass filter based on nonresonating 'T' junctions. Electronics Letters. Vol. 46, no. 16 pp: 1107-1108.

2010.

[33] Mohammad Memarian and R. R. Mansour. Dual-Band Half-Cut Dielectric Resonator Filters. Procedings of the 39th European Microwave Conference. pp: 555-558. 2009.

[34] S. B. Cohn. Direct-coupled-resonator filters. Proceedings of IRE. Vol. 45, no. 2, pp: 187-196, Feb. 1957.

[35] Matthaei George L, Jones E. L and Young Leo (1980). Microwave filters, impedance-matching networks, and coupling structures. Dedham, Mass: Artech House Books. ISBN 0-89006-099-1.

[36] R. J. Cameron, C. M. Kudsia, and R. R. Mansour, Microwave Filters for Communication Systems: Fundamentals, Design and Applications. Hoboken, NJ: Wiley, 2007.

[37] Rong Yu, Zaki K. A, Hageman M,et al. Low-temperature cofired ceramic (LTCC) ridge waveguide band-pass chip filters. IEEE Transactions on Microwave Theory and Techniques. Vol. 47, no. 12. pp: 2317-2324. 1999.

[38] Lap Kun Yeung, Ke-Li Wu. A compact second-order LTCC band-pass filter with two finite transmission zeros. IEEE Transactions on Microwave Theory and Techniques. Vol. 51, no. 2 (1). pp: 337-341.

[39] Kengyi Huang, Tsenchieh Chiu. LTCC Wideband Filter Design with Selectivity Enhancement. IEEE Microwave and Wireless Components Letters. Vol. 19,no. 7. pp: 452-454.

[40] Zhou C. X, Guo Y. X, Yan S. L, Wang Z. L. Dual-band UWB filter with LTCC technology. Electronics Letters. Vol. 47, no. 22. pp: 1230-1232.

[41] Pursula P, Karttaavi, Kantanen, M, et al. 60- GHz Millimeter-Wave Identification Reader on 90-nm CMOS and LTCC. IEEE Transactions on Microwave Theory and Techniques. Vol. 59, no. 4 (2). pp: 1166-1173. 2011.

[42] Yang T. , Tamura M. , Itoh T. Compact and high-performance low-temperature co-fired ceramic balun filter using the hybrid resonator and symmetric four-port network. IET Microwaves, Antennas & Propagation. Vol. 6, no. 2. pp: 121-126. 2012.

[43] Bing Bai, Yintang Yang, Yuejin Li. Design of band-pass filter on different materials in LTCC/LTCF technology. 11th International Conference on Electronic Packaging Technology & High Density Packaging (ICEPT-HDP), pp: 771-773. 2010.

[44] Li Yuejin, Xing Mengjiang, Yang Yintang. Design of band-pass filter based on different materials in LTCC/LTCF technology 12th International Conference on Electronic Packaging Technology and High Density Packaging, pp:1-3. 2011.

[45] ZhangCheng Hao, JiaSheng Hong. Ultra-Wideband band-pass Filter Using Multilayer Liquid-Crystal-Polymer Technology. IEEE Transactions on Microwave Theory and Techniques, Vol. 56, no. 9. pp: 2095-2100, 2008.

[46] Hao Z. C, Hong J. S. Dual-band UWB filter using multilayer liquid crystal polymer technology. Electronics Letters. Vol. 46, no. 3. pp: 265-266. 2010.

[47] Zhang-Cheng Hao, Jia-Sheng Hong. Quasi-Elliptic UWB band-pass Filter Using Multilayer Liquid Crystal Polymer Technology. IEEE Microwave and Wireless Components Letters. Vol. 20, no. 4. pp: 202-204. 2010.

[48] Hsuan-Ling Kao,Cheng-Lin Cho,Li-Chun Chang. Inkjet-Printed Interdigital Coupled Line Filter on Liquid Crystal Polymer Substrate. IEEE Electron Device Letters, Vol. 34, no, 12. pp: 1584-1586. 2013.

[49] Abbaspour-Tamijani, Abbas Dussopt L and Rebeiz, G. M. Miniature and tunable filters using MEMS capacitors. IEEE Transactions on Microwave Theory and Techniques. Vol. 51,no. 7 pp: 1878-1885. 2003.

[50] Entesari K,Obeidat K. , Brown A. R. , et al. A 25-75- MHz RF MEMS Tunable Filter. IEEE Transactions on Microwave Theory and Techniques. Vol. 55, no. 11. pp: 2399-2405. 2007.

[51] Shalaby M. M, Abdelmoneum M. A and Saitou K. Design of Spring Coupling for High-Q High-Frequency MEMS Filters for Wireless Applications. IEEE Transactions on Industrial Electronics, Vol. 56, no. 4. pp: 1022-1030. 2009.

[52] Giner J, Uranga A, Torres F, et al. Fully CMOS integrated band-pass filter based on mechanical coupling of two RF MEMS resonators. Electronics Letters. Vol. 46. no. 9. pp: 640-641. 2010.

[53] Reines I, Park S. -J, Rebeiz G. M. Compact Low-Loss Tuneable -Band band-stop Filter With Miniature RF-MEMS Switches. IEEE Transactions on Microwave Theory and Techniques. Vol. 58, no7 (1). pp: 1887-1895. 2010.

[54] Sekar V, Armendariz M, Entesari K. A 1.2-1.6 GHz Substrate-Integrated-

Waveguide RF MEMS Tunable Filter. IEEE Transactions on Microwave Theory and Techniques. Vol. 59, no. 4 (1). pp: 866-876. 2011.

[55] Omran H, Sabry Y. M, Sadek M, et al. Deeply-Etched Optical MEMS Tunable Filter for Swept Laser Source Applications.

IEEE Photonics Technology Letters. Vol. 26, no. 1. pp: 37-39. 2014.

[56] Tarot A. C, S. Collardey and K. Mahdjoubi. Numerical studies of metallic pbg structures. Progress in Electromagnetics Research, PIER 41, pp: 133-157, 2003.

[56] Guida G, A. de Lustrac, and A. Priou. An introduction to photonic band gap (PBG) materials, Progress in Electromagnetics Research, PIER 41, pp: 1-20, 2003.

[57] Zheng L. G and W. X. Zhang, Analysis of bi-anisotropic pbg structure using plane wave expansion method, Progress Electromagnetics in Research, PIER 42, pp: 233-246, 2003.

[58] Zheng L. G. and W. X. Zhang, Study on bandwidth of 2-d dielectric PBG material, Progress In Electromagnetics Research, PIER 41, pp: 83-106, 2003.

[59] Yuan H. W. , S. -X. Gong, X. Wang et al. Scattering analysis of a printed dipole antenna using PBG Structures. Progress in Electromagnetics Research B. Vol. 1, pp: 189-195, 2008.

[60] Daeyoung O. and P. Ikmo, Two-arm microstrip spiral antenna with a circular aperture on the ground plane for generating a circularly polarized conical beam. IEEE Antennas Propagation Society International Symposium. Vol. 3, pp: 866-869, 2003.

[61] Velazquez-Ahumada M. C, J. Martel, and F. Medina. Parallel coupled microstrip

filters with ground-plane aperture for spurious band suppression and enhance coupling. IEEE Transaction on Microwave Theory Tech. Vol. 52, pp: 1082-1086, 2004.

[62] Sharma R. , T. Chakravarty, S. Bhooshan, et al. , Characteristic impedance of a microstrip-like interconnect line in presence of ground plane aperture, International Journal of Microwave Science and Technology. Vol. 1, pp: 1-5, 2007.

[63] Lim J. -S. , C. -S. Kim, Y. -T. Lee, et al. A spiral-shaped defected ground structure for coplanar waveguide. IEEE Microwave Component Letter. Vol. 12, no. 9, pp: 330-332, 2002.

[64] J. Yun, P. Shin. Design Applications of Defected Ground Structures, Ansoft Corporation, 2003 Global Seminars. Available at www. ansoft. com.

[65] Boutejdar A., G. Nadim, S. Amari, et al. Control of band-stop response of cascaded microstrip low-pass band-stop filters using arrowhead slots in backside metallic ground plane. IEEE Antennas Propagation Society International Symposium. Vol. 1B, pp: 57-577, 2005.

[66] Chen H. -J, T. -H. Huang, C. -S. Chang, et al, A novel cross shape DGS applied to design ultra-wide stop-band low-pass filters. IEEE Microwave Component Letter. Vol. 16, no. 5, pp: 252-254, 2006.

[67] J. L. Li, J. X. Chen, Q. Xue, et al. , Compact microstrip low-pass filter based on defected ground structure and compensated microstrip line, IEEE MTT-S International Microwave Symposium Digest, pp: 1483-1486, 2005.

[68] J. X. Chen, J. L. Li, K. C. Wan, et al. , Compact quasi-elliptic function filter based

on defected ground structure, IEE Proceeding Microwaves Antenna Propagation. Vol. 153, no. 4, pp: 320-324, 2006.

[69] L. H. Weng, Y. C. Guo, X. W. Shi, et al. , An overview on defected ground structure, Progress in Electromagnetics Research B. Vol. 7, pp:173-189, 2008.

[70] C. J. Hwang, L. B. Lok, I. G. Thayne, et al. A wide-bandpass filter with defected ground structure for wide out-of-band suppression. 2009 Asia Pacific Microwave Conference, Singapore. pp: 2018-2021. 2009.

[71] J. P. Thakur and P. Jun-Seok. A new design approach for circular polarize antenna with DGS under the unbalanced feed-lines. 36th European Microwave Conference. pp: 1483-1485, 2006.

[72] Colin-Beltran E, Corona-Chavez. A, Itoh. T, et al. Circular Aperture Slot Antenna with Common-Mode Rejection Filter Based on Defected Ground Structures for Broad Band. IEEE Transactions on Antennas and Propagation. Vol. 61, no. 5, pp: 320-324, 2006.

[73] J. -J. Koo, S. -M. Oh, M. -S. Hwang, et al. A new DGS unequal power divider. European Microwave Conference, pp: 556-559, 2007.

[74] Yuchun Guo, Qing Wang. An Improved Parameters Extraction Method for Dumbbell- Shaped Defected Ground Structure. Engineering Scientific Research. Vol. 2 no. 3, March 2010.

[75] Abdalla Abdulhadi, Alsanousi Abdulhadi, Antumani Ashoka, et al. Combined Shaped Microstrip Line and DGS Techniques for Compact Low-pass Filter Design. International Journal of Engineering &Technology IJET-IJENS. Vol. 13, no. 03.

2013.

[76] Abdalla Abdulhadi, Alsanousi Abdulhadi, Antumani Ashoka, et al. A Compact Microstrip Low-pass Filter Based on DGS with Shaped Microstrip Line. International Journal of Engineering and Technology. Vol. 3, no. 6, June, 2013.

[77] Yujian Cheng, Wei Hong, Ke Wu. Half Mode Substrate Integrated Waveguide (HMSIW) Directional Filter. IEEE Microwave and Wireless Components Letters, Vol. 1, no. 7. pp: 504-506.

[78] Magri V. P. R, Lima R. A. A, Mosso M. M. et al. Substrate Integrated Wave Guide filter at 10 GHz using commercial FR-4 lossy substrate. 2009 SBMO/IEEE MTT-S International Microwave and Optoelectronics Conference (IMOC), pp: 595-599. 2009.

[79] Senior D. E, Xiaoyu Cheng, Machado. M. et al. Single and dual band bandpass filters using complementary split ring resonator loaded half mode substrate integrated waveguide. 2010 IEEE Antennas and Propagation Society International Symposium (APSURSI), pp: 1-4. 2010.

[80] K. Wu, D. Deslandes and Y. Cassivi. The Substrate Integrated Circuits-A New Concept for High-Frequency Electronics and Optoelectronics. 6th International Conference on Telecommunications in Modern Satellite, Cable and Broadcasting Service. Vol. 1, pp: III-X, 2003.

[81] D. Deslandes and K. Wu. Single-Substrate Integration Techniques for Planar Circuits and Waveguide Filters. IEEE Transaction on Microwave Theory and Techniques. Vol. 51, pp: 593-596, Feb, 2003.

[82] D. Deslandes and K. Wu. Integrated Microstrip and Rectangular Waveguide in Planar Form. IEEE Microwave and Wireless Components Letters. Vol. 14, pp: 446-448, Sep. 2004.

[83] Y. L. Zhang, W. Hong, K. Wu, J. X. Chen, et al. Development of Compact band-pass Filters with SIW Triangular Cavities. 2005 Asia-Pacific Microwave Conference Proceedings. pp: 4. 2005.

[84] T. Shahvirdi and A. Banai. Applying Contour Integral Method for Analysis of Substrate Integrated Waveguide Filters. 2010 10th Mediterranean Microwave Symposium, Guzelyurt. pp: 418-421. 2010.

[85] X. Zou, C. M. Tong, and D. W. Yu. Design of an X-Band Symmetrical Window band-pass Filter Based On Substrate Integrated Waveguide. Cross Strait Quad-Regional Radio Science and Wireless Technology Conference, Harbin. pp: 571-574. 2011.

Chapter 3

The Basic Theory of Filters

3.1 Introduction

The rapid development of wireless communication systems has greatly promoted the development of filters. In order to achieve modern communication system development, filter design and realization methods have undergone tremendous changes, and new technologies have been proposed.

In this chapter, a brief introduction to filter design theory including the classification of the four basic types of filter according to their attenuation characteristics, design parameters of filters, three classical types of filter, four common filter frequency conversion mechanisms, and other related knowledge, is presented.

According to the attenuation characteristics of different filters, filters can be divided into four basic types: low pass filters (LPF), high pass filters (HPF), band-pass filters (BPF) and band-stop filters (BSF). The relationship between the attenuation coefficient and the normalized angular frequency is shown in Figure 3.1. Here we take parameter $\Omega = \omega/\omega_c$ as the normalized frequency of angular frequency ω_c. For the low-pass and

high-pass filter, ω_c is the cut-off frequency of the filter, for the band-pass and band-stop filter ω_c is the centre frequency of the filter.

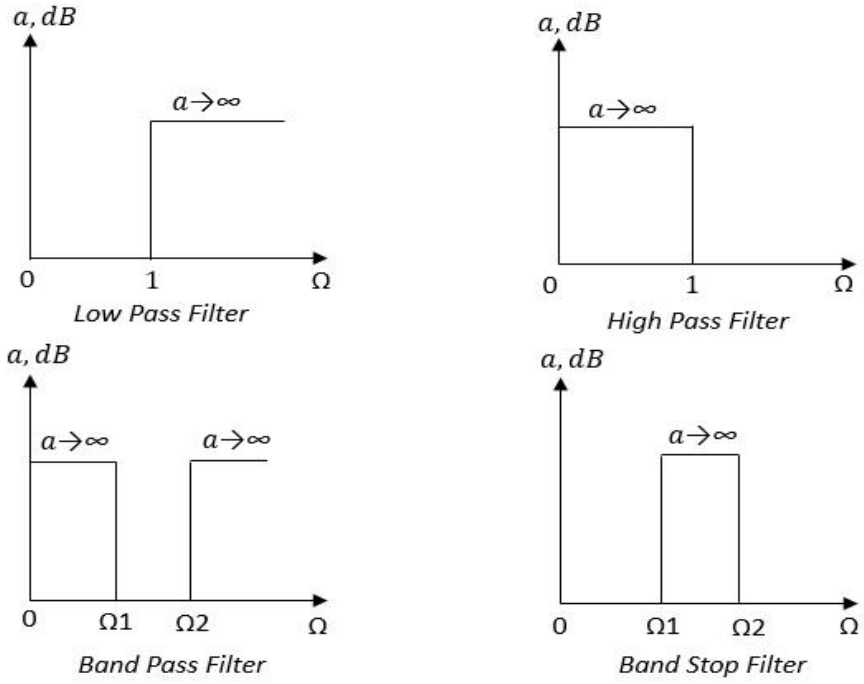

Figure 3.1. The relationship between the attenuation coefficient and the normalized angular frequency in four types of filters.

When we are comprehensively analysing filters, the design parameters below need to be considered [1]:

(a). The centre frequency: the working frequency of the filter.

(b). Insertion loss: in ideal situations, the filter has no power loss in its pass-band. But in the practical engineering application, we cannot eliminate the filter power loss, due to conductor loss, dielectric loss and radiation loss. Insertion loss L_A quantitatively describes the difference between the response amplitude and the 0 dB benchmark[1]:

$$L_A=10\log(P_{in}/P_L) = -10\log(1-|\Gamma_{in}|^2) \quad (3.1)$$

where P_L is the filter load output power, P_{in} is the input power from the signal source. Γ_{in} is the reflection coefficient observed from the signal source to the filter.

(c) Ripple coefficient: reflecting the flatness in bandwidth.

(d) Bandwidth: for the band-pass filter, bandwidth is defined as the difference in frequency between 3 dB attenuation of upper-side frequency f_{U3dB} and 3 dB attenuation of lower-side frequency f_{L3dB}:

$$BW_{3dB} = f_{U3dB} - f_{L3dB} \tag{3.2}$$

(e) Rectangular coefficient: Rectangular coefficient is defined as the ratio of 60 dB bandwidth to 3 dB bandwidth. It describes the steepness degree of the filter frequency response curve nearby the cut-off frequency.

$$SF = BW_{60dB}/BW_{3dB} = (f_{U60dB} - f_{L60dB})/(f_{U3dB} - f_{L3dB}) \tag{3.3}$$

(f) The stop-band rejection: in an ideal situation, a filter has infinite attenuation within the stop-band but in real situations the filter can only offer finite attenuation which is associated with the filter element number. Thus, in actual situations, engineers usually adopt 60 dB as the stop-band rejection design value.

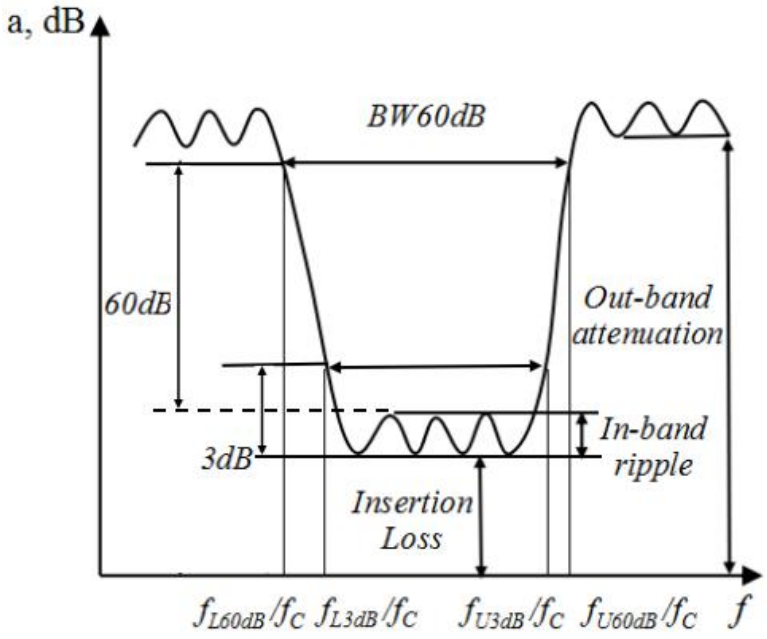

Figure 3.2. The filter design parameters

The above mentioned parameters can be illustrated by the typical band-pass attenuation curve, which is shown in Figure 3.2.

In addition, the quality factor Q can describe the filter frequency selectivity, usually defined as the ratio of average energy storage to average energy consumption in one period.

$$Q = \omega \frac{\text{average energy storage}}{\text{average energy storage in one period}} = \omega \frac{\text{average energy storage}}{\text{power loss}}\Bigg|_{\omega=\omega_c}$$
$$= \omega \frac{W_{stored}}{P_{loss}}\Bigg|_{\omega=\omega_c} \tag{3.4}$$

where P_{loss} is the energy consumption in unit time.

3.2 Three Types of Basic Filter

3.2.1 Maximally flat filter (Butterworth filter)

Since there is no ripple in the attenuation curve of this kind of filter, it is called maximally flat. For the low-pass filter, the insertion loss can be determined by the formula [1]:

$$L_A(\Omega) = -10 \log (1 - |\Gamma_{in}|^2) = 10 \log \{1 + a^2 \Omega^{2N}\} \tag{3.5}$$

where Ω is the normalized frequency, N is the number of stages of the filter. The frequency response curve can be shown in Figure 3.3. When Ω=0, L_A (Ω) =0, when Ω increases, L_A (Ω) increases monotonically. When Ω<1, L_A (Ω) increases slowly, L_A (Ω) increases fast when Ω >1. a is determined by maximum attenuation L_A (Ω=1), and:

$$a = \sqrt{10^{L_{Ar}/10} - 1} \tag{3.6}$$

where N is determined by out-of-band minimum attenuation L_A ($\Omega=\Omega_S$), that is $L_A(\Omega)$ $=10 \log \{1+a^2\Omega_s^{2N}\}$, and:

$$N > [\log(\frac{10^{L_{Ar}/10}-1}{a^2})/2\log\Omega_s] \tag{3.7}$$

In (3.7), [ ] means integer values from $\log(\frac{10^{L_{Ar}/10}-1}{a^2})/2\log\Omega_s$.

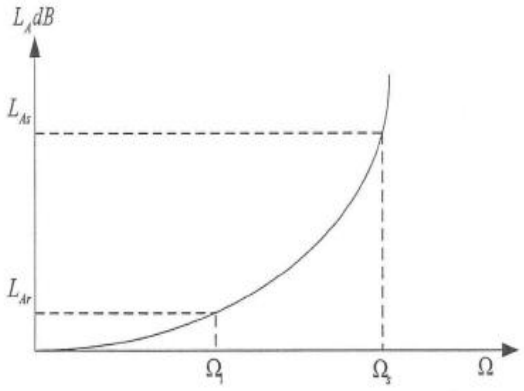

Figure 3.3. Frequency response the maximally flat low-pass prototype filter

Generally, normalized low-pass filters can be illustrated by Figure 3.4, where R_G=1, and all the values of g_i (i=0, 1, 2. . . N+1) can be found in reference [2].

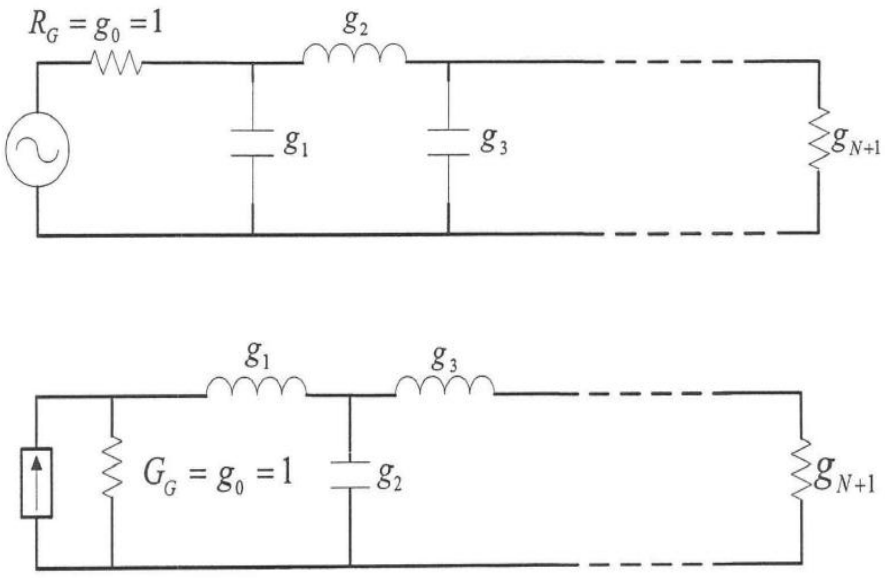

Figure 3.4. The equivalent circuits of two type multi-stage low-pass filters with normalized components.

3.2.2 Chebyshev Filter

In a Chebyshev filter, the insertion loss characteristic function is described by Chebyshev polynomials can be written as follows[2]:

$$L_A(\Omega) = \log\{LF\} = 10\log\{1+a^2T^2_N(\Omega)\} \tag{3.8}$$

The frequency response curve can be shown in Figure 3.5, $T_N(\Omega)$ is the first class of Chebyshev polynomial, that is:

$$\begin{cases} T_N(\Omega) = \cos\{N[\cos^{-1}(\Omega)]\} & (\Omega \le 1) \\ T_N(\Omega) = \cosh\{N[\cosh^{-1}(\Omega)]\} & (\Omega \ge 1) \end{cases} \tag{3.9}$$

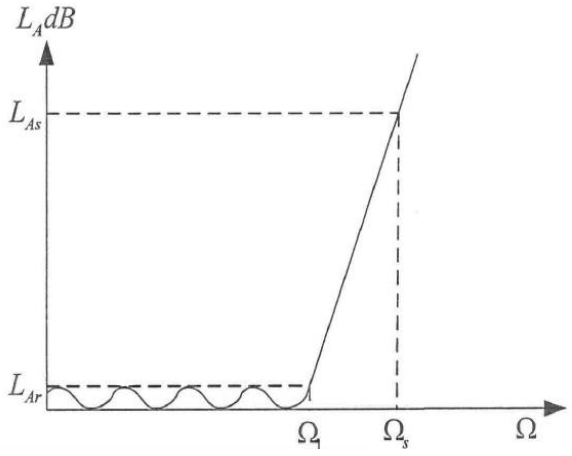

Figure 3.5. Frequency response of the Chebyshev low-pass prototype filter

In the frequency range -1<Ω<1, the minimum attenuation caused by the filter is 0 dB and the maximum one is $L_{Ar}=10\log(1+a^2)$, which is also the peak value of all the ripples in the band of the filter. Assume the peak value of the ripple is PLR_{db}, and $a=\sqrt{10^{RPL_{dB}/10}-1}$. When Ω>1, $T_N(\Omega)$ is hyperbolic cosine function, hence the attenuation would increase monotonically with the increase of Ω. Assume at the stop-band frequency Ω_s, stop-band attenuation is L_{AS}, there is:

$$L_A(\Omega) = 10 \log [1 + a^2 T_N^2(\Omega_s)] \tag{3.10}$$

The number of reactance components n is:

$$N \geq [\frac{ch^{-1}\sqrt{(10^{L_{Ar}} - 1)/a^2}}{ch^{-1}\Omega_s}] \tag{3.11}$$

Compared to the maximally flat filter, this filter has steeper pass-band stop-band step response. For the relatively high normalized frequency $\Omega >> 1$, $T_N(\Omega)$ can be approximated by $(2\Omega)^N/2$. This means that Chebyshev filter attenuation characteristic is $2^{2N}/4$ times better than that of the Butterworth filter. When the value of a and n are detailed, similar to Butterworth filter network analysis we can get the ladder circuit and nominalized values[2]:

$$\begin{cases} g_1 = 2a_1\gamma \\ g_k = 2a_{k-1}a_k/(b_{k-1}g_{k-1}) \qquad (k = 2,3\cdots n) \\ g_{n+1} = \begin{cases} 1 & (\text{n is odd number}) \\ th^2(\beta/4) & (\text{n is even number}) \end{cases} \end{cases} \tag{3.12}$$

$$\begin{cases} \beta = \ln\left(cth\dfrac{L_{Ar}}{17.37}\right) \\ g_k = sh(\beta/2n) \\ a_k = \sin\left(\dfrac{2k-1}{2n}\pi\right)(k = 1,2,\cdots n) \\ b_k = \gamma^2 + \sin^2\left(\dfrac{k}{n}\pi\right) \end{cases} \tag{3.13}$$

Where g_i(i=1 to N) is the inductance of series inductors or capacitance of shunt capacitors. β, a_k b_k are relarive parameters to calculate the parameter g_i.

3.2.3 Elliptic Filter

The middle parts of the pass-band and stop-band are flat in the frequency response of the Butterworth filter. In Chebyshev filters, the frequency response shows equal ripples in the pass-band while are maximally flat in the stop-band. Another kind of filter is the

elliptic filter. It is realized by elliptic functions and shows equal ripple in both pass-band and stop-band. Its response curve is shown in Figure 3.6, which shows that the attenuation poles are not located at infinite points, this means that we can get very high cut-off rate.

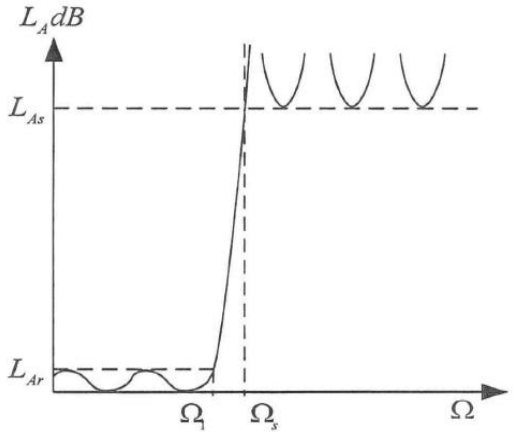

Figure 3.6. Frequency response the elliptic low-pass prototype filter

In Figure 3.6, L_{Ar} is the maximized attenuation in the pass-band, L_{As} is the minimum attenuation in stop-band and Ω_s is the border frequency of the stop-band.

The N stage elliptic function low-pass filter attenuation characteristic is[2]:

$$L_A(\Omega) = 10\lg[1+a^2 F_{2N}(\Omega)] \tag{3.14}$$

when N is an odd number, and :

$$F_N(\Omega) = \mathrm{sn}[NK_1 \mathrm{sn}^{-1}(\Omega, k)/K, k1] \tag{3.15}$$

when N is an even number:

$$F_N(\Omega) = \mathrm{sn}[K_1 + N K_1 \mathrm{sn}^{-1}(\Omega, k)/K, k1] \tag{3.16}$$

where

$$K_1 = K(k_1) \tag{3.17}$$

$$K=K(k) \tag{3.18}$$

Here K_1 and K are complete elliptic integral functions whose modulus is k_1 and k, respectively. $sn^{-1}(u,k)$ means the inversely elliptic function which is defined as: if $y=sn(u,k)$, then $u=sn^{-1}(y,k)$. Real parameters a, k_1 and k are all between 0 and 1, and they are decided by technical specifications. The relationship between parameter a, k_1 and k is shown below:

$$\frac{K_1^{'}}{K^{'}}=\frac{nK_1}{K^{'}} \tag{3.19}$$

where

$$\begin{cases} K_1^{'}=K\left(k_1^{'}\right) \\ K^{'}=K\left(k^{'}\right) \end{cases} \tag{3.20}$$

where

$$\begin{cases} k_1^{'}=\sqrt{1-k_1^2} \\ k^{'}=\sqrt{1-k^2} \end{cases} \tag{3.21}$$

where K_1'and K' are the complementary moduli of K_1 and K.

3.3 Frequency Transform from the Low-pass Prototype

Frequency conversion is bi-directional. A practical filter may be a low-pass, high-pass, band-pass or band-stop filter. By the means of frequency conversion, it can be transformed into a low-pass prototype. By the comprehensive designs, we can get normalized component values of low-pass filter, and then by the second time frequency conversion, we can get normalized component values of the practical filter. Because only the horizontal ordinate which describes the frequency value is transformed while

vertical ordinate which describes the attenuation value is not transformed, this transform is a frequency transform under the condition of equal attenuation.

3.3.1 Frequency transform between low-pass filter and low-pass prototype

Assume the frequency variable of practical and prototype low-pass filter is ω' and ω respectively, with attenuation characteristics as illustrated in Figure 3.7. Frequency transforming requires the points at frequencies ω=0, ω, ω_s, ∞ should correspond to the points at the frequencies ω' =0, 1, ω_s', ∞ and the attenuation remain equal. The frequency transform equation is:

$$\omega' = \omega / \omega_c \tag{3.22}$$

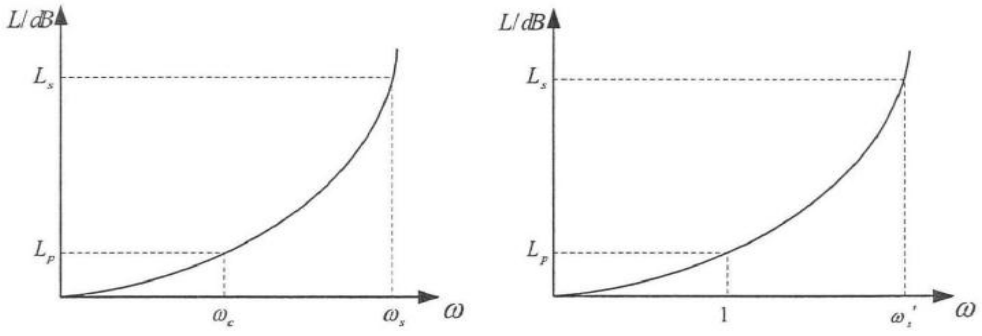

Figure 3.7. Practical/prototype low-pass filter frequency response curve

Using equal attenuation conditions and inversely normalized internal resistance R_g of signal source, the real values of the components are[1]:

$$\begin{cases} L_k = L_k' R_g = \dfrac{g_k}{\omega_c} R_g \\ C_i = \dfrac{C_i'}{R_g} = \dfrac{g_i}{\omega_c R_g} \end{cases} \tag{3.23}$$

Figure 3.8 shows an inductive input low-pass prototype filter and its corresponding practical low-pass filter. The above mentioned analyses can also be applied to the analyses of capacitive input circuits.

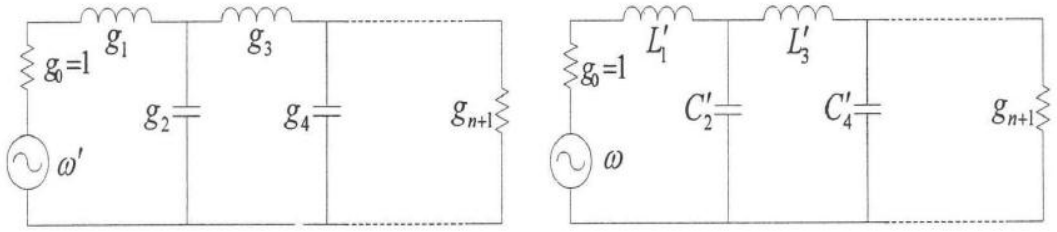

Figure 3.8. An inductive input low-pass prototype filter and its corresponding practical low-pass filter

3.3.2 Frequency transform between the high-pass filter and the low-pass prototype

Assume the frequency variable of practical high-pass filter and prototype low-pass filter is ω' and ω respectively, their attenuation characteristics are illustrated in Figure 3.9.Frequency transform requires the points at the frequency ω =0, ω_c, ω_s, ∞ should corresponds to the points at the frequency ω' =-∞,-1, -ω_s, 0 and the attenuations are equal. The frequency transform equation is:

$$\omega' = -\omega_c / \omega \tag{3.24}$$

Use equal attenuation conditions and inversely normalized internal resistance R_g of signal source, the real values of the components are:

$$\begin{cases} C_k = \dfrac{1}{\omega_c g_k R_g} \\ L_i = \dfrac{R_g}{\omega_c g_i} \end{cases} \tag{3.25}$$

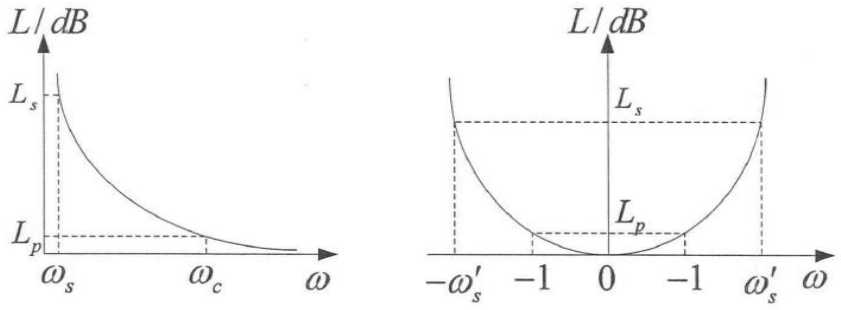

Figure 3.9. Practical/prototype high-pass filter frequency response curve

Figure 3.10 shows an inductive input high-pass prototype filter and its corresponding practical high-pass filter, the above mentioned analyses can also be applied into the analyses of capacitive input circuits.

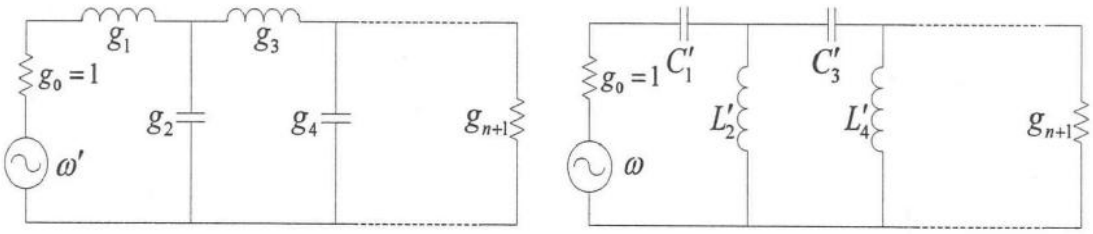

Figure 3.10. An inductive input low-pass prototype filter and its corresponding practical high-pass filter

3.3.3 Frequency transform between band-pass filter and low-pass prototype

Assume the frequency variable of practical band-pass filter and prototype low-pass filter is ω' and ω respectively, their attenuation characteristics are illustrated in Figure 3.11. The frequency transform equation is:

$$\omega' = \frac{\omega_0}{\omega_{c2} - \omega_{c1}} \left(\frac{\omega}{\omega_0} - \frac{\omega_0}{\omega} \right) = \frac{1}{W} \left(\frac{\omega}{\omega_0} - \frac{\omega_0}{\omega} \right) \tag{3.26}$$

In (3. 26), W is the relative bandwidth and is equal to $(\omega_{c2}- \omega_{c1})/2$, ω_0 is the central frequency and is equal to $\sqrt{\omega_{c1}\omega_{c2}}$.

For the series-connected branch:

$$L_k' = \frac{g_k}{W\omega_0}, \quad C_k' = \frac{W}{g_k\omega_0} \tag{3. 27}$$

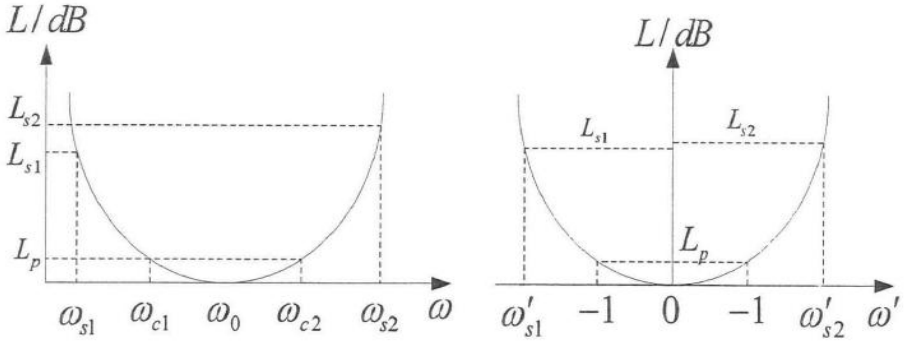

Figure 3.11. Practical/prototype band-pass filter frequency response curve

For the parallel-connected branch:

$$L_i' = \frac{W}{g_i\omega_0}, \quad C_i' = \frac{g_i}{W\omega_0} \tag{3.28}$$

The normalized circuit of the band-pass filter is shown in Figure 3.12.

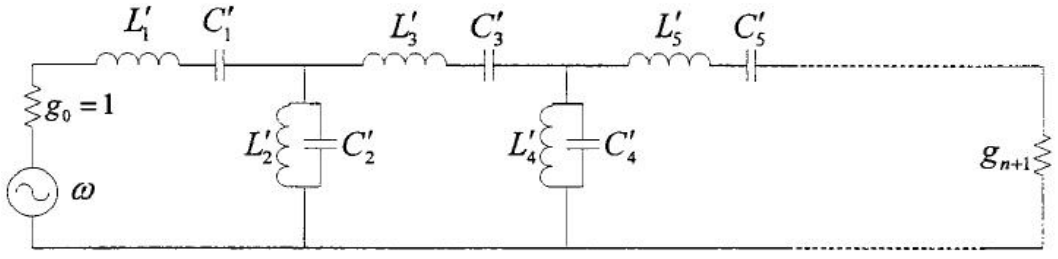

Figure 3.12. The normalized circuit of the band-pass filter

3.3.4 Frequency transform between band-stop filter and low-pass prototype

Assume the frequency variable of practical band-stop filter and prototype low-pass filter is ω' and ω respectively. The frequency transform equation is:

$$\omega' = \frac{1}{W}\left(\frac{\omega_0}{\omega} - \frac{\omega}{\omega_0}\right) \tag{3.29}$$

The ω' and ω attenuation characteristics are illustrated in Figure 3.13.

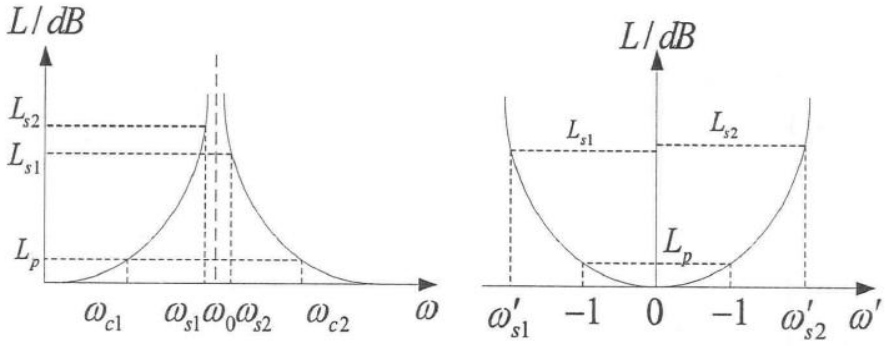

Figure 3.13. Practical/prototype high stop filter frequency response curve

In (3.29), W is the relative bandwidth and is equal to $(\omega_{s2}-\omega_{s1})/\omega_0$, ω_0 is the central frequency and is equal to $\sqrt{\omega_{c1}\omega_{c2}}$， for the series-connected branch:

$$L'_k = \frac{Wg_k}{\omega_0},\ C'_k = \frac{1}{Wg_k\omega_0} \tag{3.30}$$

For the parallel-connected branch:

$$L'_i = \frac{1}{Wg_i\omega_0},\ C'_i = \frac{Wg_i}{\omega_0} \tag{3.31}$$

The normalized circuit of the band-stop filter is shown in Figure 3.14.

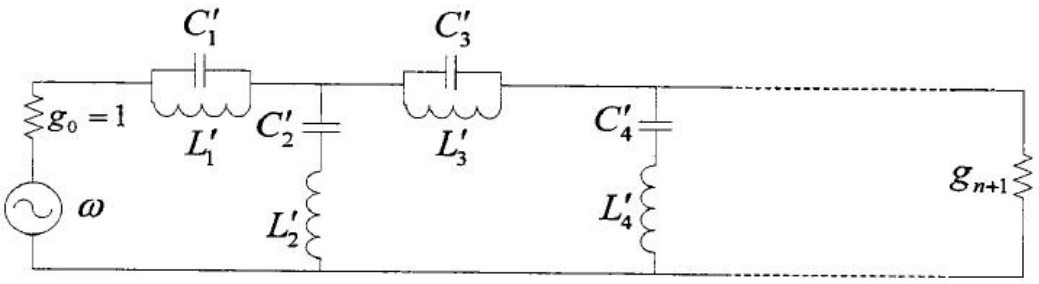

Figure 3.14. The normalized circuit of the band-stop filter

3.4 References

[1] Reinhold Ludwig, Pavel Bretchko. RF Circuit Design: Theory and Applications, Prentice-Hall, 2000.

[2] David M. Pozar. Microwave Engineering, 3rd Edition. Wiley India Pvt. Limited, 1 Sep 2009.

CHAPTER 4

A Comprehensive Study Of The Stepped Impedance Resonator (SIR) and the Asymmetric Stepped Impedance Resonator (ASIR)

4.1 The Basic Structure of the Stepped Impedance Resonator

In the field of microwave and radio frequency engineering, different resonators are utilized for different applications. Generally speaking, the stripeline or coaxial cable resonator is used as the resonator for quasi transverse electromagnetic wave or transverse electromagnetic wave.

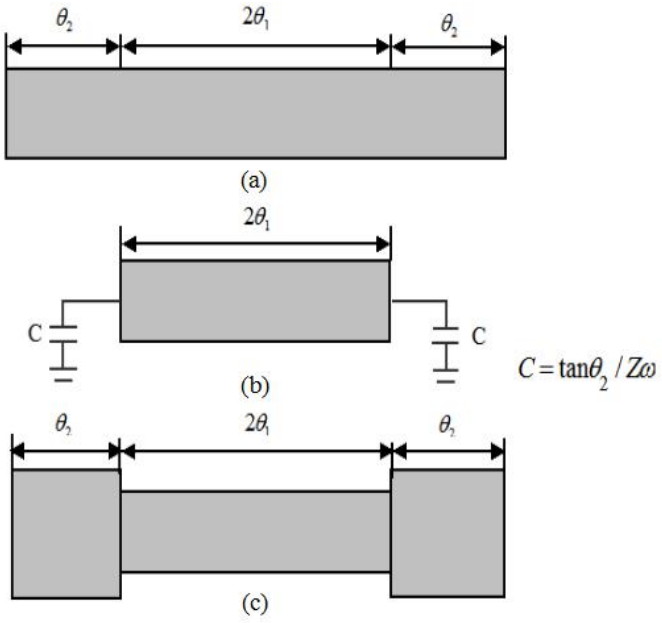

Figure 4.1. (a) UIR (b) Capacitor loaded UIR (c) SIR

Figure 4.1 (a) shows a half wave uniform impedance resonator (UIR), its substrate has the characteristic of low loss, high dielectric constant and high temperature stability.

The uniform impedance resonator (UIR) has the advantage of relatively easily calculated electrical properties and is widely used. But it has just one degree of freedom to adjust when designing. Besides, spurious frequencies appear at the frequencies which are multiples of the fundamental resonance frequency. To solve the above mentioned problems, engineers use lumped element capacitor to replace the transmission lines whose electrical lengths are θ_1 at both ends of the UIR and a capacitor loaded UIR is generated. By this means, spurious frequencies of the resonator are moved to further places and the dimension of the resonator is reduced. Therefore, capacitor loaded UIR has the advantage of smaller size and spurious frequency restriction.

In Figure 4.1 (b), the characteristic impedance of UIR is Z_1, electrical length is $2\theta_1$, half-wavelength resonator resonating frequency is, the loading capacitor is expressed as[1]:

$$C = Y_1 \tan \theta_2 / \omega_0 \tag{4.1}$$

where $Y_1=1/Z_1$, $\theta_2=\pi/4-\theta_1$.

As for the capacitor loaded UIR, circuit loss would increase considerably with the change of resonance frequency. Thus the frequency is needed to be adjusted in order to reduce loss. This disadvantage makes the capacitor loaded UIR hardly be used in frequencies higher than 1 GHz. To solve these problems, open circuit transmission line is used to replace the loading capacitor, which is shown in Figure 4.1(c).

Based on the above mentioned discussion, M. Makimoto and S. Yamashita proposed the

step impedance resonator (SIR) ,as shown in Figure 4.12.The step impedance resonator is composed of two or even more transmission lines with different characteristics and has the mode of quasi transverse electromagnetic wave or transverse electromagnetic wave. Until now, a tremendous amount of work related with step impedance resonators has been performed. The basic structure of SIR is shown in Figure 4.2.

The SIR shown in Figure 4.2 (a) contains open circuit end, short circuit end and the step impedance surface between them.

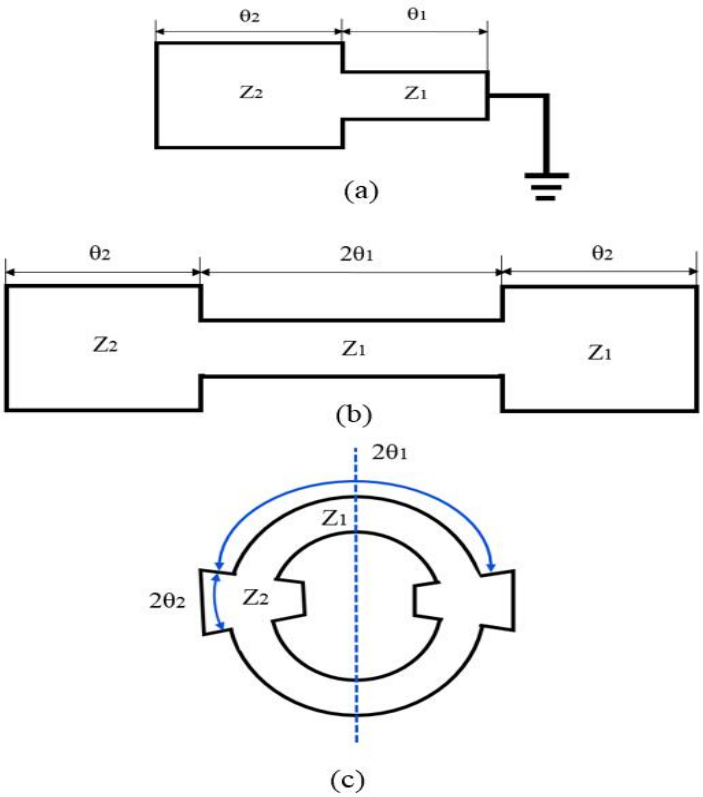

Figure 4.2. The basic structure of SIR: (a) $\lambda_g/4$ type SIR resonator.
(b) $\lambda_g/2$ type SIR resonator (c) λ_g type SIR resonator.

It is composed of two sections of transmission lines of different characteristic impedance Z_1, Z_2 and electrical length θ_1, θ_2. We define two basic parameters for simplicity:

$$K=Z_2/Z_1 \tag{4.2}$$

$$\alpha= \theta_2/(\theta_1+\theta_2) \tag{4.3}$$

where K is defined as the impedance ratio, α is defined as the electrical length ratio.

4.2 The characteristics of SIR

4.2.1 The resonance requirements of SIR

When the transmission line characteristic impedance is Z_0 with electrical length ~~is~~ θ_0, its load characteristic impedance is Z_L. According to the distributed parameter impedance theory of loss less uniform transmission line, the input impedance at the input end of the uniform transmission line is:

$$Z_{in} = Z_0 \frac{Z_L + jZ_0 \tan\theta_0}{Z_0 + jZ_L \tan\theta_0} \tag{4.4}$$

The SIR unit is shown in Figure 4.3, suppose the input impedance of the step impedance surface between open circuit end and short circuit end is Z_r, according to the above mentioned equation, there is:

$$Z_r = Z_1 \frac{Z_L + jZ_1 \tan\theta_1}{Z_1 + jYZ_L \tan\theta_1} = jZ_1 \tan\theta_1 \tag{4.5}$$

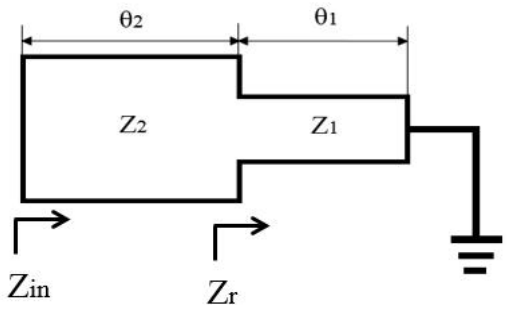

Figure 4.3. The $\lambda_g/4$ SIR Unit

If we ignore the inconsistence on the step impedance surface and the capacitor effect on the open circuit surface, the Z_r can be seen as the load of loss-less uniform transmission line whose characteristic impedance Z_2 and equivalent electrical length θ_2, therefore:

$$Z_{in} = Z_2 \frac{Z_r + jZ_2 \tan\theta_2}{Z_2 + jZ_r \tan\theta_2} \tag{4.6}$$

That is:

$$Z_{in} = jZ_2 \frac{Z_1 \tan\theta_1 + Z_2 \tan\theta_2}{Z_2 - Z_1 \tan\theta_1 \tan\theta_2} \tag{4.7}$$

The SIR will resonate when $Y_0=1/Z_0=0$, that is:

$$Z_2\text{-}Z_1\tan\theta_1\tan\theta_2=0 \tag{4.8}$$

$$Z_2/Z_1=\tan\theta_1\tan\theta_2=K \tag{4.9}$$

From the above mentioned equations, the resonance condition of SIR is determined by the ratio of impedance of two sections of transmission lines and their equivalent electrical lengths. This means that the SIR has more freedom compared to traditional UIR.

4.2.2 Electrical lengths of SIR

Assume two section line equivalent electrical lengths are θ_1 and θ_2, total equivalent electrical length is $\theta_{TA}= \theta_1+\theta_2$:

$$\theta_{TA} = \theta_1 + \theta_2 = \theta_1 + \arctan\left(K/\tan\theta_1\right) \tag{4.10}$$

The corresponding UIR electrical length is $\pi/2$, so the normalized electrical length of SIR is:

$$L_n = \theta_{TA} / (\pi / 2) = 2\theta_{TA} / 2 \tag{4.11}$$

The relationship between normalized SIR electrical length L_n and electrical length θ_1 with the variable value impedance ratio K is shown in Figure 4.4. From Figure 4.4, we know that when impedance ratio K>1, normalized SIR electrical length L_n can achieve maximum value, when K<1, normalized SIR electrical length L_n can achieve minimum value, when K=1, SIR is equal to UIR.

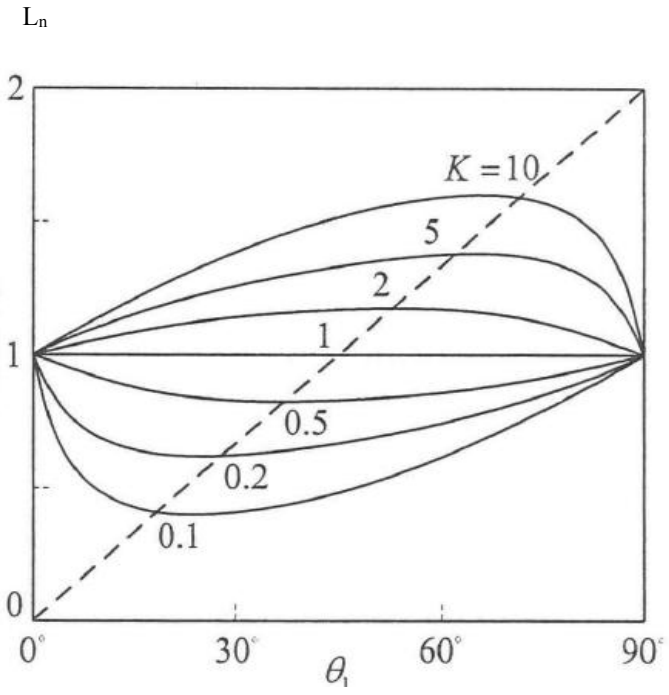

Figure 4.4. Relationship between normalized SIR electrical length L_n and electrical length θ_1 with the variable value impedance ratio K

Suppose $\lambda_g/2$ and λ_g type SIR resonator total equivalent electrical length is θ_{TB} and θ_{TC}, there are:

$$\theta_{TB}=2\theta_{TA} \tag{4.12}$$

$$\theta_{TB}=4\theta_{TA} \tag{4.13}$$

The θ_{TB} and θ_{TC} corresponding UIR electrical lengths is π and 2π, so the normalized electrical length of SIR is:

$$L_{nB}=\theta_{TB}/\pi=2\theta_{TA}/\pi \tag{4.14}$$

$$L_{nC}=\theta_{TC}/\pi=2\theta_{TA}/\pi \tag{4.15}$$

From the above mentioned expressions, three types of SIR resonance conditions can be shown by one expression, substitute $\theta_2=\theta_{TA}-\theta_1$ into Equ. (4.9), the following can be expressed:

$$K=\frac{\tan\theta_1\left(\tan\theta_{TA}-\tan\theta_1\right)}{1+\tan\theta_{TA}\tan\theta_1} \tag{4.16}$$

When $0<K<1$, $0<\theta_{TA}<\pi/2$,

$$\begin{aligned}\tan\theta_{TA}&=\frac{1}{1-K}\left(\tan\theta_1+\frac{K}{\tan\theta_1}\right)\\ &=\frac{\sqrt{K}}{1-K}\left(\frac{\tan\theta_1}{\sqrt{K}}+\frac{\sqrt{K}}{\tan\theta_1}\right)\\ &\geq 2\frac{\sqrt{K}}{1-K}\end{aligned} \tag{4.17}$$

When $\frac{\tan\theta_1}{\sqrt{K}}=\frac{\sqrt{K}}{\tan\theta_1}$, equation（4. 16）gets equality sign.

Thus, $$K=\tan^2\theta_1 \tag{4.18}$$

Thus, $$\theta_1=\arctan\sqrt{K} \tag{4.19}$$

Now θ_{TA} can get the minimum value:

$$(\theta_{TA})_{\min} = \arctan\frac{2\sqrt{K}}{1-K} \tag{4.20}$$

When $0<K<1$, $\pi/2<\theta_{TA}<\pi$,

$$\begin{aligned}\tan\theta_{TA} &= \frac{1}{1-K}\left(\tan\theta_1 + \frac{K}{\tan\theta_1}\right) \\ &= \frac{\sqrt{K}}{1-K}\left(\frac{\tan\theta_1}{\sqrt{K}} + \frac{\sqrt{K}}{\tan\theta_1}\right) \\ &\le 2\frac{\sqrt{K}}{1-K}\end{aligned} \tag{4.21}$$

When $\frac{\tan\theta_1}{\sqrt{K}} = \frac{\sqrt{K}}{\tan\theta_1}$, equation（4. 21）gets equality sign.

Thus, $$K = \tan^2\theta_1 \tag{4.22}$$

Thus, $$\theta_1 = \arctan\sqrt{K} \tag{4.23}$$

Now θ_{TA} can get the maximum value:

$$\tan(\theta_{TA})_{\max} = \frac{2\sqrt{K}}{1-K} \tag{4.24}$$

$$(\theta_{TA})_{\max} = \arctan\frac{2\sqrt{K}}{1-K} \tag{4.25}$$

Equation (4.20) and (4.25) are obtained under the condition of $\theta_1=\theta_2$, they show the maximum/minimum value of SIR. Figure 4.5 shows the relationship between normalized SIR electrical length L_{n0} and impedance ratio K when electrical length $\theta_1=\theta_2=\theta_0$. L_{n0} is expressed as:

$$L_{n0} = 2\theta_{AT}/\pi = 4\theta_0/\pi = 4\arctan\left(\sqrt{K}\right)/\pi \tag{4.26}$$

From Figure 4.5, we can use a relatively small value impedance ratio K to reduce the length of SIR resonator. The maximum length of SIR is restricted as twice of length of UIR.

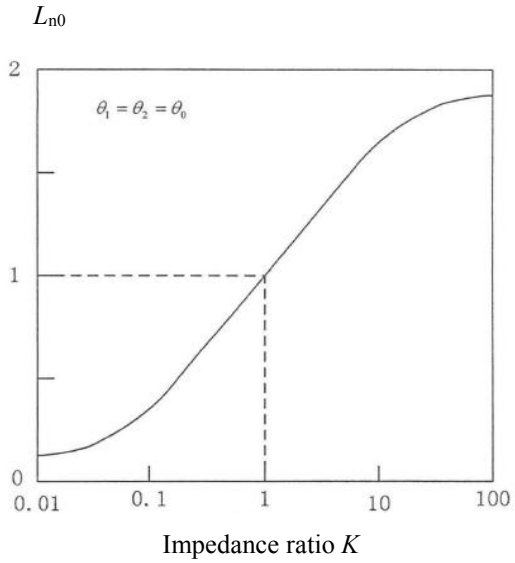

Figure 4.5. The relationship between normalized SIR electrical length L_{n0} and impedance ratio K when electrical length $\theta_1 = \theta_2 = \theta_0$.

4.3 Spurious frequency of SIR

Spurious frequencies appear at ~~the~~ frequencies which are multiples of the fundamental frequency in UIR. Spurious frequency locations can be tuned by adjusting the impedance ratio in SIR. Suppose the fundamental frequency of SIR is f_0, the first spurious frequency of $\lambda_g/4$, $\lambda_g/2$ and λ_g type SIR is f_{SA}, f_{SB}, f_{SC}, and corresponding electrical length θ_{SA}, θ_{SB} and θ_{SC}, respectively. From (4.19), we can get:

$$\tan\theta_{SA} = \tan(\pi - \theta_0) = -\sqrt{K} \tag{4.27}$$

That is:

$$\theta_{SA} = \pi - \arctan\sqrt{K} \tag{4.28}$$

From the equation below, we can get $\lambda_g/2$ and λ_g type SIR resonance condition:

$$(K\tan\theta_1+\tan\theta_2)(K-\tan\theta_1\tan\theta_2)=0 \tag{4.29}$$

Because $\theta_1=\theta_2=\theta_0$, there is:

$$(K+1)\tan\theta_0(K-\tan^2\theta_0)=0 \tag{4.30}$$

By solving the above equation, we get:

$$\theta_0=\arctan\sqrt{K} \tag{4.31}$$

$$\theta_{SB}=\theta_{SC}=\pi/2 \tag{4.32}$$

From (4.9) and (4.24), we get the spurious frequency:

$$\frac{f_{SA}}{f_0}=\frac{\theta_{SA}}{\theta_0}=\frac{\pi-\theta_0}{\theta_0}=\pi/\arctan\sqrt{K}-1 \tag{4.33}$$

$$\frac{f_{SB}}{f_0}=\frac{\theta_{SC}}{\theta_0}=\frac{\theta_{SB}}{\theta_0}=\pi/2\arctan\sqrt{K} \tag{4.34}$$

Figure 4.6 shows the relationship between impedance ratio K and normalized spurious frequency f_s/f_0. This shows that it is better to use a relatively small K value for $\lambda_g/4$ type SIR in order to move the spurious frequency far away from the fundamental frequency. Besides, the dimension of the resonator can be smaller. As for $\lambda_g/2$ and λ_g type SIRs, it is also better to use a relatively small *K* value to keep the spurious frequency far away from the fundamental frequency.

Therefore, in the design of dual-band filters, the spurious frequency is usually used to realize dual band characteristic.

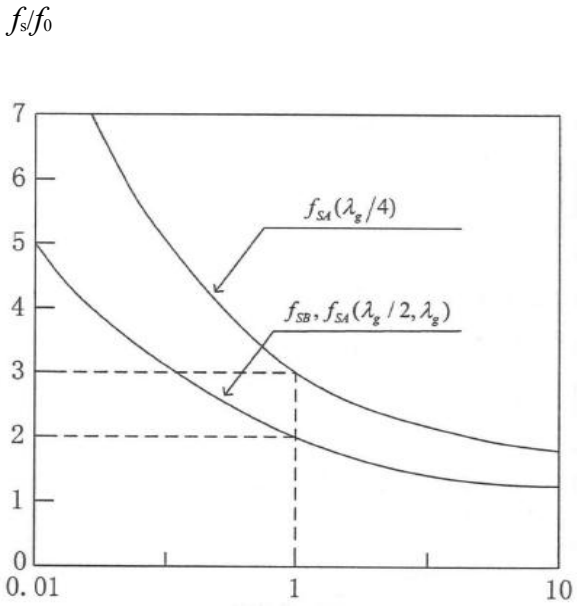

Figure 4.6. The relationship between impedance ratio K and normalized spurious frequency f_s/f_0[1].

4.4 Equivalent circuit of SIR

In practical microwave circuits, distributed parameter elements are used to realize all kinds of components while the lumped parameter elements are also used largely because of its convenience in analyses. Practical filter designs are all based on the lumped parameter elements. In the resonance condition, distributed parameter element resonator can all be described by approximated equivalent LCR resonators.

Define the susceptibility slope parameter b_s as[1]:

$$b_s = \frac{\omega_0}{2}\frac{dB_s(\omega)}{d\omega}\Big|_{\omega=\omega_0} \tag{4.35}$$

where $B_s(\omega)$ is the susceptibility of the resonator, ω_0 is the angular resonance frequency. Assume the magnetic susceptibility of the $\lambda_g/4$ type resonator is B_{SA} and the corresponding susceptibility slope parameter is b_{sa}. From (4.4) and (4.35), we get:

$$B_{SA} = \mathrm{Im}[1/Z_i] = Y_2 \frac{\tan\theta_1 \tan\theta_2 - K}{\tan\theta_1 + K\tan\theta_1} \tag{4.36}$$

$$\begin{aligned} b_{SA} &= \frac{\omega_0}{2} \frac{dB_{SA}(\omega)}{d\omega}\Big|_{\omega=\omega_0} \\ &= \frac{\theta_0}{2} \frac{dB_{SA}(\omega)}{d\omega}\Big|_{\theta=\theta_0} \\ &= \frac{\theta_{01} Y_2}{2}\left[\frac{K}{(1-K^2)\sin^2\theta_{01} + K^2} + \frac{l_1}{l_2}\right] \end{aligned} \tag{4.37}$$

Where θ_{01} is the value of θ_1 when resonating, l_1 and l_2 are the dimensions of the resonator.

When $\theta_{01} = \theta_{02} = \theta_0$, which is $l_1 = l_2$, from (4. 21):

$$\tan^2\theta_0 = K \tag{4.38}$$

$$\sin^2\theta_0 = K/(1+K) \tag{4.39}$$

Therefore,

$$\begin{aligned} b_{SA0} &= \frac{\theta_{01} Y_2}{2}\left[\frac{K}{(1-K^2)\sin^2\theta_{01} + K^2} + \frac{l_1}{l_2}\right] \\ &= \theta_0 Y_2 \\ &= Y_2 \arctan\sqrt{K} \end{aligned} \tag{4.40}$$

$$b_{SB0} = 2Y_2\theta_0 = 2Y_2 \arctan\sqrt{K} \tag{4.41}$$

$$b_{SC0} = 4Y_2\theta_0 = 4Y_2 \arctan\sqrt{K} \tag{4.42}$$

When the circuit is under the condition of resonance, the slope parameter of resonator can be expressed by the lumped element L_0, C_0, G_0, that is:

$$L_0=1/\omega_0 b_s \tag{4.43}$$

$$C_0=b_s/\omega_0 \tag{4.44}$$

$$G_0=b_s/Q_0 \tag{4.45}$$

where Q_0 is the quality factor of the resonator.

Figure 4.7 is the equivalent circuit of a resonating SIR, where the unloaded Q value of resonator is determined by material and the dimensions of the resonator. Actually, any resonator can be described in the form of Figure 4.7.

This resonator equivalent is useful for circuit calculations including the magnetic wall (or an open circuit) resonant frequency and electric wall (or a short circuit) for the condition of magnetic coupling or the condition of electric coupling, which can lead to the calculation of the magnetic coupling or the electric coupling coefficient. In Figure 4.7, $R_0=1/G_0$. Former work related to this can be seen in [2].

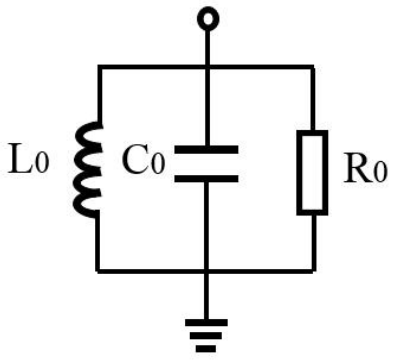

Figure 4.7. The equivalent circuit of resonating SIR

4.5 The asymmetric stepped impedance resonator (ASIR)

4.5.1. Characteristics of the Asymmetric SIR Unit

The asymmetric SIR shown in Figure 4.8 consists of sections with low and high characteristic impedance Z_1 and Z_2. The physical lengths L_1 and L_2, physical widths W_1 and W_2, and electrical lengths θ_1 and θ_2 are shown for the two sections with Z_1 and Z_2, respectively.

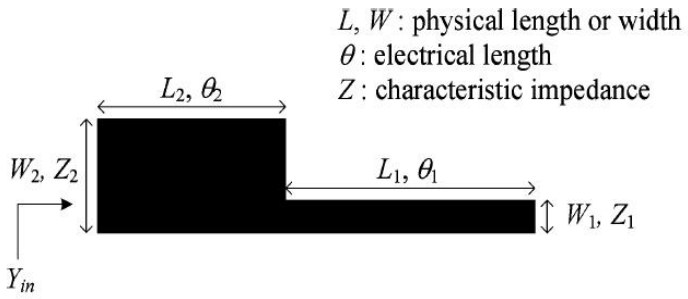

Figure 4.8. Structure of an asymmetric SIR.

The characteristic impedance ratio K and the length ratio α are defined as follows:

$$K = \frac{Z_2}{Z_1} \tag{4.46}$$

$$\alpha = \frac{\theta_2}{\theta_1 + \theta_2} \tag{4.47}$$

where α is located in the range of (0, 1).

The input admittance Y_{in} of the proposed asymmetric SIR unit is derived as:

$$Y_{in} = \frac{j}{Z_2} \frac{K \tan\theta_1 + \tan\theta_2}{1 - K \tan\theta_1 \tan\theta_2} \tag{4.48}$$

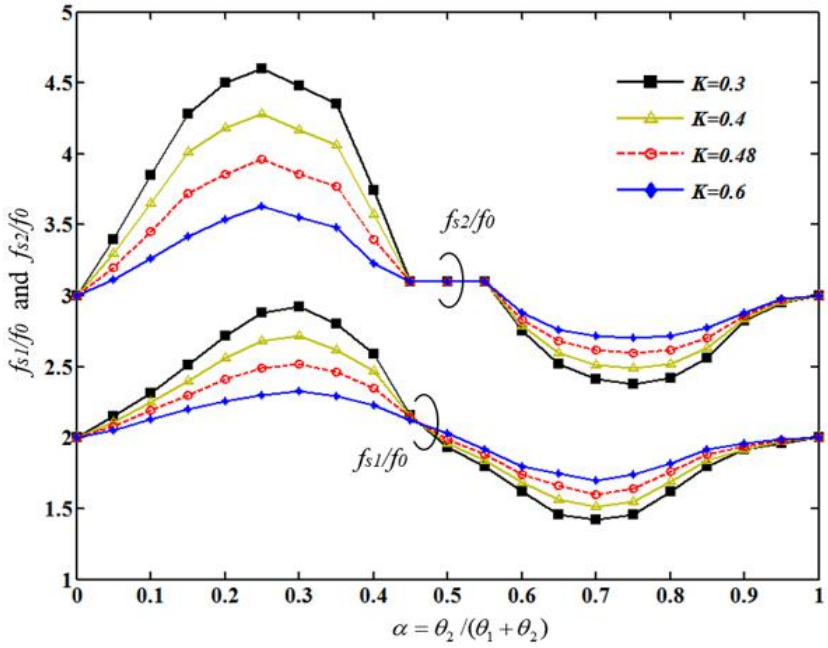

Figure 4.9. f_{s1} (the first spurious frequency) and f_{s2} (the second spurious frequency) normalized by f_0 (the fundamental frequency) for the asymmetric SIR in Figure 4.8.

It is known that the resonance of the proposed asymmetric SIR occurs when $Y_{in} = 0$. Based on (4. 48), this resonance happens when

$$\frac{K \tan \theta_1 + \tan \theta_2}{1 - K \tan \theta_1 \tan \theta_2} = 0 \tag{4.49}$$

By using the solution to (4.49), Figure 4.9 plots the first and second spurious frequency f_{s1} and f_{s2}, respectively, normalized by the fundamental frequency against α under different values of K. It is noted that when α is more than 0.5, normalized frequency f_{s1}/f_0 is greater than 2 and f_{s2}/f_0 is greater than 3, respectively. Also smaller K can result in greater normalized frequency when α is fixed. When α is greater than 0.5, normalized frequency f_{s1}/f_0 is less than 2 and f_{s2}/f_0 is less than 3. Smaller K can result in lower normalized frequency for a fixed α. When K=1, f_{s1}/f_0 is equal to 2 and f_{s2}/f_0 is equal to 3, respectively. This means that, in this limit, a uniform impedance resonator is realized

and high order resonant frequency is an integer multiple of the fundamental frequency f_0. Therefore, the higher order spurious resonant modes, which depend on the choice of the characteristic impedance ratio K and the electric length ratio α, can be found by combining (4. 47) and (4. 49).

Compared to the traditional stepped impedance resonator (SIR) with two step discontinuities, the asymmetric SIR has only one discontinuity but still keeps the characteristic of controllable spurious modes. Thus, it owns the advantage of compact size, less loss, and strong design feasibility, particularly in designing ~~of~~ high-order BPFs such as dual band [3], triple band and quad band [4] BPFs because of its inherently higher order resonant modes.

4.5.2. The Anti-Parallel Asymmetric SIR Unit

Currently, the presented coupled line asymmetric SIR structures can be classified into two types: one type is anti-parallel coupled asymmetric SIR structure. The anti-parallel coupled asymmetric SIR structure, composing of two asymmetric SIR units with their high and/or low impedance lines anti-coupled with each other, is usually folded at its open end. The high impedance lines of two asymmetric SIRs can be bent and coupled with each other to form a signal transmission route[3]. The first spurious frequency is utilized to form the second operating band by analysing the ASIR unit [5]. Because the frequency response characteristic of anti-parallel coupled line in ASIR structure is directly related with and decided by the frequency response characteristic of the ASIR unit, APC-ASIR frequency response is relative easy to get by analysing the ASIR unit. Figure 4.10 shows the anti-parallel structure formed by two ASIRs. In this structure,

two ASIRs high impedance lines are coupled with each other to realize capacitive coupling, and the resonant points can be found by using the normalized frequency plot which is similar to Figure 4.9. Figure 4.10 shows the anti-parallel structure formed by two ASIRs with the partly coupling structure in [4].

The anti-parallel structure formed by two ASIRs with tap feeding and its frequency response is shown in Figure 4.11 and Figure 4.12, respectively. It is seen from Figure 4.12 that harmonic frequencies f_{s1}, f_{s2}, f_{s3} and f_{s4} are generated with the fundamental frequency f_0 by using HFSS . These harmonic frequencies are not integer multiples of the fundamental frequency f_0 and can be studied by using the normalized frequency plot shown in Figure 4.9.

Therefore, the harmonic frequencies can be placed to the desired frequencies and generate the multiband frequency response performance, which is different from the frequency characteristic of traditional $\lambda_g/4$, $\lambda_g/2$ and λ_g stepped impedance resonator structure and has more freedom to design the needed frequency.

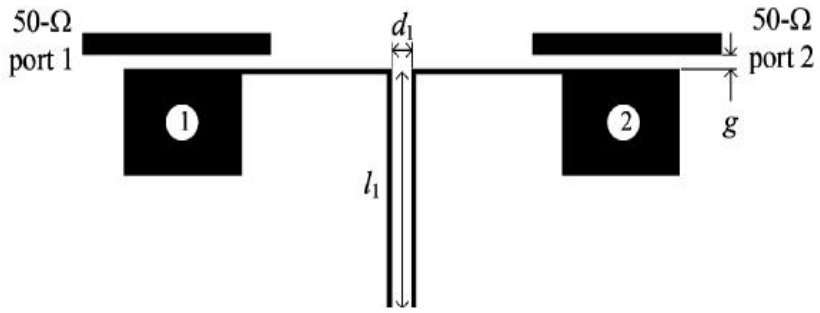

Figure 4.10. The anti-parallel structure formed by two ASIRs with the capacitor coupling shown in [3].

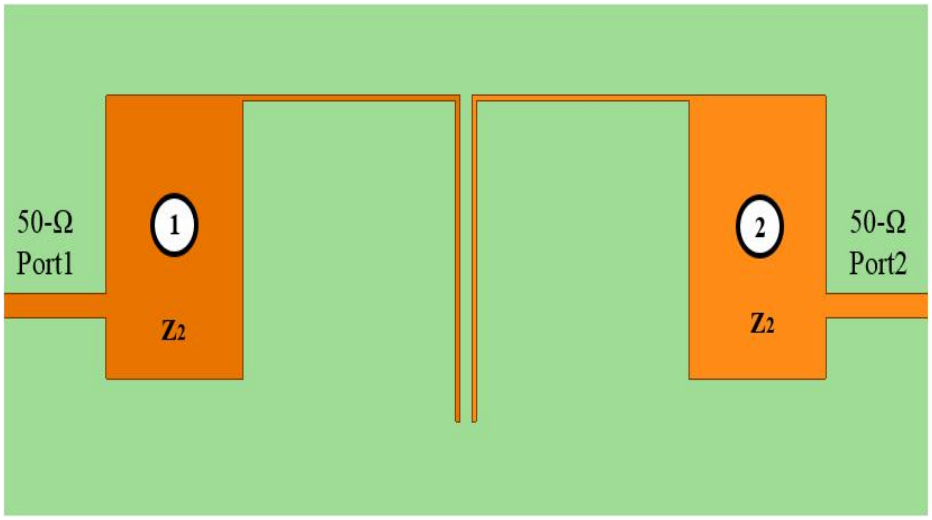

Figure 4.11. The anti-parallel structure formed by two ASIRs with tap feeding.

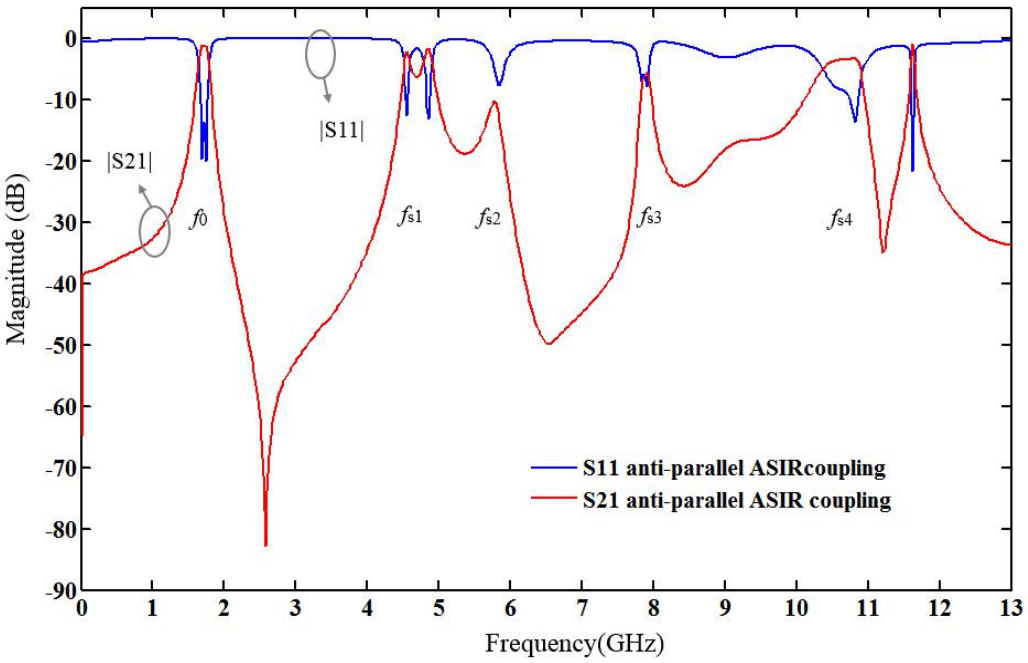

Figure 4.12. The frequency response of the anti-parallel two ASIR structure with tap feeding.

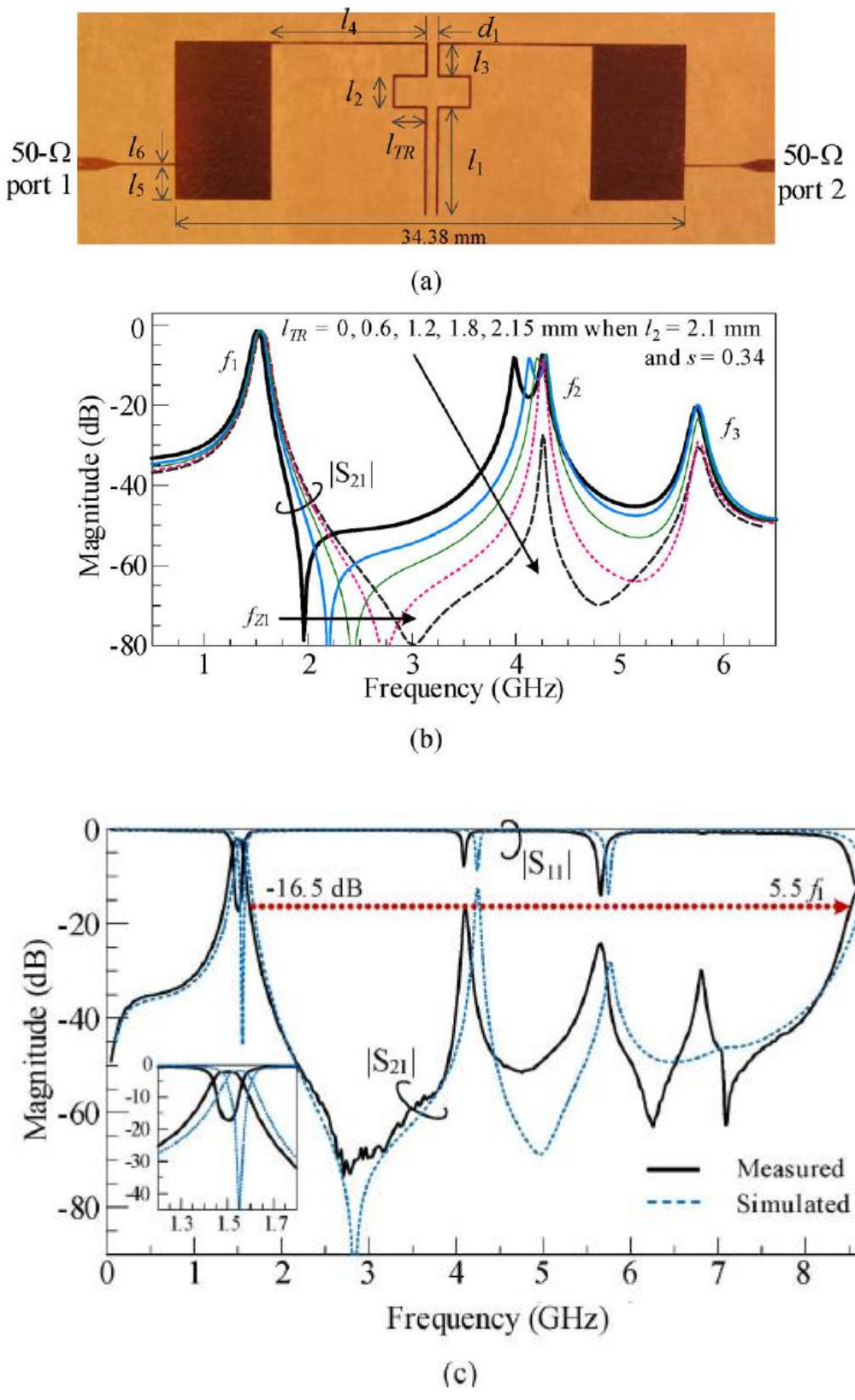

Figure 4.13. The anti-parallel structure formed by two ASIRs, for the partly coupling structure shown in [6]. (a) The configuration. (b) The frequency response with variable l_{TR}. (c) The optimized frequency response.

4.6 References

[1] David M. Pozar. Microwave Engineering, 3rd Edition. Wiley India Pvt. Limited, 1 Sep 2009.

[2] J. S. Hong and M. J. Lancaster. Couplings of microstrip square open-loop resonators for cross-coupled planar microwave filters. IEEE Transaction Microwave Theory Technique. Vol. 44, no. 11, pp: 2099-2109, Nov 1996.

[3] C. H. Kim and K. Chang. Independently Controllable Dual-Band Bandpass Filters Using Asymmetric Stepped-Impedance Resonators. IEEE Transaction Microwave Theory Technique. Vol. 59, no. 12, pp: 3037-3047, Dec. 2011.

[4] H. W. Wu and R. Y. Yang. A New Quad-Band Bandpass Filter Using Asymmetric Stepped Impedance Resonators. IEEE Microwave Wireless Component Letter. Vol. 21, no. 4, pp: 203-205, April 2011.

[5] Y. C. Chang, C. H. Kao, M. H. Weng, et al. Design of the Compact Wideband Bandpass Filter With Low Loss, High Selectivity and Wide Stopband. IEEE Microwave Wireless Component Letter. Vol. 18, no. 12, pp: 770-772, Dec. 2008.

[6] C. H. Kim and K. Chang. Wide-Stopband Bandpass Filters Using Asymmetric Stepped-Impedance Resonators. IEEE Microwave Wireless Component Letter. Vol. 23, no. 2, pp: 69-71, Feb. 2013.

[7] H. W. Liu, B. P. Ren, et al. High-Temperature Superconducting Bandpass Filter Using Asymmetric Stepped-Impedance Resonators With Wide-Stopband Performance. IEEE Transaction Applied Superconductivity. Vol. 25, no. 5, pp: 1-6, Oct. 2015.

CHAPTER 5

Novel Multi-standard Dual-Wideband and Quad-Wideband Asymmetric Step Impedance Resonator (ASIR) Filters with Wide Stop-band Restriction

5.1 Overview of Dual-Band Filters and Design Background

With the requirements in the current increasingly stringent frequency spectrum resources and the development of advanced multi-standard wireless communication systems, dual-band filters have gradually become a good candidate to meet these demands. Therefore, it is highly desirable to develop high performance dual band BPFs with compact size, low in-band insertion loss (IL), and high out-of-band rejection skirts. For this purpose, a lot of research work has been performed and design has been proposed to satisfy such stringent requirements [1-31]. Among them the most straightforward method to implement a dual-band filter is to combine two BPFs with individual pass-bands using additional impedance-matching networks [1].

Generally speaking, dual band BPFs can be classified into (1) the stepped-impedance resonator (SIR) filter [2-8], (2) loaded stub filter [9-14], (3) defected grounded structures (DGS) filter [15-18],(4) dual-mode filter [19-29], (5) dual resonator filter, (6) imbedded structure filter,etc.

As mentioned in chapter 4, the stepped-impedance resonator (SIR) can generate a tuneable first spurious frequency which can be used as the second pass-band in dual-band band-pass filters and this structure has been found in various dual-band filter designs. In 2008, paper [2] proposed a novel defected stepped impedance resonator (DSIR) structure the resonant frequency of the DSIR is found to be much lower than that of the conventional microstrip stepped impedance resonator (SIR). Besides, the circuit size can be reduced effectively by using this unit structure. By combining two designed filters together, a dual-band filter with a common input/output feed line is achieved. In the same year, paper [3] also proposed a novel stepped impedance resonator (SIR) structure to realize a dual band filter.

In 2011, paper [5] proposed an analytical method to design a dual-band filter using the short circuit terminated half-wavelength stepped impedance resonator (SIR). In the proposed method, the structural parameters of the SIR are obtained analytically according to the two pass-band centre frequencies and bandwidths of the filter. As a result, the achievable specifications of the dual-band filter can be rapidly determined. The coupling between adjacent SIRs is realized by a short-circuited stub, which is characterized as an inverter network. The dual-frequency transformer incorporated with the tapped-line input/output structure is used for the external coupling. Applying the analytical equations in the design process, a dual-band filter can be easily and quickly

realized. In 2013, paper [6] proposes a class of dual-band band-pass filters with stepped-impedance resonators (SIRs) and presents a rigorous synthesis method for these compact filters. Firstly, SIRs are designed to generate their first two resonant modes in the two specified pass-bands, and they are sequentially cascaded by alternative and inverters. In design, SIRs need to be chosen not only to satisfy the prescribed dual-band central frequencies, but also to compensate for the deficient values of inverters at these two frequencies. Following that, a generalized synthesis method is extensively described for design and exploration of novel dual-band filters on the microstrip-line topology. The two types of second-order dual-band Chebyshev band-pass filters with dual pass-bands are at 5.8 and 1.8 GHz (large frequency ratio), as well as 5.8 and 2.4 GHz (small frequency ratio), respectively.

Apart from the stepped-impedance resonator (SIR) structure, the dual-band filter can also be realized by using the resonators consisting of the open- or short-circuited stubs, which are placed in series or in parallel to create transmission zeros in the middle pass-band of a wideband BPF [9]-[14]. In 2007 and 2008, papers [9] and [10] employed simple stub loaded dual-mode resonators for the dual-band filter design and enjoy some advantages in in band performance. However, they have disadvantages of being difficult to synthesize the corresponding dual-band coupling degrees.

In 2013, paper [11] presented a novel dual-band band-pass filter with controllable frequencies and bandwidths as well as a high out-of-band rejection level. The proposed filter utilizes a novel stub-loaded quad-mode resonator. Every two modes, which can be flexibly controlled, are utilized to form a pass-band with controllable frequency and bandwidth. Source-load coupling and hook-shape feed lines are also introduced in the

paper. In the same year, paper [12] introduced the stub-to-stub coupling structure to split two identical odd-modes. Meanwhile, these two coupling stubs are folded inward, and a new transmission zero is produced, which separates four modes into two parts corresponding to two pass-bands: the first one is formed by even-modes, and the second one is composed by odd-modes. The centre frequency and bandwidth of each pass-band can be controlled by the corresponding physical dimensions. The paper [13] presented a new class of dual-, tri- and quad-band BPF by using proposed open stub-loaded shorted stepped-impedance resonator (OSLSSIR). The OSLSSIR consists of a two-end-shorted three-section stepped-impedance resonator (SIR) with two identical open stubs loaded at its impedance junctions. Two 50 Ω tapped lines are directly connected to two shorted sections of the SIR to serve as I/O ports. As the electrical lengths of two identical open stubs increase, many more transmission poles (TPs) and transmission zeros (TZs) can be shifted or excited within the interested frequency range of interest. The TZs introduced by open stubs divide the TPs into multiple groups, which can be applied to design a multiple-band band-pass filter (BPF). In order to increase many more design freedoms for tuning filter performance, a high-impedance open stub and the narrow/broad side coupling are introduced as perturbations in all filters design, which can tune the even- and odd-mode TPs separately.

In 2014, Paper [14] proposed a band-pass filter in which the frequency space between two pass-bands and bandwidths of two pass-bands can be controlled by the shorted stubs. Wide out-of-band rejection can be achieved by selecting the desired impedance and length ratios and suitable feeding point to suppress some spurious resonant frequencies. A prototype filter centred at 1.395 and 1.825 GHz is designed with the first

spurious response occurring at 7.84 GHz or 5.7 f_{01} (f_{01} is the centre frequency of the first pass-band).

As mentioned in chapter 2, various kinds of defected grounded structures in the new technology have been presented and found their applications in the design of low-pass, band-pass, and band-stop filters [15]-[17]. In 2005, paper [18] proposed an alternative approach in which the DGS themselves are considered as the building blocks of the device and the dual of the split-ring microstrip resonators. In 2008, letter [2] proposed a novel dual-band filter based on defected stepped impedance resonator (DSIR). The resonant property of DSIR is studied and compared with traditional microstrip SIR. The former is found to have a much lower resonant frequency than the latter one, which means there is a great reduction of circuit size. Making use of DSIR as the basic resonant unit, two kinds of DSIR filter operating at 1.85 and 2.35 GHz, respectively, are well designed.

Apart from previous mentioned structures, the dual-mode dual-band BPF structure is also an attractive candidate for dual-band applications due to its relatively compact size, simple physical layout, and design procedure. In general, these reported dual-mode dual-band BPF design methods can be mainly classified into two typical categories. The first one uses two dual-mode resonators, i.e., a square loop resonator [19], [20], a stub-loaded resonator (SLR) [9], or an E-shaped resonator [22], [23], operating at two different frequencies to build up a dual-band BPF. The configuration of the filter can be based on either multilayer [19] or single layer [20-23]. For the SLR presented in [9] and two different types of E-shaped resonators presented in [22] and [23], no perturbations are needed because they inherently have dual-mode characteristics. Nevertheless, the

proper perturbation is indispensable for the square loop resonator [19], [20] to excite the other mode. The other category utilizes a single resonator to realize the dual-band performance. Compared with the first category, the size and the layout complexity of this topology can be further reduced. Most of the reported dual mode dual-band BPFs using a single resonator are realized by a ring resonator [24]-[26] or patch resonator [27]-[29]. It has to be noted that these resonators exhibiting a dual-mode dual-band characteristic cannot be separated from the perturbations, such as C-sections in [24], capacitive coupling and loaded open stubs in [25], [26], embedded pair of slots in [27], cross slot and two sets of loaded stub in [28], and arc- and radial-oriented slots in [29].

With the development of wireless communication systems, multi-standard internal filters have become a necessity for the state-of-the-art multifunction “smart phones” and wireless transceivers for the mobile devices. Such filters are generally required to be capable of covering the frequency bands of Global System for Mobile Communication (GSM: 1800/1900 MHz, etc.), Universal Mobile Telecommunications System (UMTS: 1710-1880/1850-1990/1920-2170 MHz etc.) and Global Positioning System (GPS) (frequency bands centred at 1.57 GHz). Furthermore, the ever increasing implementation of Wireless Local Area Network (WLAN) such as Wi-Fi devices further increases the IEEE 802.11a bandwidth requirement in order to cover the bands centred at 5.8 GHz.

In the above mentioned dual-band filters, most of them with a miniaturized size fail to cover the required frequency bands, especially at the lower frequency band due to the narrower dual bandwidth [2], [6], [11], [12], [24]-[29] or require a considerable filter

size or thickness, which usually makes them difficult to integrate within mobile devices or portable wireless modules [6], [7], [14], [24].

In this chapter, we present new applications of microstrip hairpin resonators which lead to a new class of cross-coupled microstrip bandpass filters. The cross-coupled filters are so attractive because they exhibit ripples in both passband and stopband, which according to the early work on filter synthesis [30] can improve both frequency selectivity and bandpass loss. For instance, they are able to place transmission zeros near cut-off frequencies of a passband so that higher selectivity with less resonators can be obtained. This property is of much interest in narrow-band filters where the passband insertion loss is strongly related to the number of resonators. The cross-coupled filters, depending on the phasing of cross-coupled signals, may also flatten the group delay. Owing to the difficulty in arranging and controlling the cross couplings in planar transmission-line resonators, only a few types of cross-coupled planar filters have been developed [31]-[34]. The new cross-coupled microstrip hairpin-resonator filters offer alternative designs. They are not only simple and compact in configurations, but also have great flexibility to shape filters into different sizes. The latter is mainly due to the great freedom in choosing asymmetric impedance stepped resonator-resonator shapes.

The proposed novel multi-standard filter has a size of only 4.6 mm×41.65 mm and a thickness of 0.635 mm. This filter is capable of generating two wide operating bands that effectively cover the GSM/UMTS/GPS/IEEE 802.11a operations in mobile devices, which include GSM1800 (1710-1880 MHz), GSM1900 (1850-1990 MHz), UMTS (1920-2170 MHz), GPS (frequency band centered at 5.75 GHz) and IEEE 802.11a (frequency band centered at 5.8 GHz) bands. The proposed multi-standard filter's wide

bandwidths at the low and high frequency are attributed to the mutual coupling of the modified SIR resonators. Meanwhile, in-band and out-of-band performances of the proposed filter are enhanced by its novel folded structure and even and odd phase velocity compensation technique using shifted coupled lines. Because there is no via hole or defect ground structure included in the filter structure, the structure is relatively simple and easily realized. The theory study of the multi-standard filter and configuration performance with simulation results are described in 5.2, and the conclusion of this chapter is given in 5.3.

5.2 Filter Coupling and Configuration

5.2.1 The types of coupling

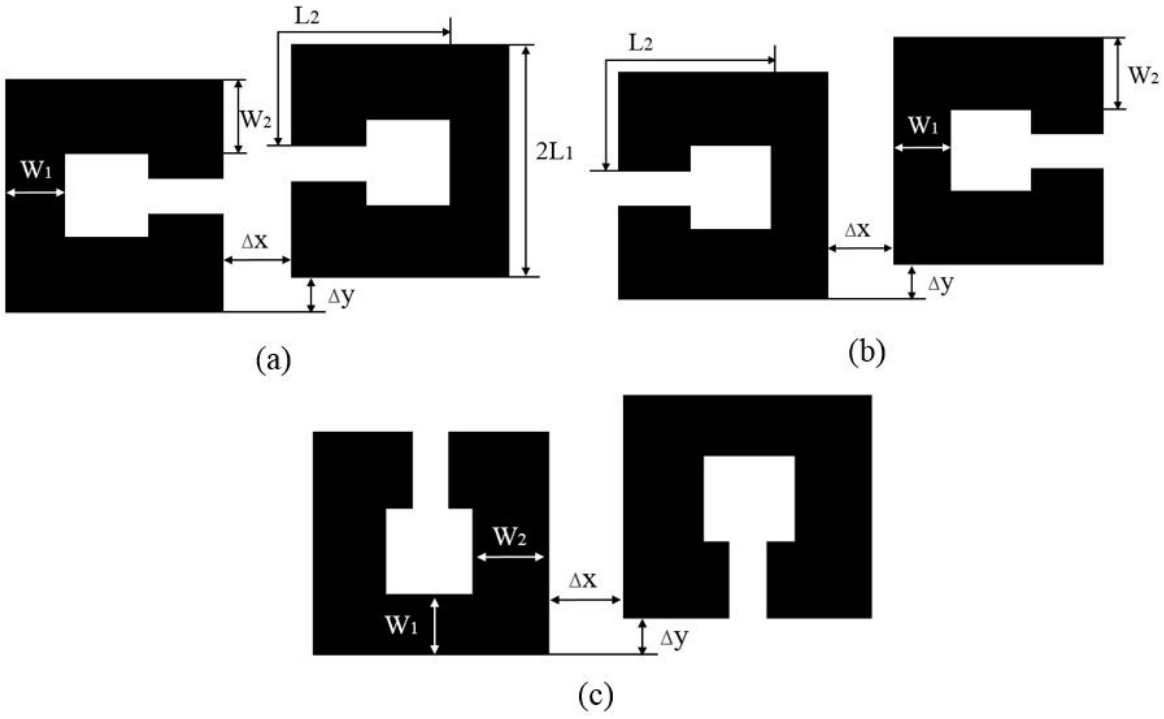

Figure 5.1. The coupling types of the resonators (a) Electric coupling. (b) Magnetic coupling. (c) Mixed coupling.

The coupling can be considered as the transfer of electrical and magnetic energy from one circuit segment to another. Figure 5.2 shows the general coupling types of the resonators. It is obvious that any coupling in those coupling structures is that of the proximity coupling, which is, basically, through fringe fields. The nature and the extent of the fringe fields determine the nature and the strength of the coupling. It can be shown that at resonance, each of the folded stepped impedance resonators (this also applies to the open-loop resonators) has the maximum electric field density at the side with an open-gap, and the maximum magnetic field density at the opposite side. Because the fringe field exhibits an exponentially decaying character outside the region, the electric fringe field is stronger near the side having the maximum electric field distribution, while the magnetic fringe field is stronger near the side having the maximum magnetic field distribution. It follows that the electric coupling can be obtained if the open sides of two coupled resonators are approximately placed as Figure 5.1 (a) shows, while the magnetic coupling can be obtained if the sides with the maximum magnetic field of two coupled resonators are approximately placed as Figure 5.1(b) shows. Mixed electric and magnetic coupling would occur when two coupled resonators are approximately placed as Figure 5.1(c) shows.

5.2.2 The Novel Skew-Symmetrical Asymmetric SIR Couple Pair

The configuration of the presented multiband filter is illustrated in Figure 5.1. The modified stepped impedance resonators (SIRs) of the proposed filter are improved from a traditional quarter wavelength SIR, which is shown in Figure 5.2. Because traditional a quarter wavelength SIR can generate a tuneable first spurious frequency, the proposed filter utilizes a pair of SIRs to form dual wide-bands which are composed of a

fundamental resonance frequency band and the first spurious frequency band. Because the traditional quarter wavelength SIR has the disadvantage of generating high order spurious frequency response, which would deteriorate filter out of band performance. To overcome this disadvantage, we propose a novel structure using folded meander couple lines instead of traditional quarter wavelength SIR coupled lines to suppress high order spurious frequency and improve out of band performance. In this work, the modified stepped impedance strips are fed by two 50 Ω microstrip feed lines. The width (W1) and length of the 50 Ω feed line are 0.6 mm and 1.2 mm, respectively.

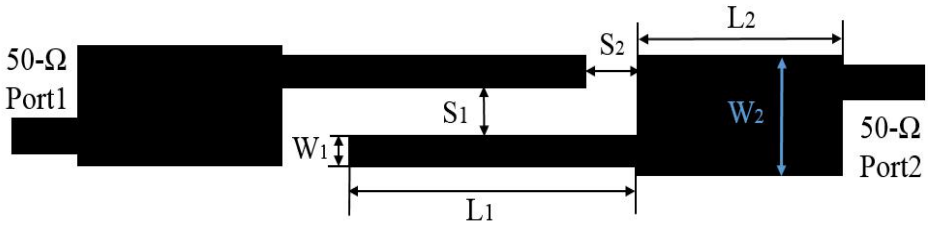

Figure 5.2. Structure of a skew-symmetrical asymmetric SIR couple pair

By tuning the value of impedance ratio, the first spurious frequency can be tuned. In this chapter, the fundamental resonant frequency and the first spurious frequency of the dual-wide-band filter is set at 1.9 GHz and 5.8 GHz, respectively. By careful calculations, the width and length of the high characteristic impedance part is set as 1.7 mm and 11.2 mm, respectively. The width and length of the low characteristic impedance part is set as 0.4 mm and 16.5 mm, respectively.

5.2.3 The Coupling Characteristic of Skew-Symmetrical Asymmetric SIR Couple Pair

In order to realize the desired values for the coupling coefficients, there are differing

coupling configurations. In each of these configurations, the coupling coefficients may be extracted using the pole-splitting method in conjunction with full-wave simulations. The coupling coefficients k can be obtained from[35]:

$$k = \frac{f_H^{\,2} - f_L^{\,2}}{f_H^{\,2} + f_L^{\,2}} \tag{5.1}$$

where f_H and f_L are the higher and lower frequencies of the splitting pole, respectively.

5.2.4. The Characteristic of electric length ratio α and of impedance ratio *K* in Skew Symmetrical Asymmetric SIR Couple Pair

The coupling matrix referring to [35] will not be discussed in this paper because of its non-wideband limitation [35] [36].The coupling between two ASIRs can be represented by a J-inverter susceptance $J_{1,2}$, where subscript 1 and 2 denotes the first and second passband. A larger value of $\overline{J_{1,2}}$ means a stronger coupling strength between two ASIRs.

The normalized $\overline{J_{1,2}}$ can be determined by [35]

$$\overline{J_{1,2}} = J_{1,2} Z_0 \tag{5.2}$$

where Z_0 represents the referred port impedance. The external quality factor $Q_{ex1,2}$ and the normalized J-inverter susceptance $\overline{J_{1,2}}$ can be related by:

$$Q_{ex1,2} = \frac{\pi}{2\overline{J_{1,2}}^{\,2}} \tag{5.3}$$

For a single resonator load, the external quality factor $Q_{ex1,2}$ can be extracted as:

$$Q_{ex1,2} = \frac{f_{c1,2}}{\Delta_{(\pm\frac{\pi}{2})1,2}} \tag{5.4}$$

where $f_{c1,2}$, , $\Delta_{(\pm\frac{\pi}{2})1,2}$ represents the central frequency and the frequency bandwidth of phase curve changing $(\pm\frac{\pi}{2})$ with respect to $f_{c1,2}$, respectively.

For a dual resonator coupling load, the external quality factor $Q_{ex1,2}$ can be extracted by

$$Q_{exl,2} = \frac{f_{c1,2}}{\Delta_{1,2}} \tag{5.5}$$

where $f_{c1,2}, \Delta_{1,2}$ represents the central frequency, -3-dB bandwidths, respectively.

From (5.3) and (5.5), $\overline{J_{1,2}}$ can be calculated by substituting the extracted $Q_{ex1,2}$ into equations in the coupling structure. Based on the quantitative analysis mentioned above, Figure 5.3 is derived and shows the extracted qualitative frequency response analysis of the skew-symmetrical asymmetric SIR coupled pair compared to the asymmetric SIR unit. It can be seen that when asymmetric SIR's electric length ratio α ranges from 0.4 to 0.5, the frequency response at frequency f_0, f_{s3} and f_{s4} enhances significantly in SS-ASIR coupled structure, while it does not change much or degrades at f_{s1} and f_{s3}. When α=0.6, the frequency response at f_0, f_{s1} and f_{s3} enhances greatly, but it does not vary much or degrade at f_{s2} and f_{s4}. The transformation table is useful to analysis and transform frequency bands where the performance-enhanced frequency response appears into desired pass-bands by considering the asymmetric SIR unit characteristic. It is also useful to analyse and transform frequency bands where the performance-degraded frequency response appears into stop-bands or excite it to become a pass-band by modifying SS-ASIR coupled structure.

(1)The influence of electric length ratio *α* in SS-ASIRs

An inherent property of the skew-symmetrical asymmetric SIR (SS-ASIR) coupled pair is that the resonant frequency location and bandwidth performance are mainly influenced by the electric length ratio α when length L1 is fixed at a certain value, and is little influenced by the impedance ratio K. This invariance characteristic is totally different from its counterparts of asymmetric SIR unit, where the normalized frequency (this also applied to the resonant frequency) is closely related with K value. This characteristic of α=0.42 is shown in Figure 5.3. In Figure 5.3, resonant frequency locations and their bandwidths are nearly fixed when α is set at 0.42, and these two parameters are little influenced by K. A similar phenomenon can be observed when α is fixed at other values. This means α is the main factor to influence the horizontal frequency response performance such as resonant frequency locations and bandwidths in SS-ASIR coupled structure.

(2) The influence of impedance ratio *K* in SS-ASIRs

From another aspect, the return loss and insertion loss performance of enhanced f_0 and f_{s2} (seen in Table 5.1 and Figure 5.3) becomes better when K varies from 0.3 to 0.6. Meanwhile, the return loss and insertion loss performance of degraded f_s1 and f_{s3} (see Table 5.1 and Figure 5.3) become better and forms two spurious peaking. Similar phenomenon can be observed when K has other values. Therefore, the impedance ratio K is a main factor to influence the vertical frequency response performance such as return coefficients of f_o and f_{si} versus α when K is fixed , as seen in Figure 5.3. Figure 5.4 shows the coupling coefficients of f_o and f_{si} versus α when K is fixed. By realizing the dual band characteristic of SS-ASIR coupled pair, α=0.42 and K=0.48 are extracted to design the proposed dual band filters. The strong coupled frequency bands at f_0 and

f_{s2} are used to form the first and second pass-band. The weak coupled frequency band at f_{s3} as well as frequency band at f_{s4} are undesired in the proposed dual-band filters. However, they can be used to form the third and fourth pass-band in the proposed quad-band filter.

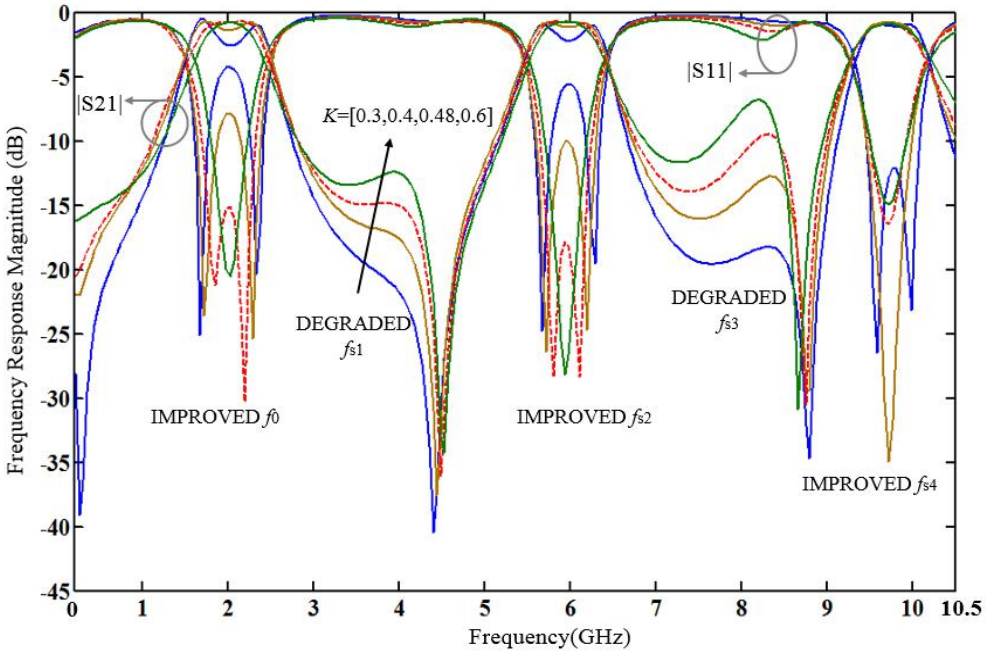

Figure 5.3. Frequency characteristic curves of SS-ASIR coupled pair when α=0.42, L1=11 mm and K=0.3, 0.4, 0.48 and 0.6.

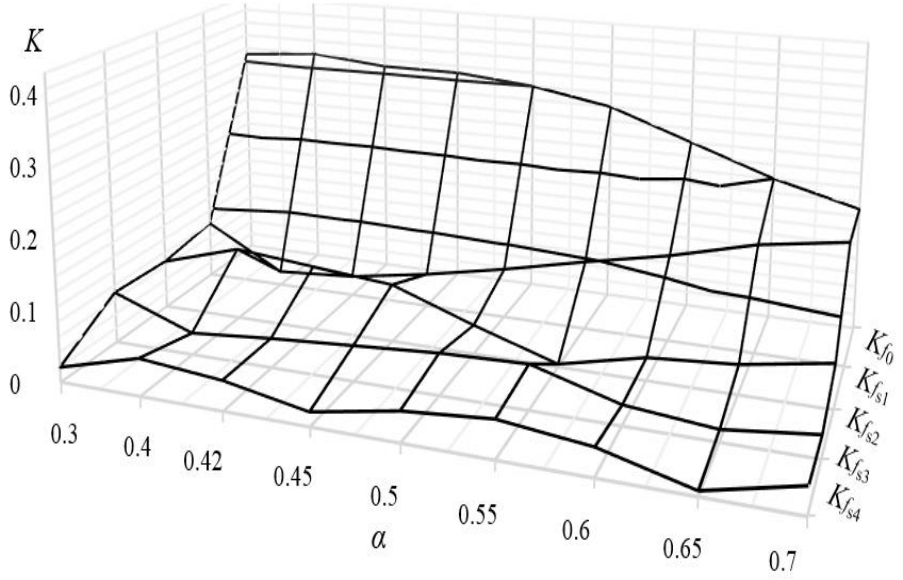

Figure 5.4. The coupling coefficients of f_o and f_{si} versus α when K is fixed.

Table 5.1
THE EXTRACTED QUALITATIVE FREQUENCY RESPONSE ANALYSIS OF THE SKEW-SYMMETRICAL ASYMMETRIC SIR COUPLED PAIR COMPARED TO THE ASYMMETRIC SIR UNIT. ‘‘IMPROVED’’ MEANS SIGNIFICANT ENHANCEMENT OF PERFORMANCE AT RELATIVE FREQUENCY,
‘‘NC/DE’’ MEANS NO SIGNIFICANT CHANGE OR DEGRADATION OF PERFORMANCE AT RELATIVE FREQUENCY POINT, WHEN α RANGES FROM 0.3 TO 0.7.

f / α	The Fundamental Frequency f_0	The First spurious Frequency f_{s1}	The Second spurious Frequency f_{s2}	The Third Spurious Frequency f_{s3}	The Fourth Spurious Frequency f_{s4}
0.3	NC/DE	Improved	NC/DE	Improved	NC/DE
0.4	Improved	NC/DE	Improved	NC/DE	Improved
0.42	Improved	NC/DE	Improved	NC/DE	Improved
0.5	Improved	NC/DE	Improved	NC/DE	Improved
0.55	Improved	NC/DE	NC/DE	Improved	NC/DE
0.6	Improved	Improved	NC/DE	Improved	NC/DE
0.65	Improved	Improved	NC/DE	NC/DE	Improved
0.7	Improved	Improved	NC/DE	NC/DE	NC/DE

5.3. THE MODIFIED SKEW-SYMMETRICAL ASYMMETRIC SIR FILTER

5.3.1 SS-ASIR Filter with Open Stub and Folded Coupled Lines

In the skew-symmetrical asymmetric SIR filter, open stubs can be added to the low impedance lines, and the high impedance coupled lines can be folded, to achieve

optimized performance. This geometry and its equivalent circuit are shown in Figure 5.5 and Figure 5.6, respectively. When two open stubs are moved from point A to C, the suppression performance of f_{s3} and f_{s4} becomes continuously better while the return loss performance of f_{s2} becomes worse from A to B and better from B to C. Meanwhile, the insertion loss and return loss performance of fundamental frequency f_o remains almost the same in this process. Therefore, two open stubs are placed at point C. Figure 5.7 shows the open stub effect on the frequency response of SS-ASIR filter. The high impedance lines are also folded to form the section of length H1 between the high and low impedance lines. Compared to conventional coupled lines that are not folded, the suppression of unwanted transmission at frequency f_{s4} is greatly improved when the interval H1 varies from 0.5 mm to 0.9 mm. The change in the frequency response for this variation of H1 is plotted in Figure 5.8.

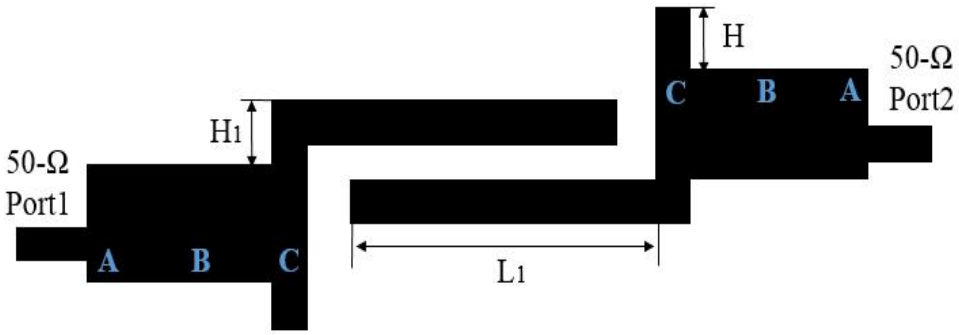

Figure 5.5 The geometry of an SS-ASIR filter with open stubs and folded coupled lines.

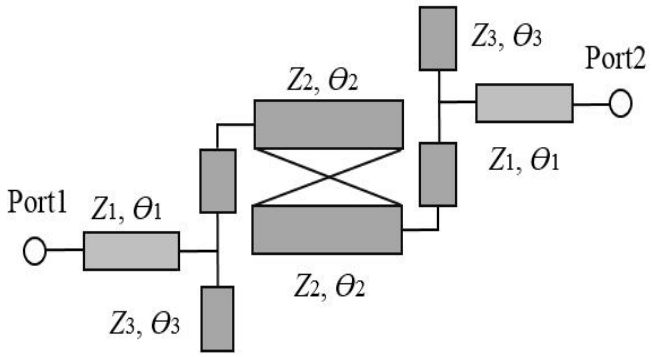

Figure 5.6. The equivalent circuit of an SS-ASIR filter with open stubs and folded coupled lines.

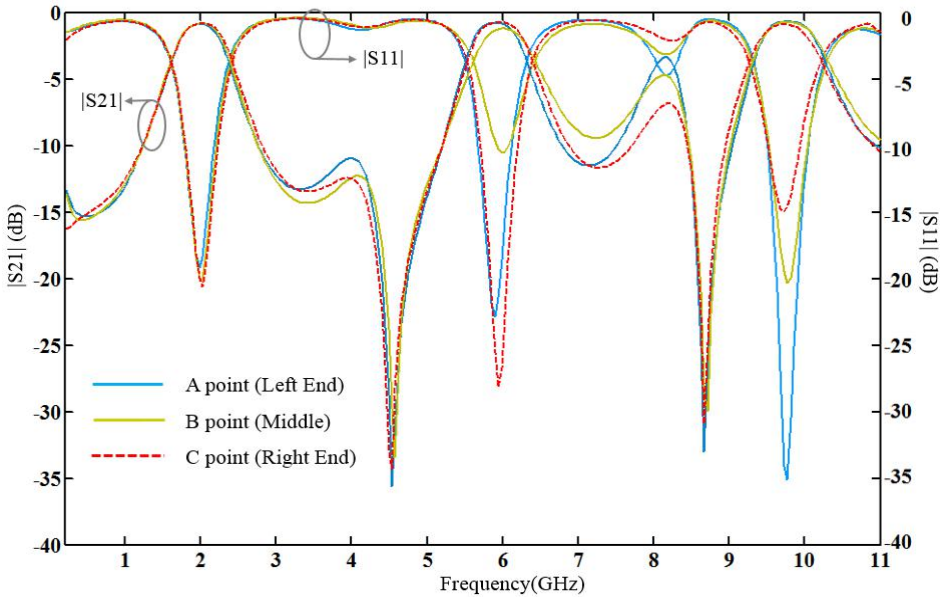

Figure 5.7. The open stub effect on the frequency response of an SS-ASIR filter.

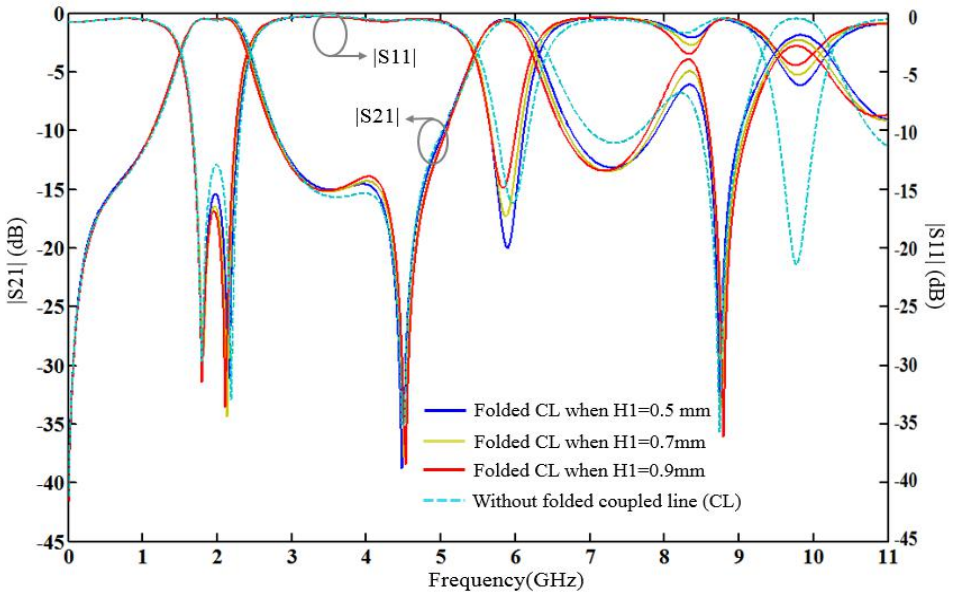

Figure 5.8. The frequency response of a modified SS-ASIR filter versus frequency when H1 varies from 0.5 mm to 0.9mm.

5.3.2. The Modified SS-ASIR Filter with Interdigital Cross-Coupled Line (ICCL)

To further optimize the in-band and out of band performance of the proposed dual-band filter, auxiliary interdigital cross-coupled lines whose width and length are W_5 and L_5

are utilized to realize the multi-path coupling effect between two modified ASIRs (MASIRs), as seen in Figure 5.9 (a). Compared to the single coupling route of A-C, at least two extra coupling routes including A-D and B-C are created by the inclusion of the auxiliary coupled lines. This interdigital multi-path coupling scheme of the modified SS-ASIR filter is shown in Figure 5.9(b). Moreover, because of the small distance between the main and auxiliary coupled lines, mutual coupling of A-B and C-D exists at the same time. This kind of mutual coupling is illustrated as dashed grey lines in Figure 5.9 (b).

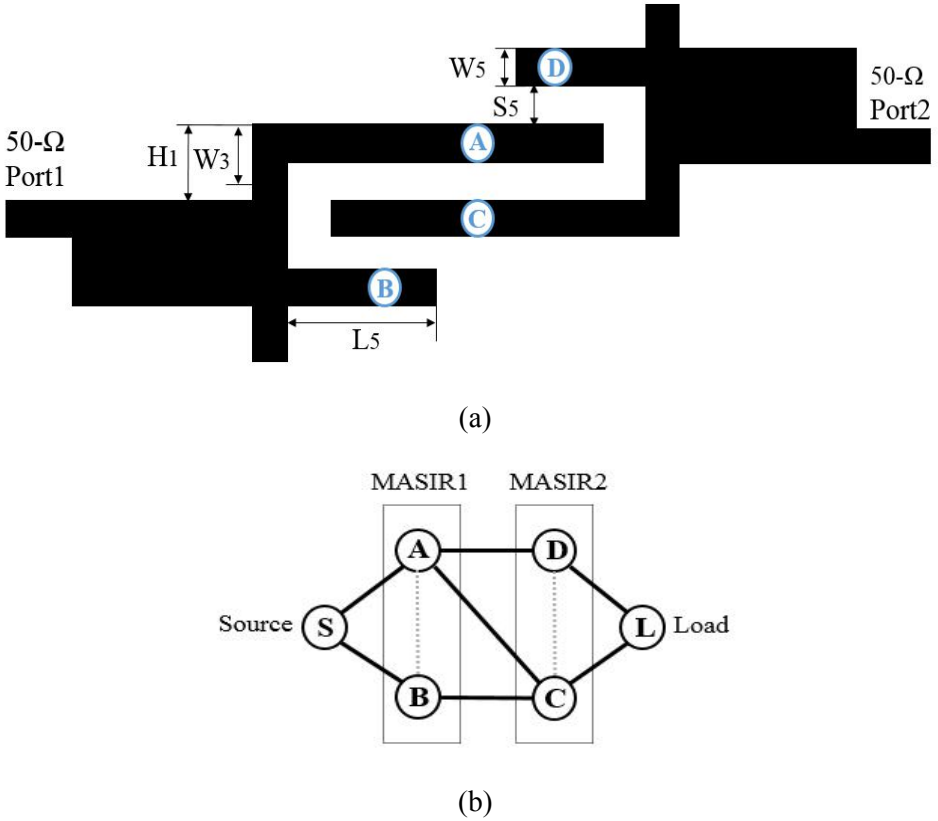

Figure 5.9. Schematic diagram of the modified SS-ASIR coupled pair with interdigital cross coupled lines. (a)Structure. (b) Coupling routing scheme. A, B denotes the main coupling line and auxiliary cross coupling in MASIR1, respectively.
C, D denotes the main coupling line and auxiliary cross coupling in MASIR2, respectively.

By including auxiliary coupled lines, the filter's out-of-band spurious frequency suppression performance and passband selectivity is considerably improved. The

designed dual-band band-pass filter (BPF) adopting an interdigital cross-coupled configuration produces a transmission zero (TZ) to approach f_{s3} and f_{s4}. The transmission zero occurs because of the cancellation of the transmitted signals passing through different routes. As seen in Figure 5.10, when the length of auxiliary coupled line L_5 ranges from 1.4-1.8 mm, the optimized suppression performance of f_{s3} and f_{s4} is achieved. Also a wide stop-band ranging from 6.3-12 GHz at the upper side of the second pass-band is realized simultaneously. Besides, the second pass-band upper side's selectivity is improved with the two pass-bands' return losses and insertion losses performance not being influenced. Figure 5.11 plots Q_{ex1}, Q_{ex2}, f_{s2}/f_0 and Q_{ex2}/Q_{ex1} versus varying S_5, which is the gap between the auxiliary-coupled and main-coupled line in the interdigital cross-coupled SS-ASIR filter.

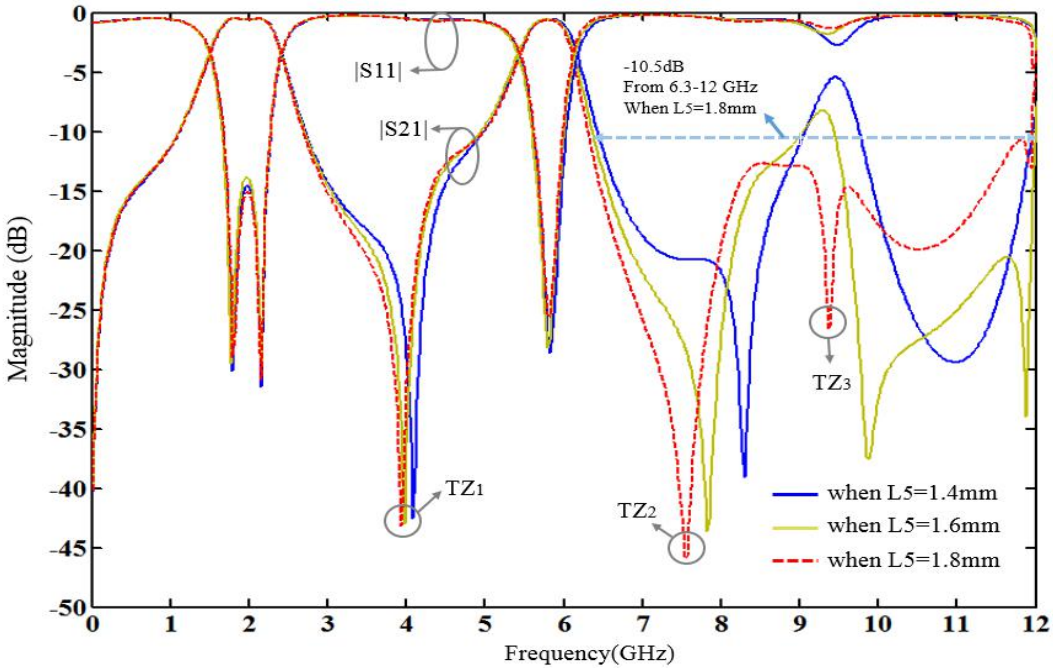

Figure 5.10. The effect of L5 on the interdigital cross-coupled SS-ASIR.

Meanwhile, Q_{ex2} decreases at first and increases a little later, which means that the bandwidth of f_{s2} can be controlled and expanded by tuning S_5. Therefore, S5 is a factor

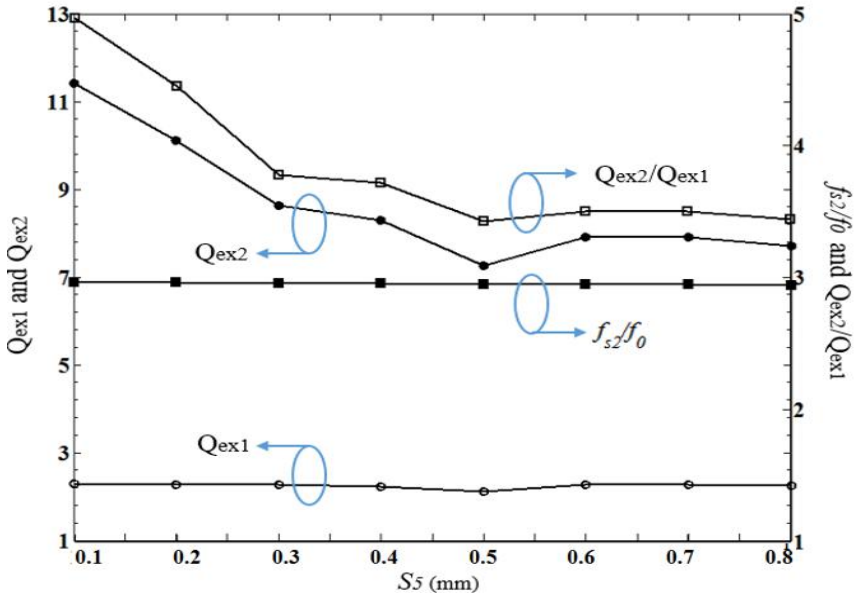

Figure 5.11. Q_{ex1}, Q_{ex2}, f_{s2}/f_0 and Q_{ex2}/Q_{ex1} versus S_5.

that can tune Q_{ex2} and $\overline{J_2}$ in SS-ASIRs with interdigital cross coupled line structure.

The proposed filters were fabricated on RO3010 substrate with a relative permittivity of 10.2, and measured using an HP8550 vector network analyser. Firstly, the calibration of the network analyser is processed. Calibration is done by attaching the various Short, Open, Load, & Thru standards to your cables and then pressing buttons on the Calibrate menu. When you push Done, the analyzer calculates the correction coefficients it will apply to all subsequent measurements. The simulated *S*-parameters which are obtained from HFSS simulation and measured *S*-parameters of the designed dual-wideband SS-ASIRs with ICCLs are plotted in Figure 5.12. Good agreement is observed between the simulated and measured results and the slight discrepancies are attributed to the loss, fabrication errors, and so on. It can be seen that dual wide-bands are realized with good in-band return loss performance. The first pass-band ranges from 1.47-2.28 GHz with central frequency of 1.875 GHz, bandwidth of 810 MHz and fractional band width

(FBW) of 43.2%. It would be applicable to bands for Global Positioning System (GPS: frequency band centred at 1.57 GHz), Global System for Mobile Communication (GSM: 1800/1900 MHz) and Universal Mobile Telecommunication System (UMTS: 1710-1880/1850-1990/1920-2170 MHz etc.). The second pass-band ranges from 5.23-5.81 GHz with central frequency of 5.52GHz, bandwidth of 580 MHz and fractional band width (FBW) of 10.5%. It can be used in IEEE802.11a WLAN applications including 5G Wi-Fi. Moreover, good isolation is achieved between the two pass-bands to eliminate the signal interference between dual-bands.

The stop-band ranges from 2.56-4.86 GHz with -10 dB suppression level. Due to the adoption of interdigital cross-coupled line structure, an extra transmission zero approaching to f_{s3} and f_{s4} is created. A wide upper stop-band ranging from 6.05-12.1 GHz with -10 dB suppression level is generated, which can be seen in Figure 5.12. The photograph of the fabricated dual-wideband SS-ASIRs with ICCLs is Figure 5.13.

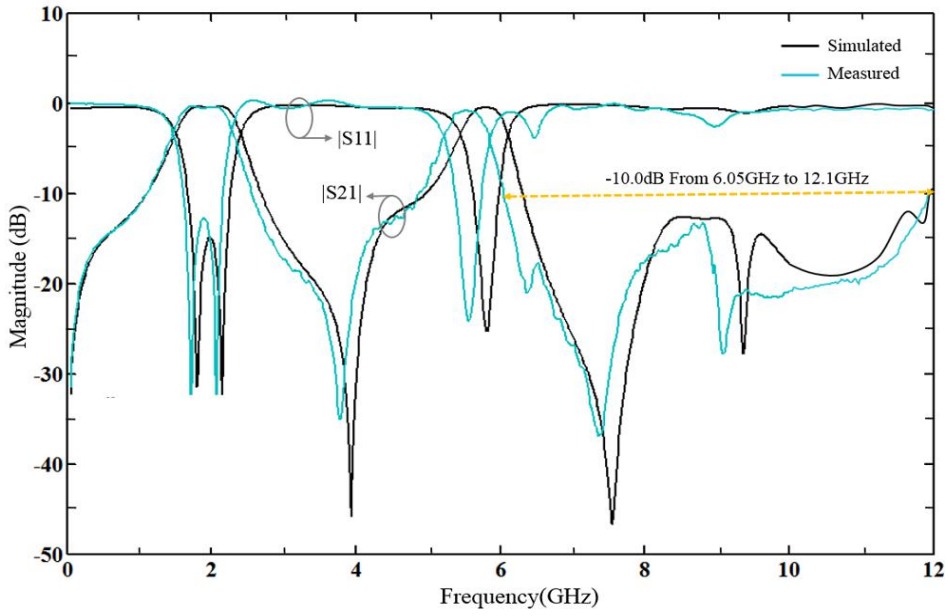

(a)

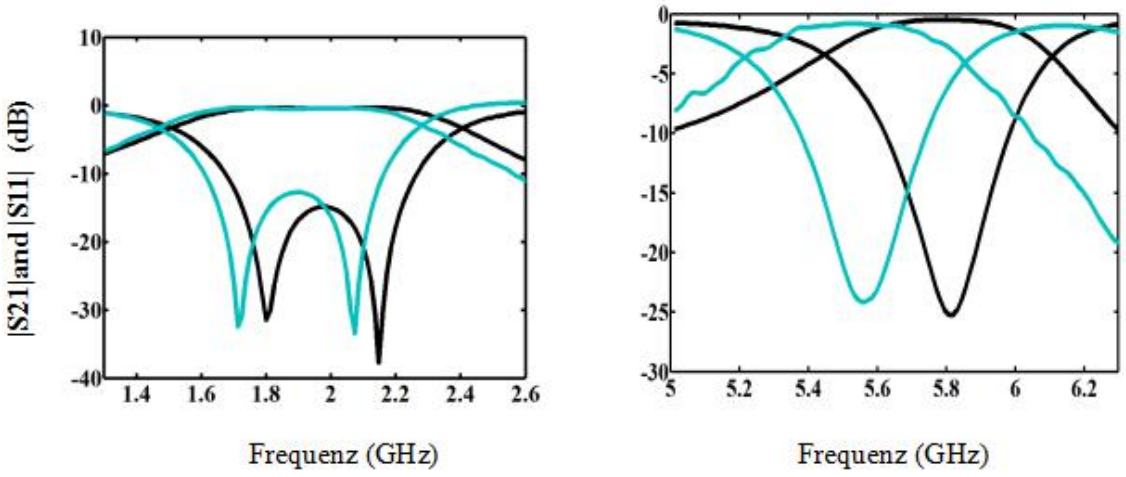

(b) (c)

Figure 5.12. (a) Simulated and measured results of in SS-ASIRs with ICCLs.
(b) Narrowband view of the first passband. (c) Narrowband view of the second passband.

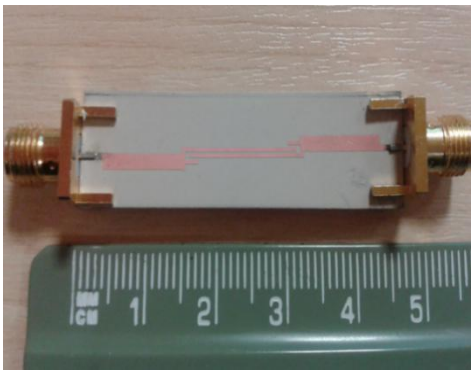

Figure 5.13. The photograph of the fabricated design.

5.3.3. The Modified SS-ASIR Filter with Parallel Uncoupled Microstrip Lines (PUMLs)

An uncoupled section located within conventional coupled lines is a useful method to achieve extra transmission zeros closing to existing zeros, created by the conventional coupled lines. Therefore, a wider stopband bandwidth with better suppression level can

be achieved. At the same time, this way can also add the freedom to optimize the in band performance of the original structure.

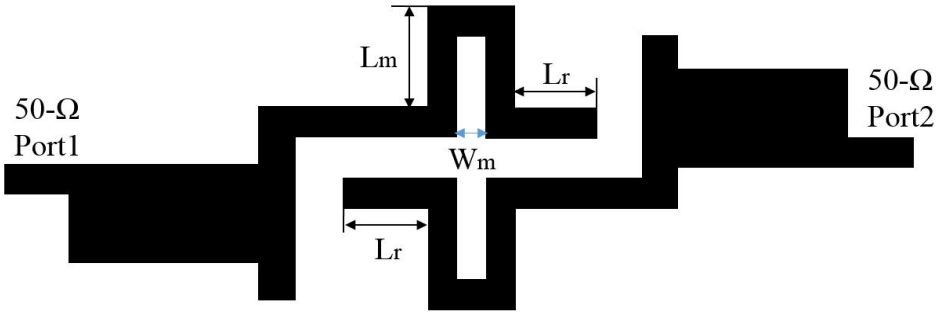

Figure 5.14. Schematic diagram of the proposed modified SS-ASIR filter with parallel uncouple microstrip lines.

Figure 5.14 shows the topological structure of the proposed modified SS-ASIR filter with parallel uncoupled microstrip lines. These parallel uncoupled microstrip lines are formed by bending the original coupled lines outwards. The parallel uncoupled microstrip line's reference location to the original coupled line open end is L_r. The parallel uncoupled microstrip line height and inner gap is Lm and Wm, respectively. Compared to the former modified SS-ASIR filter with interdigital cross-coupled line structure, the wider second pass-band is achieved by adopting the novel parallel uncoupled microstrip lines. In the former structure, $Q_{ex1,2}$ is equal to 2.28 and 9.37 when S_5=0.25 mm (as shown in Figure 11), while $Q_{ex1,2}$ is equal to 2.71 and 3.48 when L_m=2.3 mm in this novel filter with PUMLs. This means $\overline{J_2}$ is improved greatly and a stronger coupling strength between two modified ASIRs is realized. Figure 5.13 plots the reference location parameter L_r's impact on the frequency response of the filter with parallel uncoupled microstrip lines. It is noted that when L_r changes from 5.6 mm to 7 mm, the second pass-band return loss performance is enhanced considerably and its

bandwidth becomes wider resulting in forming a wide second pass-band of more than 1.5 GHz. Meanwhile, the frequency response of the first pass-band does not vary much. Hence, L_r is a vital factor to influence $\overline{J_2}$ and Q_{ex2}. Moreover, the parallel uncoupled microstrip line structure achieves one extra transmission zero nearby f_{s3} and f_{s4}, leading to the extended wide stopband bandwidth with the better suppression level, as seen in Figure 5.15.

Figures 5.16 and 5.17 show L_m's impact on the frequency response of the SS-ASIR filter with PUMLs. In Figure 5.16, when L_m ranges from 0.5 mm to 5 mm, the fundamental frequency f_0 decreases continuously while Q_{ex1} increases slightly at first and increases dramatically when Lm is greater than 2.5 mm. This represents parallel uncoupled microstrip line height Lm can increase Q_{ex1} and decrease $\overline{J_1}$ within a certain range. Figure 5.17 plots the f_{s2}, Q_{ex2}, f_{s2}/f_0 and Q_{ex2}/Q_{ex1} versus L_m. When Lm ranges from 0.5 mm to 1.5 mm, the decline speed of Q_{ex2} is much faster than the decline speed of f_{s2}, which means the bandwidth centred at f_{s2} is growing rapidly. When Lm ranges from 1.5 mm to 2.5 mm, the decline speed of Q_{ex2} is almost the same as the decline speed of f_{s2}, which means wide-band width centred at f_{s2} is formed and changes not much. When Lm ranges from 2.5 mm to 5 mm, Q_{ex2} increases as f_{s2} decreases, which means which means the band centred at f_{s2} becomes narrower. In the whole process, f_{s2} moves from 5.6 GHz to 3.8 GHz with the second pass-band being expanded to more than 1.5 GHz. Hence, Lm is also a factor to influence Q_{ex2} and strengthen $\overline{J_2}$.

The reason for this can be explained by the analysis of the parallel uncoupled microstrip line unit, whose topological structure and frequency response are plotted in Figure 5.18.

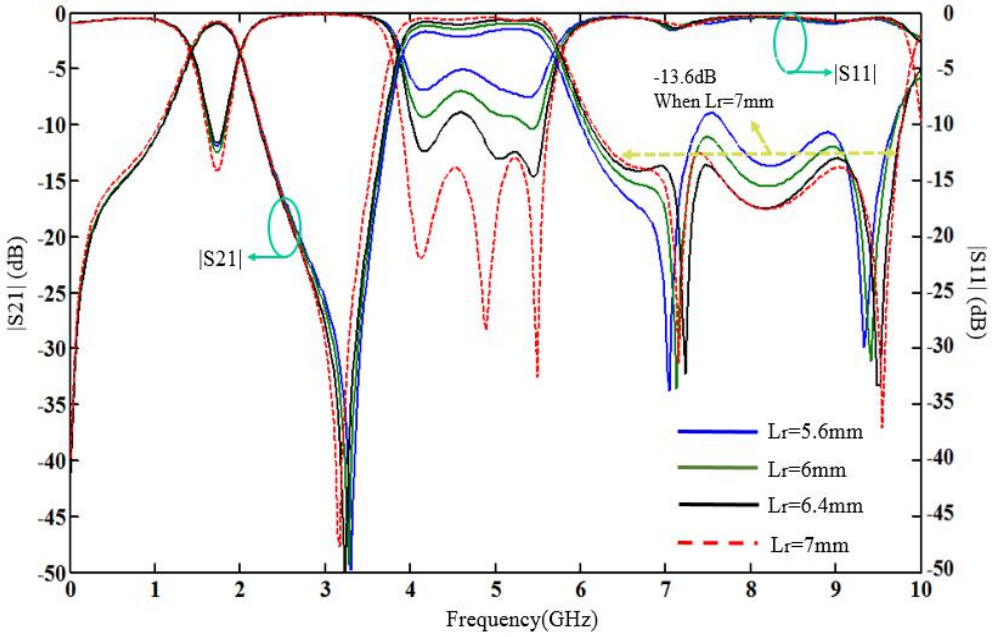

Figure 5.15. Lr's impact on the frequency response of the SS-ASIR filter with PUMLs.

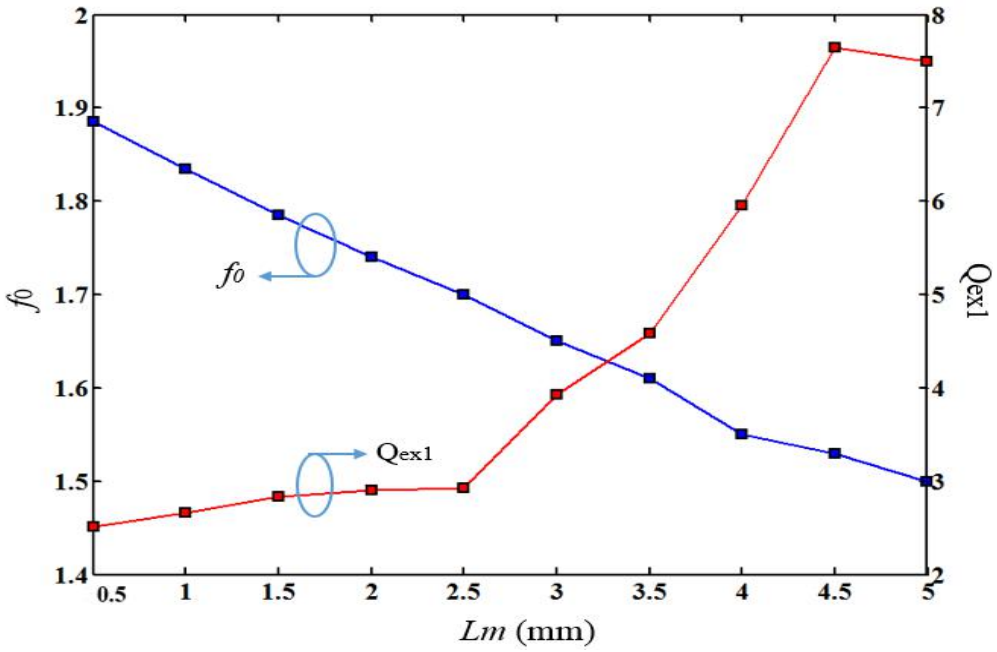

Figure 5.16. f_0 and Q_{ex1} versus Lm.

As seen in the Figure, the PUML unit forms a wide pass-band of more than 1 GHz when Lm changes from 1 mm to 3 mm. Lm. This result proves the advantage of the PUML structure to optimize the in-band performance of the filter. As for out-of-band

performance, the PUML unit generates three transmission zeros (TZs) at both sides of the pass-band, as plotted in Figure 5.18. These three TZs can improve the isolation performance between two pass-bands and the suppression level of undesired f_{s3} and f_{s4}.

The simulated and measured *S*-parameters of the designed dual-wideband SS-ASIRs with PUMLs are plotted in Figure 5.19. Good agreement can be observed between the simulated and measured results and the slight discrepancies are attributed to the loss, fabricated errors and so on.

It can be seen that dual wide-bands are realized with good in-band return loss performance. The first pass-band ranges from 1.37-1.89 GHz with a central frequency of 1.63 GHz, bandwidth of 520 MHz and fractional band width (FBW) of 31.9%. It can be applied to the Global Positioning System (GPS: frequency band centred at 1.57 GHz), Global System for Mobile Communication (GSM: 1800 MHz) and Universal Mobile

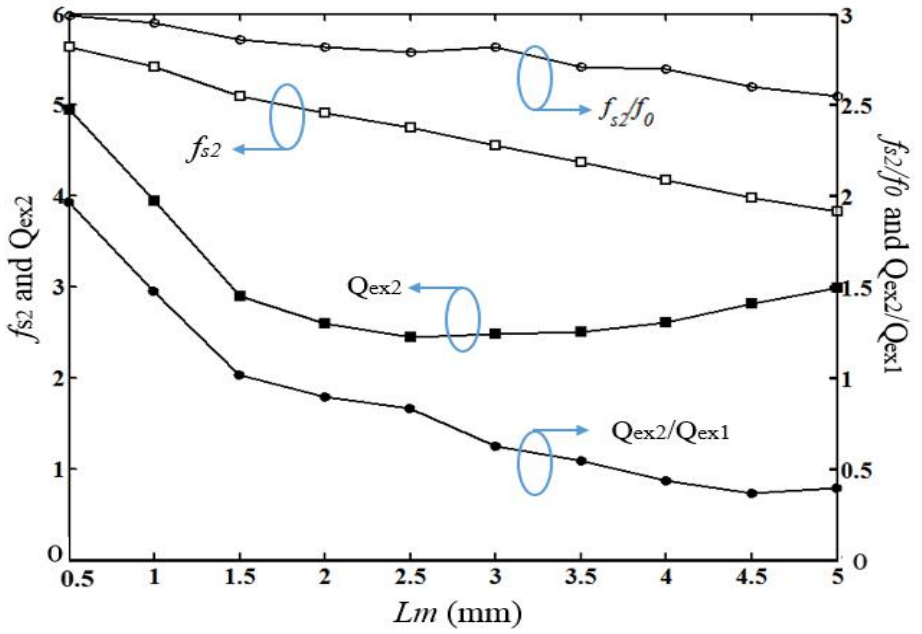

Figure 5.17. f_{s2}, Q_{ex2}, f_{s2}/f_0 and Q_{ex2}/Q_{ex1} versus Lm.

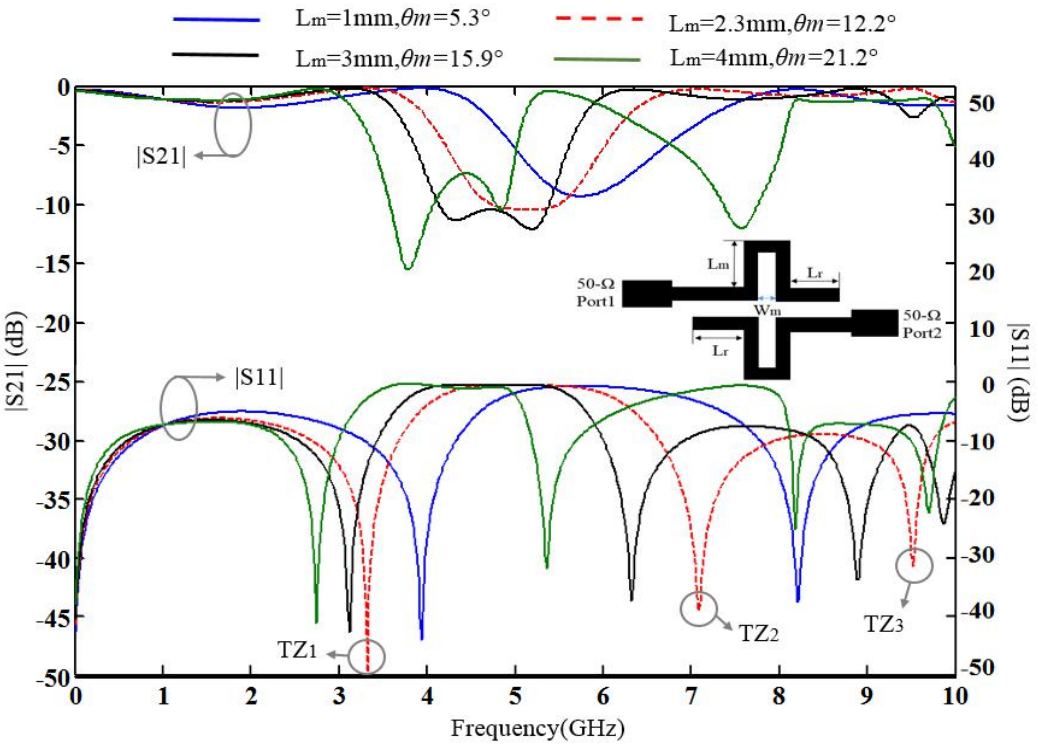

Figure 5.18. The analysis of the PUML unit.

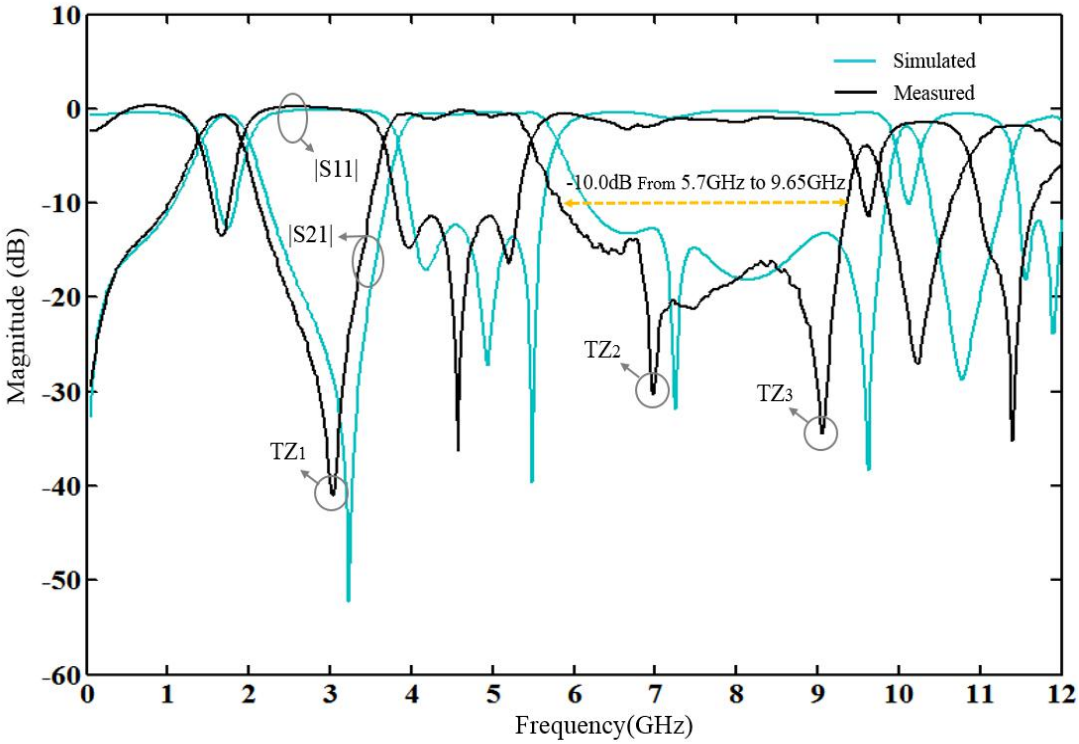

Figure 5.19. Simulated and measured results of SS-ASIRs with PUMLs.

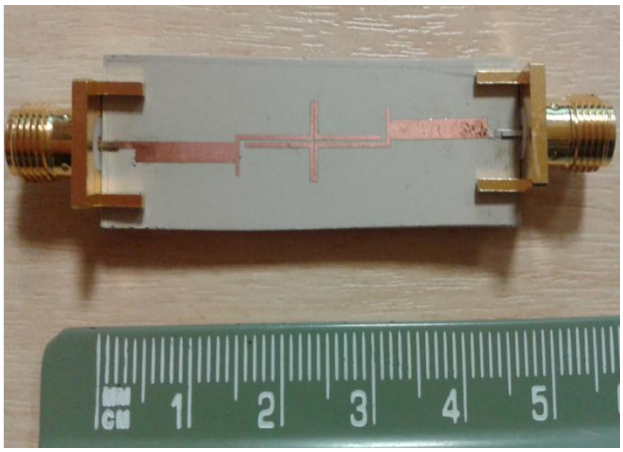

Figure 5.20. The photograph of the fabricated SS-ASIRs with PUMLs.

Telecommunication System (UMTS: 1710-1880 MHz etc.). The second pass-band ranges from 3.66-5.46 GHz with central frequency of 4.46 GHz, bandwidth of 1.8 GHz and fractional band width (FBW) of 33.0%. It can be used in IEEE802.11a WLAN applications including 5G Wi-Fi. Moreover, good isolation is achieved between two pass-bands to eliminate the signal interference between dual-bands. The stop-band ranges from 2.12-3.5 GHz with -10 dB suppression level. Due to the adoption of parallel uncoupled microstrip lines, extra transmission zero approaching to f_{s3} and f_{s4} is realized. A wide upper stop-band ranging from 5.83-9.35 GHz with -10 dB suppression level is generated, which can be seen in Figure 5.18. The photograph of the fabricated dual-wideband SS-ASIRs with PUMLs is shown in Figure 5.20.

The parameters of modified SS-ASIR with parallel uncoupled microstrip lines are shown in Table 5.2. The modified SS-ASIR filter with ICCLs and PUMLs performance comparison to previously proposed works are shown in Table 5.3. It can be seen that the proposed structures have the advantages of big fractional bandwidths,the fractional

Table5. 2

PARAMETERS OF THE PROPOSED
FOUR TYPES OF MODIFIED SS-ASIR FILTERS.
ALL DIMENSIONS ARE IN MILLIMETRES.

Filter Type / parameter	The Modified SS-ASIR Filter	The Modified SS-ASIR Filter with ICCLs	The Modified SS-ASIR Filter with PUMLs	The Modified SS-ASIR Filter with DRS
L_1	11	11	11	11
L_2	15. 6	15. 6	15. 6	15. 6
W_1	1. 6	1. 6	1. 6	1. 6
W_3	0. 4	0. 4	0. 4	0. 4
L_5		1. 81		
S_5		0. 25		
W_5		0. 42		
L_r			7. 05	
L_m			2. 32	
W_m			0. 07	
Rd				0. 6
W_d				4. 65
H_d				1. 2

Table 5.3

#PERFORMANCE COMPARISON OF THE MODIFIED SS-ASIR FILTER WITH (A) ICCLS AND (B) PUMLS.

	CF (GHz)	-3dB FBW	IL at CF(dB)	Size	Wide stop-band Restriction	Extra structure
[28]	2.4/5.26	13.7/6.3	0.6/1.4	0.46 λ_g × 0.42 λ_g	NO	NONE
[29]	2.43/3.73	4.5/6.1	2.5/1.3	0.43 λ_g × 0.69 λ_g	NO	NONE
[37]	2.4/3.5	6.88/8.57	<0.3	0.25 λ_g × 0.4 λ_g	NO	HTS
[21] Filter B	1.65/5.25	35.1/7.2	0.41/1.1	0.33 λ_g × 0.03 λ_g	NO	VIA HOLE
This work (A)	**1.875/5.52**	**43.2/10.5**	**0.39/0.87**	**0.05 λ_g × 0.56 λ_g**	**YES**	**NONE**
This work (B)	**1.63/4.46**	**31.9/33.0**	**0.70/0.12**	**0.09 λ_g × 0.56 λ_g**	**YES**	**NONE**

pass band insertion losses are less than 1dB, there is a wide stop band and no extra structures.

The design procedures are listed:

The simulations use HFSS software and optimization is set to achieve an insertion loss of less than 2dB with a return loss better than -10dB.

1) Decide the total length of the ASIR structure according to the fundamental frequency;

2) For the ICCL structure, decide the dimension of the high impedance line according to the second pass band;

3) For the PUML structure, decide the parameter Lr according to the return loss, and decide the parameter Lm according to the the second pass band.

5.3.4 The Modified SS-ASIR Filter with Defected Rectangular Structure (DRS)

The topological structure of the proposed modified skew-symmetrical asymmetric SIR Filter with defected structure is shown in Figure 5.21 (a). In contrast to the original skew-symmetrical asymmetric SIR filter, the proposed modified SS-ASIR Filter has a defected rectangular structure (DRS) in each low impedance line.

The defected rectangular structure's width and length is W_d and H_d, respectively. Its relative distance to the end of feed line is Rd.

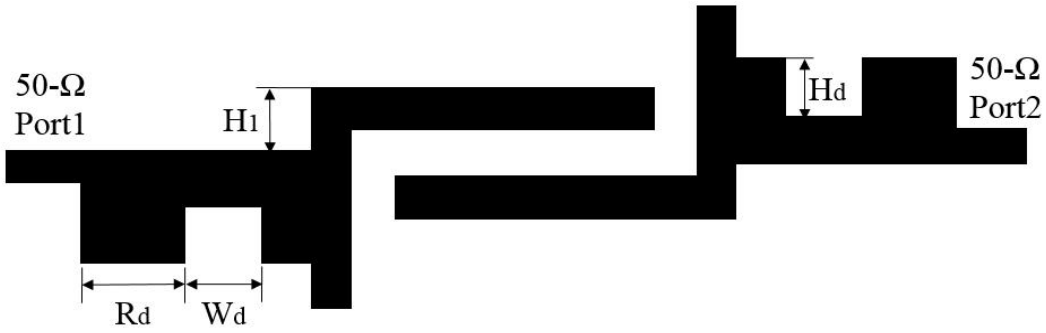

(a)

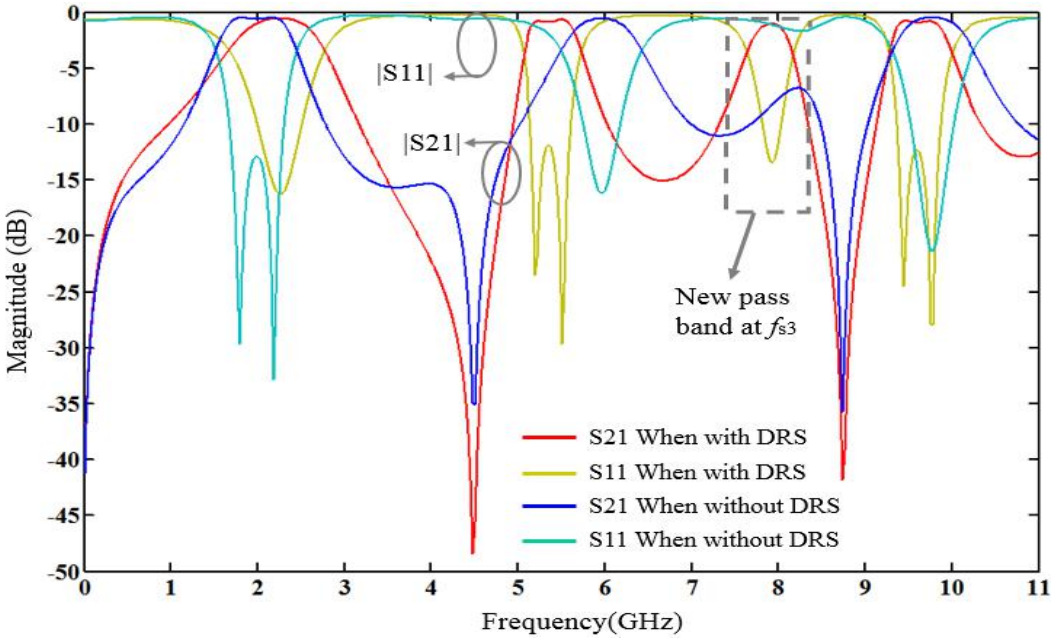

(b)

Figure 5.21. Schematic diagram of the modified SS-ASIR filter with DRS: (a) structure (b) The frequency response comparison of SS-ASIR filter with and without DRS.

By utilizing the defected rectangular structure, the performance-degraded frequency response at *f*s3 can be transformed into performance-enhanced frequency response and new wide pass-band can be excited centred at *f*s3. The frequency response comparison between the cases when modified SS-ASIR filter with and without DRS is plotted in Figure 5.21 (b).

By this means, the quad-band filter can be formed by adopting the defected rectangular structure in the SS-ASIR filter.

Figure 5.22 plots W_d's effect on the SS-ASIR filter with DRS. In (a), when W_d varies from 2.5 to 6 mm, f_{s2}/f_0 decreases while Q_{ex1} remains almost the same. And Q_{ex2} and Q_{ex2}/Q_{ex1} fluctuates in this process. This means f_{s2} does not follow the rules of invariance of resonant frequency location in the SS-ASIR coupled structure any more. In (b), Q_{ex3} varies from 12.1 to 26.8 and Q_{ex4} varies from 18.1 to 16 when W_d ranges from 2.5 to 6 mm. Q_{ex3}/Q_{ex1} increases continuously in this process.

From EM simulations, it is noted that all f_{s2}, f_{s3} and f_{s4} does not obey the rules of invariance of resonant frequency location in SS-ASIR coupled structure with DRS. And the frequency shifting exists among all four pass-bands compared to the occasion when there is no DRS. This is because the basic structure of SS-ASIR coupled pair is modified by the defected rectangular structure.

The simulated *S*-parameters and measured *S*-parameters of the designed quad-wideband SS-ASIR filter with DMS are plotted in Figure 5.23. Good agreement can be observed between the simulated and measured results and the discrepancies are attributed to the loss, fabricated errors and so on. It can be seen that dual wide-bands are realized with good in-band return loss performance. The first pass-band ranges from 1.64GHz-2.62 GHz with a central frequency of 2.13GHz, bandwidth of 980MHz and fractional bandwidth (FBW) of 46.0%. It can be used in the application of Global System for Mobile Communication (GSM: 1800 MHz/1900 MHz), Universal Mobile Telecommunication System (UMTS: 1710-1880MHz/1850-1990MHz/1920-2170 MHz

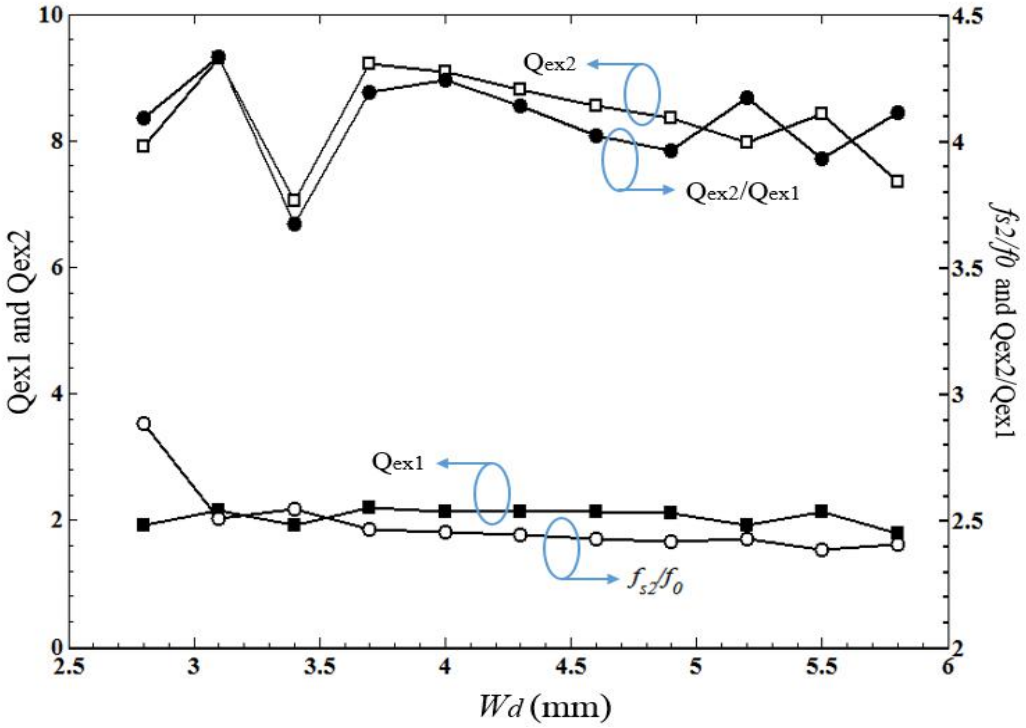

(a)

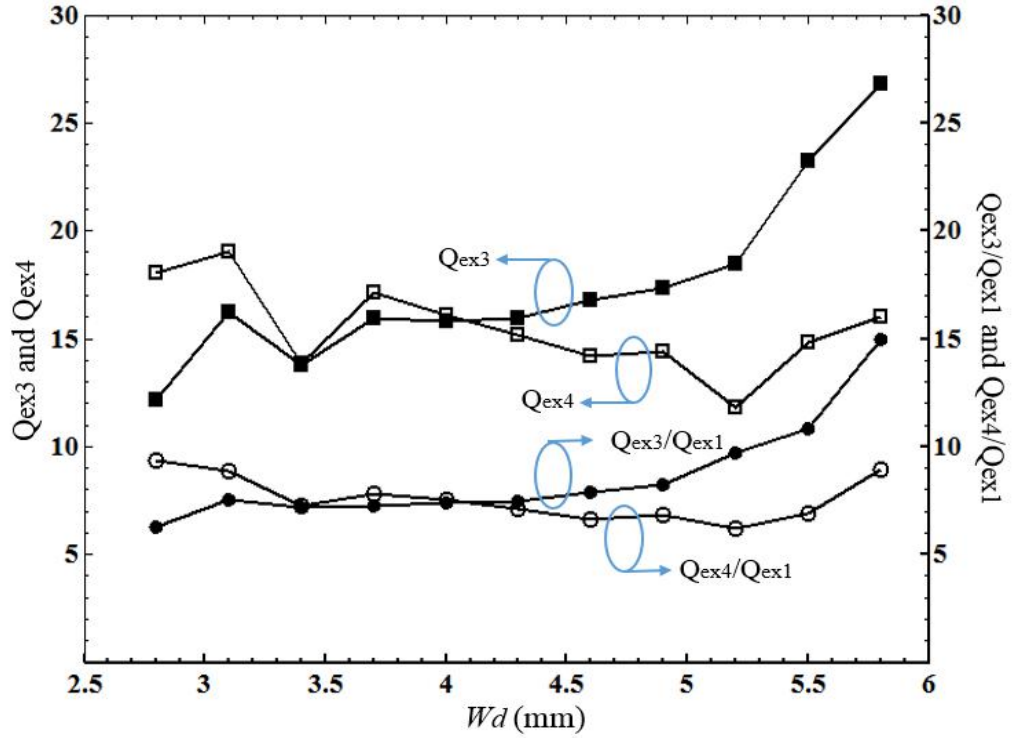

(b)

Figure 5.22. Wd's effect on SS-ASIR filter with DRS. (a) Q_{ex1}, Q_{ex2}, $fs2/f_0$ and Q_{ex2}/Q_{ex1} Versus Wd. (b) Q_{ex3}, Q_{ex4}, Q_{ex3}/Q_{ex1} and Q_{ex4}/Q_{ex1} versus against Wd.

etc.), ISM (Industry Science Medicine: 2.4GHz. The second pass-band ranges from 4.95GHz-5.55GHz with a central frequency of 5.25GHz, bandwidth of 600MHz and fractional band width (FBW) of 11.4%. It can be used in IEEE802.11a WLAN applications.

The third pass-band ranges from 7.51GHz-7.86 GHz with a central frequency of 7.685GHz, bandwidth of 350MHz FBW of 4.6%. It can be used in electronic countermeasure applications. The fourth pass-band ranges from 9.06GHz-9.56 GHz with a central frequency of 9.31 GHz, bandwidth of 500MHz and FBW of 5.4%.It can be used in X-band applications.

Moreover, good isolation is achieved between four pass-bands to eliminate the signal interference among quad-bands. The -10 dB suppression level stop-bands which ranges from 3.05GHz-4.78 GHz between the first and second pass-band,5.77GHz-7.20GHz between the second and third pass-band, 8.04GHz-8.889GHz between the third and fourth pass-band are realized.

What is more, two transmission zeroes located at 4.26GHz and 8.46GHz are formed to further enhance frequency selectivity, which are illustrated in Figure 5.23.

The parameters of modified SS-ASIR with DMS are shown in Table 5.2. The size of the modified SS-ASIRs with DMS is $0.09\lambda_g \times 0.56\lambda_g$, where λ_g is the guided wavelength. The photograph of the fabricated quad-wideband SS-ASIR filter with DMS is plotted in Figure 5.24.

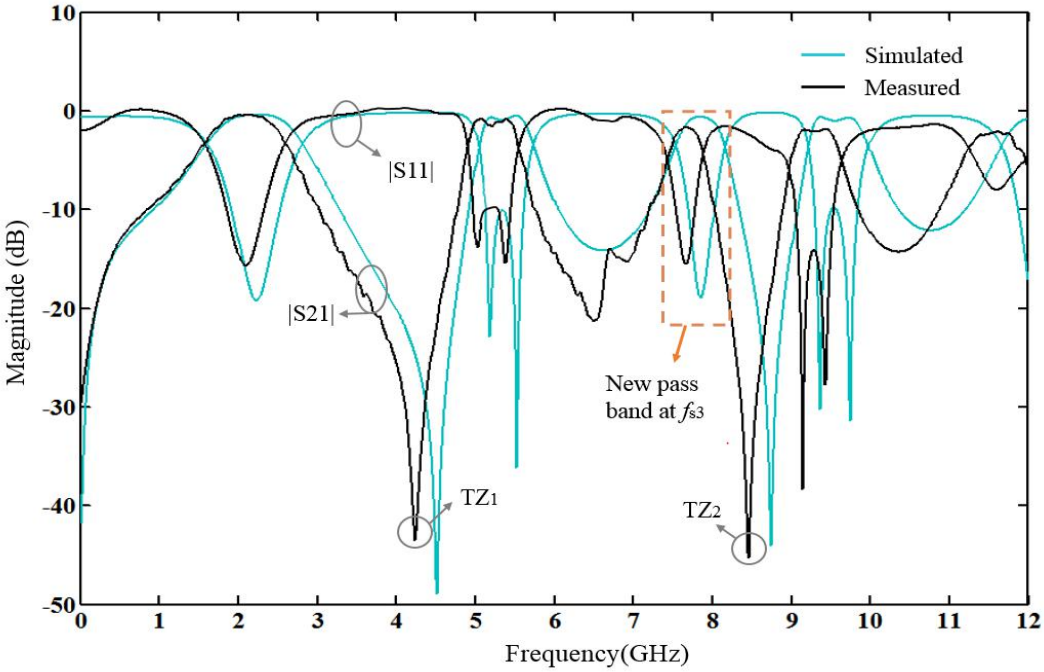

Figure 5.23. Simulated and measured of the modified SS-ASIRs with DMS.

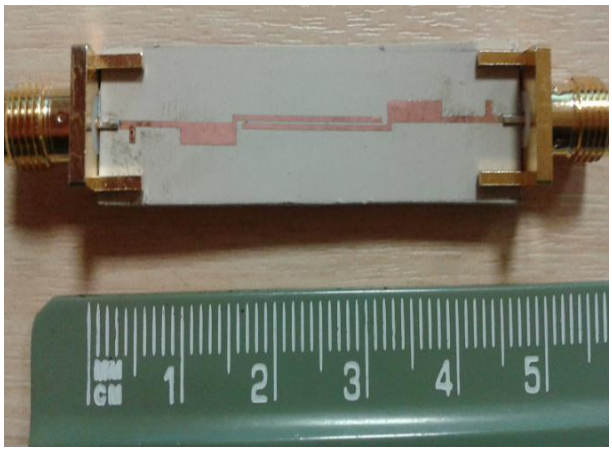

Figure 5.24. The photograph of the fabricated modified SS-ASIRs with DMS.

5.4 Conclusion

Multi-standard dual-wideband and quad-wideband filters based on the detailed analysis of the simple asymmetric SIR unit and of the skew-symmetrical asymmetric SIR

coupled pair have been presented. By utilizing a novel modified skew-symmetrical asymmetric SIR coupled pair with ICCLs and PUMLs, the proposed dual-band filters for the first time realize dual-wideband with wide stop-band restriction among the recently proposed dual-wideband filters. Their bandwidths are controllable by tuning relative parameters. By introducing DMS, the frequency band nearby the third spurious frequency is excited and formed, resulting in a quad-wideband filter. The proposed dual-wideband and quad-wideband modified SS-ASIR filters cover the communication applications including GPS, GSM, UMTS, ISM and IEEE 802.11 a/b/g/n/ac. The filters' measured results agree well with simulated results and theory predictions. The good in band and out of band performance, compact size and simple structure make the proposed filters very promising for applications in future multi-standard wireless communication.

5.5 References

[1] H. Miyake, S. Kitazawa, T. Ishizaki, et al. A miniaturized monolithic dual band filter using ceramic lamination technique for dual mode portable telephones. International Microwave Symposium. Digest. Vol. 2, pp: 789-792. June. 1997.

[2] Bian Wu, Chang-Hong Liang, Pei-Yuan Qin, et al. Compact Dual-Band Filter Using Defected Stepped Impedance Resonator. IEEE Microwave and Wireless Components Letters. Vol. 18. no. 10, pp: 674-676. 2008.

[3] Xin Gao, Lap Kun Yeung, Ke-Li Wu. A Dual-Band Balun Using Partially Coupled Stepped-Impedance Coupled-Line Resonators. IEEE Transactions on Microwave Theory and Techniques. Vol. 56, no. 6. pp: 1455-1460. 2008.

[4] Qing-Xin Chu, Fu-Chang Chen. A Compact Dual-Band band-pass Filter Using Meandering Stepped Impedance Resonators. IEEE Microwave and Wireless Components Letters. Vol. 18, no. 5. pp: 320-322. 2008.

[5] Yuan, H. -J. , Fan, Y. Compact microstrip dual-band filter with stepped-impedance resonators. Electronics Letters. Vol. 47. no. 24. pp: 1328. 2011.

[6] Wei-Shin Chang, Chi-Yang Chang. Analytical Design of Microstrip Short-Circuit Terminated Stepped-Impedance Resonator Dual-Band Filters. IEEE Transactions on Microwave Theory and Techniques. Vol. 59, no. 7. pp: 1730-1739. 2011.

[7] Songbai Zhang, Lei Zhu . Synthesis Design of Dual-Band Bandpass Filters with $\lambda/4$ Stepped-Impedance Resonators. IEEE Transactions on Microwave Theory and Techniques. Vol. 61, no. 5 (1). pp: 1812-1819. 2013.

[8] Ching-Wen Tang, Po-Hsien Wu. Design of a Planar Dual-Band band-pass Filter. IEEE Microwave and Wireless Components Letters. Vol. 21, no. 7. pp: 362 - 364, 2011.

[9] X. Y. Zhang, J. X. Chen, Q. Xue, et al. Dual-band band-pass filters using stub-loaded resonators. IEEE Microwave Wireless Component Letter. Vol. 17, no. 8, pp: 583-585, Aug. 2007.

[10] P. Mondal and M. K. Mandal. Design of dual-band band-pass filters using stub-loaded open-loop resonators. IEEE Transactions on Microwave Theory and Techniques. Vol. 56, no. 1, pp: 150-155, Jan. 2008.

[11] Li Gao, Xiu Yin Zhang. High-Selectivity Dual-Band band-pass Filter Using a Quad-Mode Resonator with Source-Load Coupling. IEEE Microwave and Wireless

Components Letters, Vol. 23, no. 9, pp: 474- 476, 2013.

[12] Shou-Jia Sun, Tao Su, Kun Deng, Bian Wu, Chang-Hong Liang. Compact Microstrip Dual-Band Bandpass Filter Using a Novel Stub-Loaded Quad-Mode Resonator. IEEE Microwave and Wireless Components Letters, Vol. 23 no. 9, pp: 465-467, 2013.

[13] Jin Xu, Wen Wu, Chen Miao . Compact Microstrip Dual-/Tri-/Quad-Band band-pass Filter Using Open Stubs Loaded Shorted Stepped-Impedance Resonator. IEEE Transactions on Microwave Theory and Techniques. Vol. 61, no. 9, pp: 3187- 3199, 2013.

[14] Jin Shi, Long-long Lin, Jian-Xin Chen, et al. Dual-Band band-pass Filter with Wide Stop-band Using One Stepped-Impedance Ring Resonator with Shorted Stubs. IEEE Microwave and Wireless Components Letters. Vol. 24, no. 7, pp: 442- 444, 2014.

[15] D. Ahn, J. S. Park, C. S. Kim, et al. A design of the low-pass filter using the novel microstrip defected ground structure. IEEE Transaction Microwave Theory Technique. Vol. 49, no. 1, pp: 86-93, Jan. 2001.

[16] A. Abdel-Rahman, A. K. Verma, A. Boutejdar, et al. Control of band-stop esponse of hi-low microstrip low-pass filter using slot in ground plane. IEEE Transactions

on Microwave Theory and Techniques. Vol. 52, no. 3, pp: 1008-1013, Mar. 2004.

[17] J. S. Yun, G. Y. Kim, J. S. Park, et al. A design of the novel coupled line band-pass filter using defected ground structure. IEEE Microwave Theory Technique Symposium, 2000.

[18] A. A-Rahman, A. R. Ali, S. Amari, et al. Compact band-pass filters using defected ground structure (DGS) coupled resonators IEEE MTT-S International Digest . Proceeding. pp: 1479-1482, 2005.

[19] J. -X. Chen, T. Y. Yum, J. -L. Li, et al. Dual-mode dual-band band-pass filter using stacked-loop structure. IEEE Microwave Wireless Component Letter. Vol. 16, no. 9, pp: 502-504, Jun. 2006.

[20] S. Fu, B. Wu, J. Chen, et al Novel second order dual-mode dual-band filters using capacitance loaded square loop resonator. IEEE Transaction on Microwave Theory Techniques. Vol. 60, no. 3, pp: 477-483, Mar. 2012.

[21] J. Xu, Wen Wu,C. Miao. Compact and Sharp Skirts Microstrip Dual-Mode Dual-Band Bandpass Filter Using a Single Quadruple-Mode Resonator (QMR). IEEE Transaction on Microwave Theory Techniques. Vol. 61, no. 3, pp. 1104-1113, March. 2013.

[22] J. Wang, L. Ge, K. Wang, and W. Wu. Compact microstrip dual-mode dual-band band-pass filter with wide stop-band. Electronic Letter. Vol. 47, no. 4, pp: 263-265, Jan. 2011.

[23] Y. -T. Kuo and C. Y. Chang. Analytical design of two-mode dual band filters using E-shaped resonators. IEEE Transaction on Microwave Theory and Techniques. Vol.60, no. 2, pp: 250-260, Feb. 2012.

[24] Y. C. Chiou, C. Y. Wu, and J. T. Kuo. New miniaturized dual-mode dual-band ring resonator band-pass filter with microwave C-sections. IEEE Microwave Wireless Component Letter. Vol. 20, no. 2, pp: 67-69, Feb. 2009.

[25] S. Luo, L. Zhu, and S. Sun. A dual-band ring resonator band-pass filter based on two pairs of degenerate modes. IEEE Transaction on Microwave Theory and Techniques. Vol. 58, no. 12, pp: 3427-3432, Dec. 2010.

[26] S. Sun. A dual-band band-pass filter using a single dual-mode ring resonator. IEEE Microwave Wireless Component Letter. Vol. 21, no. 6, pp: 298-300, June. 2011.

[27] Y. Sung. Dual-mode dual-band filter with band notch structures. IEEE Microwave Wireless Component Letter. Vol. 20, no. 2, pp: 73-75, Feb. 2010.

[28] Y. C. Li, H. Wong, and Q. Xue. Dual-mode dual-band filter based on a stub-loaded patch resonator. IEEE Microwave Wireless Component Letter. Vol. 21, no. 10, pp: 525-527, Oct. 2011.

[29] R. Zhang, L. Zhu, and S. Luo. Dual-mode dual-band band-pass filter using a single slotted circular patch resonator. IEEE Microwave Wireless Component Letter. Vol. 22, no. 5, pp: 233-235, May 2012.

[30] S. Darlington. Synthesis of reactance four poles which produce prescribed insertion loss characteristics. Journal of Mathematical Physics .Vol. 18, pp: 257-353.Sept. 1939.

[31] K. Jokela. Narrow-band stripline or microstrip filters with transmission zeros at real and imaginary frequencies. IEEE Transaction on Microwave Theory and Techniques. Vol. MTT-28, pp: 542-554, June 1980.

[32] S. J. Yao, R. R. Bonetti, and A. E. Williams. Generalized dual-plane multicoupled line filters. IEEE Transaction on Microwave Theory and Techniques. Vol. 41, no. 2, pp: 2182-2189, Dec. 1993.

[33] J. S. Hong and M. J. Lancaster. Couplings of microstrip square open loop resonators for cross-coupled planar microwave filters. IEEE Transaction on Microwave Theory and Techniques. Vol. 44, no. 1, pp: 2099-2109, Nov. 1996.

[34] J. S. Hong and M. J. Lancaster. Cross-Coupled Microstrip Hairpin-Resonator Filters. IEEE Transaction on Microwave Theory and Techniques. Vol. 46, no. 1, pp: 118-122, Jan 1998.

[35] A. L. C. Serrano, F. S. Correra, T. -P. Vuong, et al. Synthesis methodology applied to a tunable patch filter with independent frequency and bandwidth control. IEEE Transaction on Microwave Theory and Techniques. Vol. 60, no. 3, pp: 484-493, Mar. 2012.

[36]J. S. Hong and M. J. Lancaster. Microstrip Filter for RF/Microwave Applications. New York: Wiley, 2001.

[37] H. W. Liu, Pin Wen, X. M. Wang, Y. Wang, et al. Dual-Band High-Temperature Superconducting Hairpin-Resonator Bandpass Filter Based on Two Pairs of Nondegenerate Modes. IEEE Transaction on Applied Superconductivity. Vol. 25, no. 3, pp. 1-4, June 2015.

CHAPTER 6

Novel Multi-standard Single-/Tri-/Quint-Wideband Asymmetric Step Impedance Resonator Filters with tuneable transmission zeros

6.1 Overview of Single-band Filters and Design Background

Parallel-coupled microstrip lines have been found to be one of the most commonly used in many practical RF/microwave circuits such as resonators, baluns, amplifiers, couplers, and filters, due to their design simplicity, planar structure, and relatively wide-bandwidth [1]. In order to design parallel coupled-line filters with a relatively wide passband, enhancement to the coupling of the first and last coupled stages is required which increases the fabrication tolerance. Alternatively, three parallel-coupled line structures can be utilized to achieve wide-bandwidth with low fabrication tolerance due to their enhancement of coupling over the conventional two coupled lines. Various wideband or ultra-wideband bandpass filters (BPFs) using three parallel-coupled microstrip lines have been developed [2]-[37]. In [2], [3], BPFs are developed based on spectral domain technique to achieve wide pass-bands with up to 60% fractional bandwidth (FBW). In [4], a new wideband microstrip BPF with very narrow rejection

band is introduced using two sections of three coupled lines separated by one transmission line element. In [5], new configurations have been introduced to develop wideband BPFs. These types of filters achieve up to 80% FBW with poor out-of-band rejection level. Recently, three coupled lines have been increasingly implemented to develop multiple-mode resonator (MMR) filters with very wide pass-band [6]-[13].

Compared to the traditional stepped impedance resonator (SIR) with two step discontinuities, the asymmetric SIR (ASIR) has only one discontinuity but retains controllability of spurious modes. Thus, it combines the advantages of compact size, lower loss, and strong design feasibility, particularly in high-order BPFs such as dual band [31], triple band and quad band [22], because of its inherent higher order resonant modes.

Published coupled line ASIR structures can be classified into two types: anti-parallel-coupled or parallel-coupled ASIRs. The Anti-Parallel-Coupled ASIR (APC-ASIR), consisting of two ASIR units with their high and/or low impedance lines anti-coupled with each other, is usually folded at its open end. In [31], the high impedance lines of two ASIRs are bent and coupled with each other to form a signal transmission route, and the first spurious frequency is utilized to form the second operating band [32]. Because the frequency response characteristic of the anti-parallel-coupled line is determined by the frequency response characteristic of the ASIR, the APC-ASIR frequency response is easy to calculate. However, the bandwidth characteristic of the APC-ASIR structure [18, 31], as with the multi-stage coupled ASIR structure [33, 34], is usually limited within the narrow band

characteristic range and is not suitable to realize wide-band performance. Therefore, this approach cannot fully meet the multi-service requirement of current wireless communication.

The second type, the parallel-coupled ASIR structure, has ASIRs with their high impedance lines parallel coupled with each other: this is also called the skew-symmetrical ASIR (SS-ASIR) coupled pair. Using this kind of structure, characteristics of frequency response performance such as bandwidth, return loss and insertion loss can be greatly improved at some frequency points, without changing or degrading the performance generally. This facilitates designs with wide bandwidth and large fractional bandwidth, which is different from the narrow band characteristic exhibited in traditional ASIR structures [18, 31-32]. However, until now, the proposed ASIR structures could only realize narrow band characteristics [18, 31-34] or dual/quad-wideband characteristics, with the disadvantages of uncontrollable or limited transmission zeros seriously restricting their application range.

In this work, we propose novel multi-standard single/tri/quint-wideband rearranged ASIR filters to solve the problems mentioned above. The proposed filters are capable of generating wide operating bands which effectively cover the GPS/GSM/UMTS/IEEE 802.11a application in wireless communication systems, including GPS (1227 MHz, 1.57 GHZ), GSM1800/1900 (1710-1880 MHz, 1850-1990 MHz), and UMTS (1920-2170 MHz). These filters share the same original structure, with their performance optimized by tuning relative transmission zeros. Therefore, the design enjoys advantages of versatility and simplicity, with reduced

design complexity and cost. To the best of the authors' knowledge, the proposed ASIR filters realize for the first time a single wideband filter with wide stop-band and a quint-wideband filter at the same time, by using the same structure as in recently proposed single/multi-band filters [1-34]. Moreover, a quint-wideband filter can be realized with large fractional bandwidths for all operating bands in comparison with [25-27].

The proposed filters use the capacitive coupling of only two miniaturized ASIRs to realize single/tri/quint-wideband operation without adding any extra structure such as via holes or defected ground structure, which is also novel for single/multi-wideband filters [14-36].

6.2 The In-Band Performance Enhancement Method and Transmission Zeros Tuning Method

6.2.1. The In-Band Performance Enhancement Method

To enhance the filter in-band performance, the SS-ASIR structure is used. In the design, the frequency response transformation relationship between the parallel-coupled ASIR and the ASIR unit needs to be considered so as to enhance the performance in the desired frequency band. The transformation relationship table is shown in Table 6.1. The electrical length ratio $\alpha = \theta_2/ (\theta_2+\theta_1)$, where θ_1 and θ_2 are the electrical lengths of section L_2 and L_1 in the ASIR, respectively. The characteristic impedance ratio $K = Z_2/Z_1$, where Z_1 and Z_2 is the characteristic impedance of section L_2 and L_1 in the ASIR, respectively. ''Improved''

meanssignificantly enhanced performance at relative frequency, ‘‘NC/DE’’ means no significant change or degradation of performance at relative frequency point.

Table 6.1

THE TRANSFORMATION RELATIONSHIP OF IN-BAND PERFORMANCE OF SS-ASIR COUPLED PAIR AND ASIR UNIT, WHEN α RANGES FROM 0.4 TO 0.7.

f / α	Fundament-al Frequency f_0	First spurious Frequency f_{s1}	Second spurious Frequency f_{s2}	Third Spurious Frequency f_{s4}	Fourth Spurious Frequency f_{s4}
0.4	Improved	NC/DE	Improved	NC/DE	Improved
0.42	Improved	NC/DE	Improved	NC/DE	Improved
0.5	Improved	NC/DE	Improved	NC/DE	Improved
0.55	Improved	NC/DE	NC/DE	Improved	NC/DE
0.57	Improved	NC/DE	Improved	Improved	NC/DE
0.6	Improved	Improved	NC/DE	Improved	NC/DE
0.65	Improved	Improved	NC/DE	NC/DE	Improved
0.7	Improved	Improved	NC/DE	NC/DE	NC/DE

6.2.2. The Transmission Zeros Generating and Tuning Method in the SS-ASIR Structure

Figure 6.1 (a) shows the topological structure of the SS-ASIR couple pair rearranged by the meander coupled section (SSMCL-ASIR), which is shown as the grey part with

width W_3 and length L_4, respectively. The meander coupled section is added at the open end of the high impedance coupled line in the SS-ASIR coupled pair. Figure 6.1 (b) shows the coupling routing scheme of Figure 6.1 (a).

Compared to traditional single coupling route of B-E, at least two extra coupling routes including A-D and C-F are created by the adoption of meander coupled lines. This multi-path coupling routing scheme of the modified SSMCL-ASIR filter is shown in Figure 6.1 (b). Due to the multi-path coupling routing, more transmission zeros (TZs) are created, which are utilized to suppress high order spurious frequencies or to help facilitate multi-band performance.

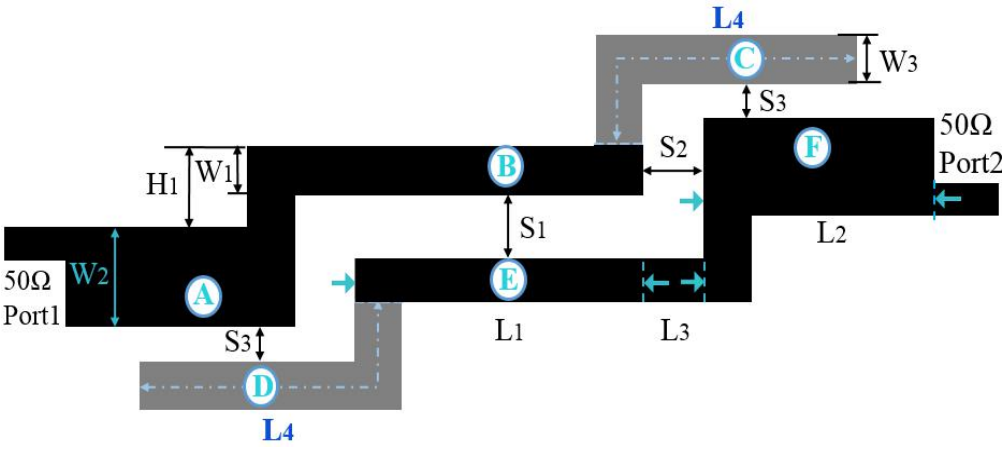

(a)

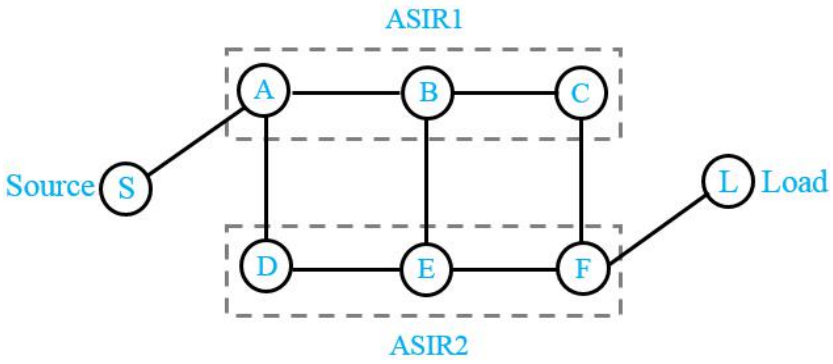

(b)

Figure 6.1. A SS-ASIR coupled pair with meander coupled section. (a) The

schematic diagram. (b) Coupling routing scheme: A-D, B-E and C-F denotes three coupling routes between ASIR1 and ASIR2, respectively.

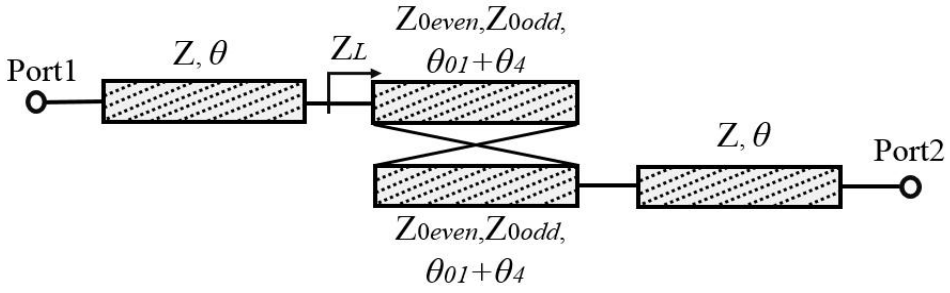

Figure 6.2. Even or odd mode equivalent circuit of SSMCL-ASIR.

Because the harmonic frequency performance would degrade when using the SS-ASIR structure, f_{si} cannot be conveniently deduced by simply analyzing $Y_{in} = 0$ in the ASIR unit. However, f_{zi} can still be obtained by setting $Z_{ine} = Z_{ino}$, where Z_{ine} and Z_{ino} are the input impedances for the even- or odd-mode equivalent circuits, respectively. The necessary and sufficient condition for Z_{ine} and Z_{ino} is $S_{21} = 0$ and the equivalent Y-parameter matrix of the even or odd mode equivalent circuit of the proposed structure can be expressed as

$$\begin{bmatrix} y_{11} & y_{12} \\ y_{21} & y_{22} \end{bmatrix} = \frac{1}{B}\begin{bmatrix} -j\frac{Z_{0even}+Z_{0odd}}{2}\cot(\theta_{01}+\theta_4) & j\frac{Z_{0even}-Z_{0odd}}{2}\csc(\theta_{01}+\theta_4) \\ j\frac{Z_{0even}-Z_{0odd}}{2}\csc(\theta_{01}+\theta_4) & -j\frac{Z_{0even}+Z_{0odd}}{2}\cot(\theta_{01}+\theta_4) \end{bmatrix} \tag{6.1}$$

where $B = -Z_{0even}Z_{0odd}\cot^2(\theta_{01}+\theta_4) + \frac{(Z_{0even}-Z_{0odd})^2}{4}$. θ_{01} and θ_4 are the electrical lengths of the original coupled line and of the meander coupled section, respectively. Z_{0even} and Z_{0odd} are the even and odd mode characteristic impedances for each coupled section, respectively. Since all elements of the normalized Y-parameters in (6.1) are purely imaginary, S_{21} of this coupled line can be expressed as

$$S_{21} = -\frac{2j\,\mathrm{Im}\{y_{12}\}}{1-\mathrm{Im}\{y_{11}\}^2+\mathrm{Im}\{y_{12}\}^2+2j\,\mathrm{Im}\{y_{11}\}} \tag{6.2}$$

Substituting from (6.1) into (6.2), gives equation (6.3). According to equation (6.3), there are three cases leading to $S_{21} = 0$. The first case is $Z_{0even} = Z_{0odd}$. The meander coupled section of length L_4 can be seen as a shifted coupled line structure which can suppress the spurious peak by compensating even- mode and odd-mode phase velocities.

$$\begin{aligned} S_{21} &= -\frac{4j(Z_{0even}-Z_{0odd})\cdot\frac{1}{\sin(\theta_{01}+\theta_4)}}{4-(Z_{0even}+Z_{0odd})^2\cdot\frac{\cos^2(\theta_{01}+\theta_4)}{\sin^2(\theta_{01}+\theta_4)}+(Z_{0even}-Z_{0odd})^2\cdot\frac{1}{\sin^2(\theta_{01}+\theta_4)}+4j(Z_{0even}+Z_{0odd})\cdot\frac{\cos(\theta_{01}+\theta_4)}{\sin(\theta_{01}+\theta_4)}} \\ &= -\frac{4j(Z_{0even}-Z_{0odd})\cdot\sin(\theta_{01}+\theta_4)}{u+jv} \\ &= \frac{4j(Z_{0even}-Z_{0odd})\cdot\sin(\theta_{01}+\theta_4)}{v^2-u^2}\cdot(u+jv) \end{aligned} \tag{6.3}$$

where

$$\begin{cases} u = 4\sin^2(\theta_{01}+\theta_4)-(Z_{0even}+Z_{0odd})^2\cdot\cos^2(\theta_{01}+\theta_4)+(Z_{0even}-Z_{0odd})^2 \\ v = 4(Z_{0even}+Z_{0odd})\cdot\cos(\theta_{01}+\theta_4)\sin(\theta_{01}+\theta_4) \end{cases}$$

The shifted coupled line structure which can suppress the spurious peak by compensating even-mode and odd-mode phase velocities. When the coupled line insertion loss is zero, the coupled length for the shifted coupled line/meander coupled line can be obtained from the following:

$$\frac{Z_{0even}}{Z_{0odd}} = \frac{\sin\beta_{even}L_4}{\sin\beta_{odd}L_4} \tag{6.4}$$

when $Z_{0even} = Z_{0odd}$, $\sin\beta_{even}L_4 = \sin\beta_{odd}L_4$. Also

$$\beta_{even}L_4 = \beta_{odd}L_4 + k_1\pi \quad (k_1 = 0,\ 1,\ 2,\ 3,...) \tag{6.5}$$

In this design, $0<\beta_{even}L_4<\pi$ and $0<\beta_{odd}L_4<\pi$, thus $k_1 = 0$ and $\beta_{\text{even}} = \beta_{\text{odd}}$. Because $v_{p,\text{even}} = \omega_{even}/\beta_{even}$ and $v_{p,odd} = \omega_{odd}/\beta_{odd}$, then $v_{p,\text{ even}} = v_{p,\text{ odd}}$ when $\omega_{even} = \omega_{odd}$. $v_{p,\text{even}}$, ω_{even} and β_{even} are even-mode phase velocity, angular frequency and phase constant, respectively. $v_{p,odd}$, ω_{odd} and β_{odd} mean odd-mode phase velocity, angular frequency and phase constant, respectively. When the even-mode and odd-mode phase velocities are equal, transmission zeros are generated and the spurious peak can be suppressed. Figure 6.3 compares frequency responses with and without a shifted coupled line/meander coupled section (SCL/MCS). As shown in the Figure 6.3, without a SCL/MCS, the unsuppressed spurious frequencies f_{s2} and f_{s3} exist and seriously limit the stop-band bandwidth. With a SCL/MCS, f_{s2} and f_{s3} are effectively suppressed and a wide stop-band is generated. Moreover, because the whole coupled line length is extended by the SCL/MCS structure, both the fundamental and spurious frequencies are shifted to lower frequencies.

The second case is $\sin(\theta_{01}+\theta_4) = 0$, namely

$$\theta_{01}+\theta_4 = k\pi \quad (k = 1,2,3) \tag{6.6}$$

The corresponding coupled line physical length can be calculated as

$$L_1+L_4 = \lambda_g/2 \tag{6.7}$$

where L_1 and L_4 are the physical lengths corresponding to θ_{01} and θ_4, respectively.

The third case is $u = 0$ and $v = 0$. When $u = 0$, there is:

$$\theta_{01} + \theta_4 = 2\sin^{-1}\sqrt{\frac{Z_{0even}Z_{0odd}}{(Z_{0even} + Z_{0odd})^2 + 4}} \tag{6.8}$$

Equation (6.8) shows the relationship between the whole coupled line electrical length

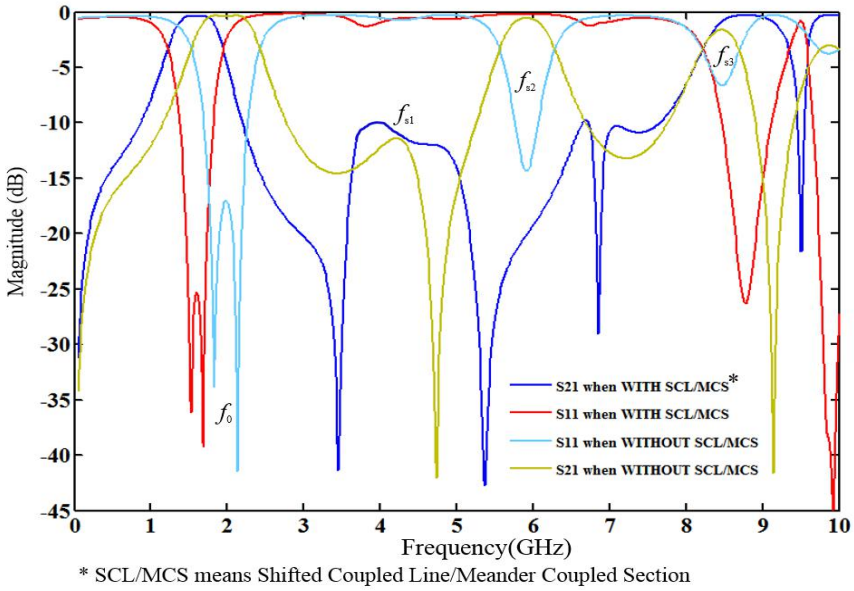

Figure 6.3. Frequency response comparison with and without SCL/MCS.

and odd-mode and even-mode impedance of the whole coupled lines.

When $v = 0$, sin $[2(\theta_{01}+\theta_4)] = 0$, and

$$\theta_{01} + \theta_4 = \frac{k\pi}{2} \quad (k = 1, 2, 3\ldots). \tag{6.9}$$

In general, the shortest whole coupled line electrical length to realize $S_{21} = 0$ can be got in the third case when k is equal to 1 and $\theta_{01}+\theta_4 = \pi/2$. The corresponding coupled line physical length can then be calculated as

$$L_1+L_4 = \lambda_g/4 \tag{6.10}$$

6.3 The Single-Wideband ASIR Filter Design

According to the frequency response transformation relationship discussed in Section A, the electrical length ratio α is 0.57 when L_2 is 11.4 mm, thus setting the fundamental frequency to around 1.51 GHz. The in-band performance of the first band, such as the insertion loss and return loss performance, is improved when the impedance ratio K is 0.48. The dimensions of the resonator are chosen as follows: L_1 = 14 mm, L_2 = 11.4 mm, L_1+L_3 = 15.2 mm, W_1 = 0.4 mm and W_2 = 1.6 mm. Through the design procedure for the coupled resonator circuits, the gaps of the whole coupled lines in Fig. 6.1(a) are determined as S_1 = 1.2 mm, S_2 = 0.2 mm and S_3 = 0.4 mm. The use of different gaps adds more design freedom for the filter. For simplicity of design, the meander coupled structure width W_3 is made 0.4 mm, which is the same as the width of coupled lines.

Because the fundamental frequency is 1.51 GHz, the relative λ_g can be calculated as 77.4 mm. Therefore, the value of (L_1+L_4) is about 19.4 mm. L_1 is 14 mm, so L_4 is set at around 5.4 mm. Although sections L_3 and H_1 would become coupled parts after adding the meander coupled section, the effects are small. The influence of these sections to the overall performance can therefore be disregarded, their coupling being much weaker than that involving sections L_1 and section L_4.

To further analyse the influence of the meander coupled section on the resonance frequency f_{sm} and transmission zero frequencies f_{zn}, the normalized f_{sm} (m = 1, 2, 3, 4) and normalized f_{zn} (n = 1, 2, 3, 4) versus γ for different values of K, are illustrated in Figure 4, where γ is the electrical length ratio between the meander coupled section θ_4 and whole coupled line (θ_1+ θ_4) and $\gamma = \theta_4/ (\theta_1+ \theta_4)$. It can be seen in Fig. 6.4 that for a fixed K value, the normalized f_{zn} (n = 1, 2, 3, 4) decline continuously and the normalized

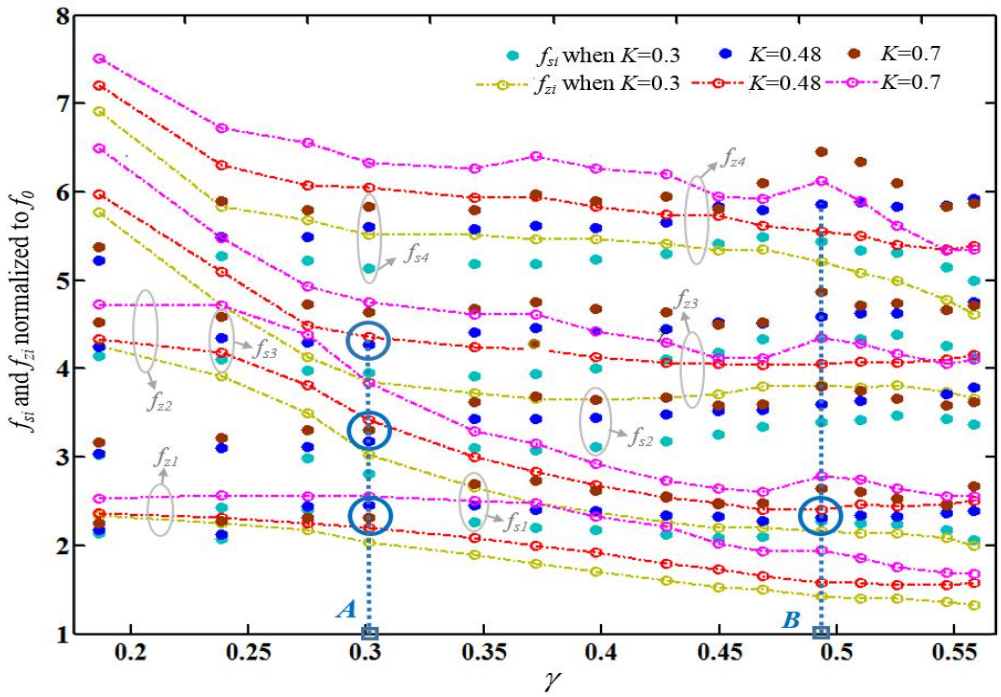

Figure 6.4. f_{si} and f_{zi} normalized to f_0 versus γ for different values of K in SSMCL-ASIR structure.

f_{sm} (m = 1, 2, 3, 4) follow an approximate sinusoidal curve when γ ranges from 0.17 to 0.58. Larger K values result in larger normalized f_{zi} and larger normalized f_{si} for a fixed γ value. Because the normalized f_{si} follow an approximate sinusoidal curve and f_{zi} follow a decreasing curve, they can intersect at a certain γ value. As illustrated, at point A, when K = 0.30, f_{z1} approaches f_{s1}, f_{z2} approaches f_{s2} and f_{z3} approaches f_{s3}, respectively. That means the first spurious frequency, the second spurious frequency and the third spurious frequency are suppressed successfully when K = 0.30. The corresponding L_4 can be calculated as 5.7 mm, which is close to the theoretical value.

The coupling matrix discussed in reference [36] will not be discussed in this paper because of its non-wideband limitation [36-37]. The coupling between two ASIRs can be represented by a J-inverter susceptance $J_{1,2}$, where subscript 1 and 2 denotes the first

and second passband. A larger value of $\overline{J_{1,2}}$ means a stronger coupling strength between two ASIRs.

The external quality factor $Q_{ex1,2}$ and the normalized J-inverter susceptance $\overline{J_{1,2}}$ can be related by [35]

$$Q_{ex1,2} = \frac{\pi}{2\overline{J_{1,2}}^2} \tag{6.11}$$

The external quality factor $Q_{ex1,2}$ can be further extracted by

$$Q_{ex1,2} = \frac{f_{c1,2}}{\Delta_{1,2}} \tag{6.12}$$

where $f_{c1,2}$, $\Delta_{1,2}$ represent the central frequency and -3 dB bandwidths, respectively. From (6.11) and (6.12), $\overline{J_{1,2}}$ can be calculated by substituting the extracted $Q_{ex1,2}$ into equation (6.11). Figure 6.5 plots f_0 and Q_{ex1} versus L_4 for different gap S_3 values in an SSMCL-ASIR single band type filter. In Figure 6.5, when L_4 ranges from 2.7 mm to 8.7 mm, the fundamental frequency f_0 decreases continuously while Q_{ex1} increases in general for a fixed S_3 value. f_0 increases when S_3 ranges from 0.1 mm to 0.4 mm and does not change much when S_3 ranges from 0.4 mm to 0.7 mm, and Q_{ex1} decreases continuously when S_3 ranges from 0.1 mm to 0.7 mm in general. Moreover, it is noted that there are two notches when S_3 = 0.1 mm and 0.7 mm, which means the bandwidth is maximum when L_4 = 5.7 mm within the range of L4 from 3.7 mm to 8.7 mm. By comprehensively considering the bandwidth, resonant frequency location and out-of-band spurious frequency suppression performance, S3 is set at 0.4 mm, which is shown as point C in Figure 6.5.

The proposed filters, fabricated on an RO3210 substrate with a relative dielectric of 10.2 and dielectric loss tangent 0.0027, have been measured using an HP8510 vector network analyser. The simulated S-parameters, measured S-parameters and zoom in-band performance of the designed single-wideband SSMCL-ASIRs are plotted in Figure 6.6.

Good agreement can be observed between the simulated and measured results and the slight discrepancies are attributed to loss and fabrication errors. It can be seen that the single-wideband filter is realized with very low insertion isolation of only 0.36 dB at central frequency and return loss of better than 25.5 dB. The pass-band ranges from 1.18-1.84 GHz with central frequency 1.51 GHz, bandwidth 660 MHz and fractional band width (FBW) 43.7%. It can be applied in the Global Positioning System (GPS: frequency band centred at 1.57 GHz), Global System for Mobile Communication (GSM: 1800 MHz) and Universal Mobile Telecommunication System (UMTS: 1710-1880 MHz, etc.).

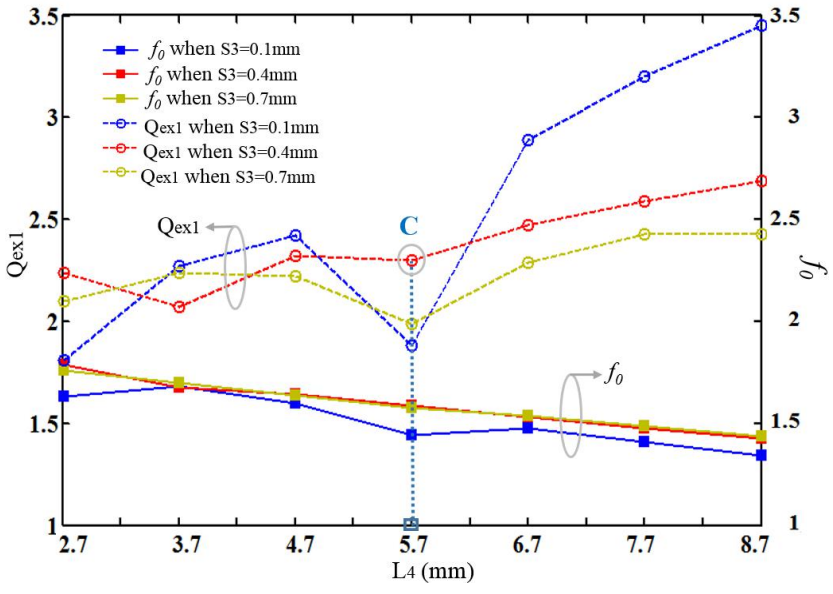

Figure 6.5. f_0 and Q_{ex1} versus L4 with different values of S_3

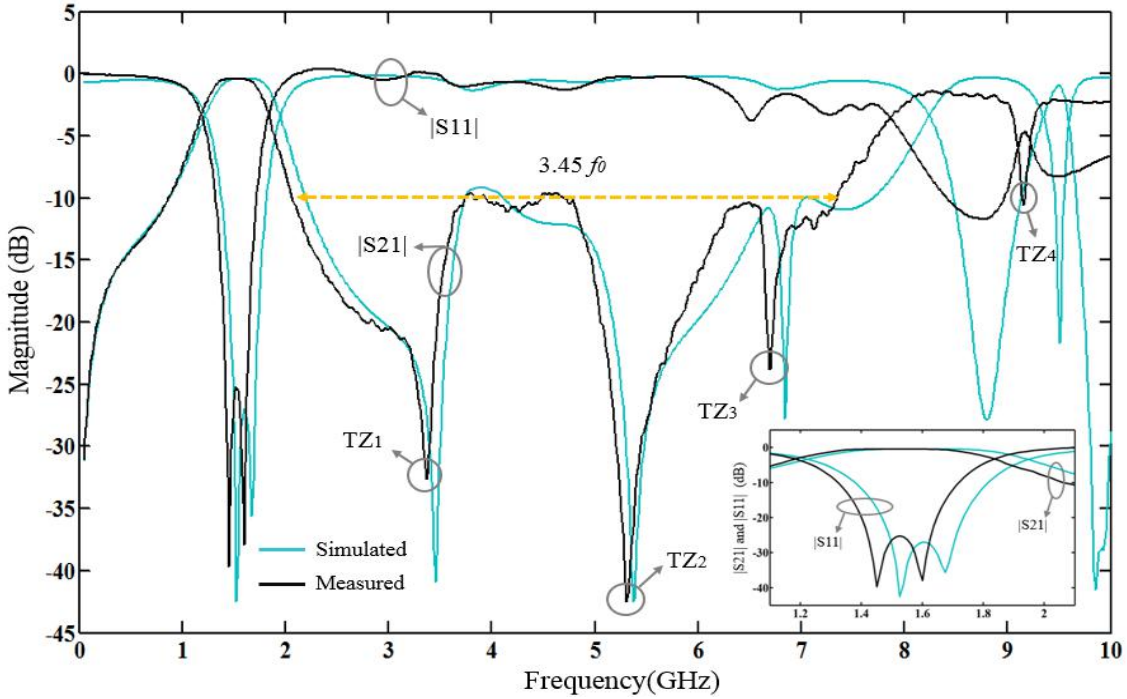

Figure 6.6. Simulated, measured results and zoom in-band performance of single-wideband type SSMCL-ASIRs.

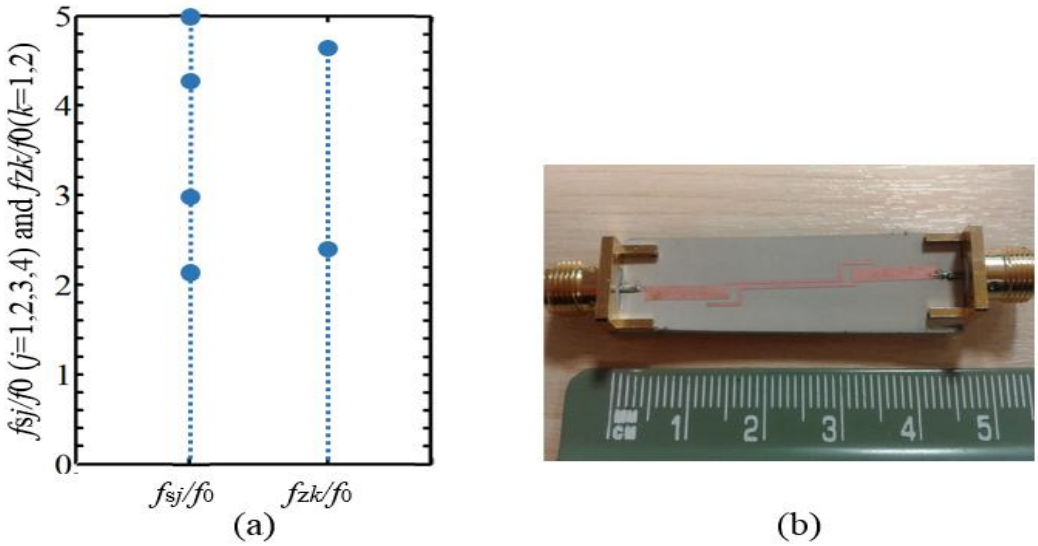

Figure 6.7. (a) f_{sj} and f_{zk} locations of the traditional structure.
(b) The single-wideband type SSMCL-ASIR filter

Table 6.2

PERFORMANCE COMPARISON WITH PROPOSED SINGLE-BAND BPF

	CF (GHz)	-3 dB FBW	IL (dB)	STOP-BAND SUPPRESSION	NUMBER TZs	SIZE	SINGLE-/MULTI-BAND VERSATI L-ITY
[5]	2.4	8.4%	2.06	up to 5.5 f_0	2	0.36 λ_g ×0.13 λ_g	NO
[9]	1.45	57.9%	1	1.45 f_0-3.35 f_0	4	0.664 λ_g ×0.133 λ_g	NO
[10]	5	40%	0.7	1.26 f_0-3.52 f_0	2	0.294 λ_g × 0.162 λ_g	NO
[11]	2.4	--	3.3	3.6 f_0	2	0.2 λ_g × 0.15 λ_g	NO
This work	**1.51**	**43.7%**	**0.36**	**1.39 f_0-4.85 f_0**	**3**	**0.063 λ_g × 0.50 λ_g**	**YES**

Since the tuneable transmission zeros f_{z1} = 3.38 GHz, f_{z2} = 5.31 GHz, f_{z3} = 6.71 GHz are close to the spurious frequencies, a wide stop-band ranging from 2.1-7.32 GHz is realized, as shown in Figure 6.6. The parameter are listed:L1+L3=15.2mm, L1=14mm, L2=11.4mm W1=0.4mm and W2=1.6mm. L4=5.7mm, S1=1.2mm, S2=0.2mm and S3=0.4mm.

Normalized resonant frequencies f_{sj} and transmission zero frequencies f_{zk} locations with

the traditional structure are plotted in Figure 6.7(a) for comparison. Figure 6.7(b) is a photograph of the single-wideband type SSMCL-ASIR.and its performance comparison with proposed single-band BPFs is shown in Table 6.2. From Table 6.2, it is seen that the proposed structure realizes bigger fractional bandwidth, which is more than 40%. The insertion loss is less than 0.5dB and is better than most published works. The stop band ranges from 1.39 f_0 to 4.85 f_0 and is wider than the published works.

6.4 The Quint-Wideband ASIR Filter Design

As stated in Section 6.2 and Section 6.3, transmission zeros can be created and utilized to give a multi-band frequency response. At point B in Figure 6.4, f_{z2} approaches f_{s1} while f_{z2}, f_{z3} and f_{z4} are distinct from f_{s2}, f_{s3} and f_{s4}, respectively. That means the first spurious frequency f_{s1} is suppressed while f_{s2}, f_{s3} and f_{s4} can be used to form the second, third and fourth operating bands respectively. The variation of S_{11} and S_{21} for different values of L_4 is shown in Figure 6.8. As shown in the figure, because of the multi-path coupling routing and transmission zeros tuning method, six transmission zeros (TZ_1-TZ_6) are generated, positioned between different pass-bands to widen the pass-bandwidths and improve the frequency selectivity.

Moreover, the fifth operating band of more than 3.5 GHz, the -3 dB bandwidth is generated, which is described as f_{s5} in the figure. Figure 6.9 plots the effect of L4 on a quint-wideband type SSMCL-ASIR. In (a), when L_4 varies from 10.1 to 16.1 mm, f_0 decreases while Q_{ex1}, normalized fs2 and Q_{ex2}/Q_{ex1} fluctuate. In (b), normalized f_{s3}, f_{s4} and f_{s5} increase slightly, and Q_{ex3}/Q_{ex1} fluctuates slightly. In contrast, Q_{ex4}/Q_{ex1} and

Q_{ex5}/Q_{ex1} decrease dramatically from 13 to 5.28 and from 7.1 to 1.2, respectively.

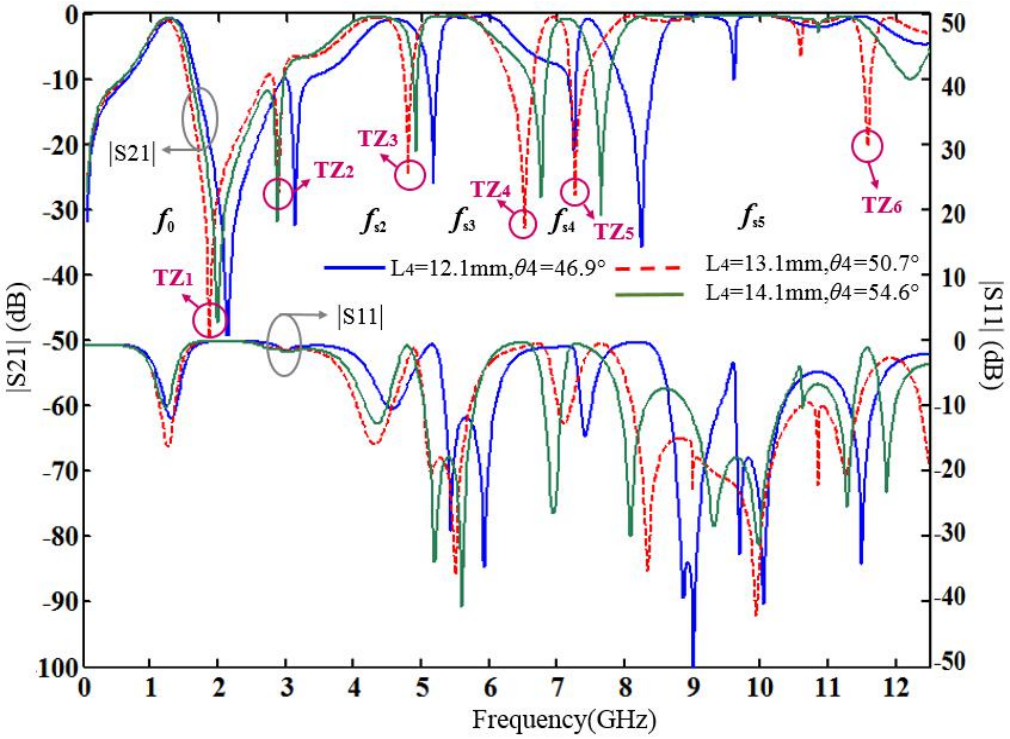

Figure. 6. 8. Variation of S11 and S21 versus different values of L_4

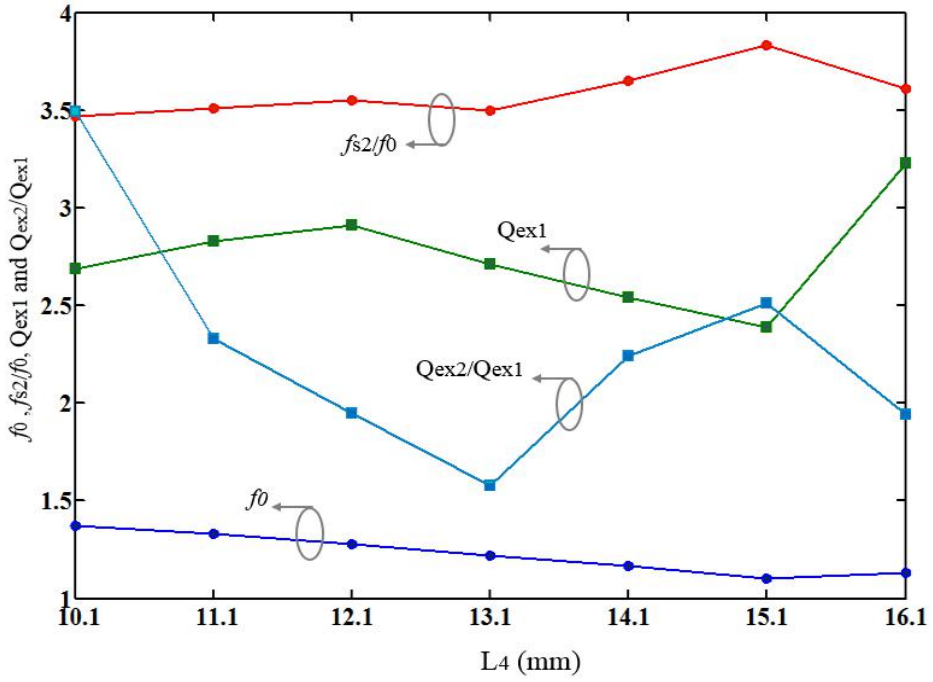

(a)

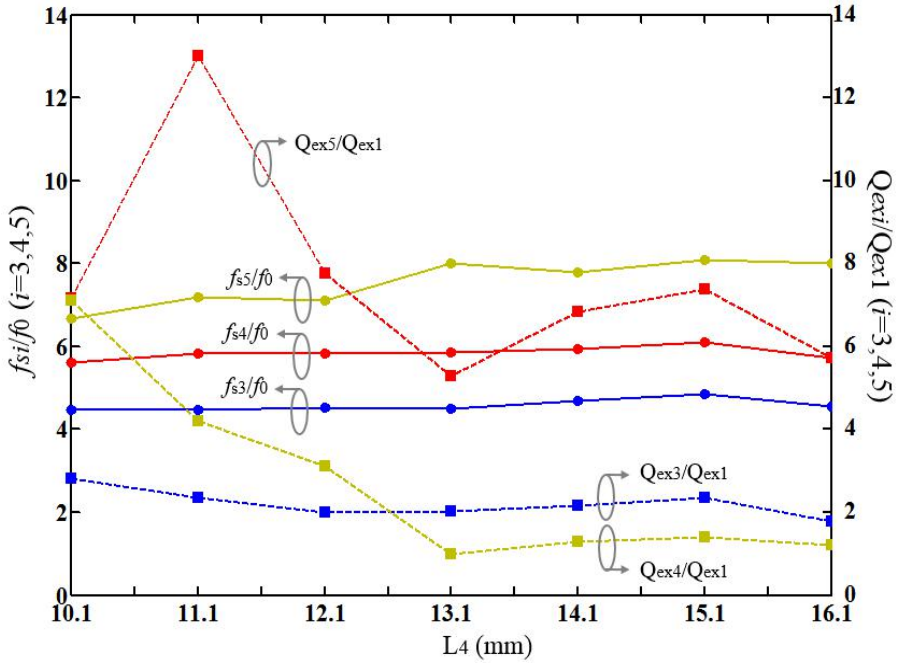

(b)

Figure 6.9. The effect of L_4 on quint-wideband type SSMCL-ASIR,
(a) f_0, Q_{ex1}, f_{s2}/f_0 and Q_{ex2}/Q_{ex1} versus L_4,
(b) f_{si}/f_0 *and* Q_{exi}/Q_{ex1} (i = 3, 4, 5) versus L_4.

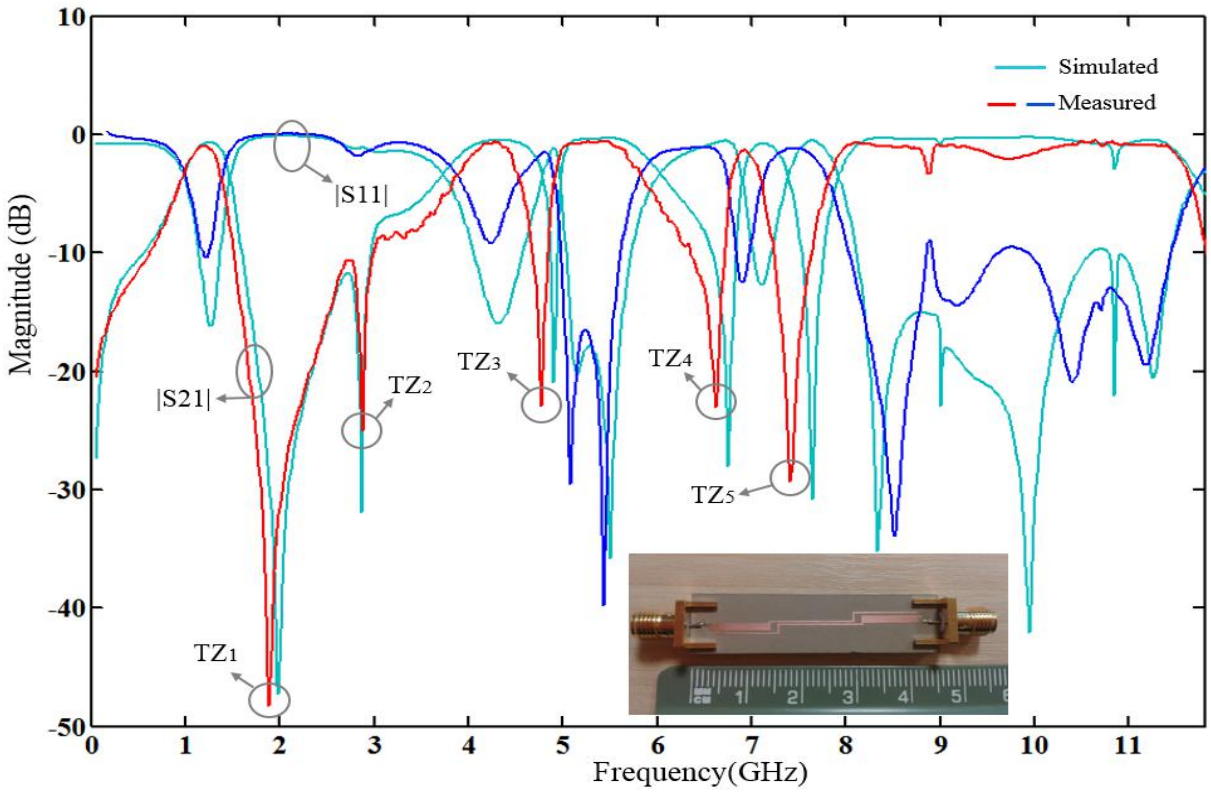

(a)

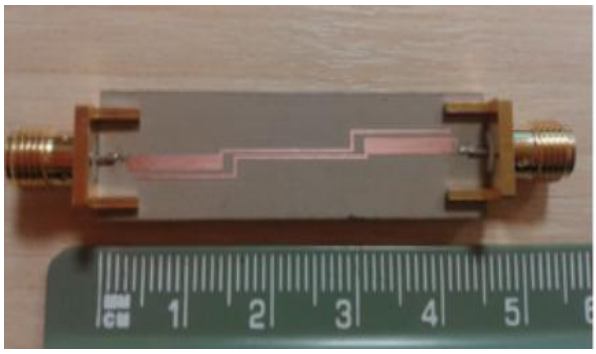

(b)

Figure 6.10. (a) Simulated and measured results;(b) photograph of a modified quint-wideband type SSMCL-ASIR.

Moreover, the notch of each Q_{exi}/Q_{ex1} (i = 2, 3, 4, 5) curve happens near L_4 = 13.1 mm, which means that relatively second, third, fourth and fifth bandwidths of the proposed quint-band filter can obtained with L_4=13.1 mm.

The design procedures for single- and quint-wideband type SSMCL-ASIR BPFs can be summarized as follows:

1) Choose the suitable electrical length ratio α, thus setting the fundamental frequency f_0, and choose the characteristic impedance ratio K in the ASIR to realize improved insertion loss and return loss performance.

2) Analyse the transmission zero generating requirement of the meander coupled section added to the SS-ASIR structure and calculate the approximate transmission zero equations S21 = 0.

3) According to the calculated results, tune the length of the meander coupled section to meet S21 = 0 and make f_{zn} approach the resonant frequency f_{sm} to form a wide

stop-band for the single-wideband type ASIR filter. The gap parameter S_1 and S_3 are also utilized and tuned to realize optimized results.

4) Tune the length of the meander coupled section to move f_{zn} away from f_{sm}, to enable a multi-band response with good isolation between operating bands for the multi-wideband type ASIR filter.

5) Because the non-wideband limitation of coupling matrix, coupling coefficient are not the vital object to consider when designing, while external quality factor Q_{ex} can be discussed for performance optimization, as mentioned above.

Simulated and measured results and photograph of the quint-wideband type SSMCL-ASIR filter are shown in Figure 6.10. Good agreement can be observed between the simulated and measured results, with discrepancies attributable to losses and fabrication errors. It can be seen that quint wide-bands are realized with good in-band return loss performance. The first pass band ranges from 1.0 to 1.38 GHz with a central frequency (CF) of 1.19 GHz, and bandwidth (BW) of 380 MHz. The second pass band ranges from 3.96 to 4.62 GHz with CF of 4.29 GHz, BW of 660 MHz. The third pass band ranges from 5.0 to 5.86 GHz with CF of 5.43 GHz and BW of 860 MHz. The fourth pass band ranges from 6.82 to 7.12 GHz with CF of 6.97 GHz and BW of 300MHz. The fifth pass band ranges from 7.96 to 11.84 GHz with CF of 9.9GHz, and a large BW of 3.88GHz. In addition, there are five transmission zeros at 1.96GHz, 2.98GHz, 4.89 GHz, 6.68GHz and 7.58GHz, which further enhance the frequency selectivity, as illustrated in Figure 6.10. The parameter are listed:L1+L3=15.2mm, L1=14mm, L2=11.4mm, W1=0.4mm and W2=1.6mm. L1=13.1mm, S1=1.2mm, S2=0.2mm and S3=0.4mm.The

quint-wideband type SSMCL-ASIR performance comparison with alternative quint-band BPFs is shown in Table 6.3. It can be seen that the proposed structure has the advantages including bigger fractional bandwidth, among them four fractional bandwidths are higher than 10%. The insertion loss is lower than published ones. All the single and quint band insertion losses are less than 2dB. Furthermore, the proposed two structures are simple and are easily made.

Table 6.3

#PERFORMANCE COMPARISON WITH PROPOSED QUINT-BAND BPF

	CF (GHz)	3 dB FBW (%)	IL (dB)	SIZE	SINGLE/ MULTI-BAND VERSA-TILITY	EXTRA STRUC-TURE
[12]	0.6/0.9/1.2/ 1.5/1.8	5.8/5.2/5.8/ 8.2/8.0	2.8/2.9/2.9/ 2.6/2.3	0.045 λ_g ×0.52 λ_g	NO	VIA HOLE
[13]	0.63/1.33/2.03/ 2.74/3.45	28.8/9.4/2.7/ 5.3/5.5	0.47/1.14/1.8/ 1.39/1.26	0.043 λ_g ×0.178 λ_g	NO	VIA HOLE
[14]	1.5/2.5/3.5/ 4.5/5.8	4.5/4.5/3.6/ 4.5/2.7	1.5/1.8/0.9/ 1.2/ 2.5	0.24 λ_g ×0.17 λ_g	NO	MULTI-LAYER
This Work	**1.19/4.29/5.43/ 6.97/9.9**	**31.9/15.4/15.8/ 4.3/39.2**	**1.0/0.47/0.50/ 1.7/ 0.6**	**0.05 λ_g ×0.40 λ_g**	**YES**	**NONE**

6.5. Tri-Wideband band-pass SS-ASIR Filter Design Using Asymmetric Parallel Uncoupled Lines

An uncoupled section located within conventional coupled lines is a useful means to achieve extra transmission zeros closing to existing zeros, created by the conventional coupled lines. At the same time, this way can also add the freedom to optimize the in-

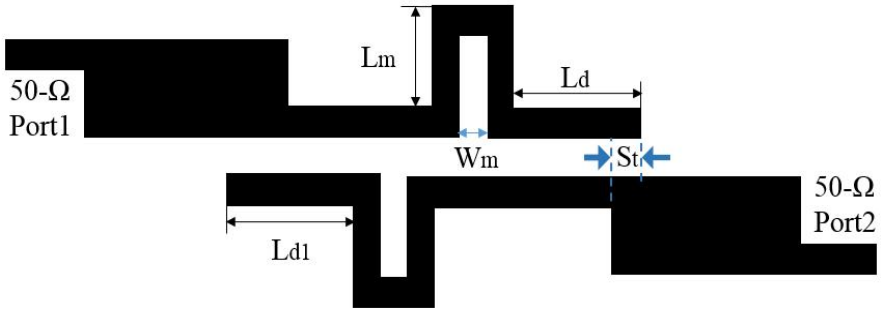

(a)

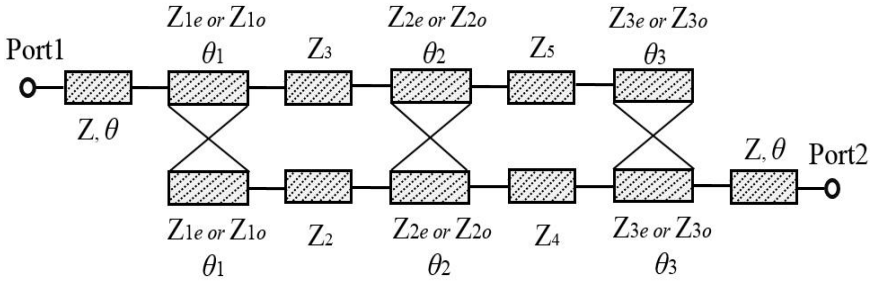

(b)

Figure 6.11. A SS-ASIR ASIR coupled pair with asymmetric parallel uncoupled meander sections. The schematic diagram. (b) Even-mode or odd-mode equivalent circuit.

band performance of the original structure. The ASIR unit can be further moved horizontally to the left/right so as to form the extra coupling between the high characteristic impedance coupled line and the low characteristic impedance line. In this

chapter, the ASIR coupling structure in vertical direction is further modified and an asymmetric parallel uncoupling microstrip line structure (APUML) is proposed. As shown in Figure 6.11 (a), the two ASIR unit impedance line has an extra coupling with the distance between two vertical symmetry axes of two parallel uncoupling microstrip line, and this distance is controlled and influenced by the APUML relative distance parameter L_d, L_{d1} to open end and parameter St. The APUML's height and inner gap is Lm and Wm, respectively. The relative even- or odd-mode equivalent circuit of the proposed structure is shown in Figure 6.11 (b). Z_{1e} or Z_{1o}, Z_{2e} or Z_{2o} and Z_{3e} or Z_{3o} are left, middle and right coupled section's even or odd-mode impedance, respectively. Z_2, Z_3 or Z_4 and Z_5 are uncoupled sections in two coupled ASIRs, respectively.

Compared to traditional skew-coupled ASIR filters, a wider second pass-band is achieved and the additional third operating band is generated by adopting the novel asymmetric parallel uncoupled microstrip lines. This means $\overline{J_2}$ is improved greatly and a stronger coupling strength between two ASIRs is realized. Figure 6.12 illustrates the influence of W_m and L_m on the response of the APUML-ASIR tri-band filter with different values of St. In (a), when Wm varies from 0.05 mm to 0.25 mm, f_0 decreases slightly and f_{s2}/f_0 increases slightly but neither are greatly influenced by varying St. Meanwhile, f_{s2}/f_0 does not change much but does less when St increases. In (b), when W_m varies from 0.05 mm to 0.25 mm f_{z1}/f_0 decreases slightly while $f_{z2,\ 3}/f_0$ hardly changes, but when St becomes greater for a fixed W_m, $f_{z1,\ 2,\ 3}/f_0$ becomes less. This means transmission zeros can be controlled by W_m and St. In (c), when Lm varies from 1.7 mm to 2.9 mm, $f_{s1,\ 2,\ 3}/f_0$ decreases slightly. When St varies from 1 mm to 4 mm, f_0 and f_{s2}/f_0 do not vary but f_{s1}/f_0 decreases.

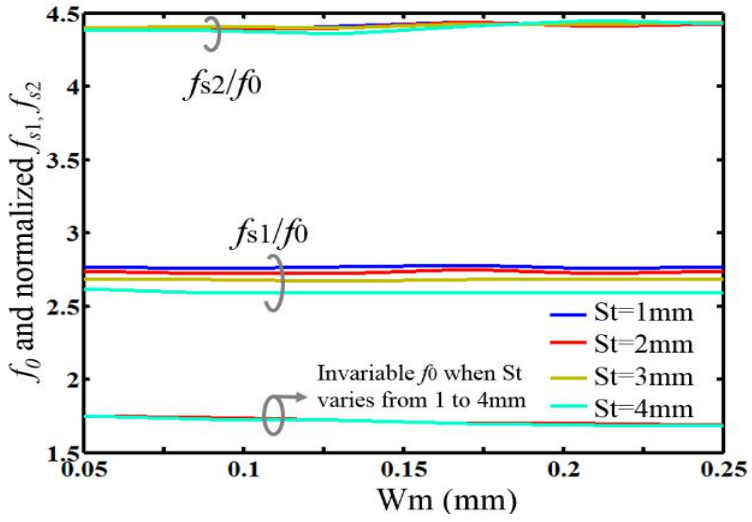
4.5
4
3.5
3
2.5
2
1.5
0.05
0.1
0.15
0.2
0.25
Wm (mm)
f_0 and normalized f_{s1}, f_{s2}
f_{s2}/f_0
f_{s1}/f_0
Invariable f_0 when St varies from 1 to 4mm
St=1mm
St=2mm
St=3mm
St=4mm

(a)

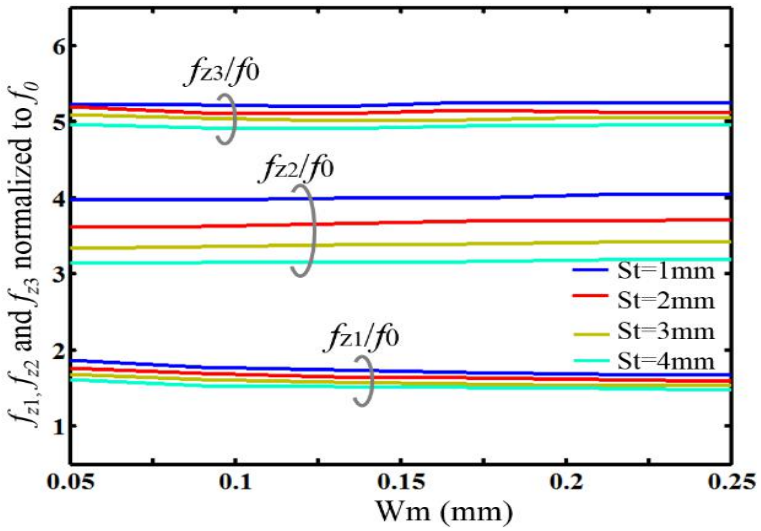
6
5
4
3
2
1
0.05
0.1
0.15
0.2
0.25
Wm (mm)
f_{z1}, f_{z2} and f_{z3} normalized to f_0
f_{z3}/f_0
f_{z2}/f_0
f_{z1}/f_0
St=1mm
St=2mm
St=3mm
St=4mm

(b)

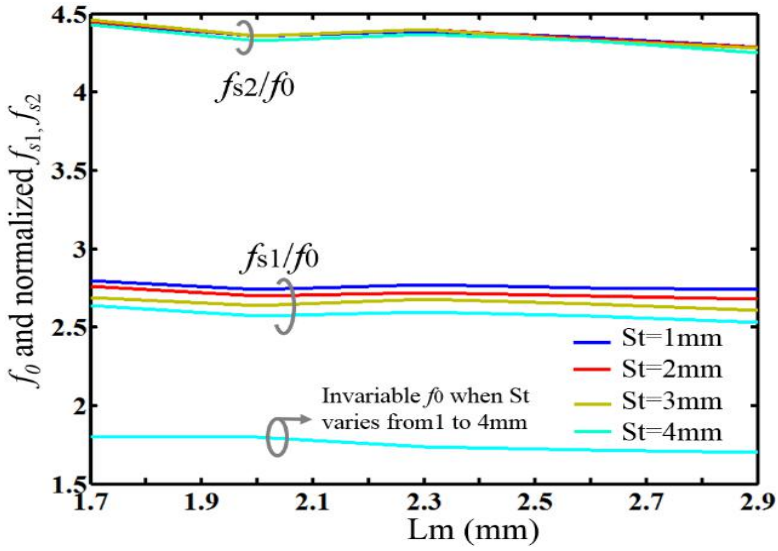
4.5
4
3.5
3
2.5
2
1.5
1.7
1.9
2.1
2.3
2.5
2.7
2.9
Lm (mm)
f_0 and normalized f_{s1}, f_{s2}
f_{s2}/f_0
f_{s1}/f_0
Invariable f_0 when St varies from1 to 4mm
St=1mm
St=2mm
St=3mm
St=4mm

(c)

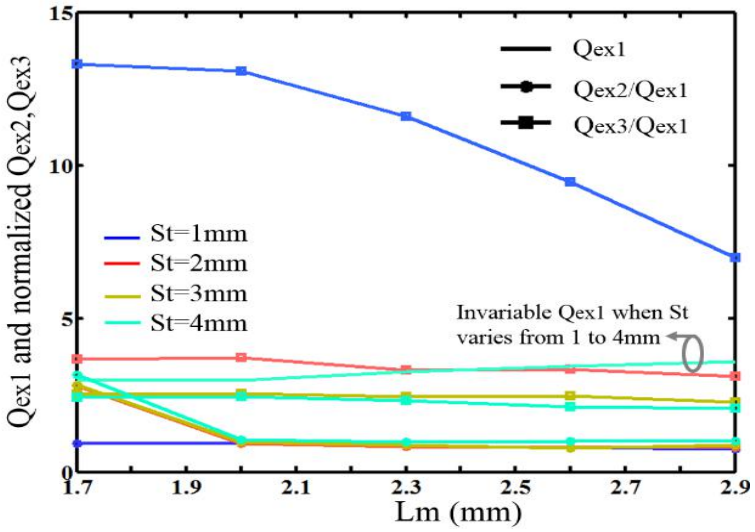

(d)

Figure 6.12. The influence of W_m and L_m on the response of the APUML-ASIR Tri-band filter for variation of St: (a) f_0 and normalized f_{si} (W_m varies):
(b) Normalized f_{zi}:
(c) f_0 and normalized $f_{si,}$ (L_m varies):
(d) Q_{ex1} and normalized Q_{exi}.
When one parameter varies, the others remain unchanged.

In (d), when Lm varies from 1.7 mm to 2.9 mm, Q_{ex1} increases and $Q_{ex2,\,3}/Q_{ex1}$ decreases, so that the fundamental bandwidth becomes narrower. When St becomes greater, Q_{ex1} does not change and $Q_{ex2,\,3}/Q_{ex1}$ decreases. Compared to f_0, f_{s2}, f_{z1} and f_{z3}, the variation of St has greater influence on the second pass-band central frequency f_{s1}, the second transmission zero f_{z2} and the third pass-bandwidth.

Figure 6.13 shows the effect of the reference location parameter L_d on the frequency response of the proposed tri-band filter. It is noted that when L_d changes from 5 mm to 7.64 mm when L_{d1} is fixed at 8.1 mm, the second pass-band return loss performance is enhanced greatly and its bandwidth becomes wider, providing a wide second pass-band of more than 3.5 GHz.

At the same time, a third pass-band is formed and its return loss as well as its insertion loss performance is improved considerably by varying Ld. Similar phenomenon can be observed when varying Ld1 with fixed Ld. Therefore, Ld and Ld1 are two important factors to tune and influence the coupling strength between two modified ASIRs and external quality factors.

The analysis of the asymmetric parallel uncoupled microstrip line unit (APUML) further helps to explain the formation of the second and third pass-band. The APUML topological structure and frequency response are plotted in Figure 6.14. As seen in the figure, the APUML unit forms two wide pass-bands between 4-6 GHz and 6-8 GHz when Ld1 changes from 9.1 mm to 7.1 mm. This result proves the advantage of the

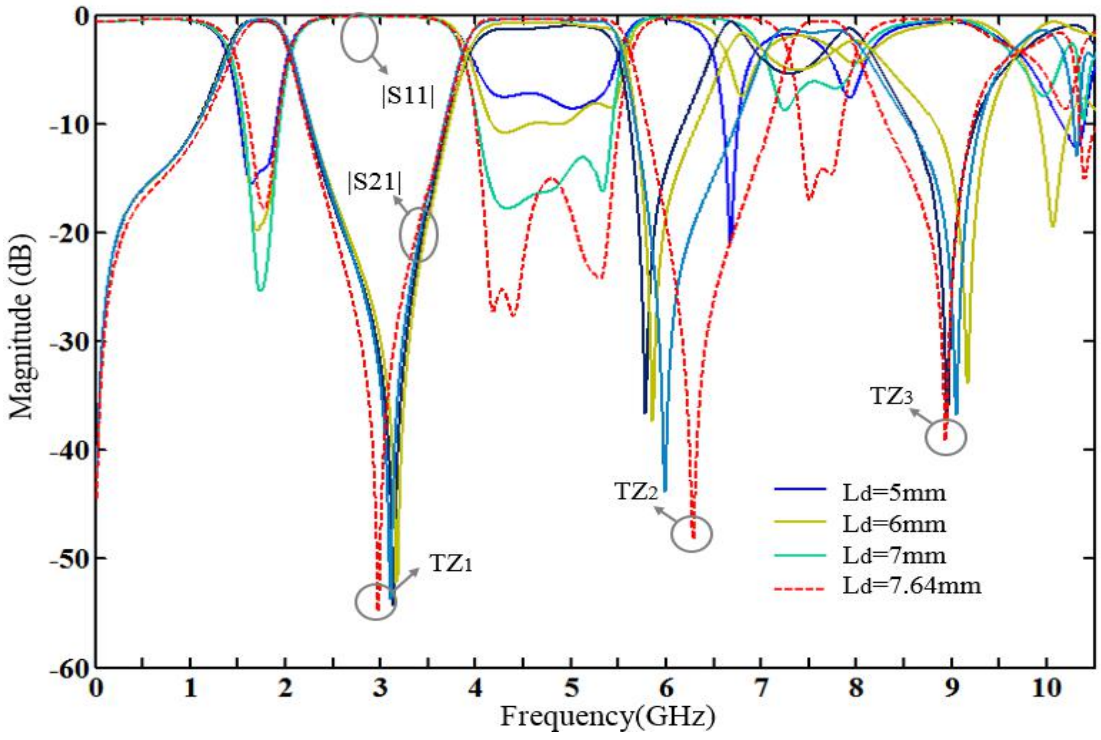

Figure 6.13. The impact of L_d impact on the frequency response of the SS-ASIR filter with APUMLs.

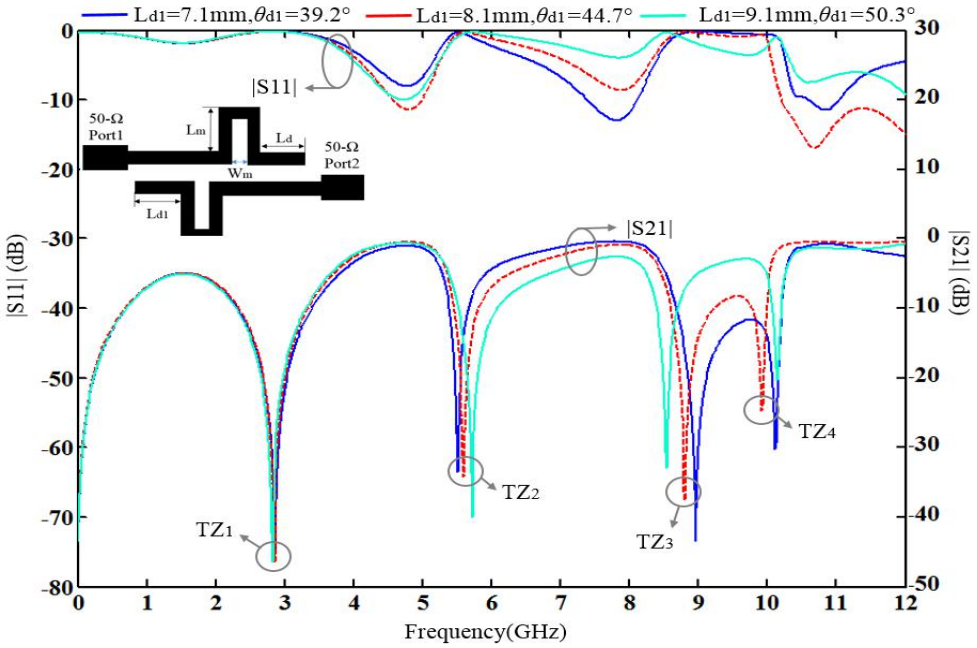

Figure 6.14. The analysis of the APUML structure

APUML structure to optimize the in-band filter performance. As for out of band performance, the APUML unit generates four transmission zeros at both sides of the pass-bands, as plotted in Figure 6.14. These four transmission zeros can improve the isolation performance between the three pass-bands, and the out of band suppression performance.

The simulated S-parameters, measured S-parameters and fabricated photograph of the tri-wideband ASIR filter are shown in Fig.6.15. Good agreement is observed between the simulated and measured results and the slight discrepancies are attributed to the loss and fabrication errors. It can be seen that triple wide-bands are realized with good in-band return loss performance. The first pass-band ranges from 1.46-1.98 GHz with the (CF) of 1.72 GHz, bandwidth (BW) 520 MHz and fractional band width (FBW) 30.2%.

It can be applied in the Global Positioning System (GPS: frequency band centred at 1.57 GHz), Global System for Mobile Communication (GSM: 1800 MHz) and Universal Mobile Telecommunication System (UMTS: 1710-1880 MHz, etc.). The

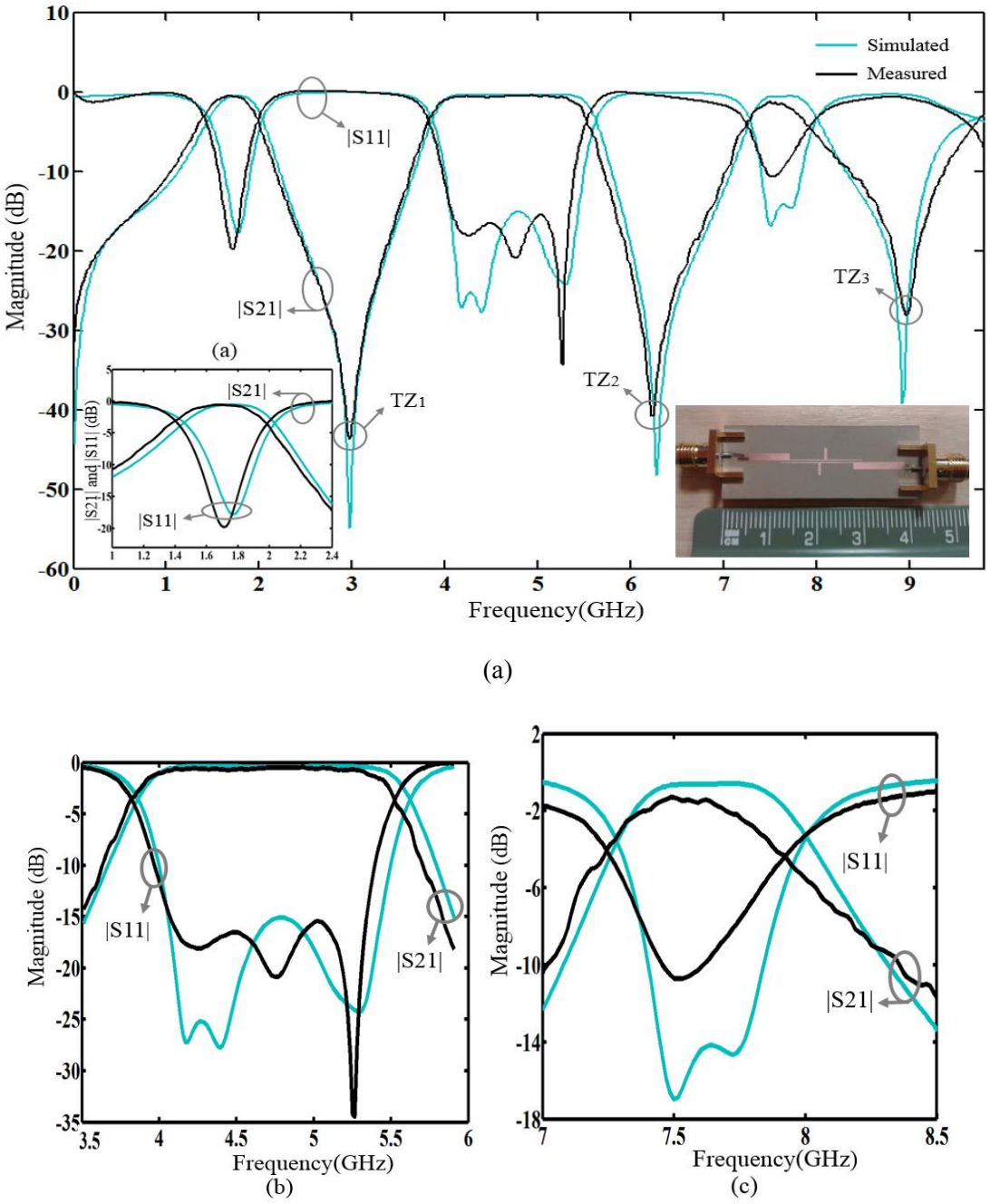

Figure 6.15. Simulated and measured results of SS-ASIRs with APUMLs; (a) Narrowband view of the first passband, (b) Narrowband view of the second passband, (c) Narrowband view of the third passband.

second pass-band ranges from 3.90-5.54 GHz with CF 4.72 GHz, BW 1.64 GHz and FBW 34.7%. It can be applied in IEEE802.11a WLAN applications including 5G Wi-Fi. The third pass-band, which ranges from 7.32-7.86 GHz with CF 7.59 GHz, BW 0.54 GHz and FBW 7.1%, can be applied in earth-satellite satellite communication. Moreover, good isolation is achieved between the three pass-bands, to eliminate signal interference. Three transmission zeros located at 3.02, 6.26 and 9.01 GHz are generated to enhance frequency selectivity, which can be seen in Figure 6.15. The triple-wideband type APUML-ASIR filter performance comparison with alternative tri-band BPFs is

Table 6.4

PERFORMANCE COMPARISON WITH PROPOSED TRI-BAND ASIR BPF

	CF (GHz)	3 dB FBW (%)	IL (dB)	$ISO_{1,2}$, $ISO_{2,3}$	SIZE	EXTRA STRUC -TURE
[13]	1.875/3.54/5.91	19.9/14/4.6	0.6/0.75/1.65	>27 / >20	$0.206\lambda_g$ $\times 0.086\lambda_g$	VIA HOLE
[15]	1.8/3.5/5.8	7/5/3.5	0.88/1.33/1.77	>40.4 / >12.78	$0.108\lambda_g$ $\times 0.521\lambda_g$	VIA HOLE
[16]	2/3.45/5.8	8.7/13.4/7.2	1.4/0.7/1.7	NA	$0.045\lambda_g$ $\times 0.52\lambda_g$	VIA HOLE
[17]	2.4/3.5/5.45	11.6/6.7/17.8	1.1/1.2/1	<40 / <40	$0.21\lambda_g$ $\times 0.11\lambda_g$	VIA HOLE
This work	**1.72/4.72/7.59**	**30.2/34.7/7.1**	**0.58/0.43/1.3**	**43.5/39.2**	**$0.09\lambda_g$ $\times 0.51\lambda_g$**	**NONE**

shown in Table 6.4. It can be seen that the proposed structure has the advantages including bigger fractional bandwidth, among them first two fractional bandwidths are higher than 30% and are bigger than the published works.The insertion losses are lower than published ones. All the tri-band insertion losses are less than 2dB. Furthermore, the proposed two structures are simple and are easily made.

6.6 Conclusion

Novel multi-standard single/tri/quint-wideband ASIR filters are proposed in this chapter. By utilizing a novel modified SS-ASIR coupled pair with meander coupled sections, and placing transmission zeros close to resonant frequencies, a single-wideband filter with good fractional bandwidth, insertion loss and return loss performance is realized. By varying the lengths of meander coupled sections, stronger coupling between two resonators is realized and more transmission zeros are generated, which are tuned to help in forming a quint operating wideband. With the help of APUML, a tri-wideband ASIR filter is realized with high fractional bandwidth. These filters effectively cover several applications including GPS, GSM, UMTS, ISM and IEEE 802.11 a/b/g/n/ac, with controllable bandwidths. Furthermore, the proposed structures successfully realize ASIR filter applications in single/dual/triple/quadruple/quint-wideband fields, but with the advantage of higher versatility. Measured results agree well with simulated results and theoretical predictions. The good in-band and out-of-band behaviour, compact size and simple structure make the proposed filters very promising for applications in future multi-standard wireless communication.

6.7 References

[1] G. L. Matthaei, L. Young, and E. M. T. Jones. Microwave Filters, Impedance-Matching Network, and Coupling Structures. Norwood, MA: Artech House, 1980.

[2] R. Schwindt and C. Nguyen. Spectral domain analysis of three symmetric coupled lines and application to a new bandpass filter. IEEE Transaction on Microwave Theory and Technology. Vol. 42, no. 7, pp: 1183-1189, Jul. 1994.

[3] J.-T. Kuo, E. Shih, and W.-C. Lee. Design of bandpass filters with parallel three-line coupled microstrips. Proceeding of Asia-Pacific Microwave Conference. pp: 157-160. Jun. 2001.

[4] R. Schwindt and C. Nguyen. Spectral domain analysis of three symmetric coupled lines and application to a new bandpass filter. IEEE Transaction on Microwave Theory and Technology. Vol. 42, no. 7, pp: 1183-1189, Jul. 1994.

[5] J.-T. Kuo, E. Shih, and W.-C. Lee. Design of bandpass filters with parallel three-line coupled microstrips. Proceeding of Asia-Pacific Microwave Conference. pp: 157-160. Jun. 2001.

[6] C. Nguyen. New compact wideband bandpass filter using three parallel- coupled lines. Electronic Letter. Vol. 30, no. 25, pp: 2149-2150, Dec. 1994.

[7] H. Shaman and J. S. Hong. Wideband bandpass microstrip filters with triple coupled lines and open/short stubs. Proceeding of Asia-Pacific Microwave Conference. pp: 1-4. Dec. 2007,

[8] L. Zhu, S. Sun, and W. Menzel. Ultra-wideband (UWB) bandpass filters using multiple-mode resonator. IEEE Microwave Wireless Component Letter. Vol. 15, no. 11, pp: 796-798, Nov. 2005.

[9] J. Fan, D. Zhan, C. Jin, and J. Luo. Wideband microstrip bandpass filter based on quadruple mode ring resonator. IEEE Microwave Wireless Component Letter. Vol. 22, no. 7, pp: 348-350, Jul. 2012.

[10] M. K. Mandal and S. Sanyal. Design of wide-band, sharp-rejection bandpass filters with parallel-coupled lines. IEEE Microwave Wireless Component Letter. Vol. 16, no. 11, pp: 597-599, Nov. 2006.

[11] X. Luo, J.-G. Ma, and E.-P. Li. Wideband bandpass filter with wide stopband using loaded BCMC stub and short-stub. IEEE Microwave Wireless Component Letter. Vol. 21, no. 7, pp: 353-355, Jul. 2011.

[12] T.-N. Kuo, S.-C. Lin, C.-H. Wang, et al. New coupling scheme for microstrip bandpass filters with quarter-wavelength resonators. IEEE Transaction on Microwave Theory and Technology. Vol. 56, no. 12, pp: 2930-2935, Dec. 2008.

[13] J. Xu, Y. X. Ji, C. Miao, et al. Compact Single-/Dual-Wideband BPF Using Stubs Loaded SIR (SsLSIR). IEEE Microwave Wireless Component Letter. Vol. 23, no. 7, pp: 338-340, July 2013.

[14] Q.-X. Chu and X.-K. Tian. Design of UWB bandpass filter using stepped-impedance stub-loaded resonator. IEEE Microwave Wireless Component Letter. Vol. 20, no. 9, pp: 501-503, Sep. 2010.

[15] H.-W. Deng, Y.-J. Zhao, L. Zhang, et al. Compact quintuple-mode stub-loaded resonator and UWB filter. IEEE Microwave Wireless Component Letter. Vol. 20, no. 8, pp: 438-440, Aug. 2010.

[16]A. Gorur. Description of coupling between degenerate modes of a dual-mode

microstrip loop resonator using a novel perturbation arrangement and its dual-mode bandpass filter applications. IEEE Transaction on Microwave Theory and Technology. Vol. 52, no. 2, pp: 671-677, Feb. 2004.

[17]S.-C. Lin, P.-H. Deng, Y.-S. Lin, et al. Wide-stopband microstrip bandpass filters using dissimilar quarter-wavelength stepped-impedance resonators. IEEE Transaction on Microwave Theory and Technology. Vol. 54, no. 3, pp: 1011-1018, Mar. 2006.

[18] H. Wang and Q. X. Chu. An EM-Coupled Triangular Open-Loop Filter With Transmission Zeros Very Close to Passband. IEEE Microwave and Wireless Components Letters. Vol. 19, no. 2, pp. 71-73, Feb. 2009.

[19] A. Torabi and K. Forooraghi. Miniature harmonic-suppressed microstrip bandpass filter using a triple-mode stub-loaded resonator and spur lines. IEEE Microwave Wireless Component Letter. Vol. 21, no. 5, pp: 255-257, May 2011.

[20] Chan Ho Kim and Kai Chang. Wide-Stopband Bandpass Filters Using Asymmetric Stepped-Impedance Resonators. IEEE Microwave Wireless Component Letter. Vol. 23, no. 2, pp: 69-71, Feb. 2013.

[21] C. F. Chen, T. Y. Huang and R. B. Wu. Design of microstrip bandpass filters with multiorder spurious-mode suppression. IEEE Transaction on Microwave Theory and Technology. Vol. 53, no. 12, pp: 3788-3793, Dec. 2005.

[22] T. N. Kuo, S. C. Lin, C. H. Wang, et al. New Coupling Scheme for Microstrip Bandpass Filters With Quarter-Wavelength Resonators. IEEE Transaction on Microwave Theory and Technology. Vol. 56, no. 12, pp: 2930-2935, Dec. 2008.

[23] S. J. Sun, T. Su, K. Deng, B. Wu, et al. Shorted-Ended Stepped-Impedance Dual-Resonance Resonator and Its Application to Bandpass Filters. IEEE Transactions on Microwave Theory and Techniques. Vol. 61, no. 9, pp. 3209-3215, Sept. 2013.

[24] J. Fan, D. Zhan, C. Jin, and J. Luo. Wideband microstrip bandpass filter based on quadruple mode ring resonator. IEEE Microwave Wireless Component Letter. Vol. 22, no. 7, pp: 348-350, Jul. 2012.

[25] X. Luo, J. -G. Ma, and E. -P. Li. Wideband bandpass filter with wide stopband using loaded BCMC stub and short-stub. IEEE Microwave Wireless Component Letter. Vol. 21, no. 7, pp: 353-355, Jul. 2011.

[26] C. W. Tang and S. F. You. Miniaturized wide stopband rejected microstrip filter with coupled spur-lines. Electronics Letters. Vol. 42, no. 5, pp: 286-288, 2 March 2006.

[27] K. W. Hsu, W. C. Hung and W. H. Tu. Compact quint-band microstrip bandpass filter using double-layered substrate. Microwave Symposium Digest (IMS), 2013 IEEE MTT-S International, Seattle, WA, pp: 1-4. 2013.

[28] S. Zhang and L. Zhu. Compact Tri-Band Bandpass Filter Based on λ/4 Resonators With U-Folded Coupled-Line. IEEE Microwave Wireless Component Letter. Vol. 23, no. 5, pp: 258-260, May 2013.

[29] L. Gao, X. Y. Zhang, B. J. Hu, et al. Novel Multi-Stub Loaded Resonators and Their Applications toVarious Bandpass Filters. IEEE Transaction on Microwave Theory and Technology. Vol. 62, no. 5, pp: 1162-1172, May 2014.

[30] L. Gao, X. Y. Zhang and Q. Xue. Compact Tri-Band Bandpass Filter Using Novel

Eight-Mode Resonator for 5G WiFi Application. IEEE Microwave Wireles Component Letter. Vol. 25, no. 10, pp: 660-662, Oct. 2015.

[31] C. H. Kim and K. Chang. Independently Controllable Dual-Band Bandpass Filters Using Asymmetric Stepped-Impedance Resonators. IEEE Transaction on Microwave Theory and Technology. Vol. 59, no. 12, pp: 3037-3047, Dec. 2011.

[32] Y. C. Chang, C. H. Kao, M. H. Weng, et al. Design of the Compact Wideband Bandpass Filter With Low Loss, High Selectivity and Wide Stopband. IEEE Microwave Wireless Component Letter. Vol. 18, no. 12, pp: 770-772, Dec. 2008.

[33] H. W. Liu, et al. High-Temperature Superconducting Bandpass Filter Using Asymmetric Stepped-Impedance Resonators With Wide-Stopband Performance. IEEE Transaction on Applied Superconductivity. Vol. 25, no. 5, pp: 1-6, Oct. 2015.

[34] H. W. Wu and R. Y. Yang. A New Quad-Band Bandpass Filter Using Asymmetric Stepped Impedance Resonators. IEEE Microwave Wireless Component Letter. Vol. 21, no. 4, pp: 203-205, April 2011.

[35] A. L. C. Serrano, F. S. Correra, T. -P. Vuong, et al. Synthesis methodology applied to a tunable patch filter with independent frequency and bandwidth control. IEEE Transaction on Microwave Theory and Technology. Vol. 60, no. 3, pp: 484-493, Mar. 2012.

[36] J. S. Hong and M. J. Lancaster. Microstrip Filter for RF/Microwave Applications. New York: Wiley, 2001.

[37] R. Azadegan and K. Sarabandi. Miniature high-Q double-spiral slot-line resonator filters. IEEE Transaction on Microwave Theory and Technology. Vol. 52, no. 5, pp: 1548-1557, May 2004.

CHAPTER 7

Novel Multi-standard Mixed-Coupled Single-Wideband And Quint-Wideband Asymmetric Stepped Impedance Resonator Filters

7.1 Introduction

One of the prevalent methods for creating finite transmission zeros is the basic cross-coupling mechanism [1]. These cross couplings are equal in magnitude and out-of-phase with the mainline one at the transmission zero frequencies. Cross-coupling paths can be introduced either by resonant nodes [2]-[4], or non-resonant nodes [5], [6]. This mechanism is only valid with the assumption of narrowband nondispersive mainline and cross couplings, and it is able to generate maximum finite N transmission zeros without considering I/O ports (N is the filter order). Another popular mechanism to create finite transmission zeros is based on mixed inter-resonator couplings, where capacitive- or inductive-dominant mixed coupling is dispersive. In the filter core-passband synthesis, it provides required capacitive- or inductive-dominant couplings. Meanwhile, these capacitive and inductive components annihilate each other at certain frequencies,

resulting in finite transmission zeros. Mixed coupling between open-loop resonators was discussed in [7], and its inductive and capacitive components are enlaced with each other. An earlier work [8] employed stepped-impedance resonators (SIRs) to separately control inductive and capacitive components in mixed inter-resonator couplings. Separated inductive coupling using iris and capacitive coupling using strips were also introduced between two cavity resonators [9] and the substrate integrated waveguide (SIW) resonators [10]-[12] for implementation of compact inline quasi-elliptic bandpass filters. For the other planar implementations, quasi-elliptic bandpass filters based on resonators and separated and mixed couplings were illustrated in [13]-[18]. Explicit formulation presented in [7] and [11] explained the existence of one lower side transmission zero for the capacitive-dominant coupling, and one upper side transmission zero for the inductive-dominant coupling.

Figure 7.1 shows the proposed second-pole mixed coupled asymmetric stepped-impedance (ASIR) filter. In the traditional ASIR structure, each resonator has a high and low- characteristic impedance section. In the proposed mixed electric coupling and magnetic coupling (MEMC) modified ASIR structure, high-characteristic impedance sections are coupled partly with each other to form the spiral and open-loop structure leading to mixed electric coupling and magnetic coupling effect. The electric coupling is generated between the gaps of the coupled high impedance sections, since the resonator has the maximum electric fringe field density at the open ends [19]. The magnetic coupling is achieved by the parallel coupled section.

According to [20], S_{21} can be calculated as:

$$S_{21} = -\frac{2j\,\mathrm{Im}\{y_{12}\}}{1-\mathrm{Im}\{y_{11}\}^2+\mathrm{Im}\{y_{12}\}^2+2j\,\mathrm{Im}\{y_{11}\}} \tag{7.1}$$

The phase of S_{21} and the group delay (τ_d) are:

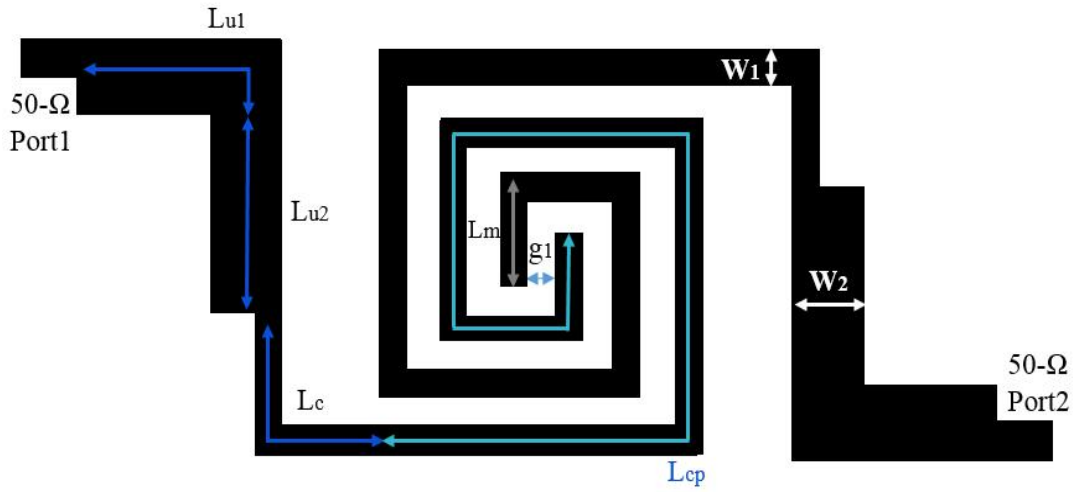

Figure 7.1 A skew-symmetrical asymmetric SIR couple pair with meander coupled section.

$$\angle S21 = \pi/2 - \tan^{-1}\left(\frac{2\mathrm{Im}\{y_{11}\}}{1-\mathrm{Im}\{y_{11}\}^2+\mathrm{Im}\{y_{12}\}^2}\right) \tag{7.2}$$

$$\tau_d = -\frac{\angle S21}{dw} = \frac{d}{dw}\tan^{-1}u = \frac{1}{1+u^2}\frac{du}{dw} \tag{7.3}$$

where

$$u = \frac{2\mathrm{Im}\{y_{11}\}}{1-\mathrm{Im}\{y_{11}\}^2+\mathrm{Im}\{y_{12}\}^2} \tag{7.4}$$

The Y-matrix [Y] of the coupled lines is expressed by the following:

$$[Y]=\begin{bmatrix} y_{11} & y_{12} \\ y_{21} & y_{22} \end{bmatrix}=\begin{bmatrix} -j\dfrac{1/Z_{0even}+1/Z_{0odd}}{2}\cot\theta_{cp} & j\dfrac{1/Z_{0even}-1/Z_{0odd}}{2}\csc\theta_{cp} \\ j\dfrac{1/Z_{0even}-1/Z_{0odd}}{2}\csc\theta_{cp} & -j\dfrac{1/Z_{0even}+1/Z_{0odd}}{2}\cot\theta_{cp} \end{bmatrix} \tag{7.5}$$

However, it seems that it needs be corrected as the Y-matrix [Y']:

$$[Y']=\begin{bmatrix} y_{11} & y_{12} \\ y_{21} & y_{22} \end{bmatrix}=\frac{1}{B}\begin{bmatrix} -j\dfrac{Z_{0even}+Z_{0odd}}{2}\cot\theta_{cp} & j\dfrac{Z_{0even}-Z_{0odd}}{2}\csc\theta_{cp} \\ j\dfrac{Z_{0even}-Z_{0odd}}{2}\csc\theta_{cp} & -j\dfrac{Z_{0even}+Z_{0odd}}{2}\cot\theta_{cp} \end{bmatrix} \tag{7.6}$$

Based on the equation above, S_{21} is equal to zero when coupled line length $L_{cp} = \lambda/4$ corresponds to $\theta_{cp}=90°$ (θ_{cp} is the electrical length of L_{cp}). Since u =0 in this case,

$$\tau_{d,\omega=\omega_0}=-\frac{\angle \mathrm{S21}}{dw}=\frac{du}{dw}=\frac{d\theta_{cp}}{dw}\frac{du}{d\theta_{cp}} \tag{7.7}$$

and the group delay of the coupled line τ_d can be expressed as

$$\tau_d=\frac{\theta_{cp}}{\omega}A\left(1-\cot^2\theta_{cp}+B\cot\theta_{cp}\right) \tag{7.8}$$

where

$$\begin{cases} A=\dfrac{Z_{0e}+Z_{0o}}{1-\dfrac{\left(Z_{0e}+Z_{0o}\right)^2}{4}\cot^2\theta_{cp}+\dfrac{Z_{0e}-Z_{0o}}{4}\csc^2\theta_{cp}} \\ B=\dfrac{\left(Z_{0e}+Z_{0o}\right)^2}{2}\cot\theta_{cp}\left(1+\cot^2\theta_{cp}\right)-\dfrac{\left(Z_{0e}-Z_{0o}\right)^2}{2}\cot\theta_{cp}\csc^2\theta_{cp} \end{cases} \tag{7.9}$$

The equivalent circuit of the coupled structure in the proposed filter is shown in Figure 7.2.

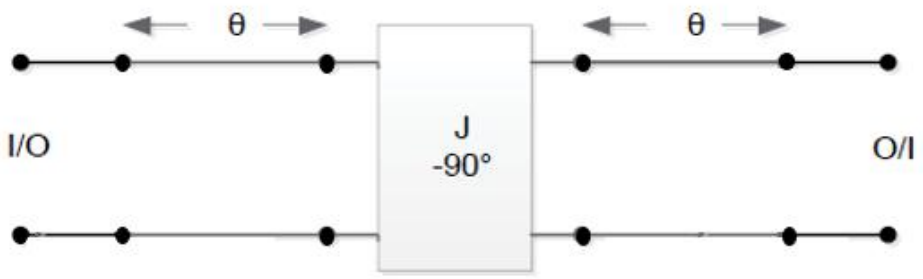

Figure 7.2. The equivalent circuit of the coupled structure in the proposed filter.

The coupling routing scheme of the proposed filter is shown in Figure 7.3. It is seen from Figure 7.3 that at least four coupling routings are created by the use of the spiral and open loop (SOL) structure, which lead to the cross-coupling and multiple transmission zeros. This can facilitate the forming of the wide stopband.

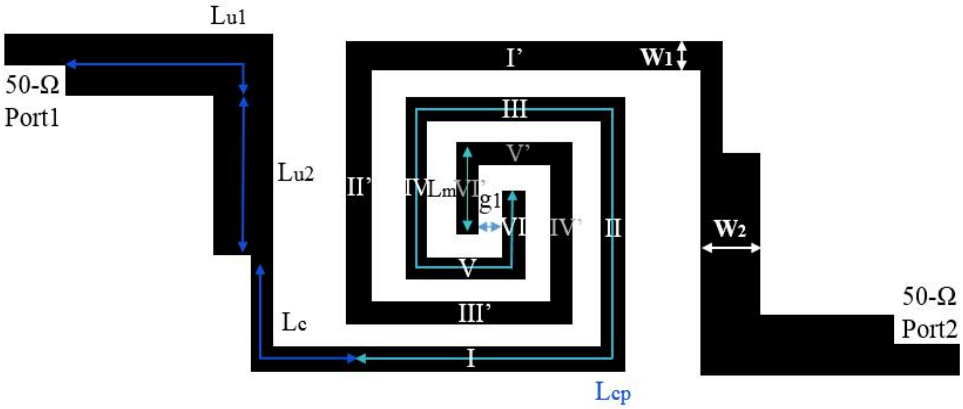

(a)

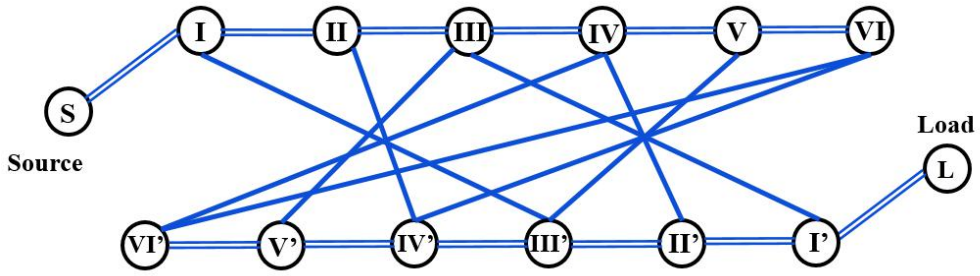

(b)

Figure 7.3. The coupling routing scheme of the proposed filter. (a) The structure. (b) The coupling routing scheme.

7.2. Single-Wideband Filter Design

(a) The effect of parameter L_{m1}: Figure 7.4 shows the effect of parameter L_{m1} in a single-wideband type mixed coupling ASIR filter. It is seen from Figure 7.3 that when L_{m1} increases, f_0 would become smaller, that means the fundamental frequency can be changed by ~~the~~ means of changing the coupling length parameter L_{m1} of the ASIR coupled structure. At the same time, the stopband suppression level would be changed with the increase of L_{m1}. When L_{m1}=1.8 mm, the stop-band ranges from 3.45-11.35 GHz with best -13.9 dB suppression level. The in-band best insertion loss (IL) is -0.85 dB. When L_{m1} = 2.2 mm, the stop-band ranges from 3.26-10.7 GHz, which is $4.2f_0$ (f_0 is the fundamental frequency of the filter). The return loss (IL) is larger than -12.0 dB. Although the stopband suppression level becomes less, the bandwidth, the insertion loss performance and return loss performance are improved, while when L_{m1} increase from 1.8 mm to 2.2 mm, the widened bandwidth ranges from 2.25-2.82 GHz with central

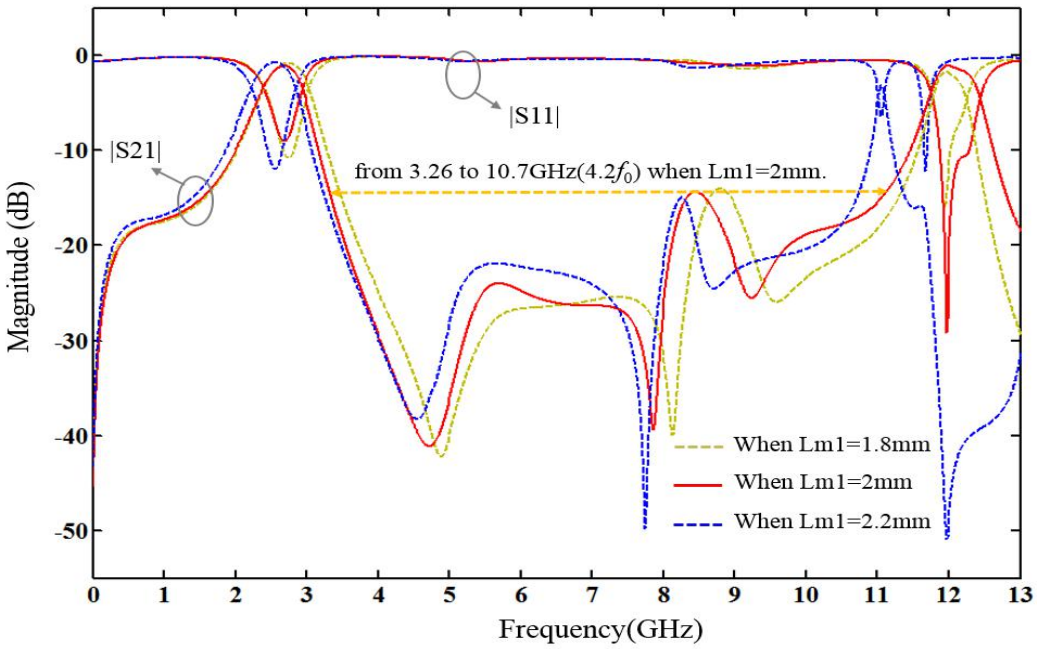

Figure 7.4. The effect of parameter L_{m1} in single-wideband type mixed coupling ASIR filter with SOL structure.

frequency of 2.535 GHz. The in-band best insertion loss (IL) is -0.77 dB.

(b) The effect of parameter g: to increase the coupling gap g between the high characteristic impedance lines from 0.25 mm to 0.31 mm, both the fundamental frequency and the harmonic frequency change little. However, the insertion loss of the pass-band would be changed from -0.75 dB to -0.76 dB and from -0.76 dB to -1.67 dB when g increases from 0.25 mm to 0.31 mm, and the return loss of the pass-band would be changed from from -11.8 dB to -12.0 dB and from -12.0 dB to -6.8 dB. This means that the coupling strength is weakened by the increasing of g.

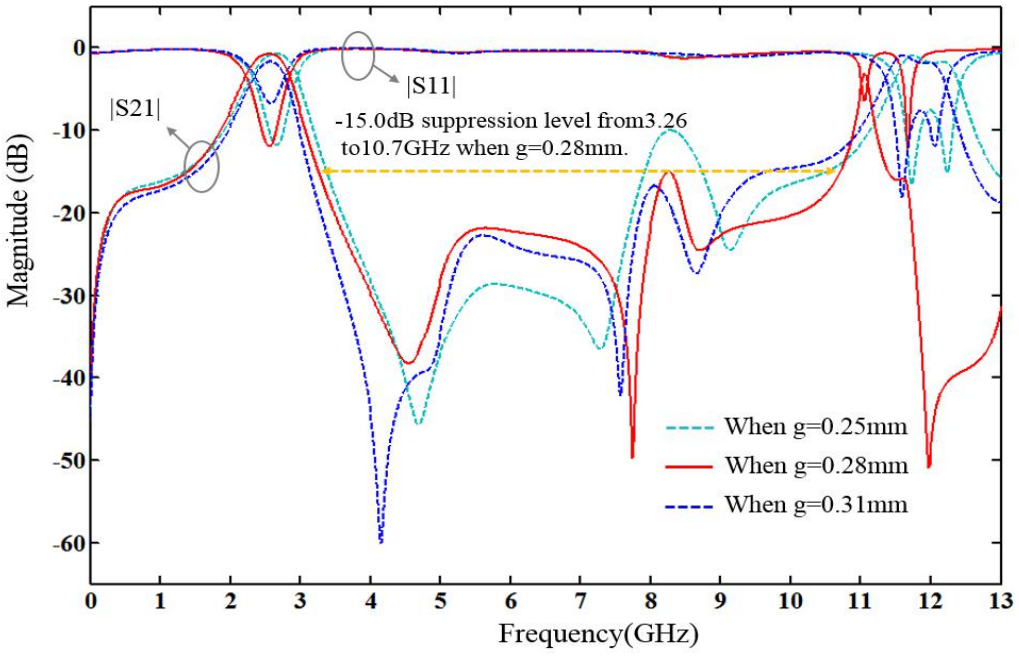

Figure 7.5. The effect of parameter g in single-wideband type mixed coupling ASIR filter with SOL structure.

At the same time, the stop-band suppression level is enhanced by ~~the~~ increasing ~~of~~ g, which changes from -10 dB to -16.7 dB with general broadened stopband bandwidth. Besides, the stop-band width would be changed by the change of g. The optimized

value of parameter g can be found as 0.28 mm from Figure 7.5, which shows the effect of parameter g in single-wideband type mixed coupling ASIR filter.

(c) The effect of parameter L_c: when the uncoupled high characteristic impedance lines L_c increase from 0.5 mm to 0.15 mm, the fundamental frequency and the harmonic frequency decrease. Meanwhile, the pass-band insertion loss and return loss performance become better, and the stop suppression level firstly becomes better then becomes worse later. This means the uncoupled part of the mixed coupling ASIR filter with spiral and open-loop coupled structure can also influence the resonance locations, insertion loss and return loss performance. Figure 7.6 shows the effect of parameter L_c in the single-wideband type mixed coupling ASIR filter. The optimized value of parameter L_c can be found as 1 mm from Figure 7.6.

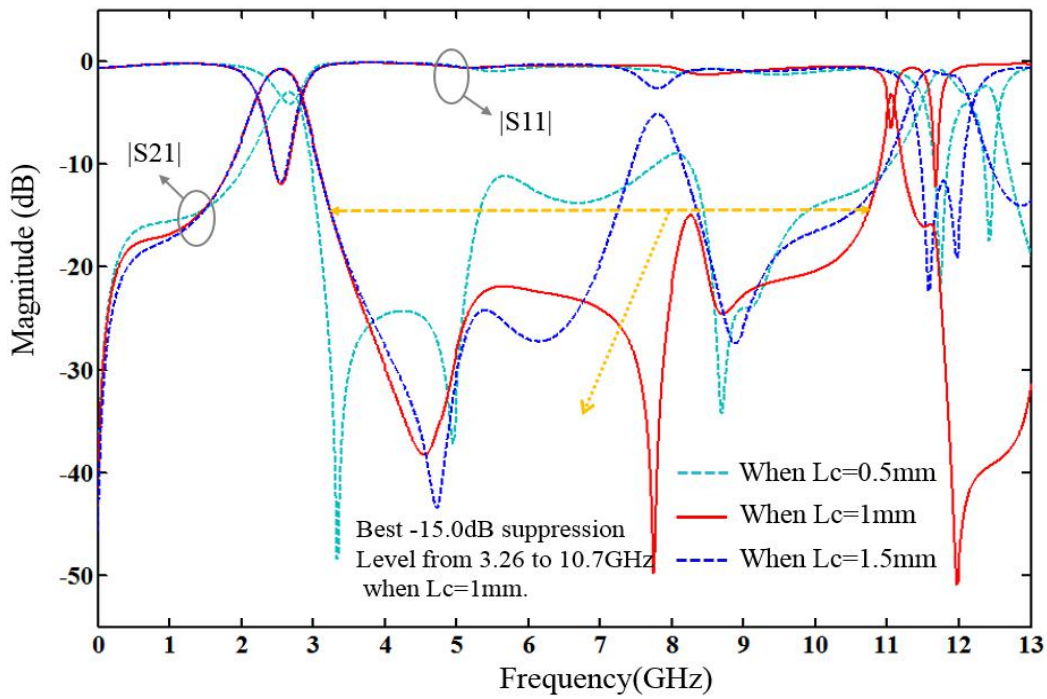

Figure 7.6. The effect of parameter L_c in single-wideband type mixed coupling ASIR filter with SOL structure.

(d) The effect of parameter L: when L increases from 3 mm to 3.8 mm, the fundamental frequency and the harmonic frequency do not change much. At the same time, the return loss changes from better than 11.9 dB to better than 8.4 dB . When L=3.8 mm, the stop

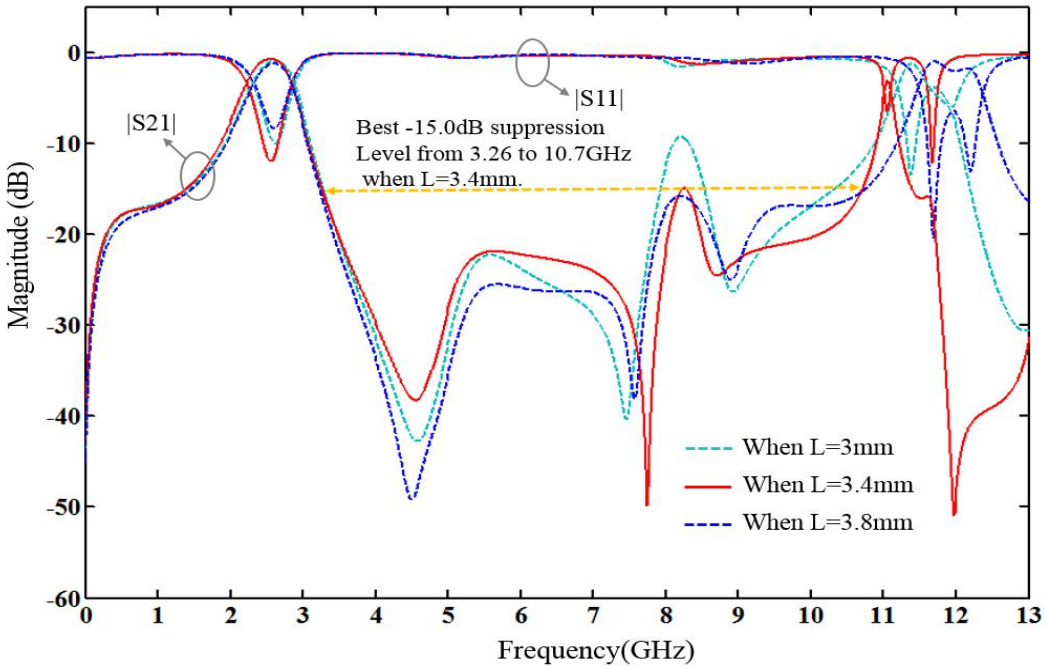

Figure 7.7. The effect of parameter L in single-wideband type mixed coupling ASIR filter with SOL structure.

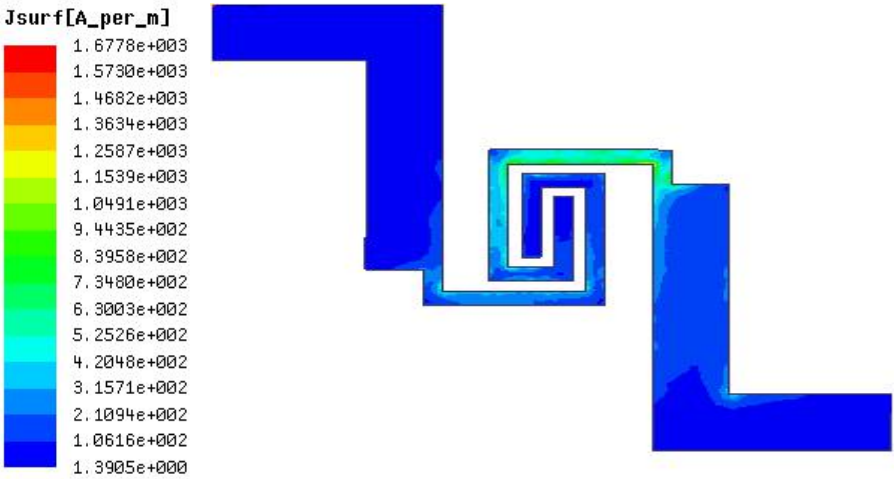

Figure 7. 8. Single-wideband type spiral and open-loop coupled ASIR band-pass filter's surface current distribution at f_0.

band ranges from 3.26-10.6 GHz. When L is equal to 3 mm, the stop-band ranges from 3.08-11.9 GHz with a suppression level of -9.3 dB. When L increases to 3.4 mm, the stop-band ranges from 3.26-11.7 GHz with a suppression level of -15.0 dB. Figure 7.7 shows the effect of parameter L in single-wideband type mixed coupling ASIR filter. The optimized value of parameter L can be obtained as 3.4 mm from Figure 7.7.

Figure 7.8 illustrates the single-wideband type spiral and open-loop coupled ASIR band-pass filter's surface current distribution at f_0, showing that when the electric coupling is weak due to the relative long distance between two open ends of the high characteristic lines, the magnetic coupling plays a main role to the fundamental mode. The dimensions of the spiral and open-loop ASIR filter in Figure 7.1 are L_{m1} =2.0 mm, L_{c1} = 1.0mm, L=3.4 mm, g=0.28mm, W_2 =0.4mm and W_1 = 1.6 mm.

7.3. The Quint-Wideband Filter Design

Many multi-band filters have been presented in literature such as in [21]-[27]. Among them, tri-band bandpass filters and quad-band filters are good candidates [21]-[24]. However, both proposed types of filter have the disadvantage of narrow-band characteristics which cannot cover the required frequency bands, insertion loss performances which are not satisfactory or occupying relatively large sizes. To further improve the filter performances and solve the problems mentioned above, the quint-band filter was firstly proposed in 2012 by [27], which proposed tri-mode stub-load stepped-impedance resonators to realize quint-band performance. A multiple stubs loaded ring resonator (MSLRR) is proposed in [26] to design directly coupled multi-band bandpass filters (BPFs) with mixed electric and magnetic coupling (MEMC), and

[25] utilizes three pairs of simple microstrip stepped-impedance resonators on the top and middle metal layer, and two pairs of slot uniform-impedance resonators on the bottom metal layer. By this means, a quint-band performance can be realized by these individual structures. However, all of the proposed quint bandpass filters have relatively complicated structures such as multiple via holes [26][27] or multi-layer structures. These disadvantages make the design and fabrication complicated, leading to high loss and cost.

In this section, a compact quint-wideband bandpass filter with low insertion loss, good return loss and wide passband is designed. The proposed filter has no extra structure such as via holes or multi-layer. The filter is designed, fabricated and measured. A good agreement between simulated and measured results is obtained. The proposed quint-wideband mixed-coupling ASIR filter with the description of electric coupling and magnetic coupling effect is illustrated in Figure 7.9. The centre and both ends of an ASIR coupled section are the fundamental mode's peak points of the magnetic field and electric field, respectively. To enhance the electric coupling of the filter, two adjacent spiral ASIRs' ends can be closely located, which can be adjusted by g_1. We can enhance the magnetic coupling of the fundamental mode by closely locating two adjacent spiral ASIRs' parallel coupling parts, which can be adjusted by g_2. The field peak points of the proposed filter using spiral and open-loop structure is shown in Figure 7.10. The coupling points of spurious modes can be adjusted by changing coupling length L_{cp}. The spurious modes can also be adjusted by changing uncoupled section lengths L_{u1} and L_c, which add the freedom for designing the quint-band filter. The effect of spiral and open-loop coupled high characteristic impedance line structures (SOLHLs) in ASIRs can be reflected by the surface current distribution at fundamental frequency and its spurious

frequencies, which is illustrated in Figure 7.11. In Figure 7.11, magnetic coupling plays a main role to the fundamental frequency because the electrical coupling is weakened by the long distance between two open ends, whereas the four spurious mode f_{s1}, f_{s3}, f_{s4} and f_{s5} current densities are high in different places of the SOLHLs, which means the SOLHLs facilitates the forming of high-order modes in the proposed quint-band filter. The simulated results' comparison between the quint-wideband type modified ASIR BPF with and without the SOLHL structure is shown in Figure 7.12.

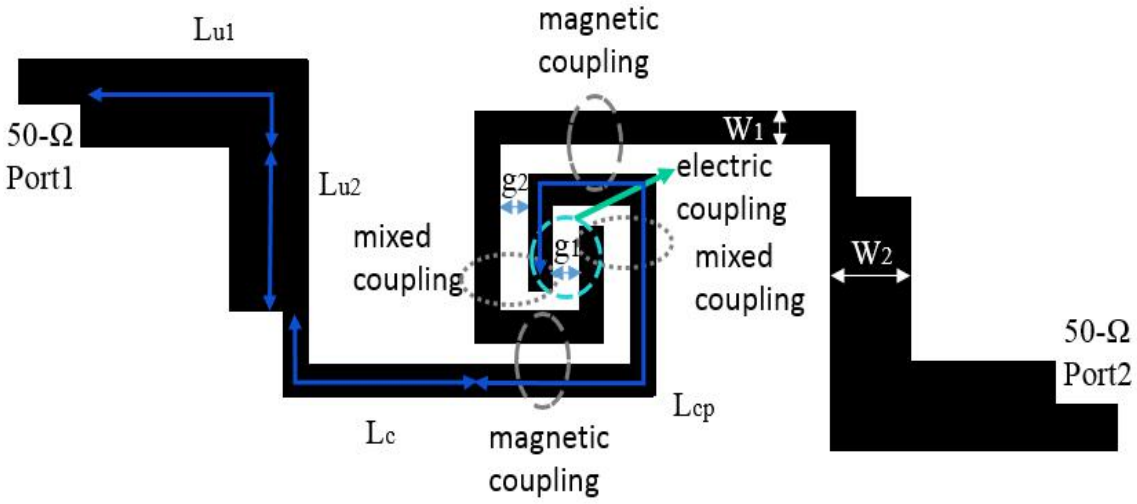

Figure 7.9. The proposed quint-wideband mixed-coupling ASIR filter with the description of electric coupling and magnetic coupling effect.

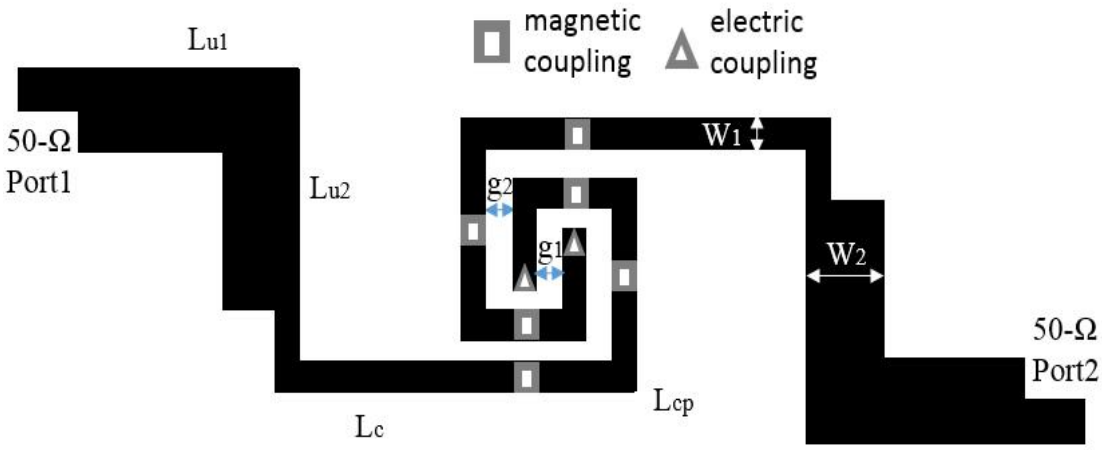

Figure 7.10. Field peak points of the filter using spiral and open-loop couple structure.

To investigate the character of the proposed structure, the filter is designed on a Rogers RO3210 substrate with dielectric parameter of 10.2, tanδ of 0.0027 and thickness of 0.635 mm, then is simulated by HFSS. The dimensions of the spiral and open-loop ASIR filter in Figure 7.9 are L_{u1} = 5.9 mm, L_{u2} = 6.6 mm, L_c =9.3 mm, L_{cp} =17.8 mm, g_1 = 0.22mm, g_2 = 0.2mm and W_1=1.6 mm. The total size of the proposed cross-coupled spiral SIR filter is 0.17 λ_g×0.4l λ_g, where λ_g is the microstrip guided wavelength at f_0. Its measured result agrees well with the simulation.

Simulated and measured results of the quint-wideband ASIR filter with SOLHLs are plotted in Figure 7.12 and Figure 7.13, respectively. Good agreement is observed between the simulated and measured results and the discrepancies are attributed to the loss, fabricated errors and so on. The first pass-band ranges from 1.03-1.52 GHz with central frequency (CF) of 1.275 GHz, and bandwidth (BW) of 490 MHz It is suitable for GPS (L1 band: 1.57542 GHz, L2 band: 1.22760 GHz, L3 band: 1.38105 GHz, L4 band: 1.84140 GHz). The second pass-band ranges from 3.03-3.42 GHz with CF of 3.225 GHz, BW of 390 MHz, and can be used in 3G Wi-Fi application. The third pass-band ranges from 5.52-6.23 GHz with CF of 5.875 GHz, BW of 710 MHz, so can be used in IEEE802.11a applications. The fourth pass-band ranges from 7.00-8.03 GHz with CF of 7.515 GHz, BW of 1.03 GHz, while the fifth pass-band ranges from 9.53-9.95 GHz with CF of 9.74 GHz, and has a large BW of 420 MHz, They can be used in satellite communication. Two transmission zeros located at 2.49 GHz and 4.98 GHz are formed to further enhance the frequency selectivity, also illustrated in Figure 7.12.

The photograph of the fabricated quint-wideband ASIR filter with SOLHLs is Figure 7.14.

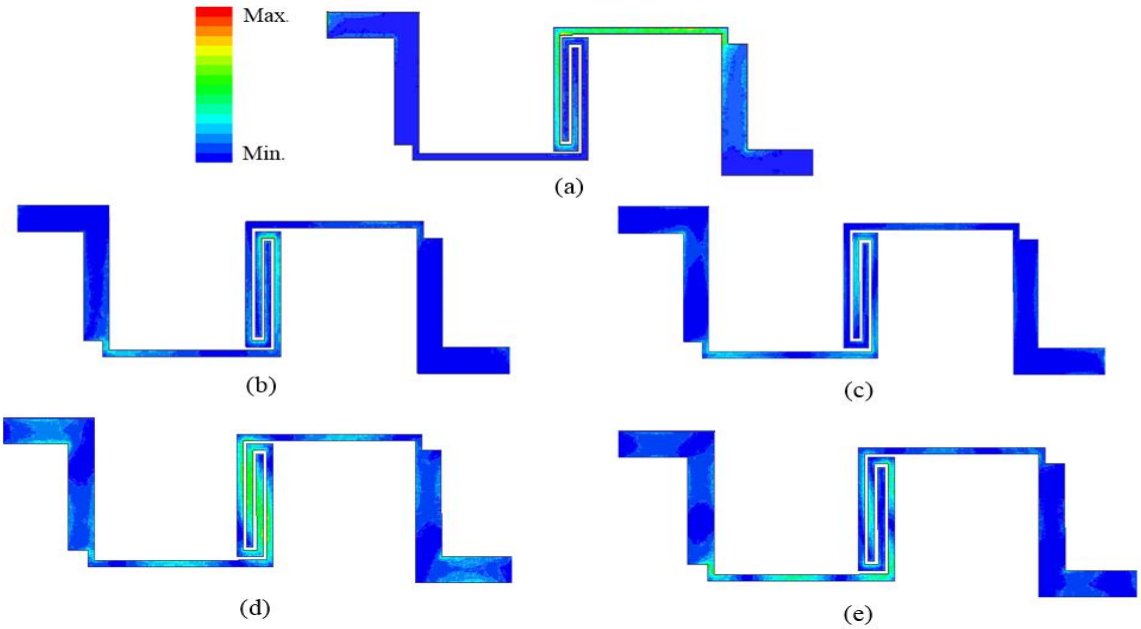

Figure 7.11. The quint-wideband type spiral and open-loop coupled ASIR band-pass filter's surface current distribution at (a) f_0, (b) f_{s1}, (c) f_{s3}, (d) f_{s4} and (e) f_{s5}.

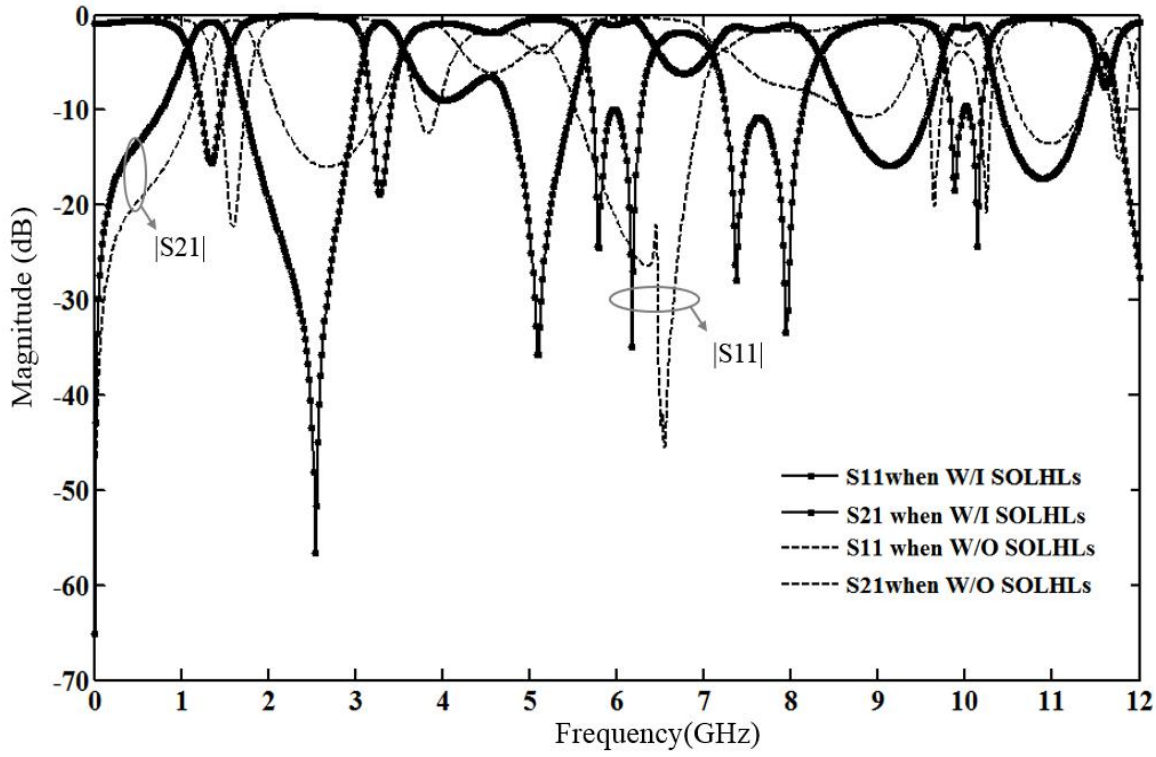

Figure 7.12. The simulated results comparison between the quint-wideband type modified ASIR BPF with and without the spiral and open loop structure.

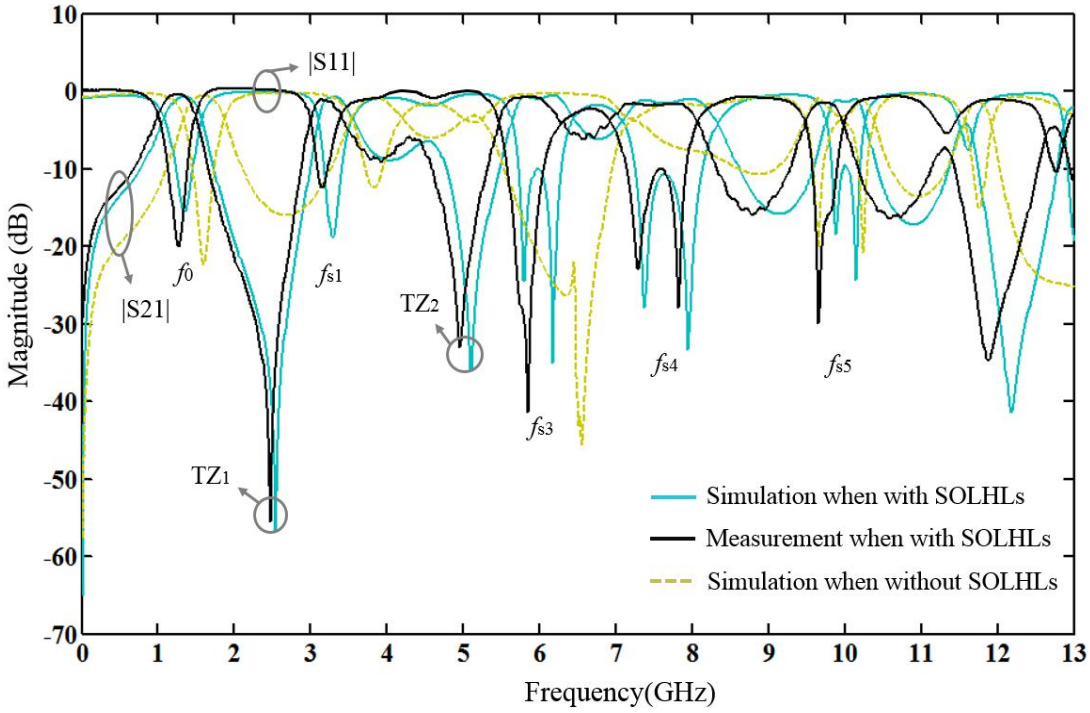

Figure 7.13. Simulated and measured results of the proposed quint-wideband ASIR filter.

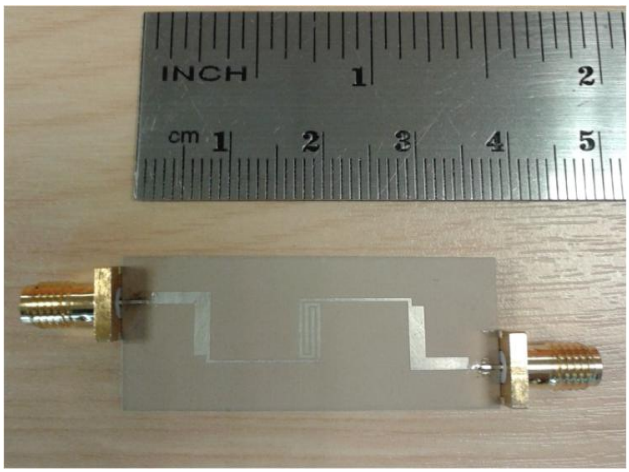

Figure 7.14. Photograph of the fabricated quint-wideband ASIR filter.

Table 7.1

PERFORMANCE COMPARISON WITH CURRENTLY QUINT-BAND BPFs

	CF(GHz)/ 3 dB FBW (%)	Insertion Loss (dB)	SIZE	EXTRA STRUC-TURE
[27]	0.6/5.8%, 0.9/5.2%, 1.2/5.8%, 1.5/8.2%, 1.8/8.0%	2.8,2.9,2.9, 2.6,2.3	0.045 λ_g ×0.52 λ_g	VIA HOLE
[26]	0.63/28.8%, 1.33/9.4%, 2.03/2.7%, 2.74/5.3%, 3.45/5.5%	0.47,1.14,1.8, 1.39,1.26	0.043 λ_g ×0.178 λ_g	VIA HOLE
[25]	1.5/4.5%, 2.5/4.5%, 3.5/3.6%, 4.5/4.5%, 5.8/2.7%	1.5,1.8,0.9, 1.2,2.5	0.24 λ_g ×0.17 λ_g	MULTI-LAYER
THIS WORK	**1.275/38.4%, 3.225/12.1%, 5.875/12.1%, 7.515/13.7%, 9.74/4.3%**	**0.41,1.27,0.83, 1.74,1.55**	**0.11 λ_g ×0.34 λ_g**	**NONE**

It can be seen that the proposed structure has advantages including bigger fractional bandwidth, amongst which four fractional bandwidths are higher than 10% and are better than the published works. The insertion losses are lower than published ones. All the tri-band insertion losses are less than 1.6dB. Furthermore, the proposed two structures are simple and are easily made.

7.4. Conclusion

In general, new mixed-coupled quint-wideband ASIR bandpass filters which consist of spiral and open-loop coupled structure to enhance fundamental mode coupling and another four spurious modes coupling with optimum insertion loss performance have been proposed. The proposed filter has the advantages of applicable quint-wideband, simple structure and compact size, which are all attractive and versatile for the microwave/RF applications in future multi-function wireless communication.

7.5 References

[1] R. Levy. Filters with single transmission zeros at real or imaginary frequencies. IEEE Transaction on Microwave Theory and Technology. Vol. MTT-24, no. 4, pp: 172-181, Apr. 1976.

[2] J. -S. Hong and M. J. Lancaster. Design of highly selective microstrip bandpass filters with a single pair of attenuation poles at finite frequencies IEEE Transaction on Microwave Theory and Technology. Vol. 48, no. 7, pp: 1098-1107, Jul. 2000.

[3] S. Zhang, L. Zhu, and R. Li. Compact quadruplet bandpass filter based on alternative J/K inverters and resonators. IEEE Microwave Wireless Component Letter. Vol. 22, no. 5, pp: 224-226, May 2012.

[4] R. J. Cameron. General coupling matrix synthesis methods for Chebyshev filtering functions. IEEE Transaction on Microwave Theory and Technology. Vol. 47, no. 4, pp: 433-442, Apr. 1999.

[5] S. Bastioli, C. Tomassoni and R. Sorrentino. A new class of waveguide dual-mode filters using TM and no resonating modes. IEEE Transaction on Microwave Theory and Technology. Vol. 58, no. 12, pp: 3909-3917, Dec. 2010.

[6] S. Bastioli and R. V. Snyder. Inline pseudo elliptic TE01-mode dielectric resonator filters using multiple evanescent modes to selectively bypass orthogonal resonators. IEEE Transaction on Microwave Theory and Technology. Vol. 60, no. 12, pp: 3988-4001, Dec. 2012.

[7] Q. Chu and H. Wang. A compact open-loop filter with mixed electric and magnetic coupling IEEE Transaction on Microwave Theory and Technology . Vol. 56, no. 2, pp: 431-439, Feb. 2008.

[8] J. Kuo, C. Hsu, and E. Shih. Compact planar quasi-elliptic function filter with inline stepped-impedance resonators. IEEE Transaction on Microwave Theory and Technology. Vol. 55, no. 8, pp: 1747-1755, Aug. 2007.

[9] H. Wang and Q. -X. Chu. An inline coaxial quasi-elliptic filter with controllable mixed electric and magnetic coupling. IEEE Transaction on Microwave Theory and Technology. Vol. 57, no. 3, pp: 667-673, Mar. 2009.

[10] W. Shen, L. -S. Wu, X. -W, et al. Novel substrate integrated waveguide filters with mixed cross coupling (MCC). IEEE Microwave Wireless Component Letter. Vol. 19, no. 11, pp: 701-703, Nov. 2009.

[11] K. Gong, W. Hong, Y. Zhang, et al. Substrate integrated waveguide quasi-elliptic filters with controllable electric and magnetic mixed coupling. IEEE Transaction on Microwave Theory and Technology. Vol. 60, no. 10, pp: 3071-3078, Oct. 2012.

[12] P. Chu. et al. A planar bandpass filter implemented with a hybrid structure of substrate integrated waveguide and coplanar waveguide. IEEE Transaction on Microwave Theory and Technology. Vol. 62, no. 2, pp: 266-274, Feb. 2014.

[13] K. Ma, J. Ma, et al. Do. A compact size coupling controllable filter with separate electric and magnetic coupling paths. IEEE Transaction on Microwave Theory and Technology. Vol. 54, no. 3, pp: 1113-1119, Mar. 2006.

[14] C. -L. Hsu, C. -H. Yu, and J. -T. Kuo. Control of transmission zero by mixed-coupling in a two-stage coupled-resonator filter. Proceeding Asia-Pacific

Microwave Conference. pp: 1-4. 2007.

[15] L. Athukorala and D. Budimir. Design of compact dual-mode microstrip filters. IEEE Transaction on Microwave Theory and Technology. Vol. 58, no. 11, pp: 2888-2895, Nov. 2010.

[16] E. Doumanis, G. Goussetis, and S. A. Kosmopoulos. Inline interdigital pseudo-elliptic helical resonator filters. IEEE Microwave Wireless Component Letter. Vol. 21, no. 8, pp: 400-402, Aug. 2011.

[17] S. Tang, J. Kuo, and S. Chung. Bandwidth and transmission zero control for compact dual-mode resonator filter by extraction of EM coupling. Proceeding of Asia-Pacific Microwave Conference. pp: 661-663. 2012.

[18] F. Zhu, W. Hong, J. Chen, et al. Quarter-wavelength stepped impedance resonator filter with mixed electric and magnetic coupling. IEEE Microwave Wireless Component Letter. Vol. 24, no. 2, pp: 90-92, Feb. 2014.

[19]J. S. Hong and M. J. Lancaster. Microstrip Filter for RF/Microwave Applications. New York: Wiley, 2001.

[20] S. S. Myoung, Y. Lee and J. G. Yook. Bandwidth-Compensation Method for Miniaturized Parallel Coupled-Line Filters. IEEE Transaction on Microwave Theory and Technology. Vol. 55, no. 7, pp. 1531-1538, July 2007.

[21] L. Gao, X. Y. Zhang and Q. Xue. Compact Tri-Band Bandpass Filter Using Novel Eight-Mode Resonator for 5G WiFi Application. IEEE Microwave and Wireless Components Letters. Vol. 25, no. 10, pp. 660-662, Oct. 2015.

[22] F. Song, B. Wei, L. Zhu, et al. A Novel Tri-Band Superconducting Filter Using Embedded Stub-Loaded Resonators. IEEE Transactions on Applied Superconductivity. Vol. 26, no. 8, pp. 1-9, Dec. 2016.

[23] H. W. Wu and R. Y. Yang. A New Quad-Band Bandpass Filter Using Asymmetric Stepped Impedance Resonators. IEEE Microwave and Wireless Components Letters. Vol. 21, no. 4, pp. 203-205, April 2011.

[24] C. Karpuz, A. K. Gorur and M. Emur. Quad-Band Microstrip Bandstop Filter Design Using Dual-Mode Open Loop Resonators Having Thin Film Capacitors. IEEE Microwave and Wireless Components Letters. Vol. 26, no. 11, pp. 873-875, Nov. 2016.

[25] K. W. Hsu, W. C. Hung and W. H. Tu. Compact quint-band microstrip bandpass filter using double-layered substrate. Microwave Symposium Digest, pp. 1-4. 2013.

[26] J. Xu, W. Wu and G. Wei. Compact Multi-Band Bandpass Filters with Mixed Electric and Magnetic Coupling Using Multiple-Mode Resonator. IEEE Transaction

on Microwave Theory and Technology. Vol. 63, no. 12, pp. 3909-3919, Dec. 2015.

[27]Chi-Feng Chen.Design of a Compact Microstrip Quint-Band Filter Based on the Tri-Mode Stub-Loaded Stepped-Impedance Resonators. IEEE Microwave and Wireless Components Letters. Vol.63, no.12,pp.357-359, July 2012.

CHAPTER 8

Summarized Conclusions And Recommendations for Future Work

8.1 Summarized Conclusions

Chapter 1: explained the motivation for this work as being the development of high performance, multi-standard filters with compact size, low in-band insertion loss (IL), and high out-of-band rejection skirts. Current developments in microwave filter design were outlined, with asymmetric stepped impedance resonator architectures providing the context for those further improvements and innovations proposed in this work.. Moreover, present day wireless communication standards and relative operating frequency bands are identified for better understanding of the microwave. radio frequency context

Chapter 2: provides an introduction and a comprehensive literature review of the state of the art in microwave filters. The recent main stream of microwave filters are classified and discussed separately in detail. This chapter also shows performance and structure analyses combining new materials, new structures and new technologies in the

microwave filter field, helpful to the enhancement of the performance of microwave filters as well as microwave systems.

Chapter 3: presents a comprehensive theoretical study of microwave filters. It includes the introduction of four basic filter types: low-pass, high-pass, band-pass and band-stop filters. Filter design parameters are presented. Three classic filter types are explained. Furthermore, the way to transform filter frequency is also presented and described in detail.

Chapter 4: provides a comprehensive study of the stepped impedance resonator (SIR) structure. All three types of quarter wavelength, half wavelength and full wavelength SIR resonator are analysed and fully explained. All of these are helpful to the detailed design of SIR filters in the next chapter. Moreover, the asymmetric stepped impedance resonator, which is a novel SIR structure and has appeared in recent publications in the last ten years, is studied because of its advantages over other structures including the SIR structure. Sensitivity of the performance to variation in dimensions is explored.

Chapter 5: Based on ideas discussed in the earlier chapters, a novel parallel coupled ASIR structure is proposed and its characteristics are fully analysed and discussed. The proposed novel interdigital cross-coupled lines structure successfully realizes fractional bandwidths of 43.2% and 10.5%, respectively. Due to the use of an interdigital cross-coupled structure, multiple routes and an extra transmission zero are generated. This leads to the realization of the wide stop band. The measurement result shows that the filter has a wide stop band ranging from 2.46-4.86 GHz with -10dB suppression level and a stop band ranging from 6.05-12.1 GHz with -10 dB suppression level. This can

suppress the signal interference from the 3.5 GHz Worldwide Interoperability for Microwave Access signal, satellite communication signals and so on.

The proposed novel parallel uncoupled ASIR structure successfully realizes the first pass-band ranges from 1.37-1.89 GHz with a central frequency of 1.63 GHz, bandwidth of 520 MHz and fractional band width (FBW) of 31.9%. The second pass-band ranges from 3.66-5.46 GHz with central frequency of 4.46 GHz, a bandwidth of 1.8 GHz and fractional band width (FBW) of 33.0%. Moreover, the stop-band ranges from 2.12-3.5 GHz with -10 dB suppression level. A wide upper stop-band ranging from 5.83-9.35 GHz with -10 dB suppression is realized.

Chapter 6: This chapter proposes an ASIR coupled structure rearranged by the meander coupled section. The novel structure's characteristics, mathematical analyses as well as the generation condition for the transmission zero point are analysed. The measurement result shows that a single-wideband filter is realized with very low insertion isolation of only 0.36 dB at the central frequency and return loss of better than 25.5 dB. The pass-band ranges from 1.18-1.84 GHz with central frequency 1.51 GHz, bandwidth 660 MHz and fractional band width (FBW) 43.7%. Due to the use of transmission zero realization method, a wide stop-band ranging from 2.1-7.32 GHz is realized, which can suppress signal interference such as IEEE802.11b, Worldwide Interoperability for Microwave Access signal, IEEE802.11a and so on. The proposed second filter realizes the first pass band ranging from 1.0 to 1.38 GHz with a central frequency (CF) of 1.19 GHz, and bandwidth (BW) of 380 MHz. The second pass band ranges from 3.96 to 4.62 GHz with CF of 4.29 GHz, BW of 660 MHz. The third pass band ranges from 5.0 to 5.86 GHz with CF of 5.43 GHz and BW of 860 MHz. The fourth pass band ranges from 6.82 to 7.12 GHz with CF of 6.97 GHz and BW of

300MHz. The fifth pass band ranges from 7.96 to 11.84 GHz with CF of 9.9GHz, and a large BW of 3.88GHz. It has many detailed application.

Chapter 7: This chapter proposes an ASIR spiral and open loop coupled structure to realize the single-wideband filter and the quint-wideband filter. The proposed first structure realizes a wide bandwidth ranging from 2.25-2.82GHz with central frequency of 2.535GHz. The in-band best insertion loss (IL) is -0.77dB. Furthermore, a wide stop band ranges from 3.26 to 10.7 GHz with -15dB suppression level is realized. It can suppress the signal inference such as Worldwide Interoperability for Microwave Access signal, IEEE802.11a and so on. The use of a spiral and open-loop structure, which can realize the mixed electric coupling and magnetic coupling effect at the same time, facilitates the quint-band performance. The structure for quint band is realized. The first pass-band ranges from 1.03-1.52 GHz with central frequency (CF) of 1.275 GHz, and bandwidth (BW) of 490 MHz. The second pass-band ranges from 3.03-3.42 GHz with CF of 3.225GHz, BW of 390MHz. The third pass-band ranges from 5.52-6.23 GHz with CF of 5.875 GHz and BW of 710MHz. The fourth pass-band ranges from 7.00-8.03 GHz with CF of 7.515 GHz and BW of 1.03 GHz, while the fifth pass-band ranges from 9.53-9.95 GHz with CF of 9.74 GHz and a large BW of 420 MHz. The proposed structures are promising for applications in multi-standard wireless communication.

Chapter 8: This chapter summarises the above mentioned outcomes and proposes the future plan.

8.2 Recommendations for Future Work

Throughout the research it was observed that there are areas for future work that can be carried out:

- Analyse the theory and performance of a novel multi-standard modified polygon resonator filter which covers GSM/UMTS/IEEE 802.11 bands. To validate the ideas, the multi-standard filter need to be simulated by Ansoft HFSS software, fabricated and measured.

- Analyse the theory and performance of a proposed novel multi-standard modified parallel resonator filter. To validate the ideas, the multi-standard filter need to be simulated, fabricated and measured.

- Analyse the theory and performance of a proposed novel multi-standard modified mixed electronic and magnetic coupling (MEMC) filter. To validate the ideas, the multi-standard filter need to be simulated by Ansoft HFSS software, fabricated and measured.

- Analyse the theory and performance of a proposed novel multi-standard modified polygon resonator coupled with ring resonator. To validate the ideas, the multi-standard filter need to be simulated by ADS software, fabricated and measured.

- Analyse the theory and performance of a proposed novel filter whose resonant frequency can be tuneable and reconfigurable. To validate the ideas, the multi-standard filter need to be simulated by Ansoft HFSS software, fabricated and measured.

1. Author's Publication Record

JOURNAL ARTICLES

1. **Y. Tu**, et al, Mixed-Coupling Multi-Function Wideband Stepped Impedance Resonator Filter with Wide Stop-band. Electronics letters. Under review.

2. **Y. Tu**, et al, Novel Multi-standard Dual-Wideband and Quad-Wideband Step Impedance Resonator Filters with Wide Stop Band Restriction. IEEE Trans. Microw. Theory Tech. under review

CONFERENCES:

1. **Y. Tu**, A. Ali, et al. A novel multi-standard dual-wide-band polygon SLSIR filter. International conference of Internet Technologies and Applications (ITA), pp. 434- 438. September. 2015.

2. A. Atojoko, R. A. Abd-Alhameed, **Y. Tu**, et al. Automatic liquid level indication and control using passive UHF RFID tags . 2014 Loughborough Antennas and Propagation Conference (LAPC), pp: 136-140. 2014.

3. M. A. G. Al –Sadoon, A. S. Abdullah, R. S. Ali, **Y. Tu**, R. A. Abd-Alhameed, S. M. R. Jones and J. M. Noras, The Effects of Mutual Coupling within Antenna Arrays on Angle of Arrival Methods, 2016 Loughborough Antennas & Propagation Conference (LAPC), in Burleigh Court International Conference Centre, Loughborough University, United Kingdom, pp. 371-375. 14-15 November 2016

2. List of Publications

A Multi-standard Filter with Folded Couple Lines and Shifted Coupled Lines

Yuxiang Tu, Ahmed Mirza, Raed A. Abd-Alhameed, Chan H See and Neil J. McEwan

Mobile and Satellite Communications Research centre,
University of Bradford, Engineering & Informatics,
Bradford, United Kingdom
y. tu1@student. bradford. ac. uk, r. a. a. abd@bradford. ac. uk

In recent years, with the requirements in the current increasingly stringent frequency spectrum resources and the development of advanced multi-standard wireless communication systems, multi-standard internal filters have become a necessity for the state-of-the-art multifunction “smart phones” and wireless transceivers for the mobile devices

In this paper, we propose a novel multi-standard filter with the size of only 4. 6mm×41. 65mm for wireless communication systems. The proposed filter has a fundamental bandwidth of 605. 9 MHz with fractional bandwidth(FBW) of 31. 4% centred at the 1. 9 GHz band, and first spurious bandwidth of 501 MHz with FBW of 8. 6% centred at the 5. 8 GHz band. This filter is able to generate two wide operating bands that effectively cover the GSM/UMTS/GPS /IEEE 802. 11a operations in mobile devices, which include GSM1800 (1710-1880 MHz), GSM1900 (1850-1990 MHz), UMTS (1920-2170 MHz), GPS(centred at 5. 75 GHz) and IEEE 802. 11a (centred at 5. 8 GHz) bands, which usually are only covered partly by recently published works[1-4]. The configuration of the presented multiband filter is illustrated inFigure 1, which uses folded couple lines instead of traditional a quarter wavelength SIR couple lines to optimize high order spurious performance. The even- and odd-mode phase velocities compensation technique with shifted coupled lines [5] are used for the first time in the quarter wavelength type resonator to enhance spurious frequency and out of band performance. What’s more, the return loss of fundamental resonance frequency and first spurious frequency become less with the help of the loaded stub. The Ansoft HFSS software simulated result agrees well with the theory predictions, which is shown in Figure 2. The featured broad bandwidths over dual applicable frequency bands and the miniaturized size of the proposed filter make it promising for applications in multi-standard wireless communication.

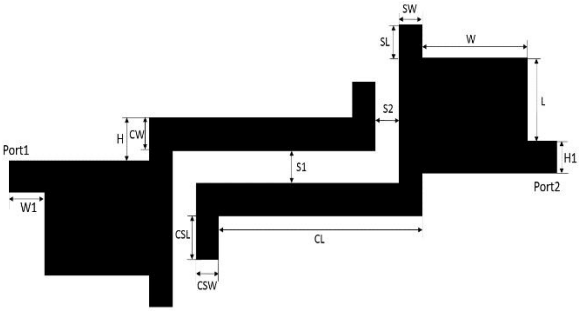

Fig1. The architecture of the proposed dual-wide-band filter

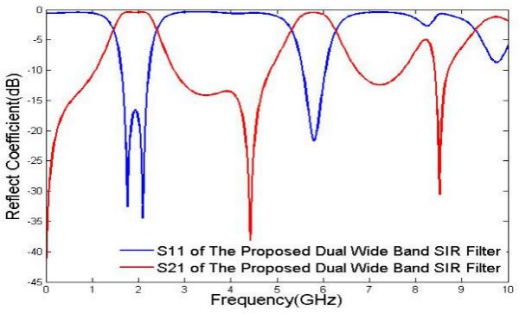

Figure 4. The final results of the proposed dual-band filter

REFERENCE

1. J. Shi, L. L Lin, Jian-Xin Chen, Hui Chu, Xu Wu, "Dual-Band Bandpass Filter With Wide Stopband Using One Stepped-Impedance Ring Resonator With Shorted Stubs," IEEE Microwave and Wireless Components Letters. Vol. 24, no. 7, pp: 442 - 444, 2014.

2. L. Gao, X. Y. Zhang, "High-Selectivity Dual-Band Bandpass Filter Using a Quad-Mode Resonator with Source-Load Coupling," IEEE Microwave and Wireless Components Letters, Vol. 23, no. 9, pp:474 - 476, 2013.

3. Shou-Jia Sun, T. Su, K. Deng, B. Wu, Chang-Hong Liang, "Compact Microstrip Dual-Band Bandpass Filter Using a Novel Stub-Loaded Quad-Mode Resonator, "IEEE Microwave and Wireless Components Letters, Vol. 23, no. 9, pp:465 - 467, 2013.

4. S. Fu, B. Wu, J. Chen, S. J. Sun, C. H. Liang, "Novel Second-Order Dual-Mode Dual-Band Filters Using Capacitance Loaded Square Loop Resonator ,"IEEE Transactions on Microwave Theory and Techniques, Vol. 60, no. 3, Part. 1, pp 477 - 483, 2012.

5. T. Lopetegi, M. A. G. Laso, J. Hernandez, M. Bacaicoa, D. Benito,M. J. Garde, M. Sorolla, and M. Guglielmi, " New microstrip "wigglyline" filters with spurious passband suppression, "IEEE Transactions on Microwave Theory and Techniques. Vol. 49, no. 9, 2001, pp: 1593-1598.

A Novel Multi-standard Dual-Wide-band Polygon SLSIR Filter

Yuxiang Tu, Raed. A. Alhameed

Mobile and Satellite Communications Research centre,
University of Bradford, Engineering & Informatics,
Bradford, United Kingdom
ytu1 @student. bradford. ac. uk, raaabd @bradford. ac. uk

Abstract. A novel multi-standard dual-wide-band filter with a compact size of only 8. 8 mm by 16. 8mm is designed and developed for transceiver devices. The proposed filter has a fundamental bandwidth of 1. 6 GHz with fractional bandwidth(FBW) of 29. 7% centreed at the 5. 4 GHz band, and second bandwidth of 300. 0 MHz with FBW of 3. 6% centreed at the 8. 15 GHz band. The basic dual-wide-bandwidth is attributed to the interaction of the novel modified polygon pair and upper stub loaded stepped impedance resonator. Moreover, the added down stub loaded stepped impedance resonator (SLSIR) further enhances the pass-band performance by widening the bandwidth and optimizing reflection coefficient performance considerably. To validate the proposed ideas, the multi-standard filter is designed and simulated by Ansoft HFSS software. The simulated results agree well with the theory predictions. The featured broad bandwidths over two frequency bands and the miniaturized size of the proposed filter make it very promising for applications in future multi-standard wireless communication.

Keywords: Dual-wide-band filter, multi-standard, stub loaded modified step impedance resonator, wireless communication.

1 Introduction

In recent years, wireless communication facilities such as wireless transceivers has been exerting an increasingly vital impact in the field of microwave and radio frequency communication. One of the most important modules in wireless communication system is the filter. Filters play a critical role in passing desired frequency bands and stopping the unwanted ones including noise signals. Therefore, performance of the filter greatly influences performance of the whole wireless communication system [1-9].

With the requirements in the current increasingly stringent frequency spectrum resources and the development of advanced multi-standard wireless communication systems, multi-standard filters have become a necessity for the state-of-the-art multifunction wireless transceivers for the mobile devices. Such filters are generally required to be capable of covering the frequency bands of IEEE 802. 11a, IEEE 802. 11h, IEEE 802. 11j and IEEE 802. 11n,all of which operate at 5 GHz bands, IEEE 802. 11ac,which was approved by IEEE in January 2014 and provides very high throughput(VHT) wireless local area networks (WLANs) in the 5 GHz band and IEEE 802. 11p, which is intended for use in vehicular communication systems as well as specifies WLAN in the licensed Intelligent Transportation Systems(ITS) band of 5. 9 GHz(5. 850-5. 925 GHz). Furthermore, ever increasing implementation of the communication between earth and space satellite further increases the Global Positioning System (GPS)(frequency bands centreed at 5. 75 GHz)requirement and X-band requirement such as International Telecommunication Union (ITU) designed earth-space satellite communication band(7. 9-8. 4 GHz), transmission frequency bands of earth observation satellite systems including Terra(frequency bands centreed at 8. 2125 GHz),Aqua(frequency bands centreed at 8. 16 GHz) and so on. Recently, many dual band filters have been designed to satisfy such stringent requirements [1-5]. However, most of them with a miniaturized size fail to cover the required frequency bands, especially at the lower frequency

band due to the narrower dual bandwidth [1-3] or require a considerable filter size or thickness, which usually makes them difficult to integrate within mobile devices or portable wireless modules [1][4][5].

In this paper, we propose a novel multi-standard filter whose size is only 8. 8mm×16. 8mm. This filter is capable of generating two wide operating bands that effectively cover IEEE802. 11a/802. 11h/802. 11j/802. 11n/802. 11ac(frequency bands cover 5 GHz),IEEE 802. 11p(frequency bands centreed at 5. 9 GHz), Global Positioning System (GPS) (frequency bands centreed at 5. 75 GHz), International Telecommunication Union (ITU) designed earth-space satellite communication band (7. 9-8. 4 GHz) and most transmission frequency bands of earth observation satellite systems.
The proposed multi-standard filter's transmission zeros, which are used to realize the isolation of two pass-bands as well as the isolation between pass-bands and out of band, are attributed to the mutual coupling of the modified polygon microstripe line. The in band performance of the proposed filter is mainly realized by upper shaped stub loaded stepped impedance resonator. This performances is further enhanced by adopting down shaped stub loaded stepped impedance resonator (SLSIR). Because there is no via hole or defect ground structure included in the filter structure, the structure is relatively simple and easily realized. The theory study of the multi-standard filter and configuration performance with simulation results are described in Section. 2, and the conclusion of this paper is given in Section. 3.

2 Filter Theory and Configuration

2. 1 The introduction of the novel modified polygon pair

The configuration of the presented multi-band filter is illustrated in Fig. 1, in which the modified polygon pair forms a symmetric structure. Two modified polygon pair exert the effect of resonators which generate the basic curve of the filter second pass-band and sufficient transmission zeros that are used to realize the isolation of two pass-bands as well as isolation between pass-bands and out of band. Further, two modified polygon resonators act as the function of feed lines for both upper and down shaped stub loaded stepped impedance resonators. Among them, the upper resonator mainly realizes dual-wide-band, and the down resonator further enhances in band performances including widening bandwidth. In this work, the modified polygon resonator pair strips are fed by two 50Ω microstrip feed lines. The width (SW) and length (SL) of the 50Ω feed line is 0. 6mm and 1. 2mm, respectively.

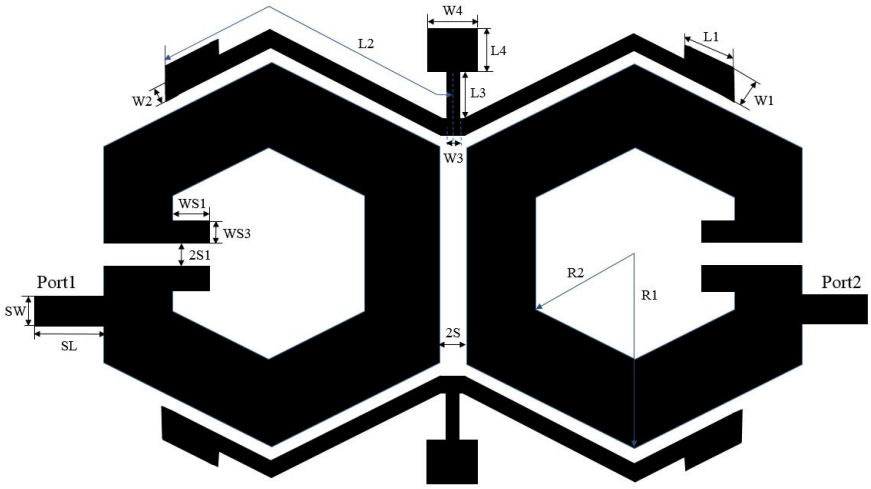

Fig1. The architecture of the proposed dual-wide-band filter

2. 2The shaped stub loaded stepped impedance resonator

The shaped stub loaded stepped impedance resonators (SLSIR) of the proposed filter in shown in Fig. 2 (a). It is seemed that upper and down SLSIR couple with two polygon resonators in a folded line form and stepped-impedance stub is embedded in invagination part between two polygon resonators. This means saves much size of resonators and results in a more compact filter size without sacrificing filter

performance. In order to simplify the analyses and calculation, SLSIR equivalent structure is derived, which is shown in Fig. 2 (b). The equivalent structure includes a traditional SIR with the characteristic admittance Y_1, Y_2, and electrical lengthΘ_1, $2\Theta_2$, which is connected to a stepped-impedance stub in the middle. The stepped-impedance stub includes high impedance line with characteristic admittance $2Y_3$ and electrical length Θ_3, and low impedance line with characteristic admittance $2Y_4$ and electrical length Θ_4. Since SLSLR is symmetrical in structure, odd- and even-mode analysis is utilized.

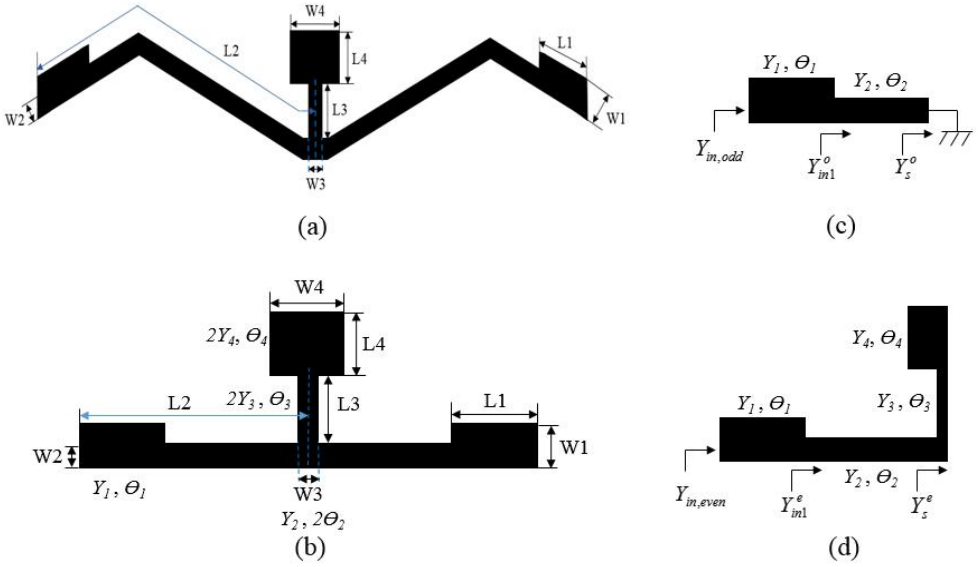

Fig2. The modified SLSIR of the proposed filter and its equivalent structure

For odd-mode excitation, the equivalent circuit is shown in Fig. 2(c). According to the transmission line theory, the input admittance for odd-mode is expressed as:

$$Y^o_{in1} = -jY_2 \cot\theta_2 \qquad (1)$$

$$Y_{in,odd} = Y_1 \frac{Y^o_{in1} + jY_1 \tan\theta_1}{Y_1 + jY^o_{in1} \tan\theta_1} \qquad (2)$$

When $Y_{in,odd}$=0,equation(2) can be deduced as:$K_1 \tan\Theta_1 \tan\Theta_2$=0. Where K_1=Y_1/Y_2. Assume the electrical length ratio of the odd-mode resonance is: α_2=$\Theta_1/(\Theta_1+\Theta_2)$. Then substitute this to (2), there is

$$K_1 \tan\Theta_2 - \cot[\Theta_1 (1-\alpha_2)/\alpha_2] = 0 \qquad (3)$$

The odd-mode solution of (3) is depend on K_1 and α_2. The ratio of the first two odd-mode resonance frequency can be determined by the length ratio α_2 and admittance ratio K_1, which are shown in

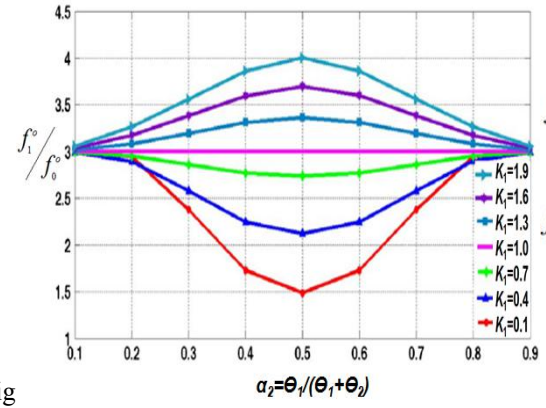

Fig **Fig. 3.** Ratios of the first two odd-mode resonant frequency

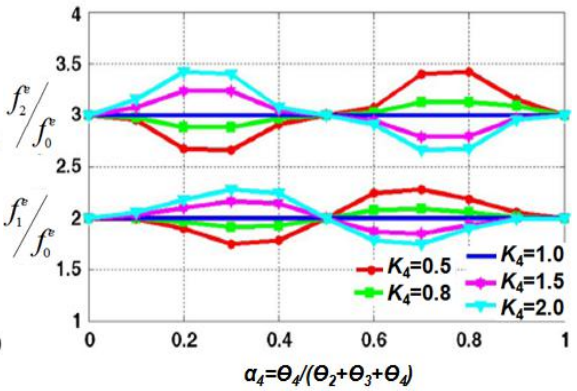

Fig. 4. Ratios of the first three even-mode resonant

f_1^o/f_0^o under different electrical length ratio α_2 and admittance ratio K_1. frequency f_1^e/f_0^e, f_2^e/f_0^e under different electrical length ratio α_4

For even-mode excitation, the equivalent circuit is shown in Fig. 2 (d). The even-mode input admittance is expressed as:

$$Y_{in,even} = Y_1 \frac{Y_{in1}^e + jY_1 \tan\theta_1}{Y_1 + jY_{in1}^e \tan\theta_1} \qquad (4)$$

In which $Y_{in1}^e = Y_2 \left(Y_s^e + jY_2 \tan\theta_2\right)/\left(Y_2 + jY_s^e \tan\theta_2\right)$, $Y_s^e = Y_3 \left(jY_4 \tan\theta_4 + jY_3 \tan\theta_3\right)/\left(Y_3 + j(jY_4 \tan\theta_4)\tan\theta_3\right)$. When $Y_{\text{in,even}}$=0,equation(4) can be deduced as: $K_4 \tan\theta_4 = \left[\tan(\theta_2+\theta_3) + K_1 \tan\theta_1\right]/\left(K_1 \tan\theta_1 \tan(\theta_2+\theta_3) - 1\right)$,in which K_4=Y_4/Y_3. The relationship among three even-modes, different electrical length ratio α_4 and admittance ratio K_4 is shown in Fig. 4. When Y_1=Y_2=Y_3 is supposed for simplicity, we can get $Y_{in,odd} = -jY_2 \cot\theta_2$ and Θ_2=90° when $Y_{\text{in,odd}}$=0. The fundamental odd-mode resonance frequency is:

$$f_0 = c/\left(4L_2\sqrt{\varepsilon_{eff}}\right) \qquad (5)$$

The input admittance for even-mode resonance frequency is express as:

$$Y_{in,even} = jY_3 \frac{Y_4 \tan\theta_4 + Y_3 \tan(\theta_2+\theta_3)}{Y_3 - Y_4 \tan\theta_4 \tan(\theta_2+\theta_3)} \qquad (6)$$

When $Y_{\text{in,even}}$=0, $K_4 \tan\theta_4 + \tan(\theta_2+\theta_3) = 0$ and further $K_4 \tan\alpha_4\theta_T + \tan(1-\alpha_4)\theta_T = 0$. (7)

In this case, the stub loaded stepped impedance resonator generates one odd-mode frequency and two even-mode frequency. A thing that needs to be mentioned is because of irregular shape of the feed line (including polygon pair) to SLSIRs and the influence of coupling between two polygon resonators, even-mode frequency of SLSIRs can be tuned by combining theory values and empirical values to make it locate into desired frequency bands.

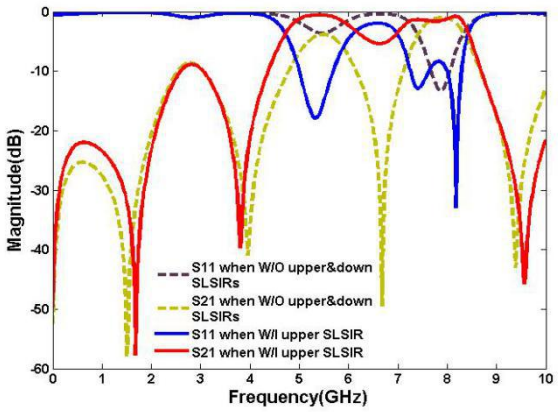

Fig. 5. The magnitude response S11 and S21when there is only polygon pair polygon pair and when polygon pair coupled with upper SLSIR

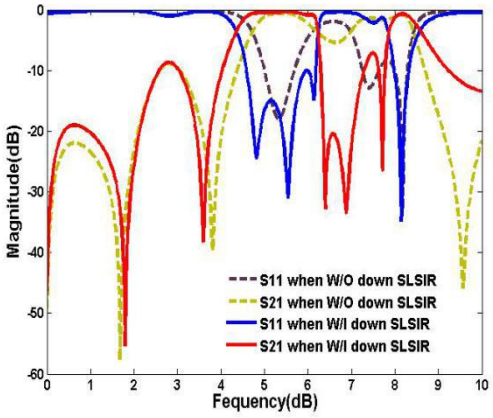

Fig. 6. The magnitude response S11 and S21 when coupled with upper SLSIR and when polygon pair coupled with upper and down SLSIR

2. 3The superimposition of Polygon Pair Waveform and Stub Loaded Stub Impedance Resonator Waveform and The Isolation between Bands

Because the modified polygon pair provides the basic curve of the filter second pass-band and four transmission zeros including the third transmission zero of 6. 68 GHz, which is shown in dash lines in Fig. 5. Using this feature, we design the upper stub loaded stepped impedance resonator's odd-mode frequency which is also SLSIR's fundamental frequency to be located at 5. 3 GHz. According to equation (5), we get the length $2L_2$ is equal to $\lambda g/2$ (a half of wavelength of SLSIR) and the value of L_2 is 4. 4mm when f_0 is 5. 3 GHz. Then external and internal radius of the polygon is set as R1=4. 1 and R2=2. 8mm, respectively. The two even-modes frequencies are tuned by changing the dimension of stepped impedance stub W_3, L_3, W_4 and L_4 in order to make it locate in 5-6 GHz band and X-band.

In this work, we set W_3=0. 2mm, L_3=0. 3mm, W_4=0. 4mm and L_4=0. 1mm. The electrical length of L_2, L_3 and L_4 is 90. 0^o, 6. 1^o and 2. 0, respectively. From solid lines shown in Fig. 5, we know that after adopting the upper SLSIR, dual wide-bands including 5. 0-5. 7 GHz centreed at 5. 34 GHz with fractional bandwidth (FBW) of 13. 0% and 8. 0-8. 3 GHz centreed at 8. 14 GHz with FBW of 3. 7% are realized with the help of polygon pair.

The magnitude response S11 and S21 of two occasions is shown in Fig. 6. The first occasion is when only the modified polygon pair with upper stub loaded stepped impedance resonator play roles, which is shown as dash lines. The second occasion is when modified polygon pair, upper and down stub loaded stepped impedance resonator play roles, which is shown as solid lines. It is seem that by adopting down stub loaded stepped impedance resonator, first pass-band performance including bandwidth performance and reflection loss performance is improved considerably. The first pass-band bandwidth of the proposed filter is broadened to 4. 6-6. 2 GHz centreed at 5. 4 GHz with fractional bandwidth (FBW) of 29. 7% and second pass-band bandwidth is 8. 0-8. 3 GHz centreed at 8. 15 GHz with FBW of 3. 6% with the interactionof down SLSIR, upper SLSIR and modified polygon pair.

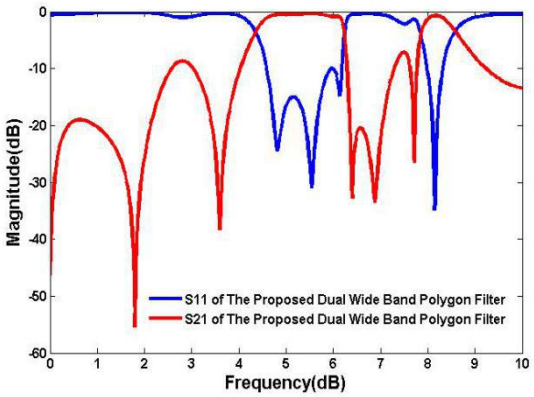

Fig. 7. The final results of the proposed dual-wide-band filter

The final results of the proposed dual-band filter is shown in Fig. 6. The substrate adopted in this work is Rogers RO3010 whose dielectric constant is 10. 2 and thickness is 0. 635mm. In the model, six transmission zeroes 0 GHz, 1. 80 GHz, 3. 60 GHz, 6. 40 GHz,6. 88 GHz and 7. 72 GHz are generated. These transmission zeroes provides well isolation between desired dual bands, suppression of out of band interruption and enhancement of the frequency selectivity. The gap width between two resonator pair is 2S=0. 2mm and another gap width 2S1=0. 2mm.

3. Conclusion

A novel multi-standard dual-wide-band filter with a compact size is designed and developed for wireless communication system such as mobile devices. This proposed filter covers a fundamental bandwidth of 1. 6 GHz with fractional bandwidth (FBW) of 29. 7% centreed at the 5. 4 GHz band and second bandwidth of 300. 0 MHz with FBW of 3. 6% centreed at the 8. 15 GHz, while occupy a miniature area of only 8. 8mm by 16. 8mm. By utilising novel modified polygon pair and upper stub loaded stepped impedance resonator, dual bands and sufficient transmission zeroes are generated. The added down stub loaded stepped impedance resonator further enhances the first pass-band performance by widening the bandwidth and optimizing reflection loss performance considerably. What's more,the folded and embedded structure of two SLSIRs saves much size of the proposed filter compared to previous SLSIRs without sacrificing filter performance. The multi-standard filter is designed, described and fully simulated. The Ansoft HFSS software simulated results agree well with the theory predictions. The featured broad bandwidths over dual applicable frequency bands and the miniaturized size of the proposed filter make it very promising for applications in future multi-standard wireless communication.

References

[1] Naeem, U. ; Bila, S. ; Thevenot, M. ; Monediere, T. ; Verdeyme, S, "A Dual-Band Bandpass Filter With Widely Separated Passbands, "IEEE Transactions on Microwave Theory and Techniques, Vol. 62, no. 3, pp. 450 - 456, 2014.

[2] Cervera, F. J. ; Jiasheng Hong, "Compact Self-Packaged Dual-Band Filter Using Multilayer Liquid Crystal Polymer Technology," IEEE Transactions on Microwave Theory and Techniques, Vol. 62, no. 11, pp. 2168 - 2625, 2014.

[3] L. Gao; X. Y. Zhang, "High-Selectivity Dual-Band Bandpass Filter Using a Quad-Mode Resonator with Source-Load Coupling," IEEE Microwave and Wireless Components Letters, Vol. 23, no. 9, pp. 474 - 476, 2013.

[4] Shou-Jia Sun ; T. Su ; K. Deng ; B. Wu ; Chang-Hong Liang, "Compact Microstrip Dual-Band Bandpass Filter Using a Novel Stub-Loaded Quad-Mode Resonator, "IEEE Microwave and Wireless Components Letters, Vol. 23, no. 9, pp. 465 - 467, 2013.

[5] S. Fu ; B. Wu ; J. Chen ; S. J. Sun ; C. H. Liang, "Novel Second-Order Dual-Mode Dual-Band Filters Using Capacitance Loaded Square Loop Resonator ,"IEEE Transactions on Microwave Theory and Techniques, Vol. 60, no. 3, Part. 1, pp 477 - 483, 2012.

[6] C. W. Tang ; P. H. Wu, "Design of a Planar Dual-Band Bandpass Filter, "IEEE Microwave and Wireless Components Letters, Vol. 21, no. 7, pp. 362 - 364, 2011.

[7] S. M. Wang ; Chun-Hsiang Chi ; Ming-Yu Hsieh ; Chi-Yang Chang, "Miniaturized spurious passband suppression microstrip filter using meandered parallel coupled lines, "IEEE Transactions on Microwave Theory and Techniques, Vol. 53, no. 2, pp. 747-753, 2005.

[8] J. Shi ; L. L Lin ; Jian-Xin Chen ; Hui Chu ; Xu Wu, "Dual-Band Bandpass Filter With Wide Stopband Using One Stepped-Impedance Ring Resonator With Shorted Stubs," IEEE Microwave and Wireless Components Letters, Vol. 24, no. 7, pp. 442 - 444, 2014.

[9] R. Phromloungsri, M. Chongcheawchamnan, and I. D. Robertson, “Inductively compensated parallel coupled microstrip lines and their applications, "IEEE Transactions on Microwave Theory and Techniques, Vol. 54, no. 9, pp. 3571-3582, 2006.

Mixed-Coupling Multi-Function Quint-Wideband Asymmetric Stepped Impedance Resonator Filter

Yuxiang Tu, Raed A. Abd-Alhameed, George A. Oguntala, Trust. Mapoka

A new mixed-coupled quint-wideband ASIR bandpass filter is proposed: spiral and open-loop coupled structures realize fundamental mode coupling and enhance another four spurious modes with optimum insertion loss. The fundamental frequency and four spurious frequencies are located at 1.275 GHz with fractional bandwidth (FBW) of 38.4%, 3.225 GHz with FBW of 38.4%, 5.875 GHz with FBW of 12.1%, 7.515 GHz with FBW of 13.7%, 9.74 GHz with FBW of 4.3%. The filter is suitable for multiple applications including GPS, Wi-Fi and IEEE 802.11a, and partially for IEEE 802.16. The quint-wideband filter has a performance superior to its currently proposed quint-wideband counterparts.

Introduction: The microstrip bandpass filter (BPF) is one of the fundamental components in microwave communication systems. Bandpass filters with good characteristics, such as low insertion loss, multi-function, wide passband and compact size, are required in communication systems [1-7]. With the current increasingly stringent demands on frequency resources, multi-band filters with multiple functions covering various communication standards and applications are highly in demand, and accordingly many multi-band filters designs have been presented [3-5]. Amongst them, tri-band bandpass filters and quad-band filters are strong candidates. However, these two types of filter have narrow-band characteristics which cannot cover the sufficient frequency bands, unsatisfactory insertion loss performance, or are relatively large in size. To improve filter performances and address the problems mentioned above, the quint-band filter was first proposed in 2012 [3], with tri-mode stub-load stepped-impedance resonators to realize quint-band performance. A multiple-stub loaded ring resonator (MSLRR) is proposed in [4] using directly coupled multi-band bandpass filters (BPFs) with mixed electric and magnetic coupling (MEMC). In [5] it is proposed to utilize three pairs of simple microstrip stepped-impedance resonators on the top and middle metal layer, and two pairs of slot uniform-impedance resonators on the bottom metal layer. Quint-band performance can indeed be realized by these individual structures, but all of these filters have relatively complicated structures such as multiple via holes [3, 4], multi-layer structure [5] and so on. These disadvantages complicate the design and fabrication, leading to high loss and cost.

In this Letter, a compact quint-wideband bandpass filter with low insertion loss, wide passband and compact size is proposed, which dispenses with complex structures. The filter is designed, fabricated and measured. Good agreement between simulated and measured results is obtained.

Proposed circuit model and analysis: Fig. 1(a) and Fig 1(b) show the configuration of the asymmetric stepped impedance resonator (ASIR) unit and the proposed second-pole mixed coupled ASIR filter, respectively. In the ASIR structure, each resonator has a high and low-characteristic impedance section. Its resonances occur when $Y_{in} = 0$ in equation (1).

$$Y_{in} = \frac{j}{Z_2}\frac{K\tan\theta_1 + \tan\theta_2}{1 - K\tan\theta_1\tan\theta_2} \tag{1}$$

In the proposed mixed coupled ASIR structure, two low characteristic impedance sections are folded to reduce the patch size, and high-characteristic impedance sections are partially coupled with each other to form the spiral and open-loop structure leading to mixed electric and magnetic coupling. The electric coupling is generated between the gaps of the coupled high impedance sections, since the SIR has the maximum electric fringe field density at the open ends [6]. The magnetic coupling is achieved by the parallel coupled section. According to [2], S_{21} can be calculated as:

$$S_{21} = -\frac{2j\,\mathrm{Im}\{y_{12}\}}{1 - \mathrm{Im}\{y_{11}\}^2 + \mathrm{Im}\{y_{12}\}^2 + 2j\,\mathrm{Im}\{y_{11}\}} \tag{2}$$

The transmission zeros occur when S_{21}=0. The Y-parameters y_{ij} (i, j=1, 2) are related elements with coupling length L_{cp}. Therefore, by adjusting L_{cp}, the transmission zeros can be relocated. This facilitates forming the multi-pass band, in conjunction with the mixed electric and magnetic coupling effect.

The centre and both ends of an ASIR coupled section are where the magnetic and electric fields in the fundamental mode peak respectively. To enhance the electric coupling of the filter, the ends of two adjacent spiral ASIRs can be closely located, which can be adjusted by g_1. We can enhance the magnetic coupling of the fundamental mode by closely positioning the parallel coupling parts of two adjacent spiral ASIRs, which can be achieved using g_2 [7]. The field peak field points of the proposed filter are shown in Fig. 2. The coupling points of spurious modes can be adjusted by changing coupling length L_{cp}. The spurious modes can also be adjusted by changing uncoupled section lengths L_{u1} and L_{u2}, which gives added freedom in designing the multi-band filter. The effect of the spiral and open-loop coupled high characteristic impedance line structure (SOLHLS) in ASIRs is reflected in the surface current distribution at the fundamental frequency and the other spurious frequencies, as illustrated in Fig. 3. Magnetic coupling is important in determining the fundamental frequency because the electrical coupling is weakened by the long distance between two open ends, whereas the four spurious modes, f_{s1}, f_{s2}, f_{s4} and f_{s5}, have current densities are distributed in different places of the SOLHLS, which means the SOLHLS facilitates the forming of high-order modes in the proposed quint-band filter.

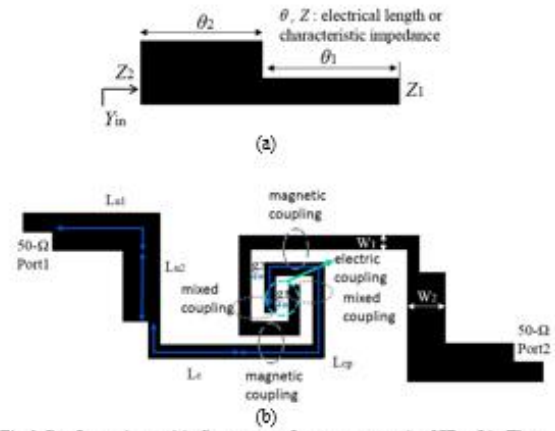

Fig.1.Configurations: (a) Structure of an asymmetric SIR. (b) The proposed quint-wideband mixed-coupling ASIR filter with the description of electric and magnetic coupling effects.

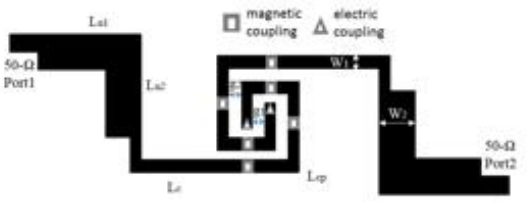

Fig. 2 Peak field points of the filter using spiral and open-loop couple structure.

AUTOMATIC LIQUID LEVEL INDICATION AND CONTROL USING PASSIVE UHF RFID TAGS

A. Atojoko[1], R. A. Abd-Alhameed[1], Y. Tu[1], F Elmegri[1], C. H. See[2], M. B. Child[1]

[1]Radio Frequency and Antenna Design Group, School of Engineering, Design and Technology,

University of Bradford, Bradford, BD7 1DP, UK

{a.a.atojok, r.a.a.abd, m.b.child}@bradford.ac.uk

[2]Bolton University, UK

{c.see@bolton.ac.uk}

***Abstract*- This paper proposes a new perspective to the liquid level monitoring and control technique by deploying energy efficient passive UHF RFID tags as liquid level sensors. The system consists of the pump, storage tank, level sensors (passive tags), RFID tag reader, pump control circuit, alarm circuit, and an indicator circuit. The tags are sealed (air and water tight), programmed with unique level labels using the Alien Reader software(860-868MHZ) and deployed to various levels of a storage tank for level monitoring and control. The mirrored P-shaped tag is designed modelled and deployed for use as the liquid level sensors. The RFID reader is disguised to form a part of the tank cover literarily few inches away from the tags. A variation of the tag readings received is used to infer level information which is communicated via the reader middleware to a computer database for monitoring.**

Keywords: Power efficient, Passive UHF RFID tag, liquid level indication and control, RFID Reader

I. INTRODUCTION

Liquid level indication and control is enormously useful particularly in places where spillage or wastage of a particular sort of liquid poses a lot of danger to human life and to the ecosystem. An effective mechanism is needed to monitor and effectively control the level of liquid pumped through and into any surface or underground storage tank. In any liquid monitoring technique, the intended threshold levels are set to be monitored and controlled. In this work, five levels are marked for indication in the tank, these are (UL-ultra Low), (L-Low) (M-Mid), (H-High), and (UH-Ultra high). The lower and upper level limits are set as the threshold levels which triggers a pump control circuit and the alarm circuit. Level sensing information from the tags are fed directly to the level indicator circuit, the threshold level information triggers the pump control circuit to engage the liquid pump to commence pumping or to terminate pumping. A safety mechanism is built into the circuit to escalate pump circuitry malfunction, this sends panic information to the alarm circuit if the pump fails to function when needed.

When these threshold levels are exceeded, a set of feedback systems escalates this unusual activity which then triggers a range of other event driven control systems to automatically curtail the situation by taking prompt and appropriate action. The demands of sophisticated automated processing systems, the need for ever-tighter process control, and an increasingly stringent regulatory environment drive process engineers to seek more precise and reliable level measurement systems. Energy efficiency and improved accuracy in liquid level measurement has led to a tremendous reduction in chemical-process variability, resulting in higher product quality, reduced cost, and less waste. Newer level measurement technologies have helped in meeting requirements for accuracy reliability and electronic reporting.

Previous approaches both manual and automated methods applied to liquid level measurement have always had limitations [1-10]. Sight glass used for manual measurement suffer from material failure and poses a serious fire and explosion hazard to personnel, the seals are prone to leak, and the sludge build up obscures visibility level and are therefore being rapidly replaced by more advanced technology. Other level detection devices include those based on specific gravity, the physical property most

The Effects of Mutual Coupling within Antenna Arrays on Angle of Arrival Methods

M.A.G. Al-Sadoon[1], A. S. Abdullah[2], R.S. Ali[2], Y. Tu[1], R.A. Abd-Alhameed[1], S.M.R. Jones[1] and J.M. Noras[1]
[1]School of Electrical Engineering and Computer Science, University of Bradford, Bradford, BD7 1DP, UK
[2]Dept. of Electrical Engineering, University of Basrah, Iraq

Abstract— In this paper, a conical helical ring antenna array is proposed for detecting direction of arrival (DOA). This array is applied two angles of arrival (AOA) methods. These are minimum variance distortionless response (MVDR) and MUSIC. The effect of mutual coupling is included on the estimation accuracy of angle of arrival. Six and eight elements ring antenna array with different spacing are studied. Results are presented that include the estimation error before and after compensation of mutual coupling.

Keywords— *Antenna array; direction finding (DF); angle of arrival; mutual coupling; tracking systems.*

I. INTRODUCTION

Direction of arrival is used to improve the communication quality of service given to mobile telephone users from the operator. Information about the direction of arrival of the incoming signals of the mobile users can be used to accurately predict their trajectories, which can be used to estimate the handoff instances [1]. Then resources for handoff requests can be reserved in advance. This will eliminate handoff failure and the associated quality of service (QoS) degradation. Smart antenna system is a promise technology of wireless mobile communication systems that supports the capacity of wireless communications applications. These systems are adopting the accurate direction of arrival technique and good beamforming approach through the use of antenna array [2].

Tracking systems will be desirable, when an AOA estimation method is integrated with compact omnidirectional antenna arrays. In Wife direction finding systems, the characteristic structure of the received signal matrix is used to obtain the information of direction. There are many techniques can be used to find the direction of arrival such as: minimum variance distortionless response (MVDR), multiple signal classification (MUSIC), maximum entropy, estimation of signal parameters via rotational invariance (ESPRIT) techniques. Normally, the mutual coupling alters the identical vectors of the antenna array, disturbing the covariance matrix. As the result, the performance and estimation accuracy of AOA method will degrade considerably [3, 4]. In many applications the size of patch and antenna array is crucial and it should be minimized as small as possible. As the distance between elements of an antenna array is decreased, the mutual coupling between these elements will affect on the performance of localization techniques negatively. The effect of mutual coupling is often analyzed by computing the mutual impedances between the antenna sensors: the values of these impedances are complex and depend on position and type of antenna array mainly [5]. It should be noticed that the behavior of mutual coupling of an antenna array in the receiving end is significantly different from that in transmitting end [6, 7]. In order to ensure an accurate estimation to direction of sources, one has to take into account mutual coupling effects. Then, a suitable decoupling approach to compensate this effect can be applied. In [8], the authors tested and investigated the performance of the AOA method by using uniform circular array (UCA) consists of 4 monopoles placed on a square metal plate. The error improved approximately by fifty percent after compensation mutual coupling of AOA technique. In this paper, the impact of mutual coupling on direction finding systems have been examined and investigated in the receiving mode. Two AOA algorithms have been used with six and eight helical UCAs with different separation distances. The error based on AOA has been calculated before and after compensation to demonstrate the operation concept. Results summarized the outcomes of AOAs are presented.

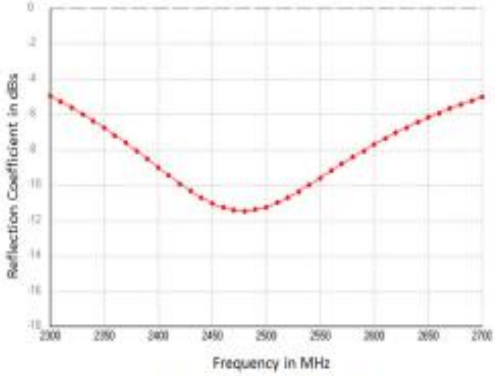

Fig. 1. Input reflection coefficient.

II. ANTENNA ARRAY MODELLING

Conical normal mode helical antenna element is selected to have a reduced antenna height, Omni-directional radiation pattern, and possible acceptable bandwidth to operate on WLAN example. The helix antenna is modeled to operate at resonant frequency 2.45 GHz for data acquisition. The height, wire radius, and spacing between turns of helix antenna are 17.5 mm, 0.5 mm and 6.4 mm respectively. The radius of the helix at the bottom and the top are 2mm and 2.8mm